

ELECTRICAL PROPERTIES OF THIN ORGANIC POLYMER LAYERS

by

Jose Luis Gil Zambrano, Lic.

A thesis submitted for the degree of Doctor of Philosophy

in the University of London

Imperial College of Science and Technology,  
London, SW7.

June 1981.

ACKNOWLEDGEMENTS

I am grateful to my supervisor, Dr. C. Juhasz, for his invaluable contribution to my education. Dr. Juhasz's dynamic and creative disposition has been a great inspiration to my interest in polymer science and engineering research.

I wish to acknowledge Professor J.C. Anderson for his interest, use of the laboratories and his helpful advice on the project.

I greatly appreciate many useful and interesting discussions I have shared with Dr. P.M. Gundry. Thanks are also due to Dr. S. Wright for reading my thesis and making corrections to the English.

I would like to express gratitude to the Universidad de Oriente of Venezuela for financial support received during the course of my research.

I would also like to thank Dr. J. van Turnhout for kindly supplying a copy of his thesis; Mr. K.G. White for technical assistance and Miss C.D.M. Collins for typing the manuscript.

Finally, I acknowledge with deepest gratitude the constant support and understanding of my wife Fanny. I dedicate this thesis to her.

ABSTRACT

The principal objectives of this research are the presentation of a short review of the electrical properties of polymers and the experimental study of the electret effect through the thermally stimulated discharge (TSD) technique. The relationship between TSD and other techniques such as d.c. step response, a.c. response and differential thermal analysis (DTA) are also discussed.

Complex internal charge distributions which are caused during the manufacturing process were found in virgin polymer films. An appreciable short-circuit current was observed during heating and cooling from nylon films sandwiched between aluminium and gold metal electrodes. It is proposed that the spontaneous current is electrochemical in nature.

$\alpha$  peaks investigated in nylon and polyvinyl butyral were found to be in agreement with the randomisation of dipoles at the glass transition and therefore this relaxation involves the onset of large-scale segmental motion.

A space charge or  $\rho$  peak was resolved by TSD in nylon films. This space charge relaxation was found to be related to a cold crystallisation mechanism occurring in the bulk of the polymer, as determined by DTA. D.C. step response also showed a low-frequency high temperature relaxation in nylon. It is believed that charge carriers are accumulated at the phase boundaries during the formation of the electret. TSD operates in the low frequency range and therefore usually shows an excellent resolution between the relaxation peaks.

CONTENTS

	<u>Page</u>
CHAPTER I:	
1.0 STRUCTURE OF SOLID POLYMERS	8
1.1 INTRODUCTION	8
1.2 MOLECULAR PACKING	8
1.3 IMPERFECTIONS IN POLYMERS	9
1.4 TRANSITIONS AND MOLECULAR MOTIONS IN POLYMERS	11
1.4.1 Introduction	11
1.4.2 Relaxations in Semicrystalline and Amorphous Polymers	11
1.4.2.1 The Glass Transition Temperature ( $\alpha$ Relaxation)	13
1.4.2.2 Theories of the Glass Transition	14
1.5 ELECTRICAL CONDUCTION IN POLYMERS	19
1.5.1 Charge Carriers in Polymers	20
1.5.2 Electronic States	23
1.5.3 Experimental Techniques to Investigate Electrical Processes in Polymers	27
1.5.3.1 Decay Methods	27
1.5.3.2 Time-of-Flight Methods	29
1.5.3.3 Contact Electrification	30
1.5.3.4 Direct Measurements of Current Voltage Curves	33
1.5.3.5 Thermally Stimulated Discharge	37
1.6 ELECTRETS	39
1.6.1 Applications	41
1.7 AIMS OF THE PRESENT STUDY AND LAYOUT OF THE THESIS	43

	<u>Page</u>
CHAPTER II: THERMALLY STIMULATED DEPolarISATION	44
2.0 INTRODUCTION	44
2.1 MECHANISMS CONTRIBUTING TO TSD	44
2.2 THERMALLY STIMULATED DISCHARGE TECHNIQUE	48
2.3 DIPOLAR THEORY OF BUCCI AND FIESCHI	50
2.4 THERMALLY STIMULATED POLARISATION TECHNIQUE	53
2.5 THE EQUIVALENT FREQUENCY OF THE TSD MEASUREMENTS	55
2.6 THERMALLY STIMULATED DISCHARGE OF HETEROGENEOUS SYSTEMS	57
2.7 DIPOLAR PROCESSES WITH A DISTRIBUTION OF RELAXATION TIMES	60
2.8 THE SCREENED HOPPING MODEL OF JONSCHER	65
2.9 EXPERIMENTAL METHODS TO DISTINGUISH BETWEEN DISTRIBUTED AND NON-DISTRIBUTED PROCESSES	68
2.9.1 Forming and Storage Conditions	68
2.9.2 Multistage TSD	69
2.9.3 Thermal Sampling Technique	69
2.9.4 Fractional Polarisation Technique	70
2.10 DETERMINATION OF THE RELAXATION PARAMETERS	71
2.10.1 Activation Energy	71
2.10.1.1 Initial Rise Method	71
2.10.1.2 Graphical Integration Method	72
2.10.1.3 The Method of Varying Heating Rate	73
2.10.1.4 Methods based on the Symmetry of the Peak	73
2.10.2 Parameters other than A	74

		<u>Page</u>
CHAPTER III:	EXPERIMENTAL APPARATUS AND MEASUREMENT PROCEDURES	76
3.0	INTRODUCTION	76
3.1	SAMPLE PREPARATION AND ELECTRODES	76
3.2	THE CRYOSTAT	78
3.3	THE CURRENT MEASUREMENT	83
3.4	DIFFERENTIAL THERMAL ANALYSIS	88
3.5	INFRARED SPECTROSCOPY	90
3.6	A.C. MEASUREMENTS	91
CHAPTER IV:	ELECTRICAL CONDUCTIVITY STUDIES ON NYLON	93
4.0	INTRODUCTION	93
4.1	STRUCTURE OF NYLONS	93
4.2	DTA OF NYLON	99
4.3	SPONTANEOUS ELECTRIC POLARISATION	101
	4.3.1 Introduction	101
	4.3.1.1 Symmetrical Electrodes ( $M_1$ -Polymer- $M_1$ )	101
	4.3.1.2 Asymmetrical Electrodes ( $M_2$ -Polymer- $M_2$ )	102
	4.3.2 Experimental Results and Discussion	106
	4.3.2.1 Symmetrical Electrodes	106
	4.3.2.2 Asymmetrical Electrodes	112
	4.3.3 Conclusions	119
4.4	D.C. CONDUCTION	120
	4.4.1 Introduction	120
	4.4.2 Hamon Approximation	121
	4.4.3 Measurements	122
	4.4.4 Previous Studies	125
	4.4.5 Discussion	135
	4.4.6 Conclusion	143

4.5	THERMALLY STIMULATED DEPOLARISATION CURRENT AT HIGH TEMPERATURE IN NYLON	144
4.5.1	Introduction	144
4.5.2	Experimental	144
4.5.3	The $\alpha$ Relaxation	146
4.5.3.1	Results	146
4.5.3.2	Discussions	150
4.5.3.3	Conclusions	155
4.5.4	The $\rho$ Peak	164
4.5.4.1	Results	164
4.5.4.2	Discussion	168
4.5.4.3	Conclusions	177
4.5.5	The $\rho'$ Peak	178
4.5.5.1	Results	178
4.5.5.2	Discussion and Conclusions	180
4.6	PYROELECTRIC EFFECT IN NYLON FILMS	181
4.7	EFFECT OF BREATHING ON NYLON FILMS	185
CHAPTER V:	THERMALLY STIMULATED DISCHARGE IN POLYVINYL BUTYRAL FILMS	187
5.0	INTRODUCTION	187
5.1	EXPERIMENTAL	188
5.2	RESULTS	188
5.3	DISCUSSION	191
5.4	CONCLUSIONS	195
CHAPTER VI:		
6.1	FINAL CONCLUSIONS	204
6.2	FUTURE WORK	206
REFERENCES		207

## CHAPTER I

### 1.0 STRUCTURE OF SOLID POLYMERS

#### 1.1 INTRODUCTION

Although this thesis is primarily concerned with the electrical properties of polymers, it seems desirable at the outset to introduce a few elementary ideas concerning their structure and molecular motions. The motion of segments in a polymer chain is responsible in large measure for the physical and mechanical properties of macromolecules in the solid or liquid state.

#### 1.2 MOLECULAR PACKING

Polymeric solids are composed of macromolecules of molecular weight greater than about  $10^4$  atomic mass units (Billmeyer 1971). The macromolecules themselves are comprised of covalently bonded molecular subunits: most commonly hydrocarbons or their compounds with oxygen, nitrogen and halogens. The intermolecular forces determine the cohesion of molecular aggregates. In the case of hydrocarbon polymers the chains are held together by van der Waals forces only. Polar chains develop, in addition, induction forces between neighbouring dipoles, which increase intermolecular cohesion. Certain polymers such as nylon, cellulose and proteins can also form intermolecular hydrogen bonds.

Polymers in the solid state can be completely amorphous, partly crystalline, or almost completely crystalline. In the bulk polymer, the ordered regions are called crystallites on account of their small size, of the order of 0.01 to 0.1  $\mu\text{m}$ . In the original fringe micelle theory, the crystallites were thought to consist of straight and parallel polymer chains which were randomly arranged in an amorphous matrix. A single polymer molecule ran through several crystalline and amorphous regions. It has now been established that the crystallites are organised into



larger groups with approximately spherical outline, called spherulites. This led to the chain folded theory. Fig. 1.1 shows a schematic representation of an amorphous and semicrystalline polymer (Kaufman 1977).

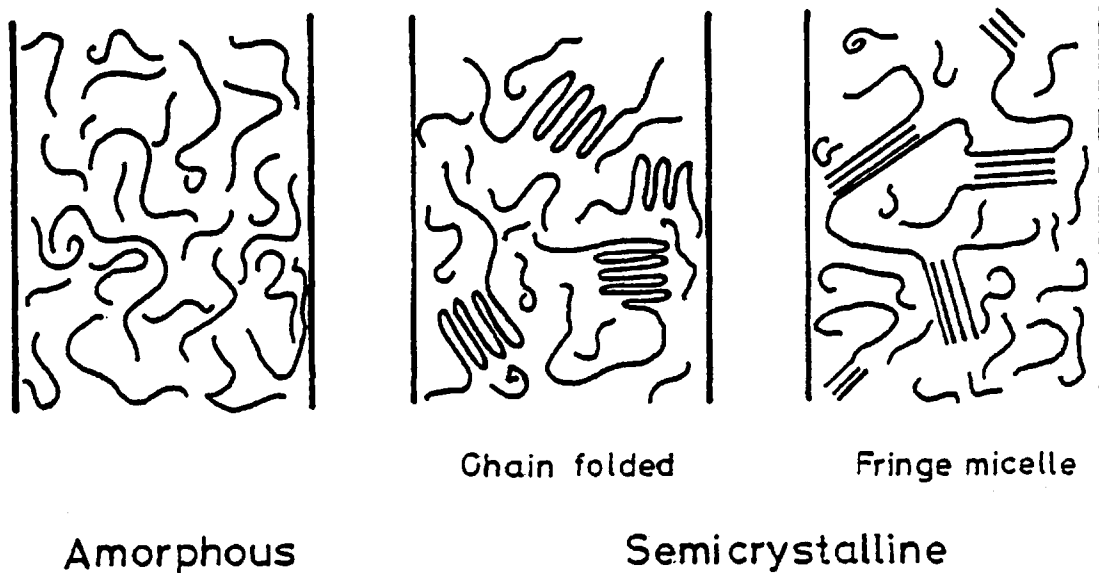


Fig. 1.1: Schematic amorphous and semicrystalline polymers

### 1.3 IMPERFECTIONS IN POLYMERS

The defects in a semicrystalline polymer are so numerous and diverse that it is impossible to characterise them completely with a single parameter. For example, the Hosemann model (Fig. 1.2) of the crystalline state contains many, but not all, types of disorders (Hosemann 1972). In the case of polyamides these may be envisaged as arising in (a) chain folds, (b) chain ends, (c) distortion, bending or twisting of H-bonded sheets, (d) intercalation of individual or small stacks of sheets, (e) vacancies, (f) voids and (g) impurities. There does not seem to be a unique way to extract all this information and relate it to a given sample.

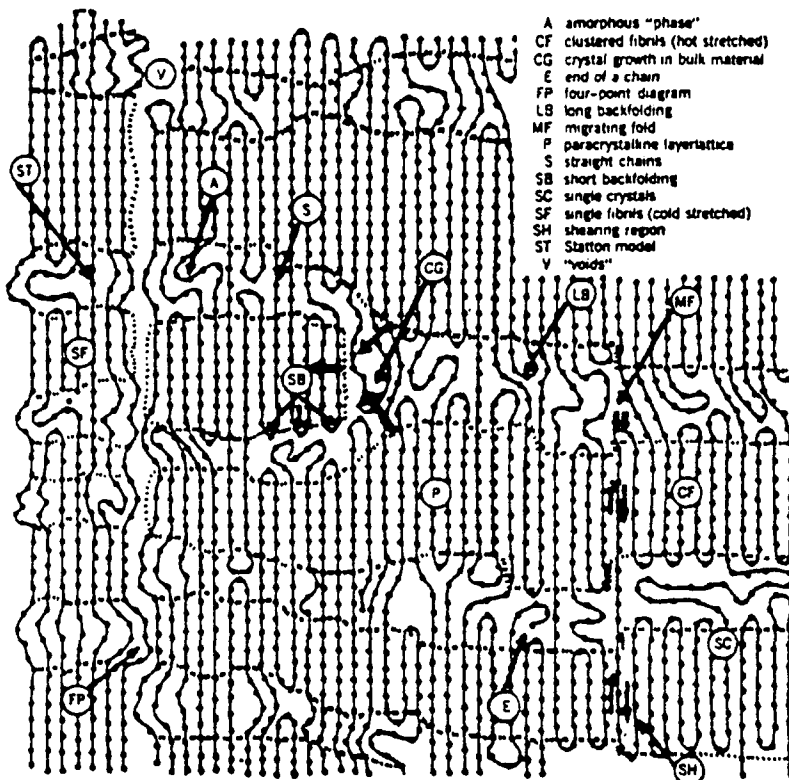


Fig. 1.2: Defects in a semicrystalline polymer (after Hosemann 1972)

The fundamental reasons for the greater concentration of defects in macromolecular solids can be expressed in thermodynamic terms. The free energy for crystallisation per mole of crystallising unit  $\Delta G_c$  can be represented as the resultant of a pair of opposing entities, the enthalpy of crystallisation  $\Delta H_c$  and the entropy factor  $T\Delta S_c$ . That is,  $\Delta G_c = \Delta H_c - T\Delta S_c$ . Compared to the enthalpy of crystallisation in simple covalent, ionic, or metallic solids, the enthalpy of crystallisation in molecular solids is quite small, for it is based on the relatively weak van der Waals forces. Highly perfect crystallisation is further impeded in the polymeric solids by the fact that the entropy of crystallisation per crystallisable unit is at least equivalent and often much greater than

in the simpler covalent, ionic, or metallic solids. In a crystallising polymer made of long chains of almost freely rotating segments, for example, the opportunity for disorder is almost astronomically greater than for the simple diamond form of carbon. As a consequence of the two unfavourable factors, low enthalpy of crystallisation and high entropy of crystallisation, the net free energy of crystallisation per crystallising unit is normally very low in polymeric molecular solids.

#### 1.4 TRANSITIONS AND MOLECULAR MOTIONS IN POLYMERS

##### 1.4.1 Introduction

In this section the different transitions that can occur in polymeric materials as well as their molecular interpretation are discussed. Emphasis will be given to the glass transition temperature,  $T_g$ .

##### 1.4.2 Relaxations in Semicrystalline and Amorphous Polymers

Typical schematic loss spectra (electrical or mechanical) for semicrystalline and amorphous polymers plotted against a relative temperature scale,  $T/T_g$  are shown in Fig. 1.3.

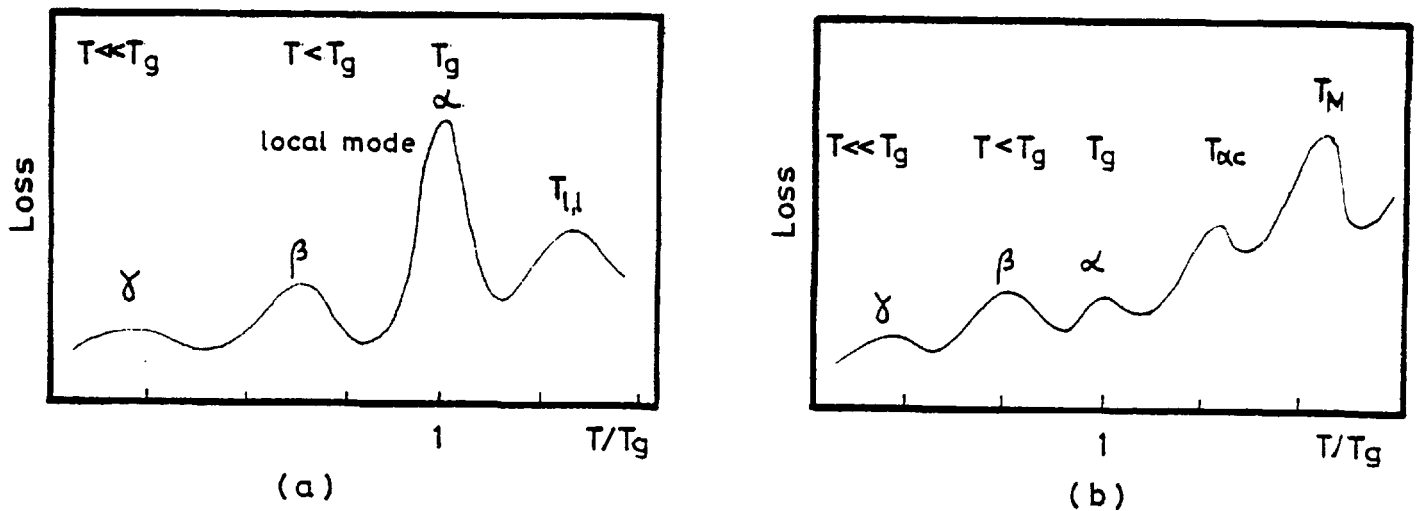


Fig. 1.3: Relaxation spectrum for amorphous (a) and semicrystalline (b) polymers (Boyer 1975)

An idealised polymer chain containing side groups will be assumed for the discussion of several types of molecular motions.

Fig. 1.4 illustrates such a chain.

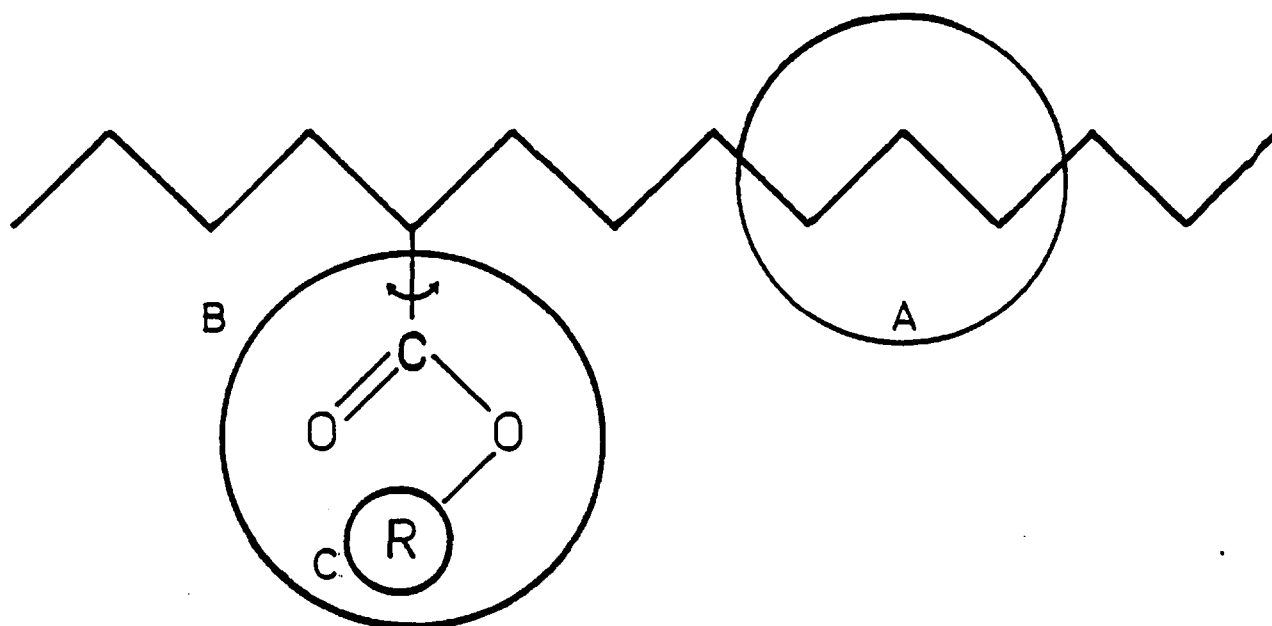


Fig. 1.4: An ideal polymer chain (after Heijboer 1978)

The  $\gamma$  relaxation is due to an internal motion within the side group itself, without interaction with the main chain (Fig. 1.4, type C). A typical example is the internal motion in R of the  $-COOR$  group in polymethacrylates.

Most polymers and copolymers show a  $\beta$  relaxation (McCrum et al 1967). In PVC this is a motion, still within the polymer chain but locally much more restricted than the motion corresponding to the glass transition (Fig. 1.4, type A). It involves 2-4 main chain atoms. In poly (methyl methacrylate) this relaxation is due to the rotation of the ester side-group about the C-C bond which links it to the main chain (Fig. 1.4, type B).

### 1.4.2.1 The Glass Transition Temperature ( $\alpha$ Relaxation)

All physical and mechanical properties of linear amorphous polymers and copolymers change in a marked fashion at the glass transition temperature,  $T_g$ . This is illustrated in Fig. 1.5 with respect to volume,  $V$ , and its first derivative,  $\alpha$ , and heat content,  $H$ , and its first derivative,  $c_p$ .

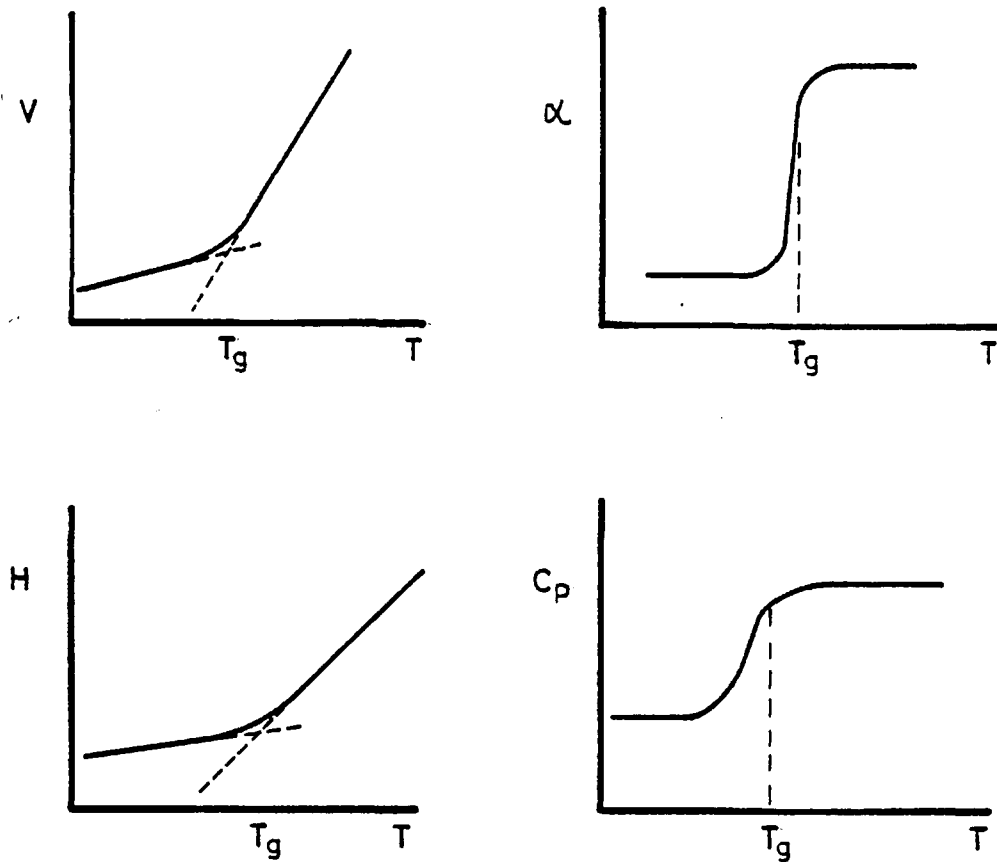


Fig. 1.5: Variation in volume,  $V$ , and heat content,  $H$ , on traversing the glass transition region

The glass transition process occurring at temperature  $T_g$  marks the freezing-in (upon cooling) or the unfreezing (upon heating) of micro-Brownian motion of chain segments 20-50 carbon atoms in length.

This micro-Brownian motion is a semicooperative action involving torsional oscillation and/or rotations about backbone bonds in a given chain as well as in neighbouring chains. For semicrystalline polymers,  $T_g$  is no longer the highly dominant loss peak.

Several factors can influence the glass transition temperature. Takayanagi et al (1963) has shown that in nylon-6 the  $\alpha$  relaxation shifts to higher temperatures as crystallinity increases. His results also show that the peak drops greatly in height and broadens significantly as crystallinity increases, suggesting that the  $\alpha$  process involves motions within the amorphous regions.

The glass transition, as well as all other relaxations and transitions including the melting point, shifts to higher temperatures with increasing frequency of observation.

Plasticisation usually results in loss of crystallinity, hence its influence in reducing  $T_g$ . Application of hydrostatic pressure increases  $T_g$ .

Many different physical methods exist to observe  $T_g$  (Boyer 1977), among which are: Differential Thermal Analysis, electrical resistivity, dielectric loss, dynamic mechanical loss, electret effect, etc.

#### 1.4.2.2 Theories of the Glass Transition

There are several approaches for a molecular interpretation of the glass transition temperature in polymers. A detailed critical survey of these is beyond the scope of this thesis. References by Saito et al (1963), McCrum et al (1967) and Ward (1979) give a detailed discussion and historical survey of  $T_g$ . This section discusses only the empirical equation of Williams, Landel and Ferry (WLF), the free volume theory and the statistical mechanical theory.

Williams, Landel and Ferry (1955) have proposed an empirical equation which describes the temperature dependence of relaxation times in the glass transition regions. This equation is now well known as the WLF equation and can be written as

$$\tau(T) = \tau_g \exp \left[ - \frac{C_1(T-T_g)}{C_2+T-T_g} \right] \quad T > T_g \quad (1.1)$$

where  $C_1$  and  $C_2$  are universal constants. For most amorphous polymers (van Turnhout 1971)  $\tau_g^{-1} = 7 \times 10^{-3} \text{ s}^{-1}$ ,  $C_1 = 40$  and  $C_2 = 52^\circ\text{C}$ . Eqn. (1.1) can be written as well in a form similar to an Arrhenius shift

$$\tau(T) = \tau'_g \exp \left[ \frac{A_w}{k(T-T_\infty)} \right] \quad T > T_g \quad (1.2)$$

where  $\tau_g^{-1} = 1.6 \times 10^{15} \text{ s}^{-1}$ ,  $A_w = 0.18 \text{ eV}$  and  $T_\infty = T_g - C_2$ .

The WLF equation has received a plausible theoretical basis in terms of free volume concepts or statistical thermodynamics. A brief discussion of both theories is given below.

Cohen and Turnbull (1959) have proposed that the free volume  $v_f$  corresponds to that part of the excess volume  $v - v_0$  ( $v$  = total measured specific volume and  $v_0$  is the occupied volume) which can be redistributed without a change in energy. It is then assumed on the basis of arguments concerning the nature of the 'cage' formed round a molecule by its neighbours that the redistribution can take place without a change in energy at temperatures above a critical temperature, which is to be identified with  $T_2$ , where the cage reaches a critical size.

Thus

$$v_f = 0 \quad \text{for } T < T_2$$

and

$$v_f = \alpha \bar{v}_m (T - T_2) \quad \text{for } T \geq T_2 \quad (1.3)$$

where  $\alpha$  is the average expansion coefficient and  $\bar{v}_m$  the average value of the molecular volume  $v_0$  in the temperature range  $T_2$  to  $T$ .

For a viscosity equation of the form (Doolittle 1951)

$$\eta = a \exp(b v / v_f) \quad (1.4)$$

where  $a$  and  $b$  are constants, this gives

$$\eta = a \exp \frac{B}{T - T_2} \quad (1.5)$$

where  $B$  is a constant and correspondingly for the average relaxation time:

$$\tau = \tau_0 \exp \frac{B}{T - T_2} \quad (1.6)$$

Substituting  $T_2 = T_g - 52$  in eqn. (1.6) gives the WLF equation and the relaxation time will become infinitely long as  $T_2$  is approached due to the disappearance of free volume.

Gibbs and Di Marzio (1958) have proposed that the dilatometric  $T_g$  is a manifestation of a true equilibrium second-order transition at the temperature  $T_2$  at which the configurational entropy of the system becomes zero. More recently Adam and Gibbs (1965) have shown how the WLF equation can be derived.

The transition probability is written as a product of a frequency factor and the probability that the system is in a state for which rearrangements are possible



$$W(T) = W_0 \exp(- n\Delta G/kT) \quad (1.7)$$

where  $W_0$  is a constant,  $\Delta G$  is the free-energy difference hindering rearrangement per segment (the barrier height) and  $n$  is the smallest number of segments that can compose a unit capable of rearrangement. This result implies that the overwhelming majority of transitions are undergone by regions whose size differs negligibly from the smallest size  $n$  that permits a transition at all. It is then argued that  $n$  is proportional to  $1/S$ , where  $S$  is the configurational entropy of the specimen. Therefore

$$W(T) = W_0 \exp(- c/ST) \quad (1.8)$$

where  $c = N_A \Delta G s^*/k$  and  $s^*$  is the configurational entropy of a unit of size  $n$ .

If  $S$  is the configurational entropy of the system, the entropy per mole of segments can be written as

$$S = \frac{N_A s^*}{n} \quad (1.9)$$

where  $N_A$  is Avogadro's number.

This is a key step because Gibbs and Di Marzio had based their earlier theory on the assumption that  $S = 0$  at  $T_2$ . Thus  $S$  at any other temperature is given by

$$S(T) = \Delta c_p \ln (T/T_2) \quad (1.10)$$

where  $\Delta c_p$  is the difference in specific heat between the equilibrium melt and the glass at  $T_g$ . Thus finally the relaxation time can be written as

$$\tau(T) = \frac{1}{W_0} \exp \frac{N_A s^* \Delta G}{k \Delta c_p} \frac{1}{T \ln(T/T_2)} \quad (1.11)$$

which can be rewritten in the form

$$\tau(T) = \tau_0 \exp \left[ - \frac{B}{(T-T_2)} \right] \quad (1.12)$$

where  $B = N_A s^* \Delta G / k \Delta c_p$  and  $\tau_0 = 1/W_0$ .

Eqn. (1.12) reduces to the WLF equation substituting  $T_2$  by  $T_g - 52$ . Free-volume ideas are widely used but the free volume is ill-defined operationally.

There exists experimental evidence that amorphous polymers and copolymers show a possible transition or relaxation above  $T_g$  (Boyer 1977). The nature of this is not too well understood but it probably involves motion of the entire polymer chain, at least up to some critical molecular weight. The onset of this motion has been designated by Boyer (1966) as  $T_{ll}$  (liquid-liquid transition).

In a semicrystalline polymer in which molecular chains meander between locally disorganised amorphous areas and more ordered folded chain regions, the effect of motion of the amorphous segments at temperatures above  $T_g$  on the crystallised regions could be to reduce the crystalline melting point locally and induce a premelting effect ( $T_{\alpha C}$ ).

The crystalline melting temperature  $T_M$  is an order-disorder transition involving a large enthalpy and entropy change, where the long-range order is destroyed.

### Cold crystallisation

Some high polymers can crystallise, on heating, at temperatures far below the melting point but above the glass-transition temperature. This type of crystallisation has been called "cold crystallisation" (Boyer 1977) and is assumed to involve the nearest neighbouring chain units in the amorphous regions. Such crystallisation occurs without molecular rearrangements and leads to production of small crystallites.

### 1.5 ELECTRICAL CONDUCTION IN POLYMERS

The electrical properties of polymers are of increasing interest and the relationship of electrical conductivity to chemical nature and morphology is one of the major unanswered problems of polymer science. It is well recognised that the concepts of solid state physics as applied to crystalline inorganic solids cannot be applied to amorphous organic polymers which, in addition to their lack of long range order, are molecular materials (Seanor 1972). Consequently such concepts as band theory are of limited applicability to organic polymers. However, it is possible to draw a phenomenological analogy between polymers and inorganic insulators and between polymers and amorphous inorganic systems such as selenium.

However, having in mind the complicated and not well known structure of high molecular weight materials it is not surprising that the picture of the conductivity mechanism is far from clear. This situation may be partly due to the large number of known polymers whose chemical and physical structures are very different. Thus it is much more difficult to establish a model of the electrical conductivity which might be applied, without question, to all types of high molecular weight solids. With few exceptions most of the polymers, especially those produced industrially, have room temperature conductivities below  $10^{-12} \text{ (ohm-m)}^{-1}$ .

In the following sections the types of charge carriers and their transport mechanism in polymers under the application of a d.c. electric field are discussed.

### 1.5.1 Charge Carriers in Polymers

In a polymer the following charge carriers can contribute to an electric current

- (i) Electric dipole moments
- (ii) Ions
- (iii) Electrons and/or holes

By varying their orientation, electric dipole moments generate a current in the external circuit. The current obtained immediately after the application of a step function voltage is known to decay with time, following the law  $I \propto t^{-n}$  where  $n \approx 1$  (Wintle 1974, Fischer and Rohl 1976, Adamec and Calderwood 1978, Vanderschueren and Linkens 1978, Das-Gupta et al (1980)). In general it is commonly accepted that due to the different configurations macromolecules may have, it is likely that rotation of the dipoles does not proceed in the same environment and therefore does not require the same energy. Different rotational masses of the dipoles will make them move at different speeds. This has led to the commonly accepted view that dipoles have a distribution of relaxation times (Daniel 1967, McCrum et al 1967).

An ionic current is always associated with the transport of matter, and should, in principle, be recognised by this property. The amount of transported substance is, however, so small that in most cases the ionic conductivity can neither be proven nor excluded. The theoretical treatment of ionic conductivity in polymers is very similar to that of

diffusion, the main difference is the superimposition of the potential field upon the potential barrier to migration as shown in Fig. 1.6.

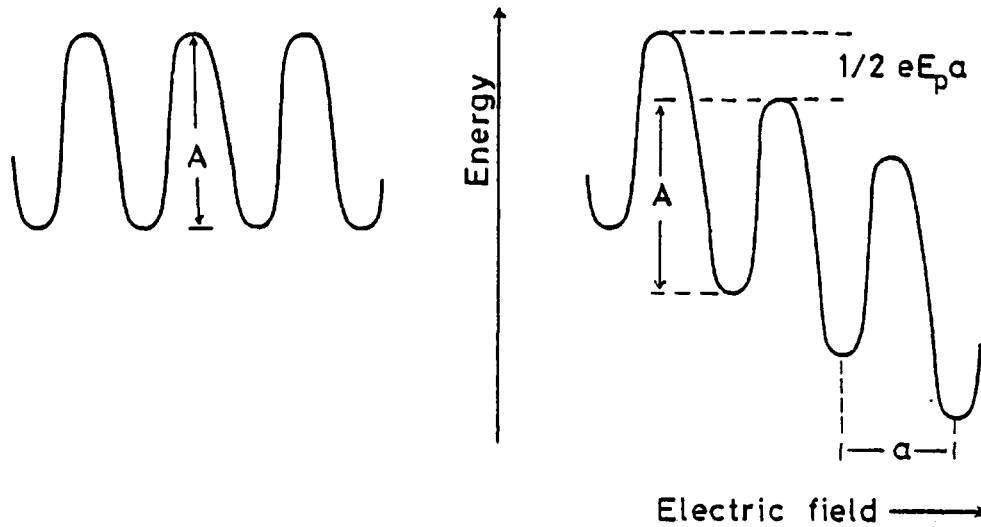


Fig. 1.6: Diagram showing the deformation on ionic potential-energy wells by an applied electric field

The current density  $J$  flowing through a specimen across which an electric field  $E_p$  is applied is given by (O'Dwyer 1973)

$$J \propto \sinh (e a E_p / 2kT) \quad (1.13)$$

where  $a$  is the jump distance and  $e$  is the magnitude of the charge on an electron.

Ionic conduction characteristics in polymers have been found by Amborski (1962), Seanor (1968), Kosaki et al (1971), Miyamoto et al (1973) and Yamashita et al (1979). The jump distance of the ions, as calculated from hyperbolic sine current-voltage relations, appears to be between  $15\text{\AA}$  at room temperature and  $60\text{\AA}$  at temperatures above  $T_g$ .

The mechanism of transport is explained qualitatively as follows. Configurations of polymer chains in amorphous regions provide various heights of potential barriers against migration of ions. Therefore, in the glassy state, where the motions of main chains are frozen, the migration of an ion may be eventually blocked by higher barriers. Interactions between neighbouring chains may constitute the potential barriers. In the glass transition region, segmental motion occurs and the high potential barriers which restricted the migration of ions may disappear or change their position temporarily or spatially. In this manner the numbers of ions which traverse the barrier increases. Fig. 1.7 illustrates this model of ion transport.

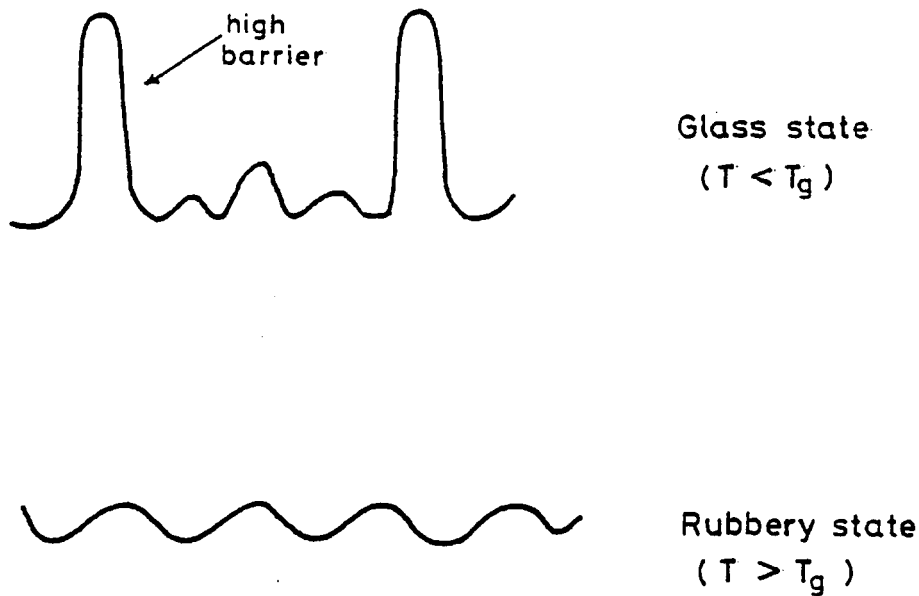


Fig. 1.7: Simplified model of potential barriers against ion transport (Kosaki et al 1971)

The main source of charge carriers is usually considered to be provided from impurities such as fragments of a polymerisation catalyst, absorbed water, and by degradation or dissociation products of the polymer itself.

### 1.5.2 Electronic States

It is well established that the molecules of organic materials are held together by weak, long range van der Waals forces. A typical separation between adjacent molecules under van der Waals forces is  $3 - 5 \text{ \AA}$  the overlapping of electron orbitals is small, the interaction energy between molecules being typically  $0.05 - 0.1 \text{ eV}$  (Duke and Schein 1980). The models developed for covalent and molecular materials have each assumed that long-range order extends through the system. It is because of the long-range order that the bands are relatively wide and the mobility relatively high. However, polymeric solids are by no means ordered, even though there may be short-range order within a given polymer chain.

The ground state highest in energy describes the most loosely bound electrons in the covalent bonds of the polymer chain often  $\pi$ - or  $\sigma$ -like in character. Separated from this, by a "gap" of  $5-10 \text{ eV}$ , lies the first excited state. Although these states resemble, in some way, the valence and conduction band in a semiconductor, there are important differences. The electrons in the molecular states of a polymer are generally strongly localised. The interaction between equivalent electronic states in the same chain and in neighbouring chains is weak, although not completely zero. Nevertheless, it is expected that, due to the weakness of this interaction, the levels widen into narrow bands. These molecular states are not expected to play any role in the dark conductivity in most of the amorphous polymers. Apart from these levels, there exist localised electronic states that are due to chemical and

structural inhomogeneities of the polymer (chemical changes in the chain, impurities, crosslinks, chain ends, folds, etc.) and they are separated from the molecular levels discussed above. Such centres give rise to trapping states, in which electrons and holes are immobilised to a certain degree. The density of these centres, their energetic position and occupancy are relevant to the conduction process. Unfortunately an exact knowledge of these parameters is not available.

The definition of the transport bands in amorphous materials has been based on the mobility of carriers (Seanor 1972, T.J. Lewis 1976, Mott 1979). This is illustrated in Fig. 1.8.

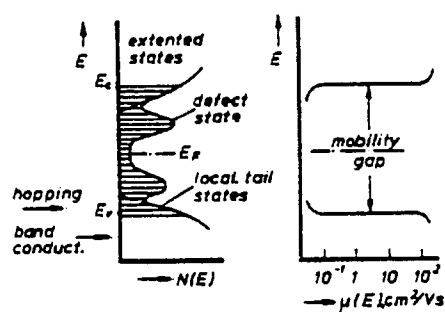


Fig. 1.8: Density of states  $N(E)$  and mobility gap.  $E_F$  is the Fermi level,  $E_C$  the critical energy for band motion, and  $E_g$  the forbidden energy gap (Seanor 1972)

The Fermi level  $E_F$  separates states able to accept an electron (acceptor,  $E > E_F$ ) from those that can deliver an electron (donors,  $E < E_F$ ). The localised states, if present in appropriate density and energetic distribution, play the main role in the conduction process, insofar as transitions of electrons between them are possible by tunneling and/or thermal activation. In general, band theory is



applicable for materials in which carrier mobilities are greater than  $1 \text{ cm}^2 \text{ v}^{-1} \text{ s}^{-1}$ , and a hopping or localised description of transport is applicable when carrier mobilities are less than  $1 \text{ cm}^2 \text{ v}^{-1} \text{ s}^{-1}$  (Wintle 1972).

The concept of molecular doping of organic polymers has proved to be a powerful means of confirming the transfer of electronic charge between localised states associated with the dispersed molecule. The charge carriers propagate through hopping among the chromophores in an intrinsically photoconductive polymeric solid like PVK and among the dopant molecules in the molecular doped polymers. The basic properties of transport in disordered organic solids are best illustrated using triphenylamine (TPA) molecularly dispersed in polycarbonate. Transport studies have been performed using the well known time-of-flight technique (Pfister 1977). Free carriers were generated by a 5 nS laser pulse of 3371<sup>0</sup>A wavelength which is exclusively and strongly absorbed by the dopant molecule. Thus the transient photoconductivity is induced by a transient photo-oxidation of the molecules. Fig.1.9 shows the hole drift mobility for various dopant concentrations as a function of temperature in the form of an Arrhenius plot  $\log \mu$  vs.  $1/T$ . It can be seen that the hole mobility is thermally activated with an activation energy  $A$  that increases with decreasing TPA concentrations. The strong dependence of the hole mobility on TPA concentration indicates that charge transport occurs by a hopping process. In this case the mobility is proportional to the overlap integral of the wavefunctions that localise the hole carrier on neighbouring dopant molecules.

The hopping mechanism can be visualised as either an oxidation-reduction or as a donor-acceptor process. In the case of hole transport for example, as a result of the photogeneration process some dopant

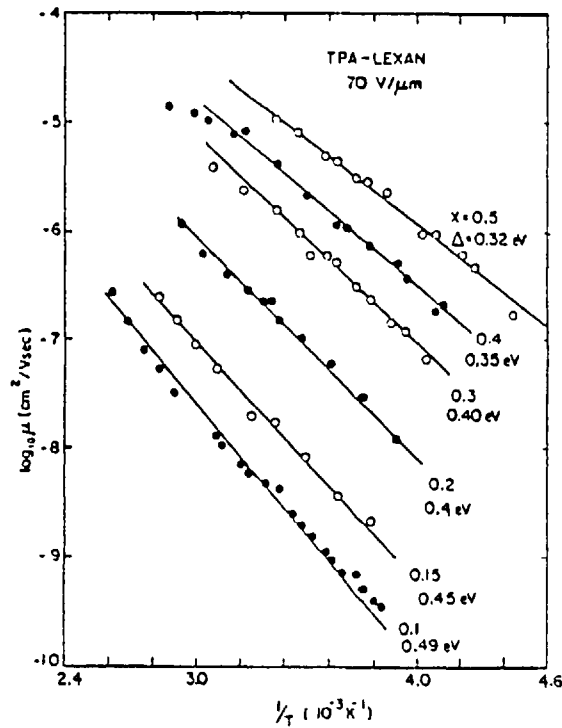


Fig. 1.9: Temperature dependence of the hole mobility at  $E = 70 \text{ V}/\mu\text{m}$  for various TPA concentrations. The activation energies and the weight radius  $X$  of TPA to Lexan are listed (Pfister 1977)

molecules are positively charged (radical cations). Under the influence of the applied electric field neutral molecules will repetitively transfer electrons to their neighbouring cations. The macroscopic manifestation of this microscope process is the motion of a positive charge across the bulk of the sample film. Therefore, for hole transport to occur one expects that the dopant molecule is donor-like in its neutral state. On the other hand for electron transport, where the electron hops from the radical anions to their neighbouring neutral molecules, the dopant molecules are acceptor-like. Fig. 1.10 illustrates those mechanisms.

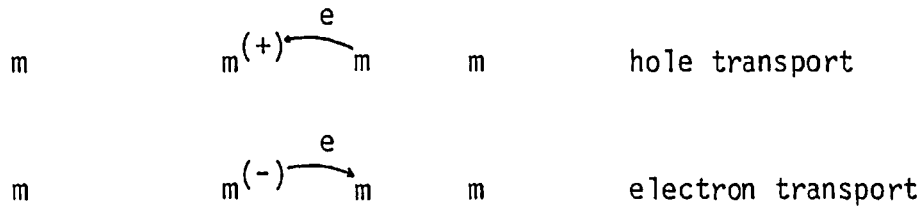


Fig. 1.10: Charge transport in doped polymer systems visualised as donor-acceptor or oxidation-reduction process (Mort 1980)

### 1.5.3 Experimental Techniques to Investigate Electrical Processes in Polymers

In this section the most used experimental methods to study electrical properties of polymers are briefly reviewed. Some experimental results are also given.

#### 1.5.3.1 Decay Methods

A thin polymer sample is charged by corona discharge. Subsequently the decay of this charge is measured, generally by a capacitive probe connected to an electrometer and measuring the surface potential. When surface conditions and discharge through the air can be neglected or eliminated experimentally, the total current density through the sample consists of three contributions: displacement current, convective current by injected charge carriers of density  $\rho_p$ , and current due to intrinsic conductivity,  $\sigma$

$$J = \epsilon\epsilon_0 \frac{\partial E(x,t)}{\partial t} + (\sigma + \mu\rho_p) E(x,t) = 0 \quad (1.14)$$

where the presence of a single type of excess charge of mobility  $\mu$  and density  $\rho_p$  have been assumed. This equation is valid if trapping is absent or if the carriers are subject to fast retrapping. Drift mobility

determinations in low-density polyethylene using this technique have been carried out by Perlman et al (1976) who assumed a region of charge density, constant in space but decreasing in time, penetrating into the sample. The resulting surface potential varies linearly in time as long as the charge front has not yet reached the opposite electrode. Fig. 1.11 shows the principle of the method.

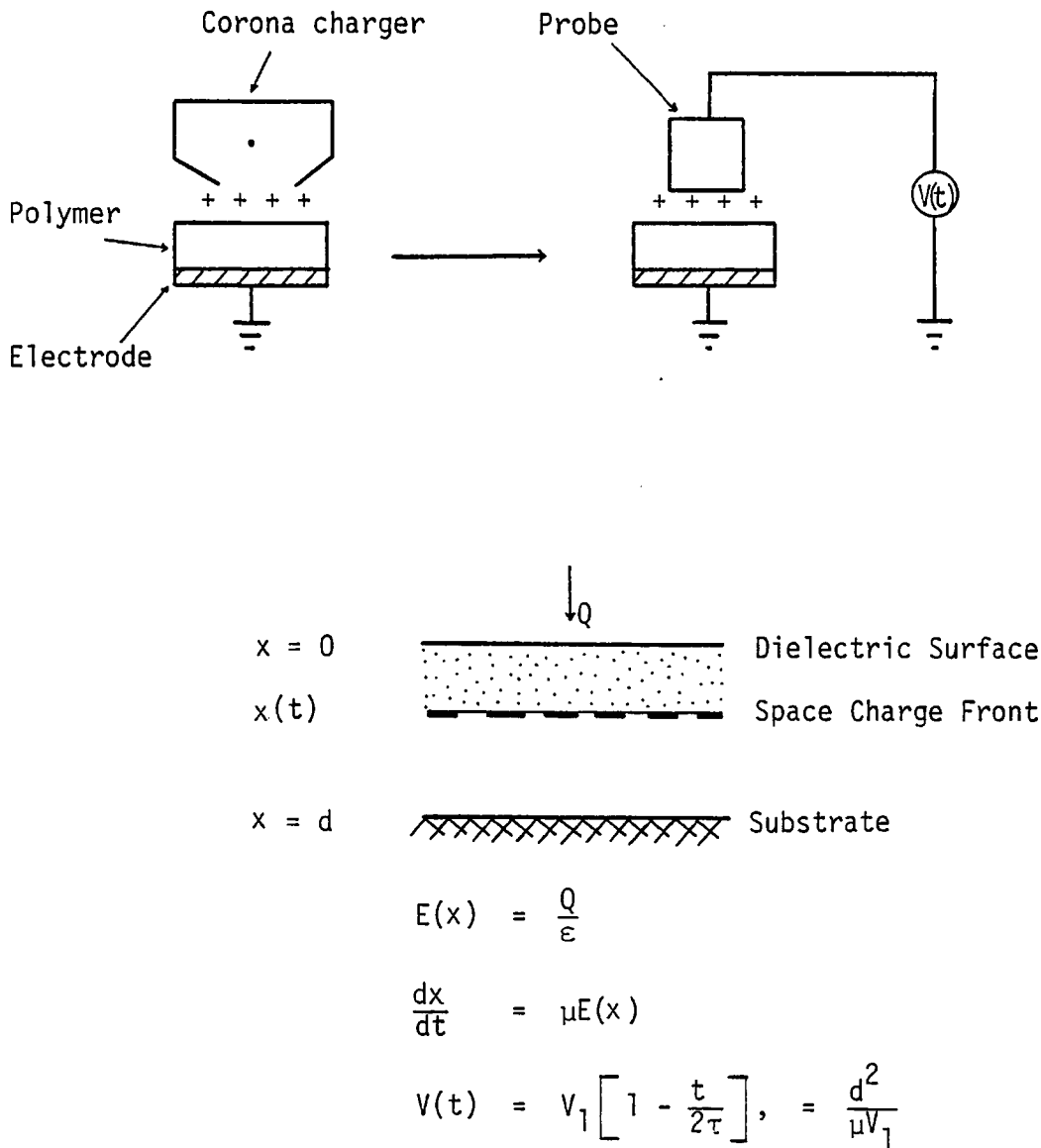


Fig.1.11(a):Flow of charge in an ideal trap-free dielectric in which charge is drifting under the influence of its own space-charge field. The field rises linearly through the space charge, reaching a value  $Q/\epsilon$  at the space-charge front.

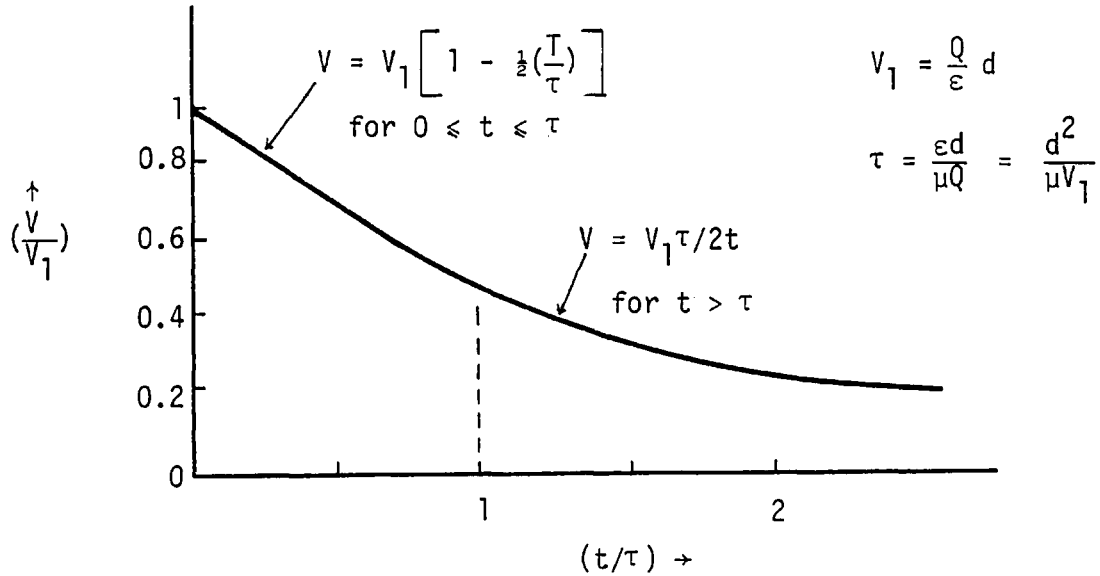


Fig.1.11(b): Decay of voltage from a pulse of charge in an ideal trap-free dielectric. In the time from zero to one transit time the voltage falls linearly from  $V_1$  to  $V_1/2$ .

### 1.5.3.2 Time-of-Flight Method

Transit time characteristics can be obtained from time-of-flight (TOF) experiments. In such an experiment the polymer, which is covered with two contacts, is subject to either a short pulse of an electron beam or by a flash of ultraviolet light (Reucroft and Ghosh 1973, Gross et al 1979, Hirsch and Tahmasbi 1980) generating a large concentration of carriers. Under a constant applied field the injected carrier sheet reaches the back electrode after a definite transit time. The arrival of the charge carriers at the counter electrode is determined by observing the current in the external circuit on an oscilloscope. Electrons and holes can be investigated separately by reversing the polarity of the field.

Fig. 1.12 illustrates the principle of the method.

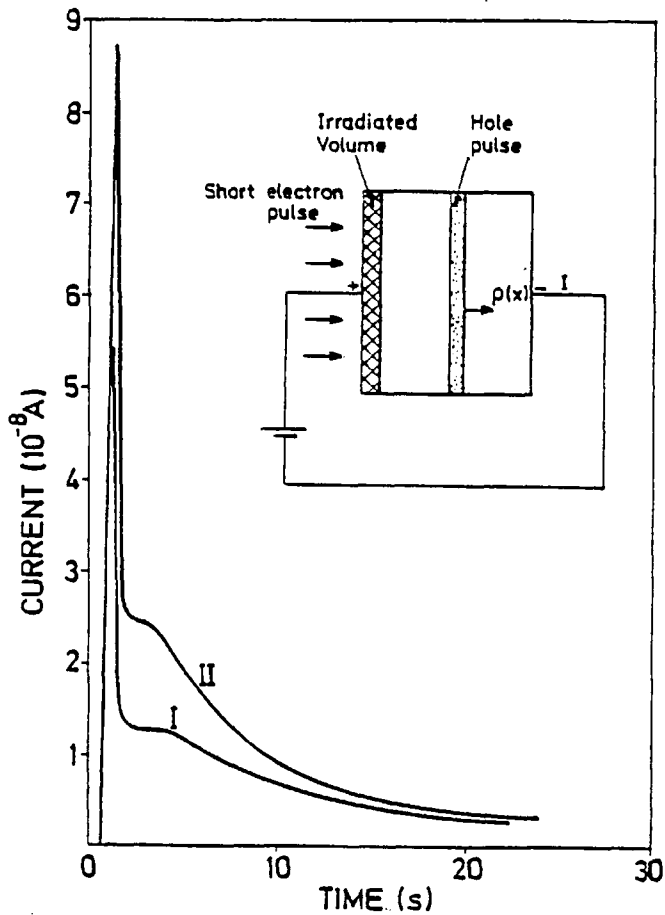


Fig. 1.12: Hole currents from 25  $\mu\text{m}$  Teflon FEP after irradiation with a 0.5 s,  $1.5 \cdot 10^{-8}$  A burst of 5 keV electrons (curve I) and 15 keV electrons (curve II). Applied voltage 600 volts, irradiated area  $20 \text{ cm}^2$ . Insert: Experimental set-up for transit and distribution measurements (Sessler 1978).

### 1.5.3.3 Contact Electrification

Contact between a metal and a polymer commonly results in the transference of charge amounting to about  $10^{11}$  electrons/ $\text{cm}^2$ . Static charge generation of polymer in contact with metals has shown that the charges transferred to the polymer depend on the work function of the

contacting materials (Davies 1969). From this finding, contact charging is interpreted as electron transfer through the interface between a metal and a polymer under contact. Since polymers pose extremely low conductivities the charge exchange should be restricted to the surface states. In this way the mechanism of electrification of polymers has been discussed assuming the existence of surface states (Lowell 1977, Lewis 1978, Murata 1979). Within the experimental scatter, which is often large, the charge density has been found to vary linearly with the work function. The energy states at the surfaces of a metal and a polymer are shown in an idealised schematic form in Fig. 1.13.

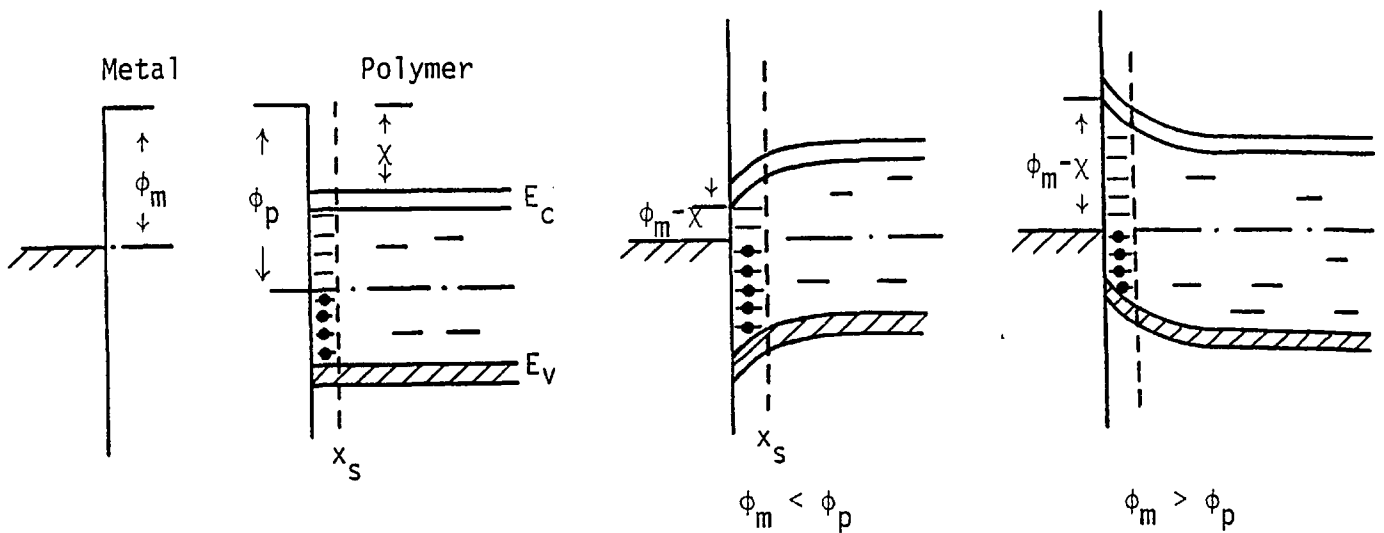


Fig. 1.13: Equilibrium conditions for a metal-polymer contact. The number of occupied surface states depends on the relative magnitudes of  $\phi_m$  and  $\phi_p$ .

The schematic diagram of an electrification apparatus is shown in Fig. 1.14.

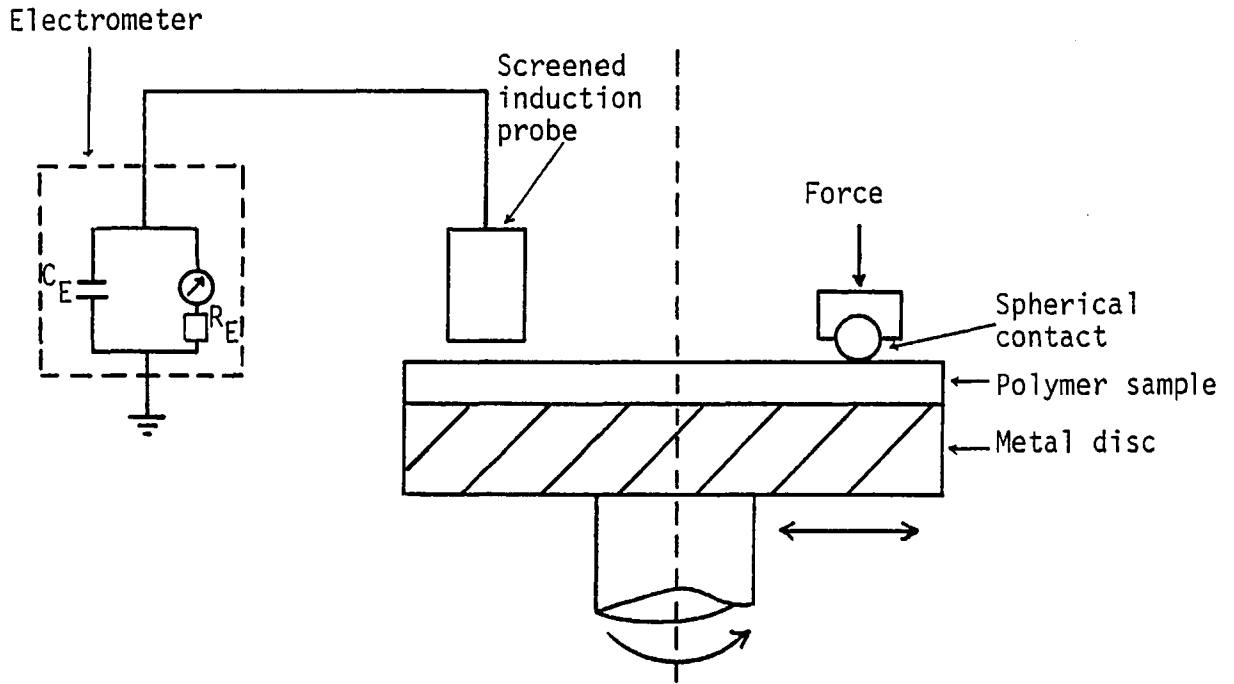


Fig. 1.14: Electrification apparatus

Tables I and II give the work functions of some polymers and order of magnitude of charge density observed on various polymers after contact with metals.

Polymer	$\phi$ (eV)
PVC	$4.85 \pm 0.20$
Polyimide	$4.36 \pm 0.06$
PTFE	$4.26 \pm 0.05$
Polycarbonate	$4.26 \pm 0.13$
PET	$4.25 \pm 0.10$
Polystyrene	$4.22 \pm 0.07$
Nylon 66	$4.08 \pm 0.06$

Table I: Work functions  $\phi$  for some polymers (Davies 1969)



Polymer	Charge density (Cm <sup>-2</sup> )	Remarks
Polyethylene	5 x 10 <sup>-6</sup> - 10 <sup>-4</sup> 5 x 10 <sup>-5</sup> 2 x 10 <sup>-5</sup>	In air, mercury contacts in air, sliding contact In vacuum
Polytetrafluoroethylene	3 x 10 <sup>-5</sup> 2 x 10 <sup>-3</sup>	In vacuum In vacuum, prolonged rolling contact
Nylon	10 <sup>-3</sup> 10 <sup>-3</sup>	In vacuum, mercury contact In vacuum, prolonged rolling contact
Polycarbonate	10 <sup>-3</sup>	In vacuum, prolonged rolling contact
Polyimide	3 x 10 <sup>-3</sup>	In vacuum, prolonged rolling contact

Table II: Charge densities observed in some polymers

#### 1.5.3.4 Direct Measurements of Current-Voltage Curves

Using high input impedance electrometers, very low currents can be measured in polymers. Thus, it is possible to obtain current-voltage curves realising, of course, the formidable experimental difficulties in establishing steady-state conditions only after very long times. However, at high enough temperatures the steady current  $I_0$  can be reached at reasonable times. Steady-state current through the polymer will be controlled either by electrode processes or by processes in the bulk. The behaviour of  $I_0$  is often analysed in terms of the following conduction mechanisms, whose relevant expressions will be presented here

(Simmons 1971, Jonscher and Hill 1975).

(a) Tunnelling

Very thin insulating films (<10 nm) are required to observe tunnelling of electrons directly from one electrode to the other. The tunnelling current can be expressed as follows.

$$\begin{array}{ll} \text{low } V & J \propto V \\ \text{high } V & J \propto V^m \exp(-A/V) \end{array} \quad (1.15)$$

where A and m are constants.

(b) Schottky emission

This conduction process is essentially a thermionic emission from a metal electrode into the conduction band of a dielectric over the potential barrier at the metal-dielectric interface, with the image force correction taken into account. The current density takes the form

$$J \propto \exp \left( \frac{\beta_S E^{\frac{1}{2}} - \phi_S}{kT} \right) \quad (1.16)$$

where  $\phi_S$  is the energy difference between the Fermi energy in the contact and the conduction band of the dielectric, E is the applied field and  $\beta_S$  the Schottky constant  $e^{3/2} (4\pi\epsilon\epsilon_0)^{-1/2}$ .

(c) Poole-Frenkel effect

This process is a bulk effect, caused by the field-lowering of the Coulombic barriers surrounding charge donor sites. Examination of the field surrounding an ionised centre under high field conditions yields an expression formally identical with eqn. (1.16) but with the Schottky constant replaced by the Poole-Frenkel constant  $\beta_{pf}$  which is numerically equal to twice the Schottky value.

(d) Poole's law

When the density of ionised centres is high the Coulombic potentials which give rise to the Poole-Frenkel effect overlap, and the peak in the potential barriers becomes pinned midway between the ionised centres, giving Poole's law characteristics. The current density for this mechanism is given by

$$J \propto \exp\left(-\frac{\phi_p}{kT}\right) \sinh\left(\frac{eES}{2kT}\right) \quad (1.17)$$

where  $\phi_p$  is the ionisation energy under zero field conditions and  $S$  is the average ionised centre separation.

(e) Space-charge limited flow

If the electrode is injecting and supplies carriers faster than they can be extracted from the polymer, the current is limited by the space charge that builds up. In the absence of traps the current is given by

$$I \propto \frac{V^2}{d^3} \quad (1.18)$$

where  $d$  is the thickness of the polymer films. In the presence of shallow traps the current takes the form

$$I \propto \theta \frac{V^2}{d^3} \quad (1.19)$$

where  $\theta$  is a trap-limiting parameter given by the ratio of free to trapped electrons.

(f) Hopping conduction

Conduction can occur by hopping of a carrier from one localised level to another. This type of conduction is characterised by the current

varying with T as

$$\log (IT^{-a}) \propto T^{-1/b} \quad (1.20)$$

where a and b are small numbers (usually  $a \sim b$ ,  $b \sim 3, 4$  or  $7$ ).

At very low temperatures

$$I \propto V^m \quad 4 < m < 20 \quad (1.21)$$

Some conduction mechanisms in polymers of the types mentioned above are given by Lilly and McDowell (1968), Lengyel (1966), Adamec and Calderwood (1975), Chybicki (1977) and Mehendru et al (1977).

Figure 1.15 presents the schematic diagram to obtain current-voltage characteristics.

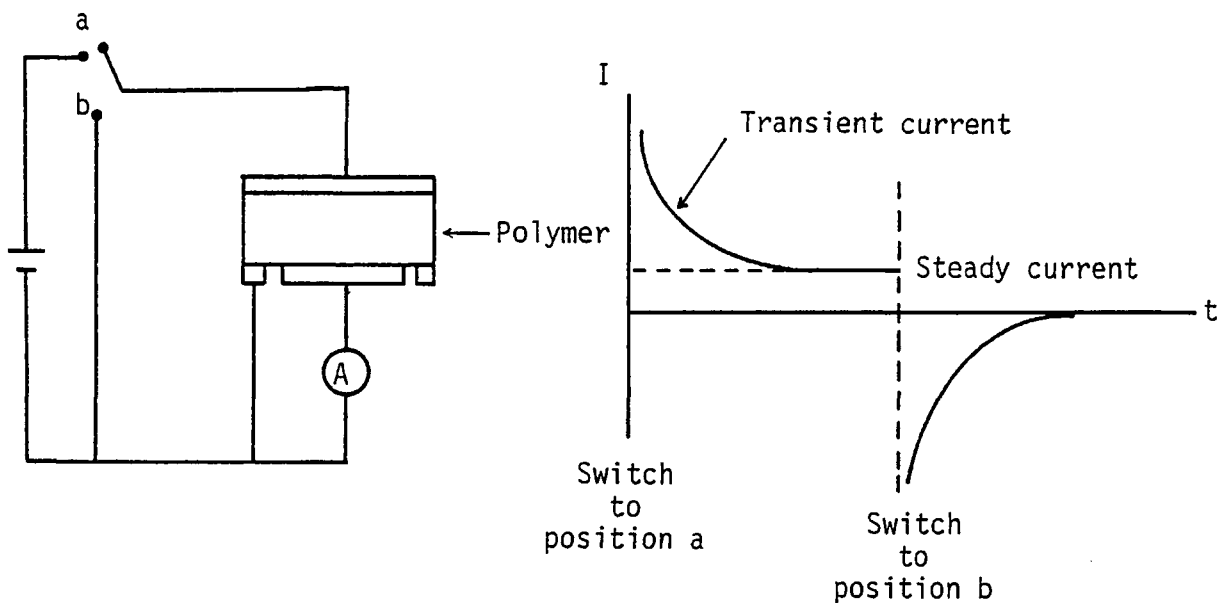


Fig. 1.15:

### 1.5.3.5 Thermally Stimulated Discharge

The thermally stimulated discharge (TSD) technique has proved to be a very suitable method to investigate (i) traps, (ii) space charges and (iii) dipolar processes in polymer electrets (van Turnhout 1975, Sessler 1977, Ito and Nakakita 1980, Mizutani et al 1980). The principal concern of TSD research is to study the charge decay by heating the polymer electret at a constant rate. The decay processes are thus investigated as a function of temperature instead of time. Such a technique can be operated under open circuit or short circuit conditions as shown in Fig. 1.16. This technique will be explained in more detail in Chapter II.

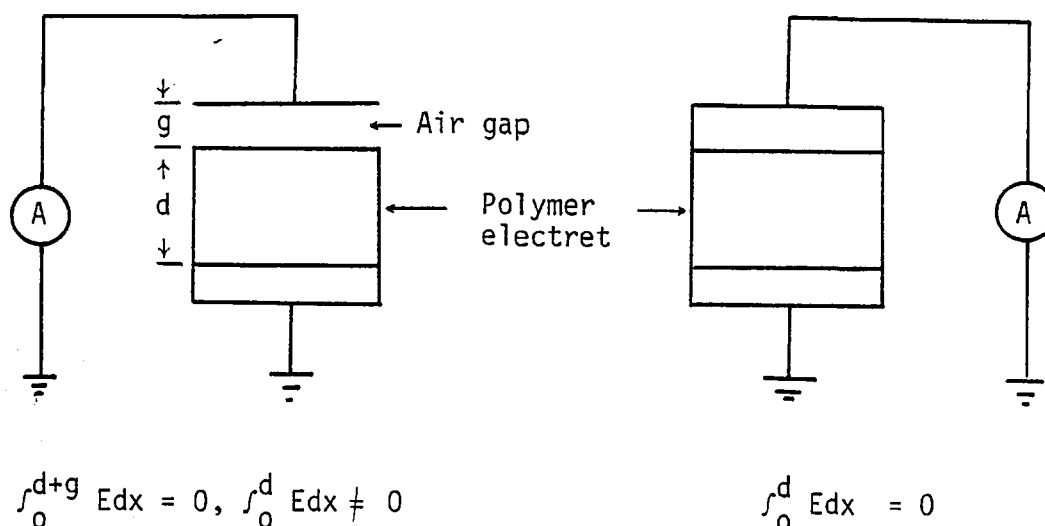


Fig. 1.16:

Some experimental data on trap density and energies in polymers is presented in Table III (Lowell and Rose-Innes 1980).

Polymer*	Technique	Trap density ( $m^{-3}$ )	Trap energy (eV below cond. band)
PE	TSD	$10^{22}$	
PC	UV excitation		band 0.5-1
PET	TSD	$10^{22}$	0.55-0.85 discrete
PVF, PS, PTFE, PVC	TSD	$10^{21}$ - $10^{22}$	1-2 discrete

Table III:

Experimental values for mobilities in some polymers are shown in Table IV.

Polymer*	Carrier type	Temperature (k)	Mobility ( $m^2/Vs$ )	Activation energy A (eV)	Method	Reference
PKV	p	295	$1 \times 10^{-10}$		TOF, light	Gill 1972
PC		358	$1.9 \times 10^{-16}$	0.73	decay, contact charging	Kiess and Rehwald 1980
PE		295	$4.3 \times 10^{-14}$		decay, Corona charging	Perlman et al 1976
PS	p	293	$1.3 \times 10^{-10}$	0.2	TOF, electron beam	Martin and Hirsch 1972
FEP	p	295	$1 \times 10^{-13}$		TOF, electron beam	Gross et al 1979
Nylon 66		295	$1.4 \times 10^{-11}$		decay, contact charging	Elsdon and Mitchell 1976

Table IV

\*Abbreviations: PE = Polyethylene; PC = Polycarbonate; PET = Polyethylene-terephthalate; PVF = Polyvinylfluoride; PTFE = Polytetrafluoroethylene; PVC = Polyvinylchloride; PVK = Polyvinylcarbazole.

## 1.6 ELECTRETS

An electret is a piece of dielectric material having a frozen-in, relatively long-lived (compared with the observation time), non-equilibrium charge.

Heaviside (1892) was apparently the first to speculate about using permanent polarisation to make the electrical counterpart of a magnet. Eguchi (1925) was the first person to experiment with electrets. He took a slab of Carnuba wax, heated it up until it melted, applied a strong electric field to polarise it, and cooled it down before switching the field off again. He found that samples prepared in this way exhibited a strong negative charge on the face which had been in contact with the positive anode, and vice versa. This initial charge he found to decay within a few days, followed by the building up of charges of opposite sign. This typical but rather surprising behaviour was explained by Gross (1949) as an interplay between surface heterocharges, due to volume polarisation, of opposite sign to the potential of the adjacent electrode during polarisation, and homocharges, due to the presence of free charges of the same sign as the potential of the adjacent electrode. The origin of the homocharges was explained in the following way. As the volume polarisation increases at the beginning of the poling the field in the gap between the dielectric and an electrode increases until discharges occur across the air gap, depositing ions of the same sign as the electrode material. At the end of the forming period a mixture of hetero- and homocharges will then be present at the dielectric surfaces. Any experimental detector of the surface charge density will give the algebraic sum (or net) value. When the forming field is removed, the voltage source is disconnected and the electrodes short circuited. At this moment the heterocharge prevails over the homocharge. However the

decrease in the internal polarisation, which even at low temperatures always follows the removal of the polarising field, reduces the amount of heterocharge. The net surface charge therefore also decreases; it becomes zero when the heterocharge just balances the homocharge and subsequently increases in the opposite direction because now the homocharge predominates. A steady-state is finally reached where the electret has a net homocharge. This is shown schematically in Fig. 1.17.

The heterocharge is a uniform volume polarisation and can be produced by dipole orientation and/or migration of ions over microscopic distances with trapping. The homocharge is a surface charge (non-uniform volume polarisation) and can be produced by space charge build-up associated with migration of ions over macroscopic distances and/or charge injection from the electrodes.

While the classical electrets were made of thick plates of Carnuba wax or similar substances, present electret research deals with thin film polymers such as polyfluorethylene propylene (FEP), polytetrafluoroethylene (PTFE) and polyvinylidene fluoride (PVDF) (Sessler and West 1975, Murayama et al 1976).

Typical electrets in present use are 10-50  $\mu\text{m}$  films of few  $\text{cm}^2$  area, often coated on one or both surfaces with evaporated metal layers. The materials are polarised to charge densities of  $10^{-8} - 10^{-6} \text{ C cm}^2$ , the charges trapped being real charges in Teflon and predominantly dipolar in PVDF.



### 1.6.1 Applications

The electret effect finds application in a wide variety of fields. The electret microphone was successfully developed by Sessler and West (1966). It was placed into commercial production in 1970 by Sony (Japan). The field of electrophotography uses charge-storage effects in one way or another (Schaffer 1975). The demand for high efficiency filters, which remove submicron particles from polluted gases, has led to the development of electret filters consisting of charged polymer fibres (van Turnhout 1975). PVDF is a semicrystalline polymer which can be made piezo- and pyroelectric by the electret effect (Wada and Hayakawa 1976). Such electrets have found widespread use in, for example, headphones, push buttons and infrared detectors.

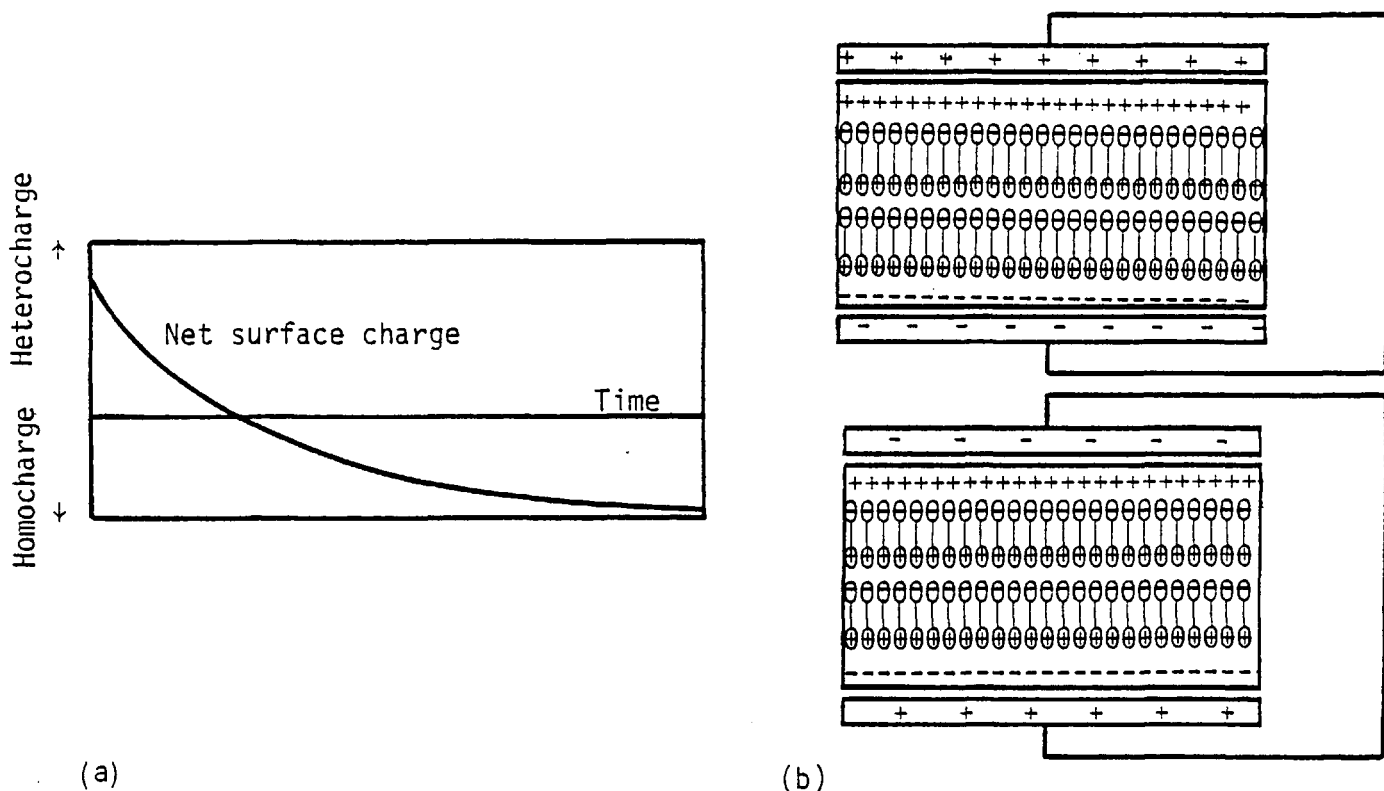


Fig. 1.17: (a) Polarity reversal: Net surface charge of an electret as a function of time. (At zero time the electrodes were short-circuited.) (b) Polarity reversal: Charge distribution for electret with dipole polarisation before (top) and after (bottom) reversal. (Gross 1971)

Polymers with metallic-like properties are being looked at by many investigators. For a material to be conducting there must be a supply of charge carriers, electrons or "holes", and an easy high mobility path for them to follow through the material. Thus one class of polymeric conductors consists of conjugated chains, with alternating single and double bonds, such that the  $\pi$ -bonding orbitals overlap to form a path along the chain. Sulphur nitride  $(-S=N-)_x$  and polyacetylene  $(-CH=CH-)_x$  are examples of intrinsically metallic synthetic polymers. This observation that polymers can be made to exhibit metallic or even superconducting properties has encouraged the belief that they may eventually challenge the more classical materials in certain applications. For instance, conducting polymers could function as antistatic coatings,  $(SN)_x$  and  $(CH)_x$  can form Schottky barriers and act as solar cells, and undoped  $(CH)_x$  has been used as the photoelectrode in a photochemical (photogalvanic) cell (Street and Clarke 1981). However, conducting polymers are probably best considered not as competitors for the classical metals or semiconductors, but as opportunities for new applications. This is so because the attractive polymer properties such as melt and solution processibilities, low density, and plasticity or elasticity.

## 1.7 AIMS OF THE PRESENT STUDY AND LAYOUT OF THE THESIS

The aims of the present investigation are to provide a short review of the electrical properties of polymeric materials and to study the electret properties of some polymers by thermally stimulated discharge methods (TSD). This technique has a great significance in electret research since it is capable of resolving processes characterised by very different activation energies or pre-exponential factors in a single, relatively short experiment. The TSD method, applied in a variety of ways, has provided extensive information on dipolar and trapped-charge in polymers. The layout of the thesis is as follows. After an introduction Chapter II deals with the theoretical aspect of TSD currents. Dipolar relaxation processes are discussed and analysed in terms of either a single or a distribution of relaxation times. TSD due to space charge polarisations are also discussed. Modern theories which do not use the concept of distribution of relaxation times are also presented.

In Chapter III, description of the experimental apparatus and measuring procedures will be given, together with the system used to prepare the polymer films. Differential thermal analysis and infra-red spectroscopy is also presented.

Chapters IV and V deal with the study of nylon and polyvinylbutyral films respectively. In Chapter VI, main conclusions reached during the present study will be given together with some suggestions for future work.

## CHAPTER II

### THERMALLY STIMULATED DEPolarISATION

#### 2.0 INTRODUCTION

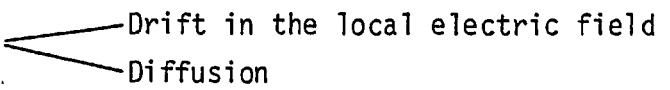
In the following sections the electret effect is discussed together with the method of electret formation. Then the polarisation acquired by the material is analysed by thermally stimulated depolarisation (TSD) methods, which are in general useful to investigate the electrical properties of high-resistivity solids. TSD is in particular very suitable for polymeric solids by using thermal relaxation effects and as such, it offers an attractive alternative to the conventional bridge methods or current-voltage-temperature measurements. The more general theories related to the main polarisation processes are outlined next, then the identification of the microscopic origin of a given current spectrum is presented. The concept of distribution of relaxation times is introduced to interpret the TSD current spectra. Modern theories which do not involve the concept of distribution function are also discussed.

#### 2.1 MECHANISMS CONTRIBUTING TO TSD

Several processes contribute to the discharge mechanism in electrets, the driving force being the restoration of charge neutrality. The total charge of an electret is usually composed of oriented dipoles and space charges, which cause deviation from local charge neutrality. Before the electret is formed the neutral polymer already contains free charges. At high temperatures these carriers are uniformly generated throughout the entire specimen by dissociation of neutral entities, resulting in the conductivity of the material, which can be of either an

ionic or electronic nature. Therefore in addition to the excess charges there must be free equilibrium charges in the electret. These do not contribute to the net charge, but are responsible for the ohmic conductivity.

The decay of the net charge of an electret during TSD will result from

- (i) Dipole reorientation
- (ii) Excess-charge motion 
  - Drift in the local electric field
  - Diffusion
- (iii) Local ohmic conduction

The disorientation of dipoles involves the rotation of a coupled pair of positive and negative charges, and requires a certain energy. The space charges are non-uniformly stored, and often reside near the electrodes. During heating they will be mobilised and neutralised either at the electrodes or in the sample by recombination with charges of opposite sign. The forces driving the charges are their drift in the local electric field, and diffusion, which tends to remove concentration gradients. The local ohmic conduction neutralises part of the excess charge by supplying opposed equilibrium charges and does not contribute to the external current at all during TSD.

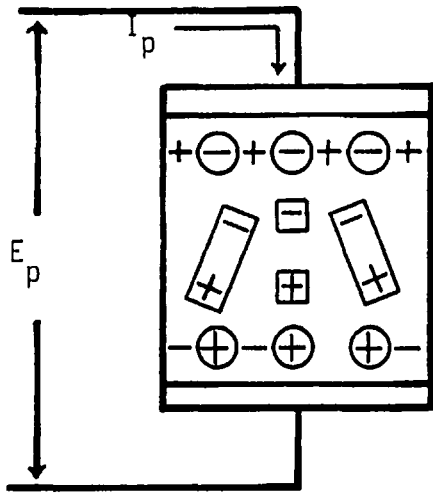
For heterogeneous polymers consisting of different components or phases, the decay of the polarisation arises from interfacial charges which were accumulated near the interfaces during the formation of the electret (Maxwell-Wagner effect).

Fig. 2.1 shows in a schematic form how the neutralisation of the polarising species could give rise to an external current during the discharge of the electret. The polarisation due to dipole orientation is shown by  $\boxed{+ -}$ , the charge due to the microscopic displacement of ions with trapping by  $\boxed{+}$   $\boxed{-}$ , the space charge build-up by the

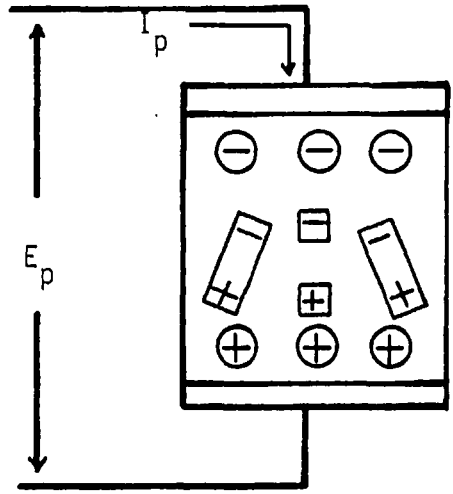
migration of ions over macroscopic distances by  $\oplus$   $\ominus$  and the space charge injected from the electrodes by  $+$   $-$  . The former two kinds give a uniform volume polarisation, which is a heterocharge, the third gives a non-uniform heterocharge, and the fourth a non-uniform homocharge.

With increasing temperature disorientation of dipoles occurs first (Stage c), followed by neutralisation of ions by conduction currents in opposite directions (stage d). The direction of these depolarisation currents is opposite to that of the polarisation current. Next, the space charge due to the free ions disappears by the recombination with counter ions as shown in stage e. The direction of the current is also opposite to that of the polarisation.

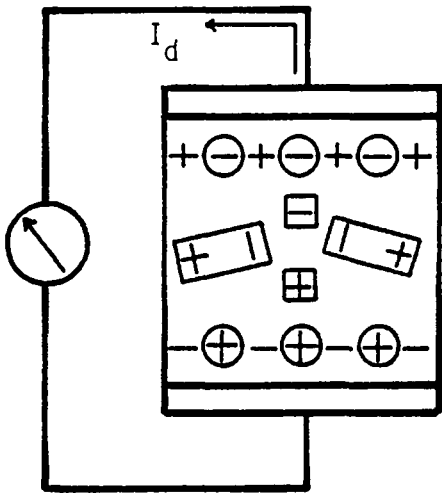
If the polarising field is sufficiently high the homocharge is produced by the injection of charge carriers from the electrodes (stage a). The homocharge remains stable until all the heterocharge disappears. When the electrodes are fully contacted with both surfaces of the specimen the homocharge should be drawn towards the nearest electrode by the electrical image force. The direction of the depolarisation current should then be the same as that of the decay of the heterocharge. However, if there is an air gap between the electrode and the surface of the specimen (stage f), the magnitude of the image force becomes negligibly small and the homocharge may diffuse into the specimen due to the internal field. A displacement current is generated by image charges released from the non-contacting electrode.



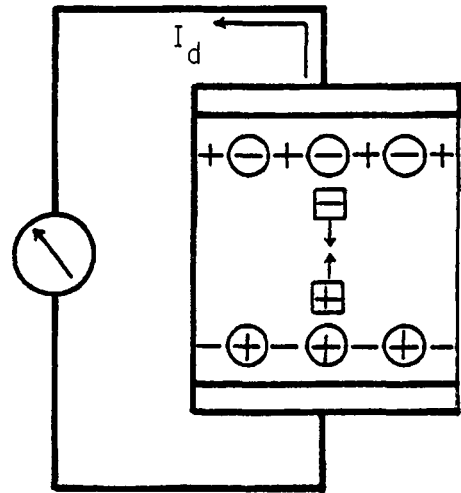
(a)



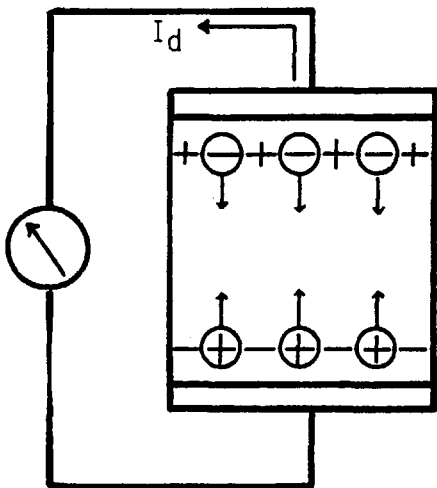
(b)



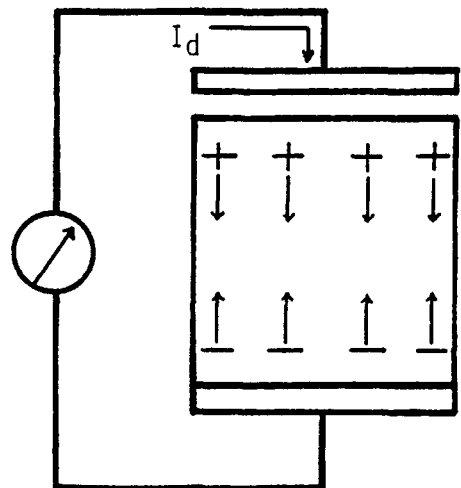
(c)



(d)



(e)



(f)

Fig. 2.1: Schematic diagram showing the different polarising species responsible for the electret effect

## 2.2 THERMALLY STIMULATED DISCHARGE TECHNIQUE

The thermally stimulated discharge (TSD) technique constitutes a basic tool for the identification and evaluation of dipole reorientation processes, trapping of charges by structural defects and impurity centres, and a build-up of charges near heterogeneities such as the amorphous-crystalline interfaces in semicrystalline polymers (van Turnhout 1975). The TSD technique consists of the following steps. The polymer is provided with vacuum evaporated electrodes on both faces and the structure heated to some polarising temperature,  $T_p$ . At this stage the sample is polarised by applying a polarising field,  $E_p$ , for an extended period. All polarisation processes which are active at or below the temperature  $T_p$ , and within the time the field has been on, will contribute to an overall polarisation. If the field were now removed at temperature  $T_p$ , the polarisation could be discharged. However, in TSD the temperature is reduced to some value  $T_0 < T_p$  with the field still on. Any polarisation process which is non-active at  $T_0$  but active between  $T_0$  and  $T_p$  has thereby been frozen in at  $T \leq T_0$ , even when the field is removed as in the TSD technique. The material so produced with its residual polarisation in the absence of an external electric field, is termed a thermoelectret.

Next, the polarised material is caused to discharge by thermal stimulation at a constant heating rate. This procedure enhances the mobility of the frozen-in dipoles and charges, so that the decay experiment is done within a reasonable time. A discharge current becomes measurable in the external circuit which first increases with increasing temperature, and then decays when the supply of charges is depleted. A current peak thus will be observed at a temperature where dipolar disorientation, ionic migration or carrier released from traps is activated. The principle of the method is outlined in Fig. 2.2.



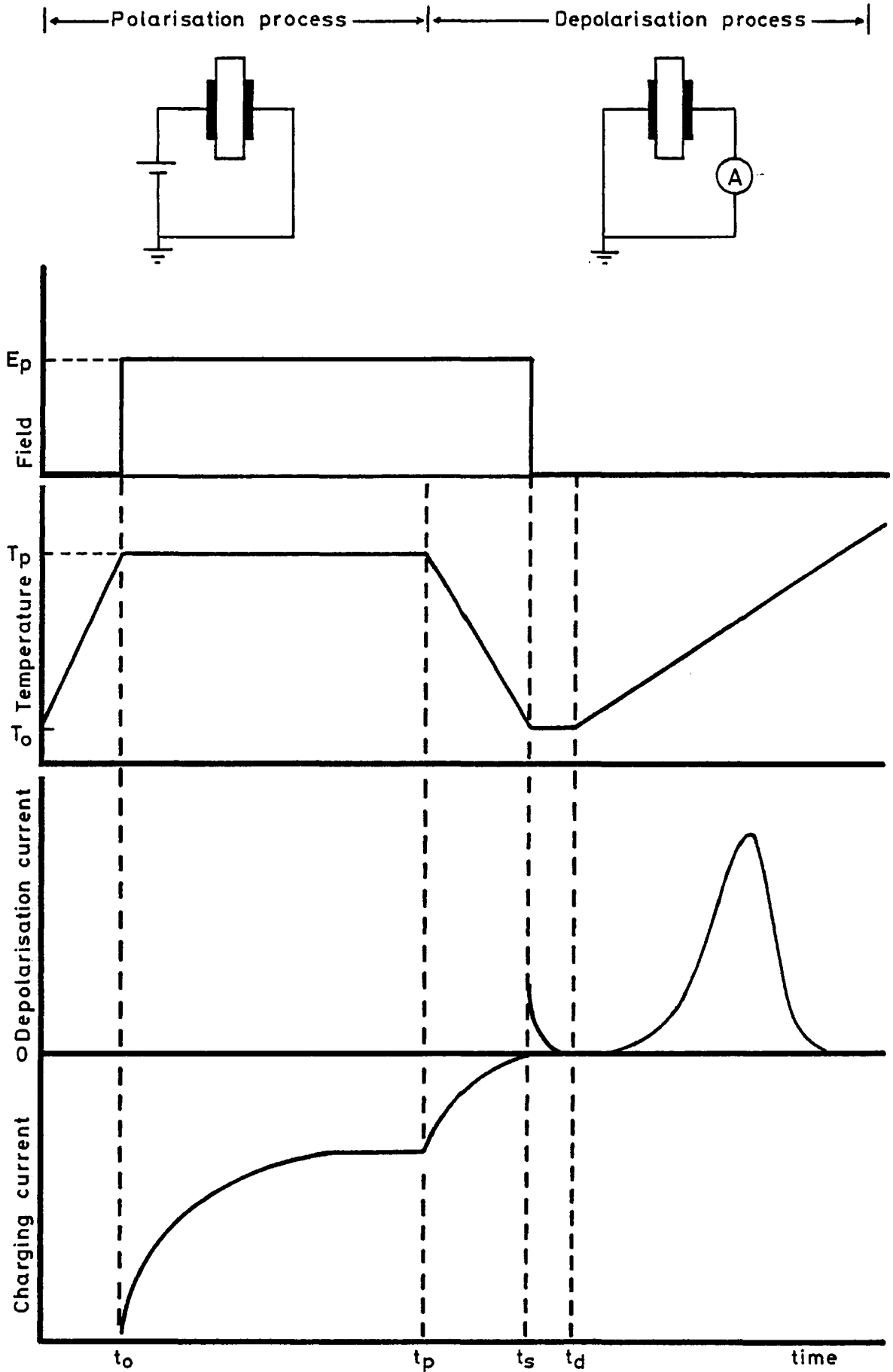


Fig. 2.2: Thermoelectret formation and principle of the TSD method

The amount of charge released during the discharge of an electret can be obtained by integration of the area under a TSD curve

$$Q_r = \int_0^{\infty} I[t, T(t)] dt$$

The frozen-in or stored charge contained in the electret after formation is  $Q_s$ . This charge is defined as the time integral over the transient component of the charging current. According to Gross (1968) the released charge is equal to the stored charge only in the case of charge invariance. The released charge is a constant which depends only on the initial state of the system at the moment of short circuit, not on subsequent heating rate and temperature.

### 2.3 DIPOLAR THEORY OF BUCCI AND FIESCHI

Bucci and Fieschi (1964) have proposed an ionic thermoconductivity method for the study of defects in ionic crystals. Because of its resolving power it is particularly well suited to the study of molecular motion in complex materials such as polymers (Perlman 1971, Hedvig 1977). The theory of Bucci and Fieschi is summarised here.

Let a static polarising field  $E_p$  be applied to a polar polymer, in which interactions between dipoles are neglected, at time  $t = t_0$  and at the polarising temperature  $T_p$ . The electric field tends to align the dipoles so that if there are  $N$  dipoles per  $m^3$  of moment  $\mu$ , the total dipole moment per unit volume in thermal equilibrium is

$$P_e = N\mu \langle \cos \theta \rangle = N\mu L\left(\frac{\mu E_p}{kT_p}\right) \quad (2.1)$$

where  $\theta$  is the angle that the dipoles make with the applied field,  $L$  the 'Langevin function' and  $k$  Boltzmann's constant. For

$$\mu E_p / kT_p \ll 1, L(\mu E_p / kT_p) \approx \mu E_p / 3kT_p.$$

The build-up of polarisation  $P$  during the formation of the electret is given by an exponential function of time

$$P(t) = P_e [1 - \exp(-wt)] \quad (2.2)$$

where  $w$  is the dipole relaxation frequency.

In TSD the polarised sample at temperature  $T_0$  is short-circuited through an electrometer. Heating at constant rate  $r(T = rt + T_0)$  then results in depolarisation by disorientation of dipoles.

The corresponding depolarisation current density can be written as

$$J(t) = - \frac{dP(t)}{dt} = wP(t) \quad (2.3)$$

The polarisation  $P(t)$  follows from eqn. (2.3) after integration

$$P(t) = P(T_0) \exp\left[- \int_0^t w dt\right] \quad (2.4)$$

where  $P(T_0)$  is the initially frozen-in polarisation.

The relaxation frequency  $w$  is generally found to obey an Arrhenius equation

$$w(T) = w_0 \exp(-A/kT) \quad (2.5)$$

where  $w_0$  is the natural relaxation frequency and  $A$  is the activation energy to disorient a dipole. The relaxation time is given by the inverse of Eqn. (2.5), that is,

$$\tau(T) = \frac{1}{w(T)} = \tau_0 \exp(A/kT) \quad (2.6)$$

where  $\tau_0$  is the relaxation time at high temperatures.

Postulating that (i) Eqn. (2.4) also holds for varying temperature and (ii) the initial frozen-in polarisation  $P(T_0)$ , before the TSD experiment is started, is equal to the equilibrium polarisation reached at the polarising temperature  $T_p$ , the thermally stimulated depolarisation current density  $J(T)$  during a TSD experiment is

$$J(T) = \frac{w_0 N \mu^2 E_p}{3kT_p} \exp(-A/kT) \exp\left[-\frac{w_0}{r} \int_{T_0}^T \exp(-A/kT') dT'\right] \quad (2.7)$$

Eqn. (2.7) is similar to thermoluminescence or thermally stimulated conductivity processes obeying first order kinetics. It represents an asymmetrical 'glow curve', the amplitude of which is a function of the previously applied field.

The temperature at which the maximum of the peak occurs,  $T_m$ , is connected with the relaxation frequency at  $T_m$  and its activation energy  $A$  by the following equation

$$T_m = \left[ \frac{rA}{kw(T_m)} \right]^{\frac{1}{2}} \quad (2.8)$$

From Eqn. (2.8) it can be seen that  $T_m$  does not depend upon either the polarising field  $E_p$  nor the polarising temperature  $T_p$ , therefore it can be concluded that for any depolarisation process obeying first order kinetics,  $T_m$  will have a fixed value.

In the case where the frozen-in polarisation of the sample  $P(T_0)$ , before a TSD experiment is started, cannot be considered to be equal to the equilibrium polarisation at  $T_p$ , i.e.  $P(T_0) \neq P_e$ , the function  $H(T,t)$  which characterises the filling state of the polarised sample (Ong and van Turnhout 1973) has to be introduced, so that

$$P(T_0) = P_e H(T,t) \quad (2.9)$$

where

$$H(T,t) = \{1 - \exp[-w(T_p)t_p - 1/r \int_{T_p}^T w(T)dT]\} \exp[-w(T_0)(t_d - t_s)] \quad (2.10)$$

Here the last exponential accounts for the decay of polarisation during the storage period. The two contributions of the first exponential determine the degree of filling produced by the polarising field during the isothermal formation at  $T_p$  and during the cooling period from  $T_p$  to  $T_0$ . The increase in polarisation during the cooling phase can sometimes be quite large depending upon the cooling rate (Hedvig 1973).

#### 2.4 THERMALLY STIMULATED POLARISATION TECHNIQUE

As has been seen, to form the thermoelectret the sample is charged isothermally at a sufficiently high temperature before it is subjected to TSD. However the thermoelectret can be formed while being heated linearly (Pfister and Abkowitz 1974, McKeever and Hughes 1975, Vanderschueren et al 1980). This procedure is termed thermally stimulated polarisation (TSP) and has several advantages. For instance it reveals how the orientation of the dipoles is proceeding. Another advantage is that the optimum temperature for the poling is easily found, thus unnecessary overheating of the sample is eliminated. Also TSP current measurements reveal the temperature at which ohmic conduction becomes significant. Fig. 2.3 shows the principle of the method.

During the TSP experiment the polarisation current density is given by

$$J_p(t) = \frac{dP(t)}{dt} + \sigma(T) E_p \quad (2.11)$$

where  $\sigma(T)$  represents the ohmic conductivity of the polymer, which usually assumes an Arrhenius type of temperature dependence, i.e.

$\sigma(T) = \sigma_0 \exp(A_c/kT)$  where  $A_c$  is the activation energy for intrinsic

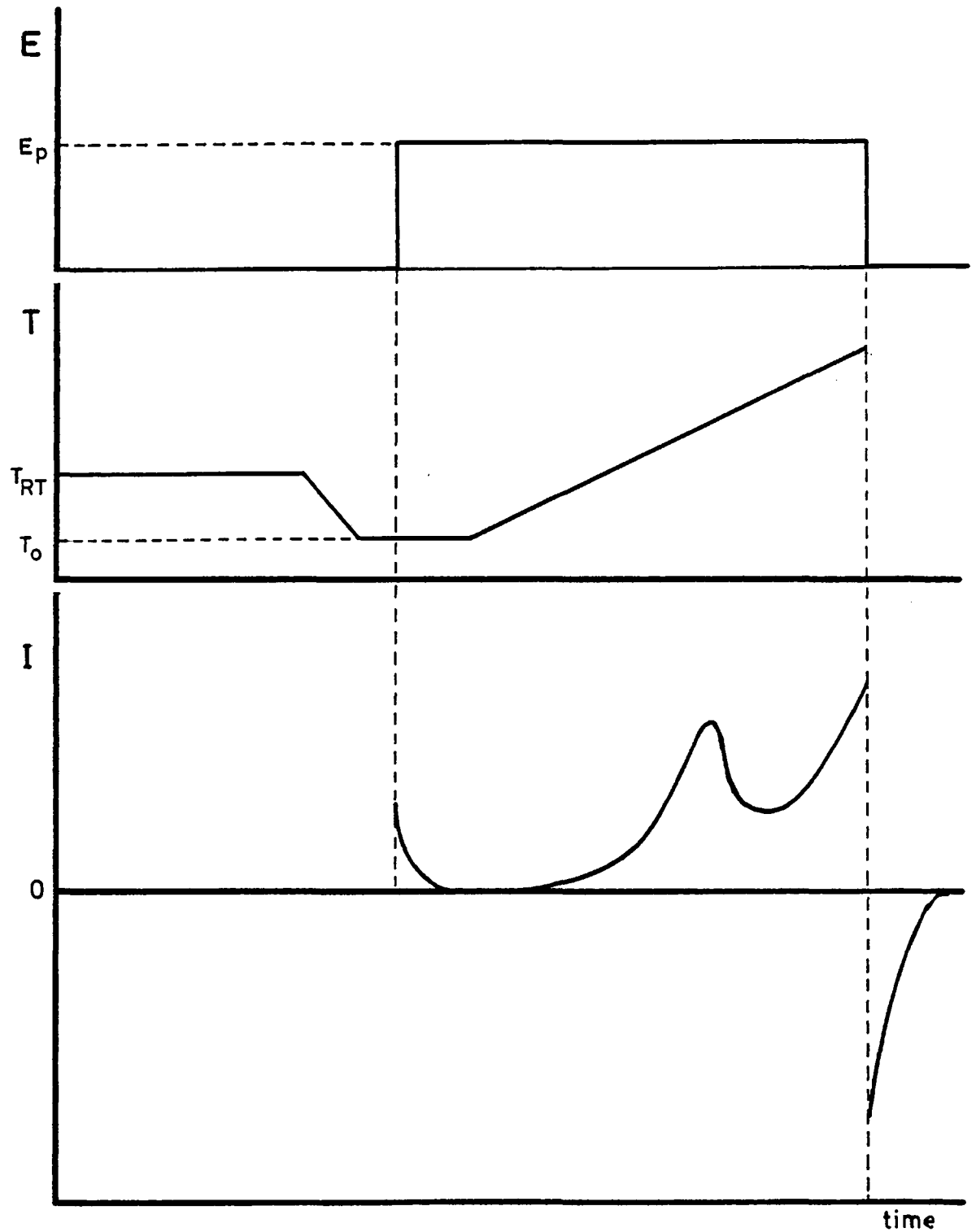


Fig. 2.3: Thermally stimulated polarisation method

conductivity.

Using Eqn. (2.2) and assuming that the temperature dependence of the saturation polarisation is negligible, the polarisation current density can be written as

$$J_p(T) = \frac{w_0 N \mu^2 E_p}{3kT} \exp \left[ - \left[ \frac{A}{kT} + w_0/r \int_{T_0}^T \exp(-A/kT') dT' \right] \right] + \sigma_0 E_p \exp(-A_c/kT) \quad (2.12)$$

As can be seen from Fig. 2.3 there are two contributions to the current density. The dipolar orientation contribution is a transient process which gives rise to a peak, whereas the conduction current, which comes from the motion of equilibrium charges, steadily increases with temperature.

## 2.5 THE EQUIVALENT FREQUENCY OF THE TSD MEASUREMENTS

The equivalent frequency of TSD measurements can be estimated by relating the heating rate  $r$  and the a.c. angular frequency  $w = 1/\tau$  via the equation that defines the maximum temperature of the TSD peak. The relation between TSD and a.c. loss data can be most easily understood when one considers a single Debye dipole relaxation, for which (Van Turnhout 1975)

$$\frac{\epsilon''(w, T)}{\epsilon_s - \epsilon_\infty} = \frac{w\tau(T)}{1 + w^2\tau^2(T)} \quad (2.13)$$

$$\frac{\tau(T) J(T)}{\epsilon_0(\epsilon_s - \epsilon_\infty) E_p} = \exp \left[ - \int_0^t dt/\tau(T) \right] \quad (2.14)$$

where  $\epsilon''$  is the dielectric loss factor and the other symbols have their usual meaning.

The conditions for the maxima in the  $\epsilon''$  and  $J$  curves are

$$w\tau(T_m) = 1 \quad (2.15)$$

and

$$d\tau(T_m)/dt = -1 \quad (2.16)$$

For a linear heating rate  $r$  and an Arrhenius type of  $T$ - $\tau$  dependence, Eqn. (2.16) can be written as

$$\left(\frac{Ar}{kT_m^2}\right) \tau(T_m) = 1 \quad (2.17)$$

For  $\epsilon''$  and  $J$  maxima to occur at the same temperature the TSD data must correspond to a.c. data at the equivalent frequency of

$$f_{eq} = \frac{1}{2\pi} \left(\frac{Ar}{kT_m^2}\right) \quad (2.18a)$$

Adopting typical values of the TSD parameters  $r$ ,  $A$  and  $T_m$ , Eqn. (2.18a) leads to  $f_{eq} \sim 10^{-4} - 10^{-1}$  Hz. These values lie well within the ultra-low frequency range.

In a similar way, for relaxations obeying a WLF equation (i.e. eqn. (1.1)) the equivalent frequency takes the form

$$f_{eq} = \frac{1}{2\pi} \frac{rC_1C_2}{(C_2 - T_m - T_g)^2} \quad (2.18b)$$

where  $C_1$  and  $C_2$  are the universal constants defined in section 1.4.2.2.



## 2.6 THERMALLY STIMULATED DISCHARGE OF HETEROGENEOUS SYSTEMS

One of the most important effects in commercial polymers is interfacial polarisation (Maxwell-Wagner effect) (Blythe 1980). Although normally associated with the physical dispersion of one phase in a second continuous plastic phase, there are many other situations in which it occurs. The phenomenon is due to the presence of two phases, one of much higher conductivity than the other. The amorphous phase will give rise to higher mobilities than the crystalline phase. If the amorphous phase contains a sufficiently large number of conducting species, interfacial polarisation results, i.e. charge carriers are trapped at phase boundaries. Alternatively, when the polymer contains many irregularly distributed traps with widely different depths, carriers might move in the direction of the field until they fall into deep traps from which they do not have enough energy to escape unless reactivated by a temperature increase. Both these interfacial polarisation effects constitute a volume effect. The M-W losses are only apparent for low measuring frequencies, usually below 1Hz. It seems, therefore, that the thermally stimulated depolarisation technique, which commonly works in the range of equivalent frequencies of  $10^{-1} - 10^{-4}$  Hz, could be used as a useful complementary tool for the dielectric study of such materials.

Fig. 2.4 illustrates the polarisation and the depolarisation of a heterogeneous polymer composed of two phases. During formation of the electret charges accumulate near the interfaces. These charges are frozen-in if the field is maintained during cooling. During TSD the charge stored will be neutralised by new carriers of opposite polarity that are transported to the interfaces by conduction currents in the opposite direction. This neutralisation process is a transient one, giving rise to a peak.

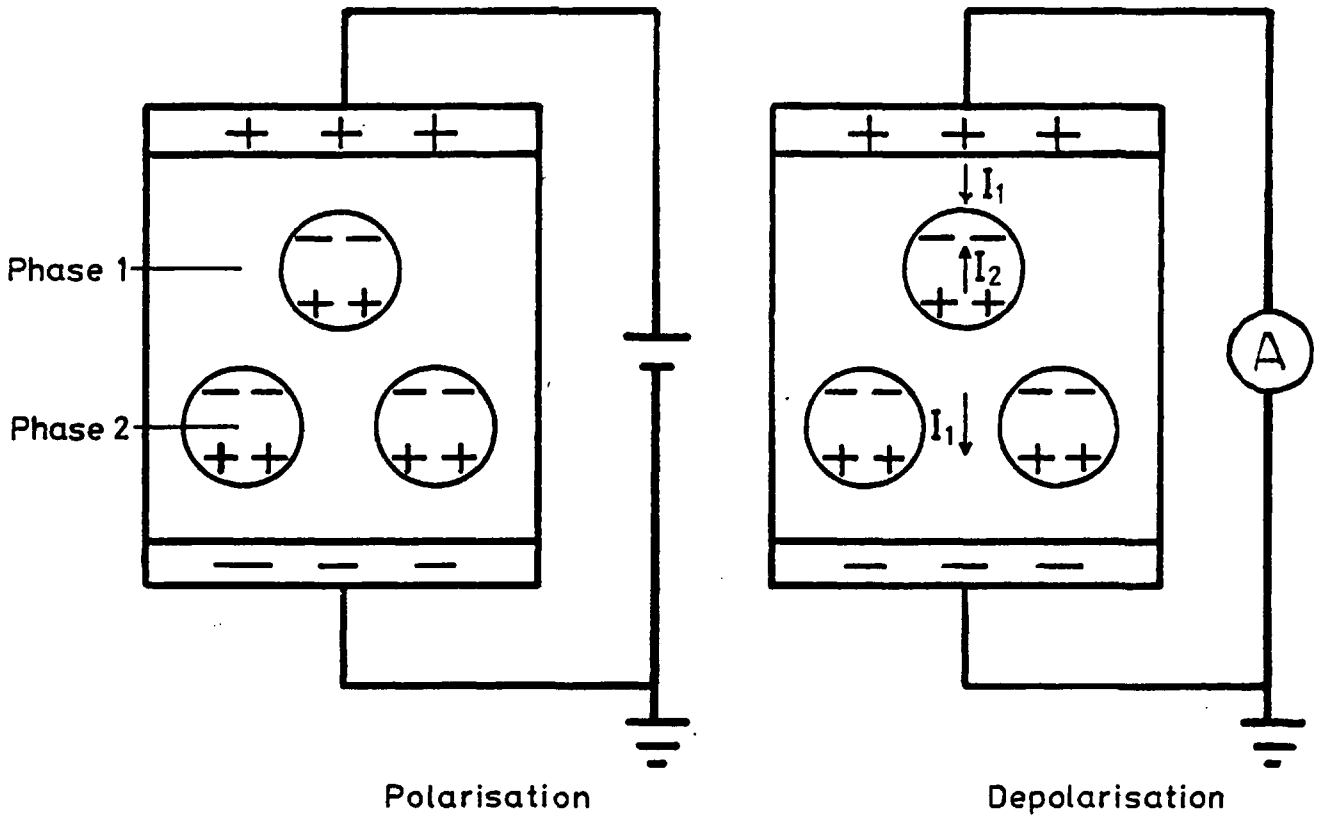


Fig. 2.4:

The theoretical aspect of space charge depolarisation due to the interfacial mechanism is much more complicated than, for instance, the TSD due to dipoles. A simplified TSDC theory of interfacial polarisation has been proposed by van Turnhout (1971), by considering the model of a charged two-layer capacitor and neglecting the possible dependencies of the permittivities of the two layers on temperature. In particular he considers a structure of two layers having dielectric constant  $\epsilon_1$ ,  $\epsilon_2$ , conductivities  $\sigma_1(T)$ ,  $\sigma_2(T)$ , and thicknesses  $d_1$  and  $d_2$ . During formation of the electret a planar charge  $Q$  is formed at the interface. In the process of TSD the planar charge will create in both layers a uniform field. According to Gauss's law

$$Q(t) = \epsilon_0 \epsilon_2 E_2(t) - \epsilon_0 \epsilon_1 E_1(t) \quad (2.19)$$

Because the voltage across the sample is zero, the following equation can be written

$$E_1(t)d_1 + E_2(t)d_2 = 0 \quad (2.20)$$

In the layers, the fields generate ohmic conduction currents which neutralise the interfacial charge, therefore

$$\frac{dQ(t)}{dt} = \sigma_1(T)E_1(t) - \sigma_2(t)E_2(t) \quad (2.21)$$

Eliminating  $E_1(t)$  and  $E_2(t)$  with Eqns. (2.19) and (2.20), eqn. (2.21) can be written as

$$\frac{dQ(t)}{dt} + \frac{[\sigma_2(t)/d_2 + \sigma_1(t)/d_1]}{\epsilon_0(\epsilon_2/d_2 + \epsilon_1/d_1)} Q(t) = 0 \quad (2.22)$$

which has the same form as the Debye relaxation. The current released during the thermal stimulation of the sample can be found from

$$J(t) = \epsilon_0\epsilon_1 \frac{dE_1(t)}{dt} + \sigma_1(T) E_1(t) = \epsilon_0\epsilon_2 \frac{dE_2(t)}{dt} + \sigma_2(T) E_2(t) \quad (2.23)$$

Combining Eqns. (2.19), (2.20) and (2.21) in eqn. (2.23) the expression for the current density is then obtained as

$$J(t) = \frac{dQ(t)}{dt} \cdot \frac{[\epsilon_2/\epsilon_1 - \sigma_2(T)/\sigma_1(T)]}{[d_2/d_1 + \sigma_2(T)/\sigma_1(T)] [1 + \epsilon_2 d_1/\epsilon_1 d_2]} \quad (2.24)$$

Depending upon the ratios  $\epsilon_2/\epsilon_1$  and  $\sigma_2/\sigma_1$ , the TSD current may be positive or negative. In general, however, the discharge current has the opposite direction to that of the charging current (Hayashi et al 1979, Vanderchueren 1980). It can also be seen from eqn. (2.24) that since

$J \neq dQ/dt$  the charge ultimately recovered during TSD will be less than the initial charge stored. This is so because the conduction currents neutralising  $Q$  oppose each other in the upper and lower layers.

The current efficiency of the process will be poor when the conductivities of the components are almost equal, because it is the average current that equals the external current. On the other hand, if one of the components is a perfect insulator, all of the image charges previously induced will be released, and the efficiency will be maximum.

## 2.7 DIPOLAR PROCESSES WITH A DISTRIBUTION OF RELAXATION TIMES

In a material characterised by a single value of the activation energy  $A$ , there is only one type of response, regardless of the values of  $T_p$  and  $T_o$ , and also largely independently of the polarising time  $t_p$  at  $T_p$  and of the storage period at  $T_o$ . This is because the system can only respond in one way, except for the amplitude of response, since there is only one activation energy and  $T_p$  either is or is not sufficient to enable the excitation to establish a state of non-equilibrium.

In polymers, a single relaxation time is inadequate to explain the observed relaxation processes. One physical reason for that is the fact that the macromolecules have different conformations and therefore the rotation of each of the dipoles does not proceed in the same environment. This situation results in a distribution of activation energies. Also, different values of the rotational masses of the dipoles give rise to different values of the pre-exponential factor  $w_o$ .

Considering an Arrhenius equation for describing the temperature dependence of relaxation times, either the pre-exponential factor or the activation energy, or both, may be distributed. That is,

$$w_i(T) = w_{oi} \exp(-A_i/kT)$$

or

$$\tau_i(T) = \tau_{0i} \exp(A_i/kT) \quad (2.25)$$

For a continuous distribution in  $\tau_0$  only, and assuming that the dipole-dipole interactions are negligible and that the time-temperature superposition principle is respected, the total polarisation can be obtained by summing the differential polarisation contributions over the whole relaxation time range

$$P(t) = \int_0^\infty P_i(t, \tau_0) d\tau_0 \quad (2.26)$$

If the sample is subjected to the forming, storage and TSD scheme of Fig. 2.2, and neglecting the temperature dependence of the equilibrium polarisation, one can write, at each temperature during a TSD experiment, the following equation

$$P(T) = P_e(T_p) \int_0^\infty H(\tau_0) f(\tau_0) \exp\left[-(r \tau_0)^{-1} \int_{T_0}^T \exp(-A/kT') dT'\right] d\tau_0 \quad (2.27)$$

where  $H(\tau_0)$  is the filling state function of each individual polarisation and  $f(\tau_0)$  is the normalised distribution function

$$\int_0^\infty f(\tau_0) d\tau_0 = 1 \quad (2.28)$$

Finally the TSD current density is given by

$$J(T) = P_e(T_p) \exp(-A/kT) \int_0^\infty \tau_0^{-1} f(\tau_0) H(\tau_0) \exp\left[-(r \tau_0)^{-1} \int_{T_0}^T \exp(-A/kT') dT'\right] d\tau_0 \quad (2.29)$$

A similar equation is obtained for a continuous distribution of activation energies, namely

$$J(T) = P_e(T_p)\tau_0^{-1} \int_0^\infty g(A)H(A) \exp[-A/kT - (r\tau_0)^{-1} \int_0^T \exp(-A/kT')dT'] dA \quad (2.30)$$

where  $g(A)$  is the normalised distribution function in activation energies

$$\int_0^\infty H(A)dA = 1 \quad (2.31)$$

and  $H(A)$  the filling state function.

As can be seen from Eqns. (2.29) and (2.30), the current density remains proportional to  $P_e(T_p)$  and thus to the polarising field,  $E_p$ . The peaks resulting for both distributions will obviously be broadened and, owing to the appearance of the filling state functions  $H(\tau_0)$  and  $H(A)$  within the integrals, not only their amplitude but also their shape and position will be strongly affected by the formation and storage conditions. This observation was predicted by Bucci and Riva (1965) and is obvious since each individual polarisation will be specifically affected contributing thus more or less to the final shape of the curve.

At each temperature  $T$ , the TSD currents given by Eqns. (2.29) and (2.30) can be thought of as being due to a Debye relaxation of which the current has its maximum at  $T$ .

The most common distribution functions applicable to dipolar relaxation processes are given in Table V.

Table V: Distribution Functions (Vanderschuren and Gasiot 1979)

Name	f(U)	Limits
Symmetrical distributions:		
Gevers	$(U_2 - U_1)^{-1}$	$\tau_1 < \tau < \tau_2$
Wagner	$(\bar{\alpha}\sqrt{\pi}) \exp(-\bar{\alpha}^2 U^2)$	$-\infty < \tau < +\infty, 0 < \bar{\alpha} < \infty$
Cole-Cole	$\frac{\sin(\bar{\beta}\pi)}{2\pi [\cosh(\bar{\beta}U) + \cos(\bar{\beta}\pi)]}$	$-\infty < \tau < +\infty, 0 < \bar{\beta} < 1$
Fuoss-Kirkwood	$\frac{\bar{\gamma} \cos(\bar{\gamma}\pi/2) \cosh(\bar{\gamma}U)}{\pi [\cos^2(\bar{\gamma}\pi/2) + \sin^2(\bar{\gamma}U)]}$	$-\infty < \tau < +\infty, 0 < \bar{\gamma} < 1$
Asymmetrical distributions:		
Davidson-Cole	$\frac{\sin(\bar{\delta}\pi)}{\pi} \left[ \frac{1}{\exp(-U)-1} \right]^\delta$ 0	$-\infty < \tau < \tau_m, 0 < \bar{\delta} < 1$ $\tau > \tau_m$
Havriliak-Negami	$(1/\pi) \exp[U\bar{\epsilon}(1-\bar{\eta})] \times$ $\sin\{\bar{\epsilon} \arctan [\sin\pi(1-\bar{\eta}) / \exp[U(1-\bar{\eta}) + \cos\pi(1-\bar{\eta})]]\} \times$ $\{\exp[2U(1-\bar{\eta})] + 2\exp[U(1-\bar{\eta})] \cos[\pi(1-\bar{\eta})] + 1\}^{-\bar{\epsilon}/2}$	$-\infty < \tau < \infty$ $0 < \bar{\epsilon} < 1$ $0 \leq \bar{\eta} < 1$

where  $U = \ln(\tau/\tau_m)$

$f(U) =$  logarithmic distribution function

$f(\ln \tau/\tau_m) = \tau/\tau_m f(\tau/\tau_m)$

$\int_{-\infty}^{+\infty} f(U) dU = 1$

The integral transforms appearing in eqns. (2.29) and (2.30) usually have to be solved by numerical integration using a computer programme but van Turnhout (1971) has shown that it is generally satisfactory to apply approximations derived by Schwarzl and Staverman (1952) for isothermal measurements. A first approximation leads to

$$P_e F_1(\tau_0/\tau_{om}) \approx \left( \frac{kT^2}{rA} J(T) \right)_{\xi(T) = \tau_0} \quad (2.32)$$

where the logarithmic distribution  $F(\tau_0) = \tau_0 f(\tau_0)$  is used, and  $\xi(T) \approx kT^2 r^{-1} A^{-1} \exp(-A/kT)$  for an Arrhenius shift.  $\tau_{om}$  is the most probable value of  $\tau_0$ .

A second-order approximation leads to

$$P_e F_2(\tau_0/\tau_{om}) \approx \left[ P_e F_1(\tau_0/\tau_{om}) - \left( \frac{kT^2}{rA} \right)^2 r \frac{dJ(T)}{dT} \right]_{\xi(T) = 2\tau_0} \quad (2.33)$$

From these equations and the experimental data it is then possible to build step by step the distribution function of the relaxation times of the process. Obviously, this method necessitates a well-isolated peak of thermal current but this is generally possible by a judicious choice of polarisation conditions.

The concept of distribution function  $f(\tau)$  is superficially very plausible (Jonscher 1975). There is no doubt that physical systems must contain distributions of parameters rather than show strictly discrete values, especially in disordered materials and where stochastic processes govern the behaviour. However, the concept of distribution function has been questioned by Jonscher and the next section discusses very briefly the ideas behind Jonscher's model.



## 2.8 THE SCREENED-HOPPING MODEL OF JONSCHER

Jonscher (1975, 1977a) has questioned the generally accepted interpretation of the loss peaks in terms of a distribution of relaxation times for Debye-like processes, because of its arbitrariness and lack of a simple physical significance.

A very important finding in the Jonscher model is that the ratio of the real and imaginary parts of the dielectric susceptibility is constant, independent of frequency

$$\frac{X''}{X'} = \text{constant} \quad (2.34)$$

Eqn.(2.34) represents the ratio of energy lost per cycle to the energy stored per cycle.

The proposed screened-hopping model which Jonscher suggests to satisfy the 'Universal' criterion given by Eqn. (2.34) is based on the following two assumptions:

- (i) The charged particles or dipoles responsible for the polarisation change their positions/orientations between preferred states in an abrupt manner by hopping or jumping movements such that the time taken by the actual transition is negligible in comparison with the time spent on average in the respective preferred states.
- (ii) The interaction with other particles/dipoles may be expressed in terms of a screening process which reduces the effective charge/dipole moment to a fixed fraction of its unscreened value.

Jonscher extended his model based on many-body interactions and simple physical criteria to cover the TSD response not based on Debye-like relaxations (Jonscher 1977b). He starts off with the following expressions for the isothermal discharge current

$$J(t) = P_0 a [w(T)]^{1-n} t^{-n} \quad \text{for } t < 1/w_p \quad (2.35)$$

$$J(t) = P_0 a [w(T)]^{-m} t^{-m-1} \quad \text{for } t > 1/w_p \quad (2.36)$$

where  $a$  is the normalisation constant

$$a = \frac{m+1-n}{\pi} \sin \frac{(1-n)\pi}{m+1-n} \quad (2.37)$$

and  $P_0$  is the initial polarisation (i.e.,  $P_0 = P(\tau_0)$ ).

The logarithmic derivative of the current density found in his work is

$$\frac{d \log J(T)}{d(1/kT)} = -A [1 - nE(U, U_0)] \quad \text{for } t < 1/w_p \quad (2.38)$$

$$\frac{d \log J(T)}{dT} = \frac{A}{kT^2} [1 - (m+1)E(U, U_0)] \quad \text{for } t > 1/w_p \quad (2.39)$$

where  $E(U, U_0)$  is the special function

$$\frac{1}{E(U, U_0)} = \frac{\int_U^{U_0} s^{-2} \exp(-s) ds}{U^2 \exp(-U)} \quad (2.40)$$

with  $U = A/kT$  and  $U_0 = A/kT_0$ .

Under experimental conditions  $U_0 \gg 1$  and  $U$  are relatively large.  $E(U, U_0)$  is slightly larger than one, tending to unity as both  $U$  and  $U_0$  become large. Also in the limit as  $U$  approaches  $U_0$ , the value of  $E(U, U_0)$  becomes large.

This signifies that after the onset of the temperature ramp the square bracket in Eqn. (2.38) is negative, implying that the current is actually falling with rising temperature. This is then reversed and the current begins to rise as  $T$  increases until  $t < 1/\omega_p$ .

Eqn. (2.38) shows that the activation energy derived from the current in the rising part of the TSD peak is smaller than the loss peak activation energy  $A$ , being given approximately by  $(1-n)A$ . Experimental evidence exists (Vandershueren and Linkens 1977) to show that the values of the activation energies determined from the rising part of a TSD peak are lower than the values determined from dielectric measurements.

Eqn. (2.39), which is valid for times  $t > 1/\omega_p$ , shows that the logarithmic slope is always negative, which means that the current falls with rising temperature.

From Jonscher's model the following conclusions can be drawn:

- (i) Only a single activation energy corresponding to the transition from the primary to the secondary depolarisation process in the time domain is sufficient.
- (ii) TSD in 'non-Debye' systems are broader in temperature than the corresponding Debye peaks.
- (iii) The activation energy determined from the rising part of a TSD peak is smaller than the activation energy derived from the shift of the peak temperature with heating rate and also from the activation energy of the loss peak frequency.
- (iv) The model allows one to calculate the initial and final shapes of TSD maxima but does not give information on the shape of the peak and on the position of the maximum on the temperature axis.

In a recent paper by Zielinski et al (1980) on the application of the many-body model of universal dielectric response to TSD, a new method was proposed to solve the equations of TSD. A solution was found in their study by placing  $m = 1 - n$ . The current density found was

$$J(T) = \frac{2mP_0}{\pi} w(T) \frac{\xi^{m+1}}{1+\xi^{2m}} \quad (2.41)$$

where

$$\xi = \frac{1}{r} \int_{T_0}^T wdT \quad (2.42)$$

Simulated TSD current spectra were obtained from Eqn. (2.41) for various parameters  $m$ , and constant activation energies. The plot obtained showed that the peaks were broad and their width depended on  $m$ . Contrary to experimental results the position and shape of the TSD peak did not depend on the forming conditions. It might be concluded that the many-body model, at least in its present form, is not satisfactory to describe the microscopic dielectric properties of polymers in non-isothermal regimes.

## 2.9 EXPERIMENTAL METHODS TO DISTINGUISH BETWEEN DISTRIBUTED AND NON-DISTRIBUTED PROCESSES

The purpose of this section is to describe some experimental methods which can be used to determine whether a dipolar TSD peak arises either from a single relaxation or from a distributed relaxation.

### 2.9.1 Forming and Storage Conditions

Varying the conditions of charging and storage can serve as a criterion for differentiating between a distributed and non-distributed peak.

If there is a single relaxation, the shape and position of the current peak do not depend on these conditions, but if there is a distribution of relaxations, they do (van Turnhout 1975). This is because the rapidly and slowly reacting dipoles of a distributed relaxation will be affected differently, e.g. by too short a formation time or too long a storage time.

The shift of a peak with heating rate may also be helpful in deciding whether a broad peak is due to a single dipole relaxation with a low activation energy, or rather to a distributed dipole relaxation. When the shift is slight, the peak is undoubtedly due to a distributed polarisation.

### 2.9.2 Multistage TSD

This technique consists of interrupting the heating at increasingly higher temperatures. After each interruption the electret is cooled and reheated for another TSD. The distributed polarisation, if any, is thus investigated in parts. In the first runs the fast dipoles are mobilised, while in the latter runs, when the temperature becomes higher, the slow dipoles get a chance to disorient.

### 2.9.3 Thermal Sampling Technique

The objective of the thermal sampling (TS) technique is to 'sample' the relaxation process within a narrow temperature range. The TS experiment consists (Zielinski and Kryszewski 1977) of polarising the 'sample' at a constant temperature,  $T_p$ , for a certain time,  $t_p$ . This excitation causes orientation of the mobile relaxation units and all molecular motions for which the relaxation time  $\tau(T_p)$  is of the order of  $t_p$  or smaller, become oriented. After that the temperature is lowered to  $T_d$  and the sample is partly depolarised in a short-circuited condition

for a period of time,  $t_d$ . Finally the sample is cooled down to  $T_0$ . Because of that 'loading' programme, only a small fraction of the molecular motion processes, for which the relaxation times lie within a certain range, become frozen in with permanent polarisation. Fig. 2.5 shows the TS technique.

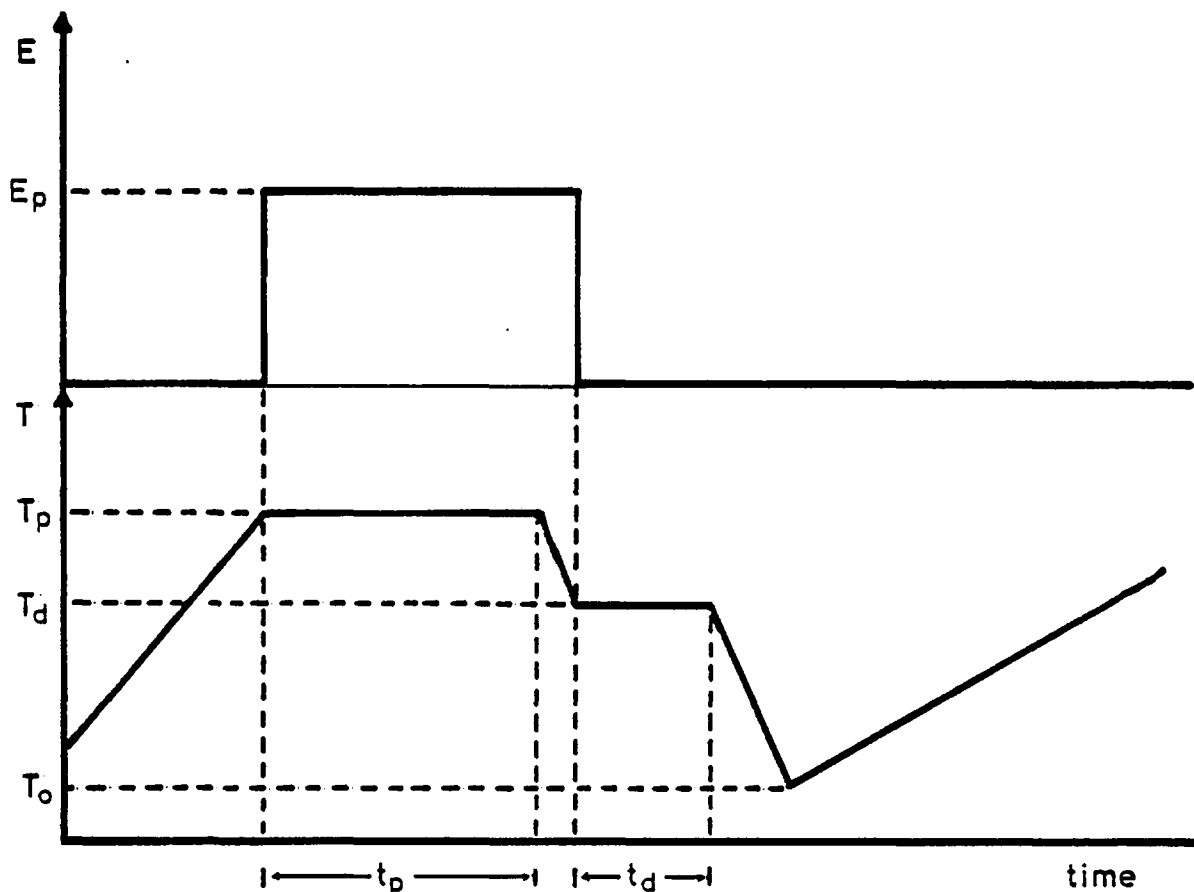


Fig. 2.5: The thermal sampling technique

#### 2.9.4 Fractional Polarisation Technique

This technique is due to Vanderschueren (1977) and is illustrated in Fig. 2.6.

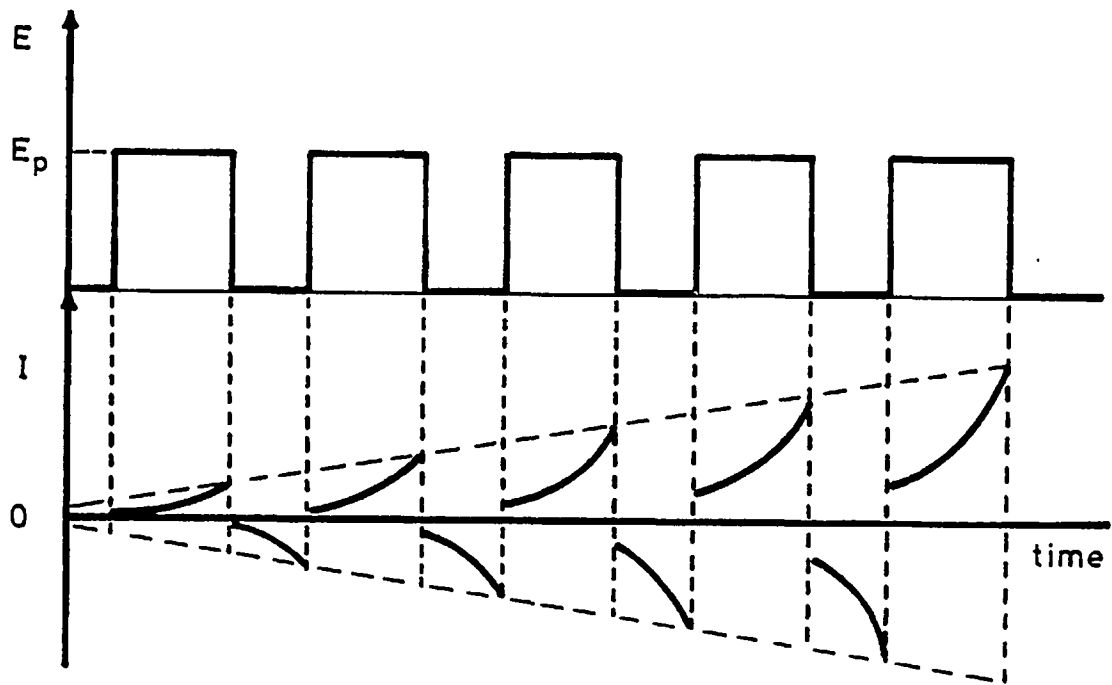


Fig. 2.6:

During slow linear cooling the polarising electric field is not applied continuously but in several steps, separated by short-circuit periods. In this way, if the initial process is distributed, there must appear during the subsequent heating a corresponding number of partial peaks, each characteristic of some components of the distribution. Typical experimental parameters are: cooling rate  $1-2^{\circ}\text{C}/\text{min}$ , heating rate  $1-5^{\circ}\text{C}/\text{min}$ , polarising steps  $5$  to  $20^{\circ}\text{C}$  and separated from each other by  $15$  to  $20^{\circ}\text{C}$ .

## 2.10 Determination of Relaxation Parameters

### 2.10.1 Activation Energy

Several methods exist for calculating the activation energy of a non-distributed process. The most used are given below.

#### 2.10.1.1 The Initial Rise Method of Garlick and Gibson (1948)

The integral term of eqn. (2.7) is negligible at low temperatures. Therefore the first exponential dominates during the rising part of a TSD peak. In this case

$$\ln J(T) \sim \text{const} - A/kT \quad (2.43)$$

By plotting  $\ln J(t)$  against  $1/T$  the activation energy can be obtained from a single measurement with good accuracy.

### 2.10.1.2 Graphical Integration Method

By taking into account the fact that the residual polarisation  $P(T)$  at an intermediate temperature  $T$  is proportional to the area of the TSD peak from  $T$  to  $\infty$ , Bucci et al (1966) proposed the use of the whole curve to calculate the activation energy. Eqn. (2.3) can therefore be written as follows

$$\begin{aligned} \tau(T) &= \frac{P(T)}{J(T)} \\ &= r^{-1} \int_T^{\infty} J(T') dT' / J(T) \end{aligned} \quad (2.44)$$

hence

$$\ln \tau(T) = \ln \left[ r^{-1} \int_T^{\infty} J(T') dT' \right] - \ln J(T) \quad (2.45)$$

Assuming an Arrhenius shift

$$\ln \tau(T) = \ln \tau_0 + A/kT \quad (2.46)$$

The integral in eqn. (2.45) can be estimated accurately by graphical integration of the TSD peak. The activation energy is calculated by plotting  $\ln \tau(T)$  vs  $1/T$ . The straight line obtained is often referred to as the BFG\* plot.

---

\*BFG stands for Bucci-Fieschi-Guidi



### 2.10.1.3 The Method of Varying Heating Rate

This method is based on the shift of a TSD peak with heating rate. If the heating rate is changed from  $r_1$  to  $r_2$ , the activation energy can be deduced using the shift of the temperature maxima  $T_{m1}$ ,  $T_{m2}$ . From eqn. (2.8) one gets

$$A = \frac{k T_{m1} T_{m2}}{T_{m1} - T_{m2}} \ln \left( \frac{r_1 T_{m2}^2}{r_2 T_{m1}^2} \right) \quad (2.47)$$

In the case where the heating rate is changed several times to different values, A can be found from a plot of  $\ln (T_m^2/r)$  against  $1/T_m$ .

### 2.10.1.4 Methods Based on the Symmetry of the Peak

One way of analysing a 'glow' peak, obtained using a linear heating rate, is by considering its symmetry properties.

First and second order kinetics are only special cases, whereas many 'glow' single peaks are neither of first nor second order. The second order peaks are characterised by a practically symmetric peak, whereas the first order peaks are asymmetric. Chen (1969a) has shown that for a first order peak  $f = 0.42$  whereas, a second order peak is characterised by  $f = 0.52$ , where  $f$  is a symmetry factor defined as  $f = \eta/\gamma$ , where  $\gamma = \delta + \eta$  is the total half width,  $\delta$  the half width at the low temperature side of the peak and  $\eta$  the half width towards the fall-off of the peak.

In another paper, Chen (1969b) showed that when one has a 'general order' case, the kinetic order  $\ell$  can be evaluated by the value of  $f$ . A calculated graph of  $f$ , ranging from 0.36 to 0.55 for values of  $\ell$  between

0.7 and 2.5 is given, which can be used for the evaluation of  $\ell$  from a measured  $f$ . The activation energy is calculated using the equation

$$A_{\delta} = c_{\delta} (kT_m^2/\delta) - b_{\delta} (2kT_m) \pm 2\% \quad (2.48)$$

where

$$c_{\delta} = 1.51 + 3.0 (f - 0.42) \quad (2.49)$$

$$b_{\delta} = 1.58 + 4.2 (f - 0.42) \quad (2.50)$$

### 2.10.2 Parameters other than A

Once the activation energy has been calculated by using one of the previous methods,  $w_0$  or  $\tau_0$  can be calculated from eqns. (2.5) and (2.6). They can also be estimated from the BFG plot. The equilibrium polarisation,  $P_e$  originally stored can be obtained by integrating the current density

$$P_e = \int_{T_0}^{\infty} J(T) dT \quad (2.51)$$

The dielectric relaxation strength  $\Delta\epsilon = \epsilon_s - \epsilon_{\infty}$  can be found if the sample has been charged to its equilibrium value. Its value is given by (Hill et al 1969)

$$\Delta\epsilon = \epsilon_s - \epsilon_{\infty} = \frac{P_e}{\epsilon_0 E_p} = \frac{N\mu^2}{3\epsilon_0 kT_p} \quad (2.52)$$

where  $\epsilon_0$  is the permittivity of free space,  $\epsilon_s$  and  $\epsilon_{\infty}$  are the limiting values of the real part of the permittivity of the material at low and high frequency respectively.

Eqn. (2.51) is also valid for distributed polarisation if the polymer is fully charged. For distributed processes, the method of varying the heating rate still applies. This is so because the maximum temperature of the TSD peak is expected to be essentially determined by the dipoles having the average value of activation energy. However, its accuracy is rather low and this is more especially true for distributed peaks, the maxima of which are often "flat" and thus difficult to determine with precision.

## CHAPTER III

### EXPERIMENTAL APPARATUS AND MEASUREMENT PROCEDURES

#### 3.0 INTRODUCTION

In its simplest form in any TSD experiment the current released from the electret is measured as a function of time during which the temperature is continuously changing. This means that there are five key parts of any TSD system : the sample which consists of polymer, electrodes and leads; the cryostat and the associated sample holder; the heating unit giving a variable but linear heating rate; the current meter and the recording unit. The sample, the cryostat and the current meter will be discussed separately. Differential thermal analysis and infrared spectroscopy techniques will be described very briefly at the end of the chapter.

#### 3.1 SAMPLE PREPARATION AND ELECTRODES

Samples were solvent cast from a polymer solution. The solvent utilised for the nylon resin was methanol. For polyvinylbutyral MEK:toluene mixtures were used. 10% in weight of solids were used to prepare the polymer solutions. The solid polymer was added to the solvent with continuous stirring and the mixture heated to 5-10<sup>0</sup>C below the reflux point of the solvent or solvent mixture, i.e. around 55<sup>0</sup>C. The total time utilised for complete solution was about four hours. Fig. 3.1 illustrates the equipment built for dissolving the polymer resins. It consists of a 50 ml glass beaker with cover, an electric motor with speed control, a heated water bath and an agitator.

Soda glass microscope slides were used as substrates. They were first washed with Teepol and distilled water. The substrates were then chemically cleaned by using organic solvents (trichloroethylene, acetone and isopropyl alcohol) in an ultrasonic bath. Evaporated aluminium or gold layers were used as bottom and top electrodes. They were prepared in a vacuum coating unit evacuated by an oil diffusion pump. A multi-strand helical tungsten filament, which had been thoroughly cleaned, was used as a source heater. Fig. 3.2a shows the arrangement of the glass slides and the mask built to deposit the bottom electrode.

After depositing the bottom electrode on the glass slide, the next step was to form the polymer film. The films were obtained by using the rod coater technique (Booth 1968). A special unit was constructed to prepare the polymer films. Fig. 3.3a shows it, which consists of a stainless-steel wire-wound coating rod, a movable platform to adjust the distance between the rod-edge and the surface of the substrate, and screws to move the platform. The diameter of the rod used was 6.3 mm and that of the wire 0.6 mm.

The way in which the polymer film was obtained is as follows. After aligning and setting the rod coater unit, a few drops of a fresh polymer solution were placed close to the wire-wound rod as shown in Fig. 3.3b. The droplets on the surface of the glass slide were made to coalesce by bringing them up to the rod, and then spread out to form a film by movement of the glass slide relative to the rod. In this manner a clear homogeneous polymer film was obtained. Typical film thicknesses varied between 10 and 20  $\mu\text{m}$ . The films were placed in an air oven at 50°C for two days to get rid of any residual solvent.

The top electrodes were evaporated next with an evaporation source sample distance of 18 cm. Guard ring configuration electrodes were much used for the top electrode as shown in Fig. 3.2a. Before evaporation the samples were left in vacuum for about two days to drive out the residual solvent (if any). Fig. 3.2b shows a schematic diagram of the metal-polymer-metal devices obtained. A length of thin copper wire was attached to each of the three electrodes using silver dag paste. The contacts were checked to ensure they adhered to the electrodes well. In addition to the above contact method, pressure contacts were also used. Film thicknesses were measured either with a comparator gauge or with a talysurf instrument.

In addition to solvent cast nylon films, hot pressed films were also produced. A commercial polymer press (Moore and Son) was used for this purpose. Aluminium foil was used as substrate. The temperature and pressure used to prepare the films were about 120°C and 0.5 ton/sq. in. respectively.

### 3.2 THE CRYOSTAT

All measurements were carried out in a metal vacuum cryostat designed to operate in the range between liquid nitrogen temperatures and about 180°C. Fig. 3.4 illustrates the system used, which is similar to the one designed by Norian (1977). Basically the cryostat consists of a metal chamber, a liquid-nitrogen cooled 'cold finger', the sample holder and the lead-throughs.

The metal chamber was built of aluminium (dural) and had an internal diameter of 15 cm. The 'cold finger' was made of copper and had a diameter of 1.9 cm. Copper was chosen because of its high thermal conductivity thus allowing quick transfer of heat. The copper rod was hard soldered onto a stainless steel sheath. The sheath did not touch

the copper rod above the seal. Hence, after pump-down, a vacuum existed between the copper rod and the sheath, which minimised heat transfer between the two. Stainless steel was chosen as the sheath material because of its low thermal conductivity. This, together with the fact that the sheath wall was made as thin as possible (approximately 1 mm), resulted in preferential heat conduction along the copper rod, rather than the sheath, resulting in a lower consumption of liquid nitrogen.

The sample holder consisted of a copper block of dimensions 3.8 cm x 3 cm x 2.2 cm with holes in which Philips thermocoax nichrome heater wire was placed. An advantage of using thermocoax was that the sheath could be earthed, because the measured d.c. currents are usually small and flow while the a.c. heater current is on. Care was taken not to short circuit the inner conductor to the sheath at the two ends of the thermocoax, where the inner conductor was bare.

The 'cold finger' fitted tightly into a hole made in the copper block, resulting in a good thermal contact. The end of the rod was exposed and came into contact with the liquid nitrogen used to cool the sample holder.

The temperature control was achieved by using a programmable heating unit of variable but linear rate (Stanton Redcroft model 681). A platinum resistance thermometer was used as a sensor for the controller. A good thermal contact between the sample substrate and the copper block was achieved by a thin film of either heat sink compound or silver dag. The temperature of the sample was measured using two chromel-alumel thermocouples attached close to the sample. The lid of the vacuum chamber had a 3 mm thick optical window. It allowed one to inspect the sample physically or to shine light on it if necessary. An Edwards multi-pin leadthrough was used to complete the necessary electrical connections.

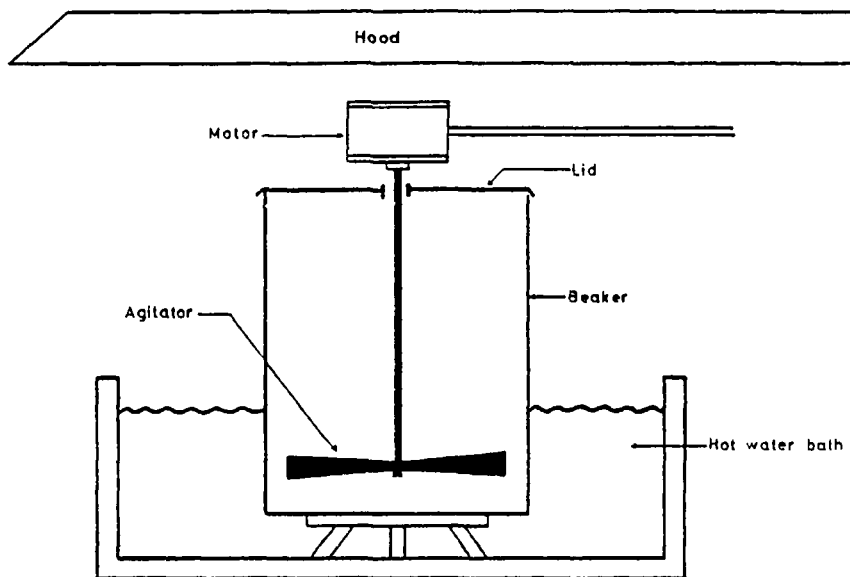
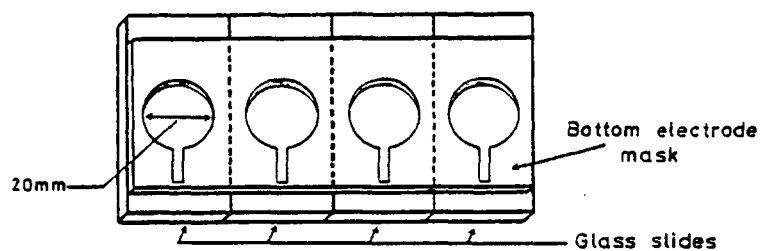
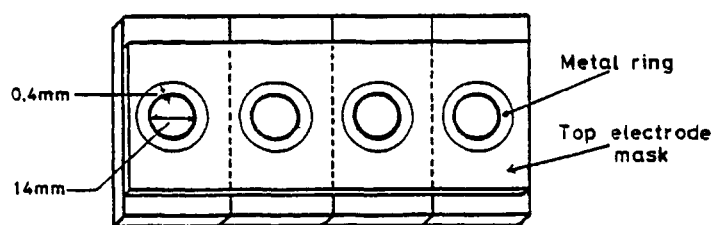


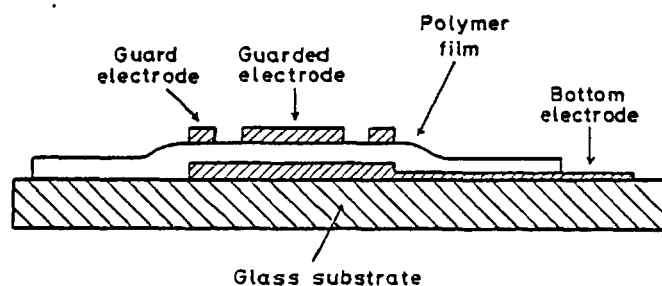
Fig. 3.1: Equipment used for preparing polymer solutions



(a) Mask arrangement



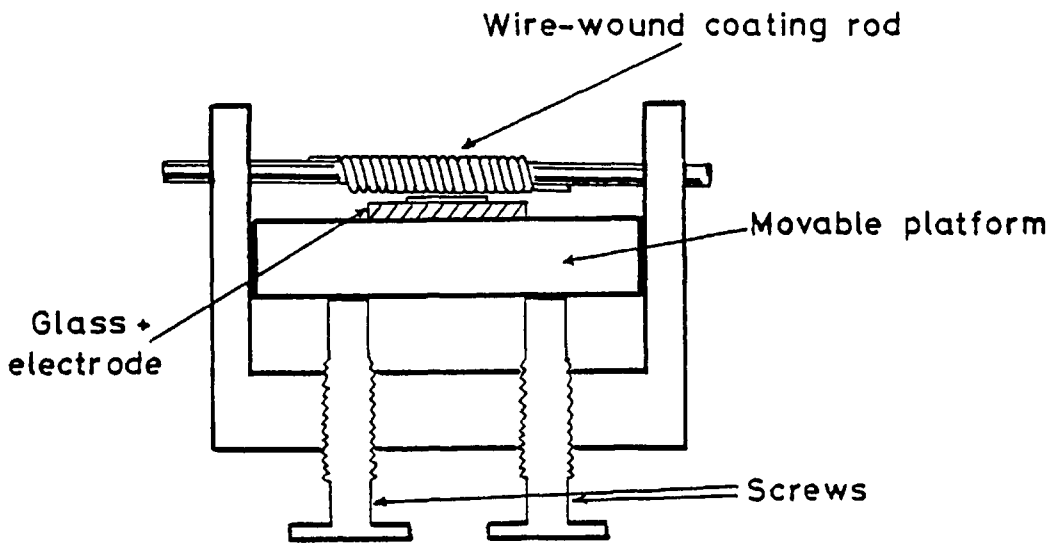
(a) Mask arrangement



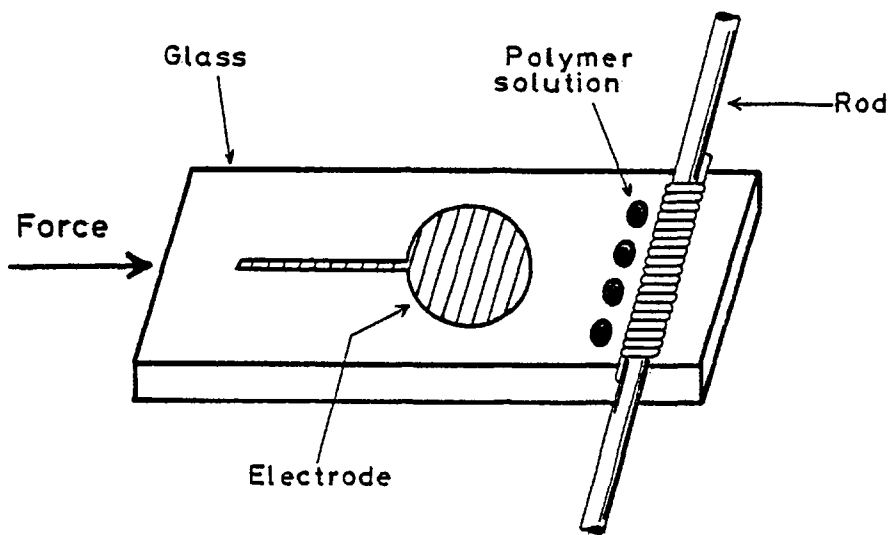
(b) Cross-sections of a metal-nylon-metal structure

Fig. 3.2:





(a) Rod coater unit



(b) Schematic arrangement showing the way polymer films were prepared

Fig. 3.3:

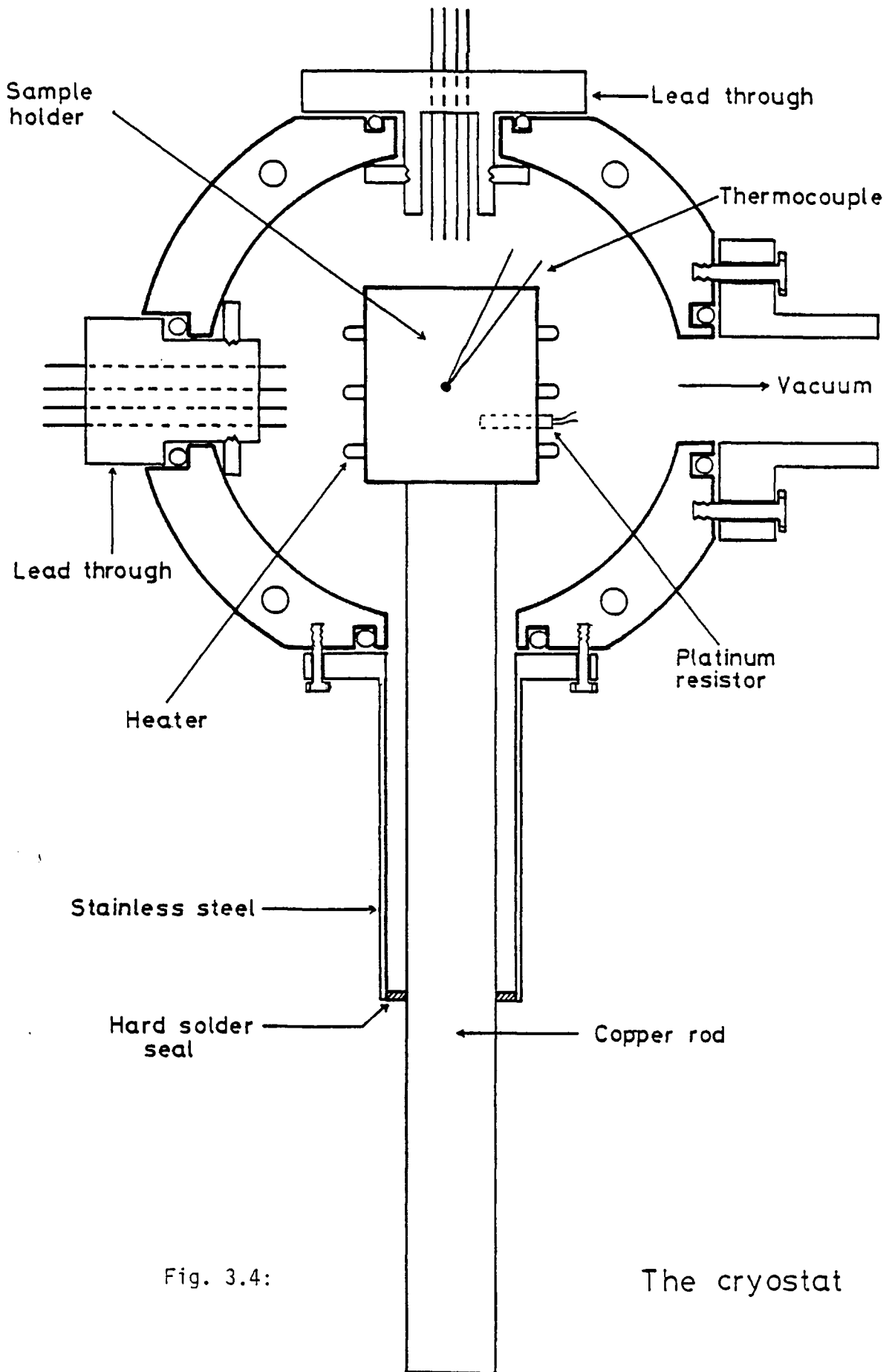


Fig. 3.4:

The cryostat

The recorder unit utilised was a Bryans chart recorder model 2000 x(t) recorder. A silicon oil pumped liquid nitrogen trapped vacuum system was used to evacuate the cryostat to a pressure better than  $2 \times 10^{-6}$  torr. A general view of equipment used is shown in Figs. 3.5 and 3.6.

### 3.3 THE CURRENT MEASUREMENT

The current detector used in the current measurements was a Keithley 610C electrometer. The electrometer is capable of measuring currents which may range from  $10^{-14}$  to 0.3A. Two techniques exist to measure low currents: the shunt-type circuit and the feedback-type circuit. The relevant circuits are shown in Fig. 3.7a and 3.7b. The feedback-type was used to measure the low currents. This circuit largely neutralises the effect of input capacitance and greatly increases the response speed, with a maximum voltage drop of 1mV.

Rise time varies primarily with the current range, the input capacity and the method used. With the feedback switch in the fast position, the rise time on the most sensitive range is less than 2 seconds, and on the  $10^{-6}$  amp range, less than 3 milliseconds (Keithley 1972). Another advantage of using the fast mode is that the common point A in the feedback is virtually at zero potential and the grounding ensures that the field lines are parallel and also perpendicular to the input electrode. In addition there is no current flow between the guard ring and the output electrode.

Low-noise coaxial cables were used for the electrical connections. They were kept short, and it was made sure that all the soldered joints were good. The electrometer was placed as close as possible to the cryostat. A protection resistor  $R_p$  of value  $100 \text{ K}\Omega$  was used in the circuit. The heating rate of the temperature controller was checked for linearity.

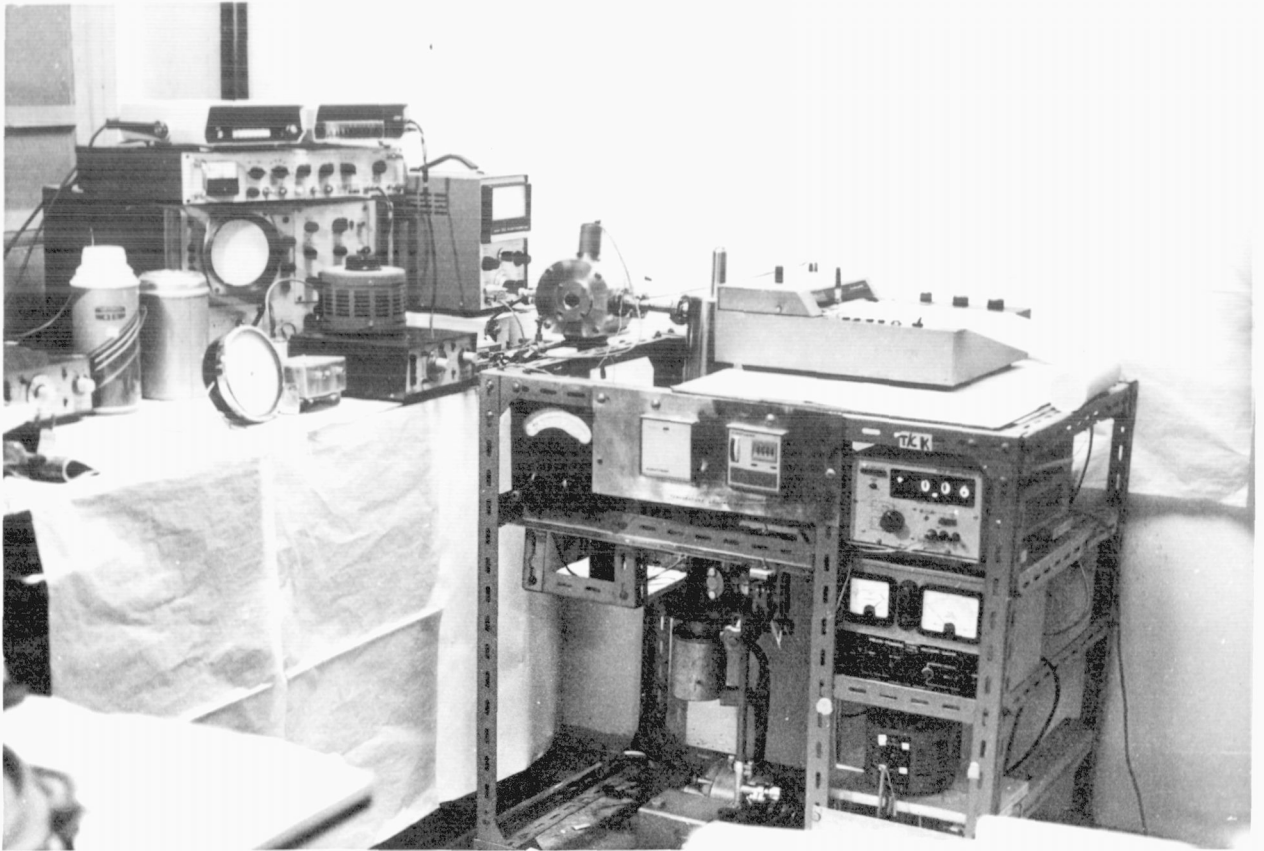


Fig. 3.5: The Experimental Set-up

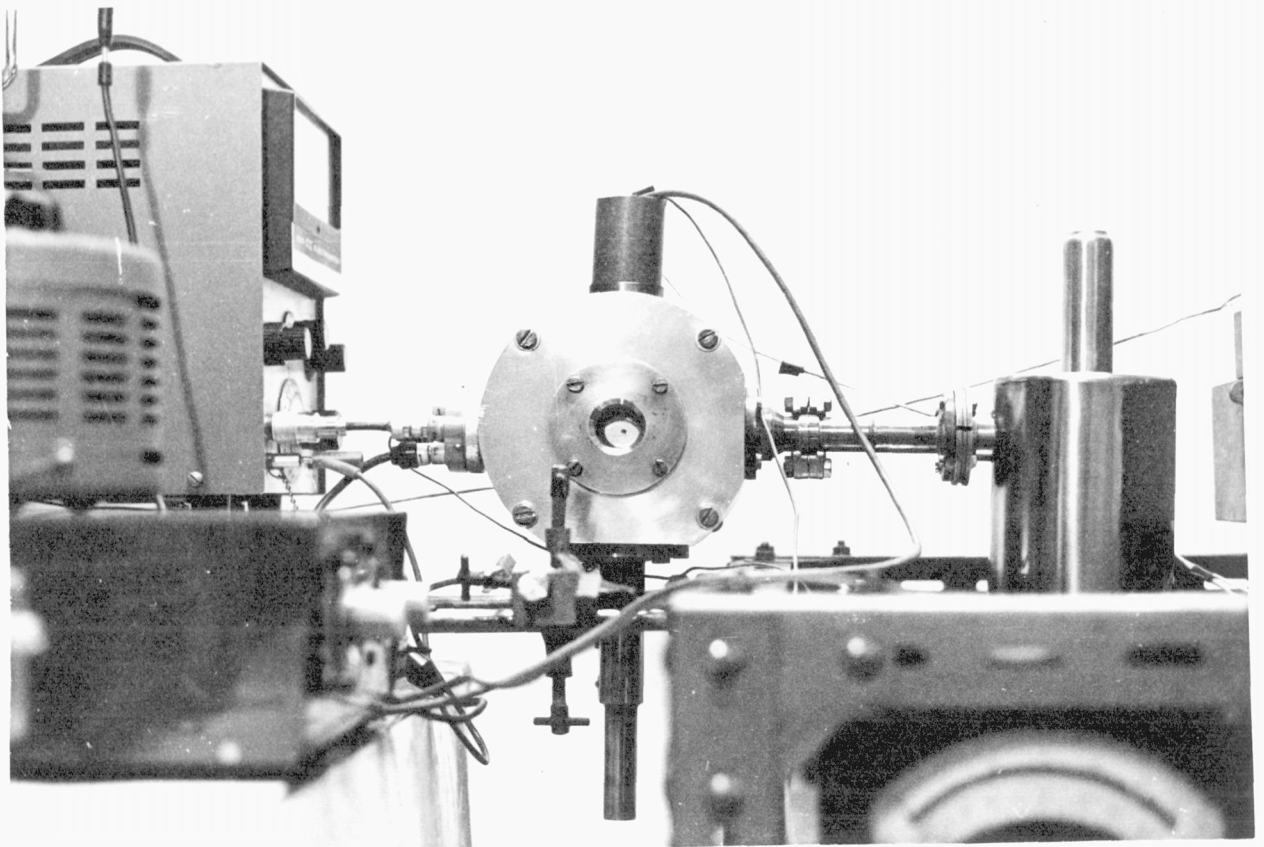
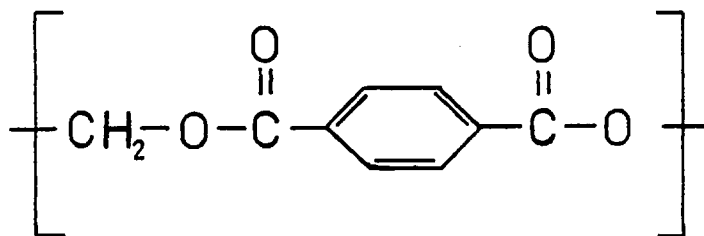


Fig. 3.6: Close-View of the Cryostat

Two thermocouples were placed in the configuration shown in Fig. 3.8. The sample was cooled down to about  $-15^{\circ}\text{C}$  and heated up at  $2^{\circ}\text{C}/\text{min}$  to high temperatures. The outputs of the thermocouples were measured as a function of time. The experimental result obtained is shown in Fig. 3.8. It can be seen that the heating is linear, and that both thermocouples agreed very well with each other. Similar results were obtained for 4 and  $6^{\circ}\text{C}/\text{min}$  rates.

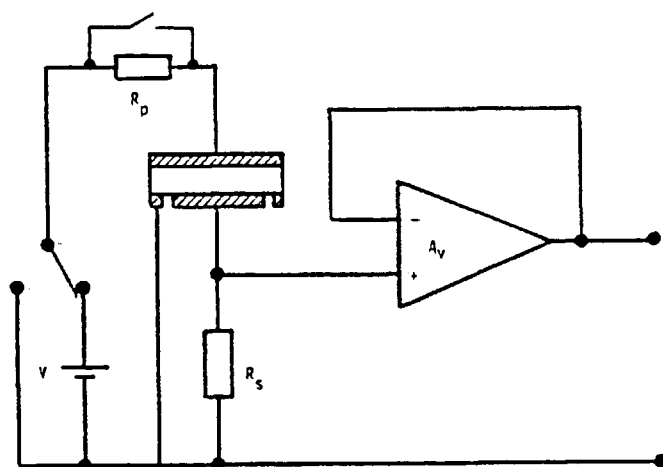
Since the TSD spectrum and other relaxation data for polyethylene terephthalate (PET) are well documented (Creswell and Perlman 1970, van Turnhout 1975, Hedvig 1977), a preliminary calibration experiment on PET was conducted for the purpose of checking the performance characteristics of the apparatus. Samples were cut from  $12\ \mu\text{m}$  sheet of commercial PET (DuPont 'Mylar', type C). Circular aluminium electrodes were evaporated on both faces of the film. The metal-polymer-metal structure obtained was stuck onto a microscope slide using silver paste. The virgin sample was first heated in short circuit conditions at  $4^{\circ}\text{C}/\text{min}$ . Very little current was observed during this blank run as seen in Fig. 3.9. The polymer electret was formed at  $100^{\circ}\text{C}$  for 20 minutes with a polarising field of  $80\ \text{kV}/\text{cm}$ . After the charging period the sample was rapidly cooled down to liquid nitrogen temperatures. At that temperature the voltage was taken off and the sample heated in a short circuit condition. The spectrum obtained is shown in Fig. 3.9. Two peaks, which are labelled  $\beta$  and  $\alpha$ , are clearly seen.

PET is a semicrystalline polymer having a chemical structural formula

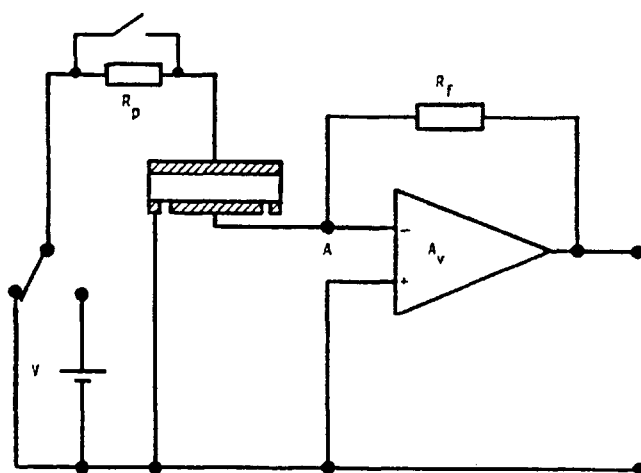


As can be seen in Fig. 3.9 the  $\beta$  peak is very broad. The maximum of the peak occurs at about  $-110^{\circ}\text{C}$ . This  $\beta$ -relaxation is believed to be made up of a number of overlapping dipolar processes. It is attributed to local relaxation of the polar CO groups. The  $\alpha$ -relaxation process has its maximum at about  $87^{\circ}\text{C}$  and is due to segmental motion of the main chain in the amorphous parts of the polymer. It arises from the cooperative motion of the glycol residues, together with the  $-\text{COO}$  dipoles of the main chain.

In conclusion it can be said that a versatile TSD apparatus has been designed for measurements from  $-196^{\circ}\text{C}$  to about  $180^{\circ}\text{C}$ . Results of initial calibration experiments on PET at low and intermediate temperatures are in good agreement with published data.



(a) Basic circuit for shunt-type measurements



(b) Basic circuit for feedback measurements

Fig. 3.7

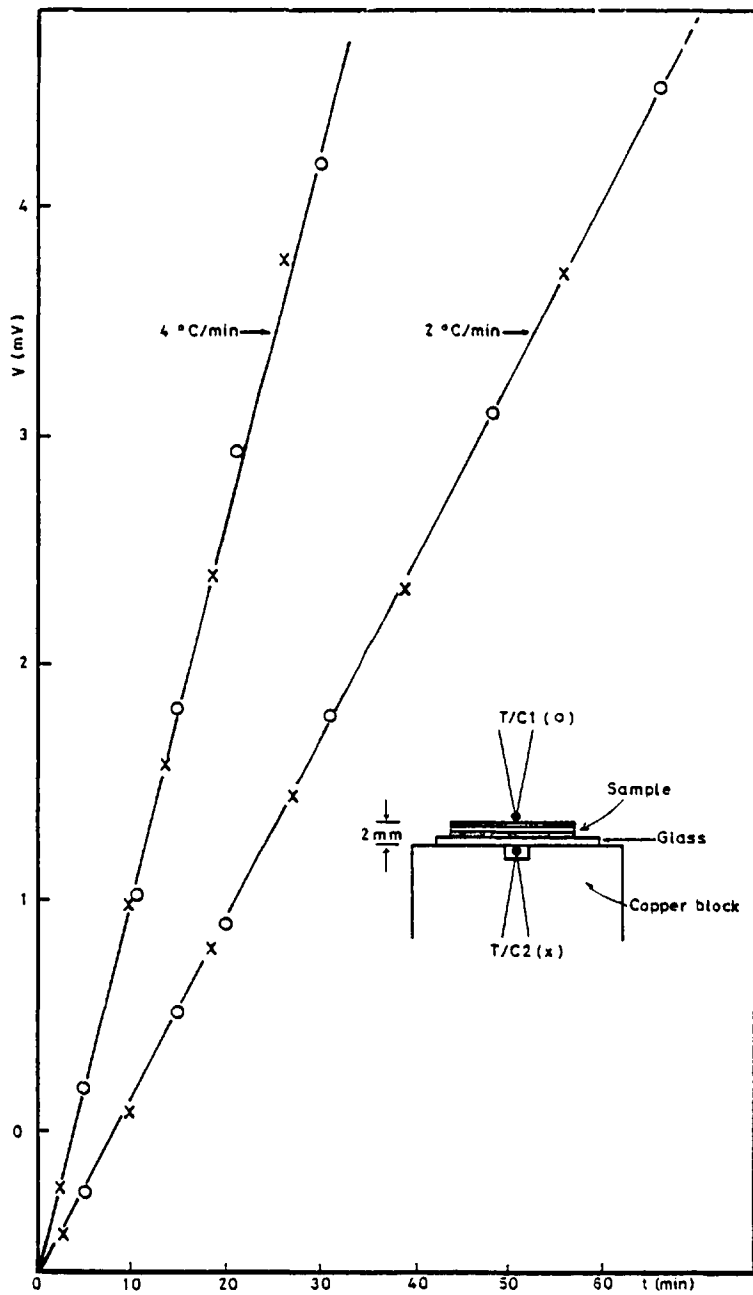


Fig. 3.8: The heating rate of the programmer

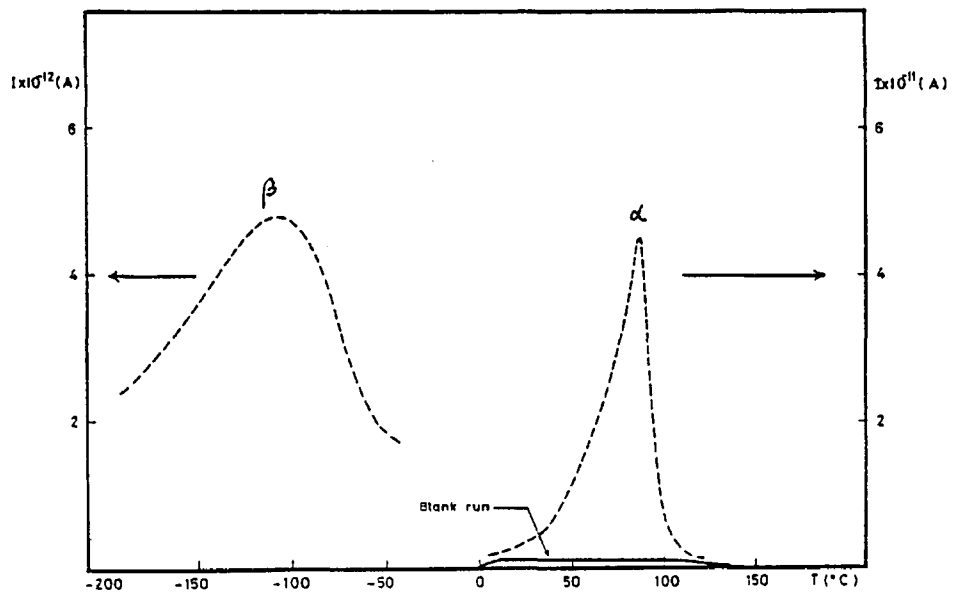


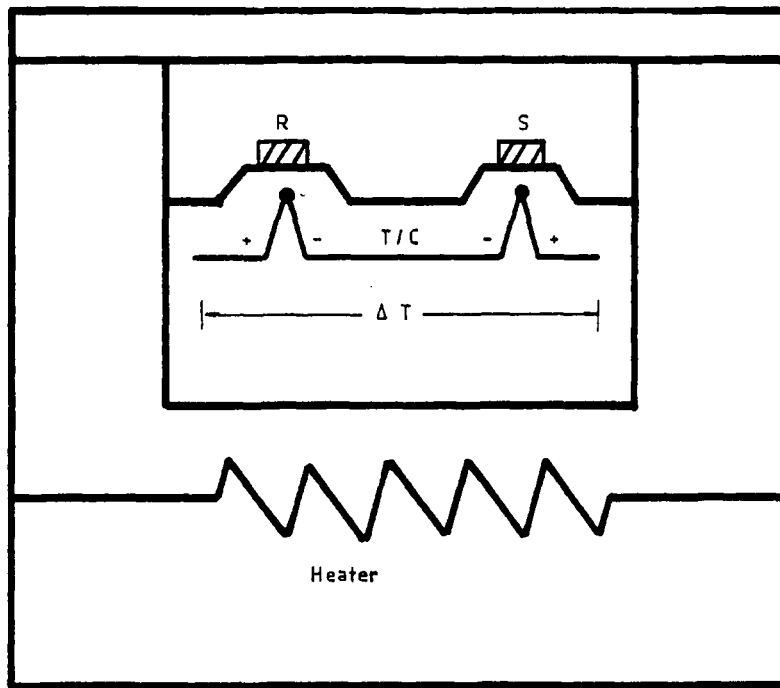
Fig. 3.9: TSD spectrum of PET

### 3.4 DIFFERENTIAL THERMAL ANALYSIS

Differential thermal analysis is a technique in which a record is made of the temperature difference between the sample and a reference material, against time or temperature, as the two specimens are subject to identical temperature regimes in an environment heated or cooled at a constant rate. The graphical record, the DTA curve, shows sharp increases or decreases in temperature difference, depending on whether a change in the sample causes absorption or liberation of heat. The method records all changes in enthalpy, whether accompanied by a change of weight or not, e.g. phase transitions of first or second order (change of crystalline structure, boiling, sublimation, evaporation, melting), or chemical reactions such as redox reactions, decomposition, dehydration and dissociation. However, DTA indicates nothing about the kind of change taking place, whether it is a phase change or a chemical reaction, or whether the change takes place in one or several steps. The nature and mechanism of the change can be analysed further by other methods (e.g. x-ray and thermogravimetry).

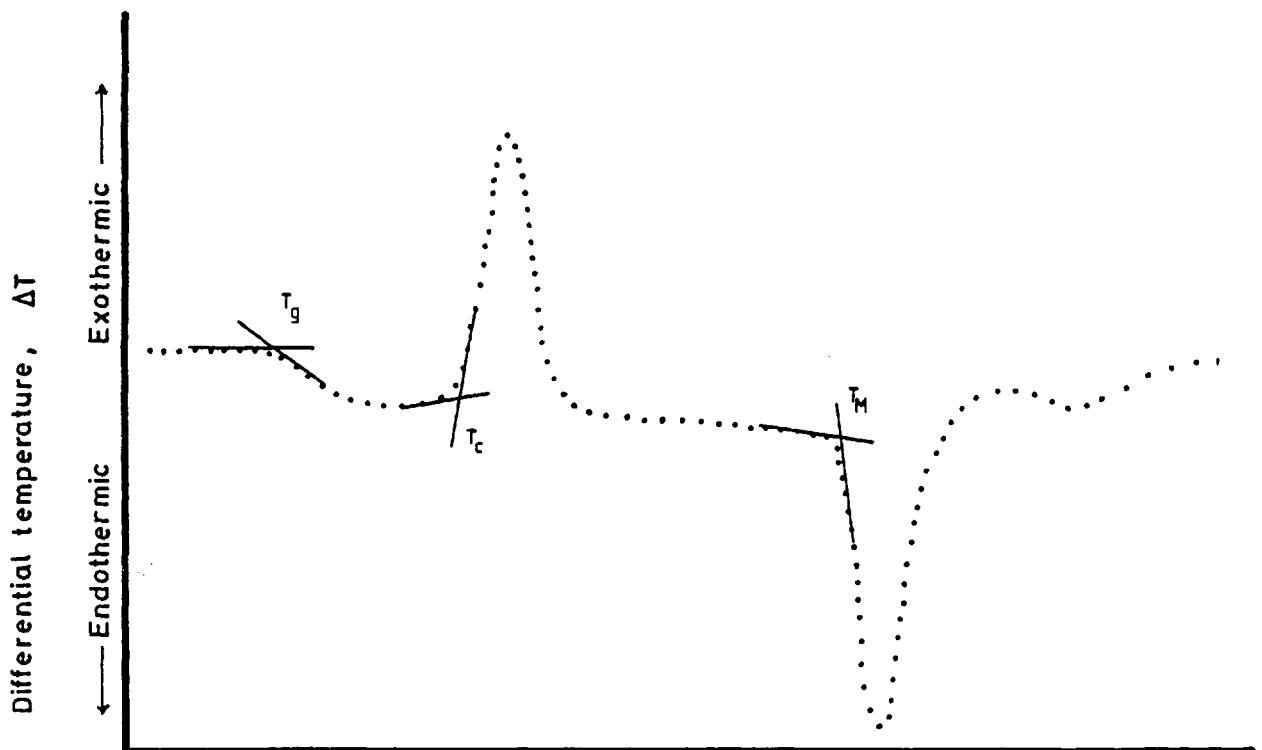
Fig. 3.10a shows a basic DTA circuit. An idealised DTA curve is represented schematically in Fig. 3.10b.  $T_g$  is the glass transition temperature,  $T_c$  corresponds to the temperature of the start of the exothermic effect and  $T_M$  is the melting point of the material. The thermal transitions of the polymers investigated here were studied using the DuPont 900 differential thermal analyser. The polymer samples were contained in a small aluminium pan. The mass of the sample used in the experiment was about 10 mg and the heating rate was  $10^{\circ}\text{C}/\text{min}$ .





R: reference material  
S: sample ; T/C: thermocouple

(a) Basic DTA circuit



(b) Schematic DTA thermogram

Fig. 3.10

### 3.5 INFRARED SPECTROSCOPY

Infrared spectroscopy is the most widely used technique for the identification of polymers. The atoms in a molecule have positive or negative charges. If a characteristic vibration causes a periodic change in the electric dipole moment of the molecule, electromagnetic radiation of the same (infrared) frequency will interact with the molecule. This interaction excites the fundamental vibrational mode and results in a resonant energy transfer in which radiant energy is absorbed by the molecule. Such a fundamental mode is said to be infrared active. When the frequency of the incident energy differs from that of the characteristic vibration, no such transfer occurs and the radiation is not absorbed. The degree of absorption is a function of the change in dipole moment that occurs during a vibration.

The identification of the polymers used in this thesis was done using a Perkin-Elmer infrared spectrophotometer model 580B. The thickness of the samples used was about 15  $\mu\text{m}$ . Figs. 3.11, 3.12, and 3.13 show the spectra of nylon, polyvinyl butyral and polyethylene terephthalate.

Absorption bands in nylons are those corresponding to the C-C, C-H, N-H and C = O bonds. The C-C stretching vibrations produce weak absorptions in the 8.0  $\mu\text{m}$  to 12.5  $\mu\text{m}$  region. Strong absorptions related to the C-H bond appear at 3.4 and 3.5  $\mu\text{m}$  and a weaker one of 6.85  $\mu\text{m}$ . The N-H and C = O absorptions are strong ones characteristic of the amide function, and appear at about 3.0  $\mu\text{m}$  and 6.1  $\mu\text{m}$ .

The polyethylene terephthalate is recognised from the C-O absorption bands at 8.0  $\mu\text{m}$  and 9.0  $\mu\text{m}$ , and the benzene ring substitution band which occurs at 13.8  $\mu\text{m}$  (Haslam et al 1972).

The spectrum of polyvinyl butyral is characterised above all by two very intense band complexes in the 8.9  $\mu\text{m}$  and 10.1  $\mu\text{m}$  regions

(vibrations of the 1,3-dioxane ring). It was found that the polymer contained small amounts of vinyl alcohol units (2.9  $\mu\text{m}$ ) and vinyl acetal structures (5.8  $\mu\text{m}$ ) (Hummel and Scholl 1972).

The transmission spectra recorded from the polymer samples showed good correlation with the previously published spectra for these polymers.

### 3.6 A.C. MEASUREMENTS

Dielectric measurements have been used extensively to investigate molecular motion and behaviour in polymers (McCrum et al 1967, Jonscher 1976). In the present work dielectric loss and permittivity were briefly studied as a function of frequency (500-600 kHz) and temperature (0-120°C). The equipment used consisted of a Wayne Kerr Universal bridge model B224, a General Radio detector type 1232A and a Farrell oscillator model LFM2. All measurements were carried out in the cryostat described in section 3.2.

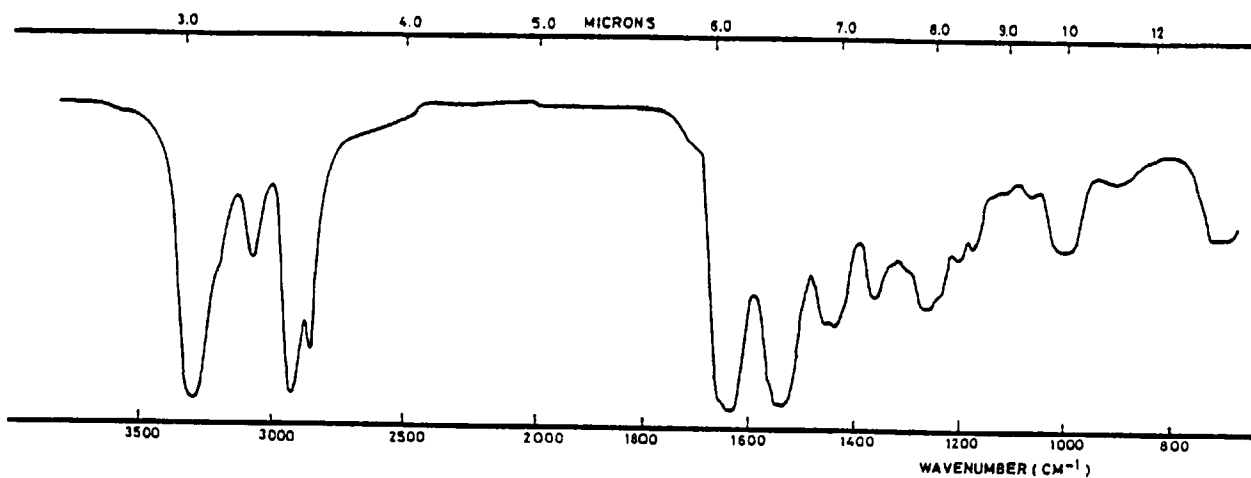


Fig. 3.11: Infrared spectrum of nylon

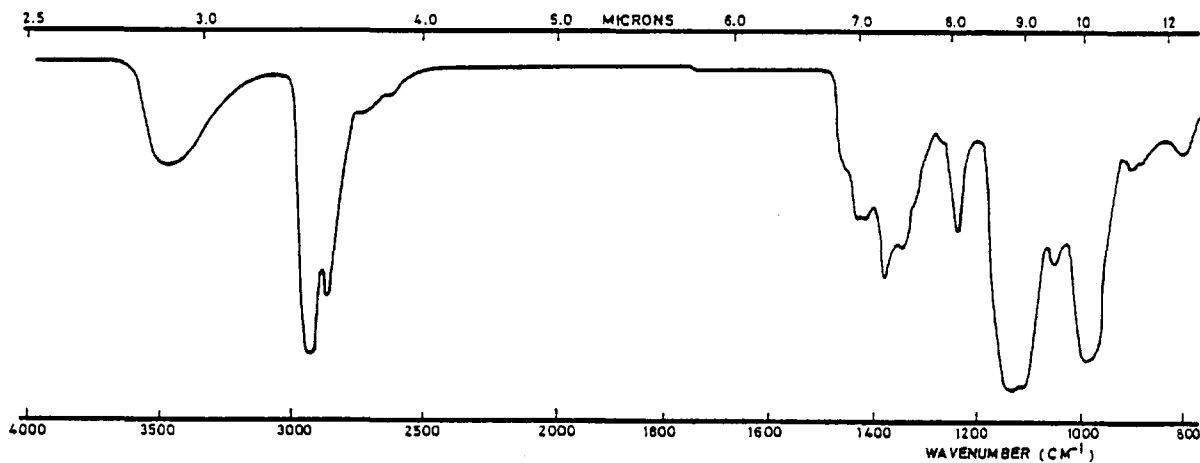


Fig. 3.12: Infrared spectrum of polyvinylbutyral

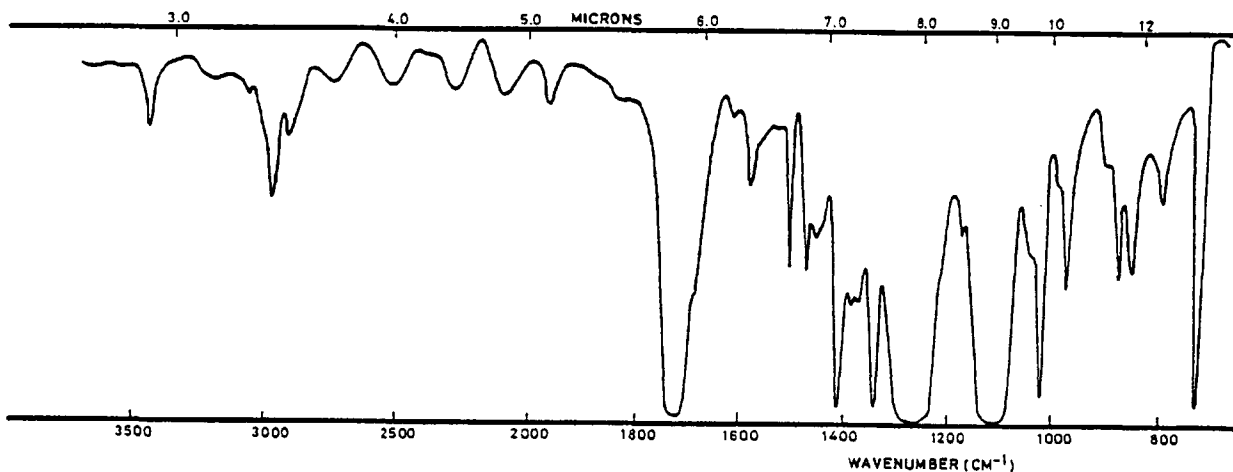


Fig. 3.13: Infrared spectrum of polyethylene terephthalate

CHAPTER IV

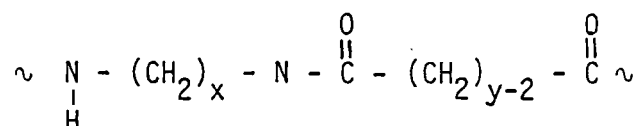
ELECTRICAL CONDUCTIVITY STUDIES ON NYLON

4.0 INTRODUCTION

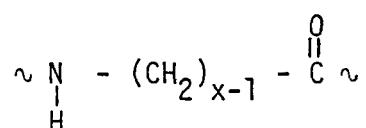
Nylon or Polyamides are important commercially and also from a theoretical point of view. The purpose of this chapter is to present, briefly, an overview of properties of polyamides. Experimental results on the nylon investigated are presented, discussed and compared with previous studies.

4.1 STRUCTURE OF NYLONS

Polyamides, or nylons, are a group of linear high polymers formed by both condensation and in addition polymerisation. The common feature of the many diverse types of nylons is the presence of the amide groups (-CONH) in a chain of methylene groups (-CH<sub>2</sub>-). The general formula for one class of polyamide is



where x and y are variable. The polyamide exhibiting x = 6, y = 6 is conventionally referred to as nylon -66, that of x = 6, y = 10 as nylon -610. Another group of polyamides has the following general structural formula



These polymers are also named by the value of x; x = 6 is referred to as nylon -6.

Table VI gives some formulae of current commercial nylons homopolymers with their respective melting points.

<u>Nylon</u>	<u>Repeat Unit</u>	<u>Tm(°C)</u>
6	$-\text{HN}(\text{CH}_2)_6\text{CO}-$	210 - 225
66	$-\text{HN}(\text{CH}_2)_6\text{NHCO}(\text{CH}_2)_4\text{CO}-$	250 - 260
610	$-\text{HN}(\text{CH}_2)_6\text{NHCO}(\text{CH}_2)_8\text{CO}-$	208 - 220
11	$-\text{HN}(\text{CH}_2)_{10}\text{CO}-$	180 - 190

TABLE VI

Not included in Table VI are the many commercial nylon copolymers (mixtures of nylons 66, 610, etc.), the compositions of which are in most cases proprietary. Among some nylon copolymers are: nylon -66/6, nylon -66/610, nylon -66/6/610, etc.

### The Amide Group

The amide groups of nylons participate in hydrogen bonding, that is, the hydrogen on a nitrogen atom is associated with the oxygen atom of an adjacent molecule. Fig. 4.1 illustrates such a bond.

Hydrogen bonds are relatively strong (Hedvig 1977) (dissociation energy  $\sim 7$  Kcal/mole). They serve to tie the nylon molecules together and play a very important part in the properties of nylons. The permanent dipole moment of the amide group is illustrated in Fig. 4.2.

The resultant orientation of the dipole,  $\theta$ , is of the order of  $56^\circ$  and the resultant dipole moment vector  $\mu$  has a magnitude of 3.7D (Pethig 1979).

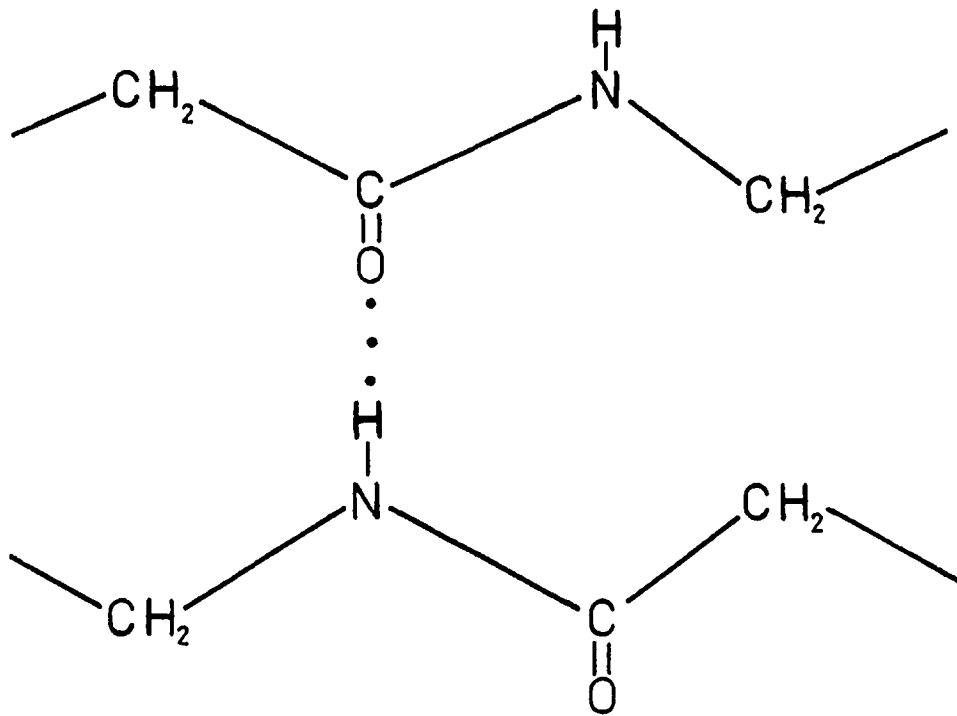


Fig. 4.1: Hydrogen bond linkage between adjacent chains

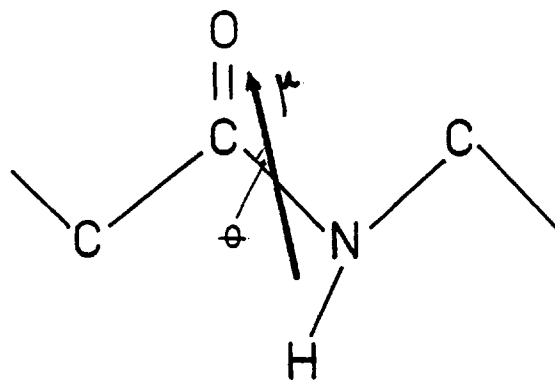


Fig. 4.2: The permanent dipole moment vector of the amide group

### Crystal Structure

Bunn and Garner (1947) first determined the unit cell structure of nylons 66 and 610. The stable structure is the  $\alpha$ -phase, which is comprised of planar sheets of hydrogen bonded molecules stacked upon one another. The molecules are in fully extended zig-zag conformation as shown in Fig. 4.3

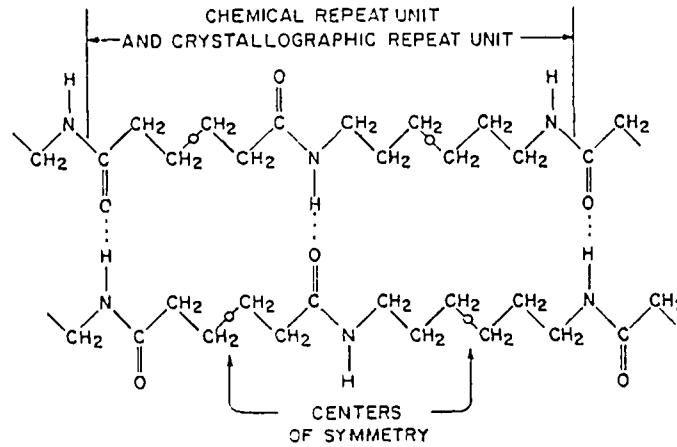


Fig. 4.3: Schematic representation of nylon-66

In crystallographic terminology, the structure is triclinic with one chemical repeat per unit cell. The triclinic is of low symmetry with all axes and interaxial angles unequal. The only symmetry element is a centre of symmetry, which is possessed by the molecule itself (see Fig. 4.3). In both the diamine and the diacid there is a centre of symmetry at the mid-point of the monomer. The arrangement of the chains in the unit cell of nylon-66 is shown in Fig. 4.4(a).

Each chemical repeat unit runs along the c-axis of the cell, but since each segment is shared by four unit cells there is one per unit cell in the crystal. The molecules are hydrogen bonded in the a-c faces of the cell. The hydrogen-bonded sheets are developed by extension of the a-c faces.

Fig. 4.4(b) shows the crystallographic planes of major interest superimposed on the outline of the unit cell of Fig. 4.4(a).

The  $\beta$ -phase, which apparently is not a distinct phase in the thermodynamic sense, amounts to a slight perturbation of the  $\alpha$ -phase.



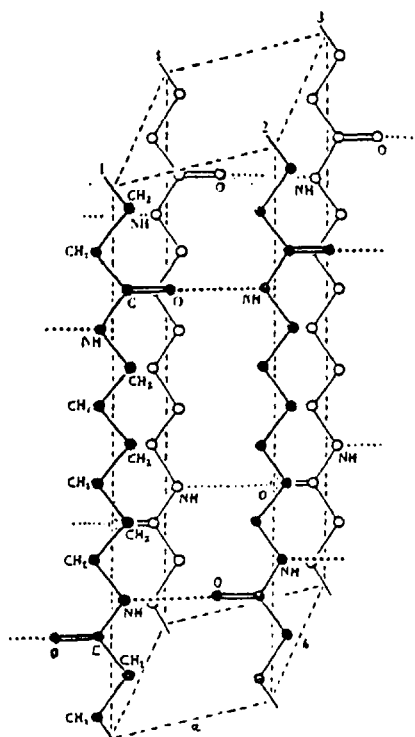


Fig. 4.4(a): Arrangement of molecular chains in nylon-66, poly(hexamethylene adipamide). (Bunn and Garner 1947).

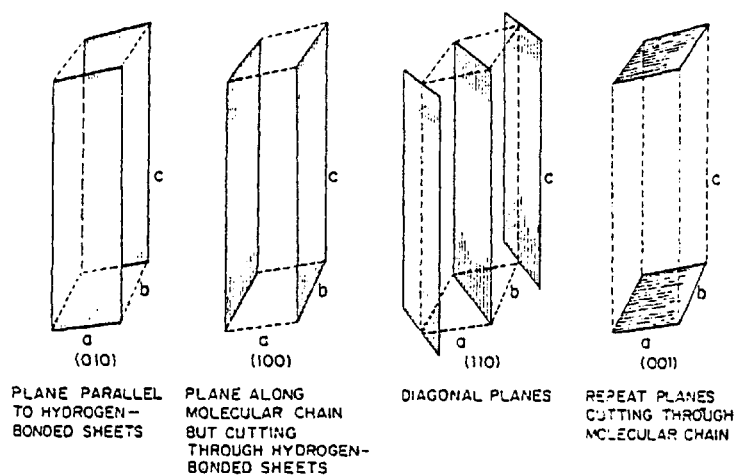


Fig. 4.4(b): Principal crystallographic planes of nylon-66

Nylons 4 and 6 usually crystallise into both the  $\alpha$ - and  $\gamma$ -phases. The hydrogen-bonded sheets of the  $\alpha$ -phase of nylon-6 involve adjacent molecules which have opposite directionality and are said to be antiparallel. Fig. 4.5 shows the  $\alpha$ -phase of nylon-6.

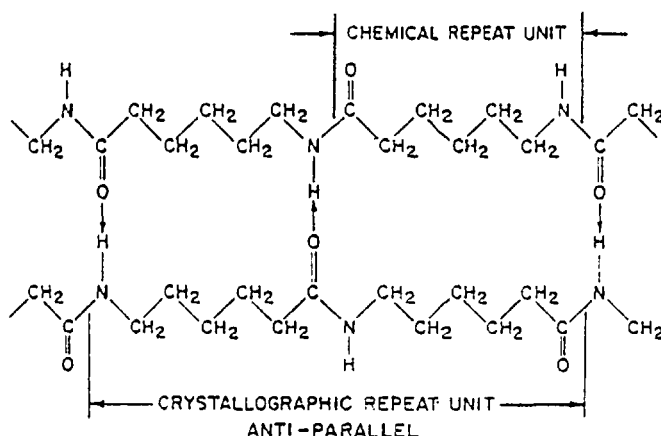


Fig. 4.5: Schematic representation of nylon-6

The hydrogen-bonded sheets are staggered up and down in such a way that the resulting structure is monoclinic instead of triclinic. The  $\gamma$ -phase is pseudo-hexagonal in which the packing of the molecules is such that the location of the molecules can be described by a lattice of hexagonal form but the structure lacks true hexagonal symmetry.

The polyamide investigated in this work has Elvamide (Du Pont) nylon resin. It is a tough and flexible polyamide supplied in granular form. It has excellent resistance to oxygen, alkali solutions, most salt solutions, and most organic solvents-hydrocarbons (including lubricating oils, greases, conventional fuels), ketones, esters, ethers and amides - but is soluble in many alcohols (Du Pont 1976). Elvamide nylon resin is a multicomponent nylon also known as nylon 66/610/6 terpolymer. Multi-ingredient nylons involve more monomers than do copolymers, and such nylons lead to low values of crystallinity. Disordering a given polyamide structure reduces the melting point and broadens the melting range. Crystallisation

of the disordered structure becomes sluggish, nucleation is slow, and the structure quenches to the amorphous state upon rapid cooling from the melt.

#### 4.2 DTA OF NYLON

Differential thermal analysis (DTA) is widely used for studying the thermal transition in nylons and other polymers. Physical and mechanical properties of polyamides are directly related to molecular mobility. The thermal transitions of the nylon investigated in this thesis were studied using the Du Pont 900 differential thermal analyser. The polymer samples were contained in small aluminium dishes. The mass of sample used in the measurements was about 10 mg and the heating rate 10°C/min. The thermograms obtained are shown in Fig. 4.6. Curve (a) refers to the first heating without reaching the melting point of the nylon. The change in the slope of the baseline is associated with the glass transition  $T_g$  in nylon. The value of  $T_g$  obtained was about 57°C. Curve (b) corresponds to a complete heating from about 0°C up to about 180°C. It can be seen that the melting range is rather broad. This is an indication that the material is extremely disordered. The temperature at which the endothermic peak occurs is about 155°C. In curve (c) the sample was run again from 0°C to 180°C after the previous thermal treatment which included the rapid cooling of the sample to 0°C. It can be seen that the nylon shows an exothermic transition above  $T_g$ , having a peak temperature of about 90°C. This crystallisation, well below the equilibrium melting temperature, has been called "Cold Crystallisation" (Ke 1962). This phenomenon is believed to involve the alignment of neighbouring chain segments in the amorphous regions. Such crystallisation occurs without molecular rearrangements and leads to the formation of small crystallites.

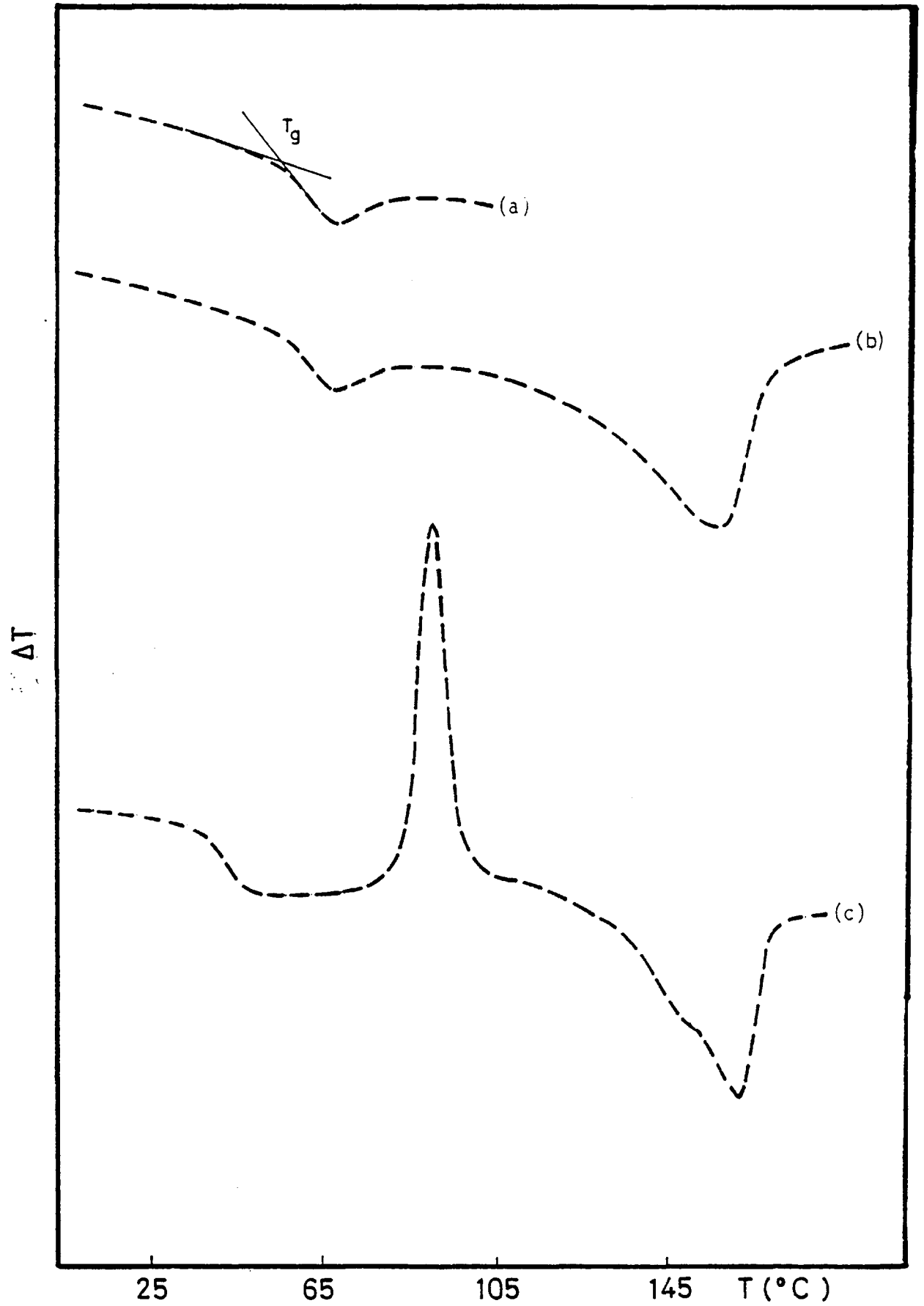


Fig. 4.6: DTA thermogram of nylon

### 4.3 SPONTANEOUS ELECTRIC POLARISATION

#### 4.3.1 Introduction

The existence of a spontaneous electric polarisation in polymeric solids has been shown very recently. In the present investigation, a metal-nylon-metal sandwich has been found to generate electric current for a considerable time (i.e. acting like a current source) while being heated uniformly under short-circuit conditions. Before giving the experimental results of the present study, a brief review of the spontaneous currents found in other polymers will be given.

##### 4.3.1.1 Symmetrical Electrodes ( $M_1$ -Polymer- $M_1$ )

Sacher (1970,1972) has observed that commercial PET films exhibit a spontaneous current, which flows under zero voltage bias on raising the temperature of the sample. The peaks observed were attributed to the depolarisation of dipoles oriented by random local stresses introduced in the manufacturing process.

TSD peaks in unpolarised polyacrylonitrile (PAN) films have been reported by Stupp and Carr (1975). The initial internal field in the solvent-cast samples was explained by assuming a charge gradient along the thickness direction of the film. The origin of the charge gradient was possibly due to the more complete evaporation of the solvent on the surface exposed to the vacuum during casting, as opposed to that on the surface in contact with the bottom electrode.

van Turnhout (1975) has found a parasitic current in PET samples never previously polarised. He attributes its origin to a weak electrochemical potential, which arises in spite of the presence of identical electrodes.

Production of carriers due to chemical degradation of PAN films was observed by Stupp and Carr (1977) at temperatures near 200°C. Chemical

degradation was found to take place asymmetrically in regions near opposite surfaces of solvent cast films.

Spontaneous current emission has been found in polyvinyl chloride (PVC) by Radhakrishna and Haridoss (1978). They have proposed that reorientation of C-Cl dipoles followed by degradation reactions were responsible for the observed currents.

#### 4.3.1.2 Asymmetrical Electrodes ( $M_1$ -Polymer- $M_2$ )

An appreciable open-circuit voltage and short-circuit current have been found by Ieda et al (1975) from  $M_1$ -PET- $M_2$  systems, where a polymer film was sandwiched in between two different metals  $M_1$  and  $M_2$ . They concluded that, if the polymer has at least a partially ionic conduction process the  $M_1$ -PET- $M_2$  system forms a galvanic cell. They suggested that the source of emf was associated with electrode oxidation-reduction processes.

Sawa et al (1977a) have approached the determination of carrier species in organic polymers differently. They used a galvanic cell consisting of the Au-Polymer-Al system. Because they have presented results on Nylon 66, their method will be described and adopted to explain the observed effect in the nylon films studied in this research. Initially they consider the  $M_1$ -Polymer- $M_2$  system as a galvanic cell, the equivalent circuit of which is shown in Fig. 4.7

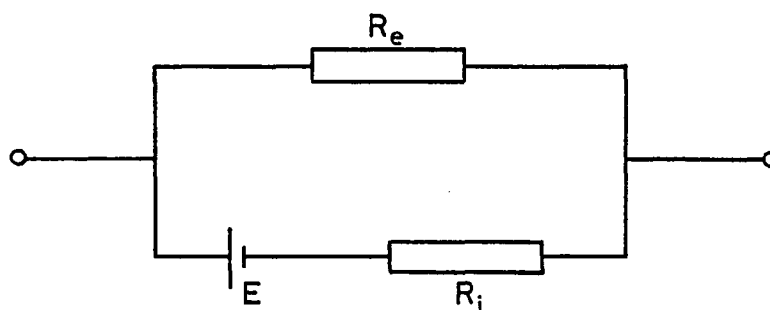


Fig. 4.7: The equivalent circuit for the  $M_1$ -Polymer- $M_2$  system.  $E$  is the electromotive force and  $R_i$  and  $R_e$  are resistances originating from the ionic and electronic contribution.

The open-circuit voltage  $V_o$  and the short-circuit current  $I_s$  can be measured by using an electrometer, as illustrated in Fig. 4.8a.

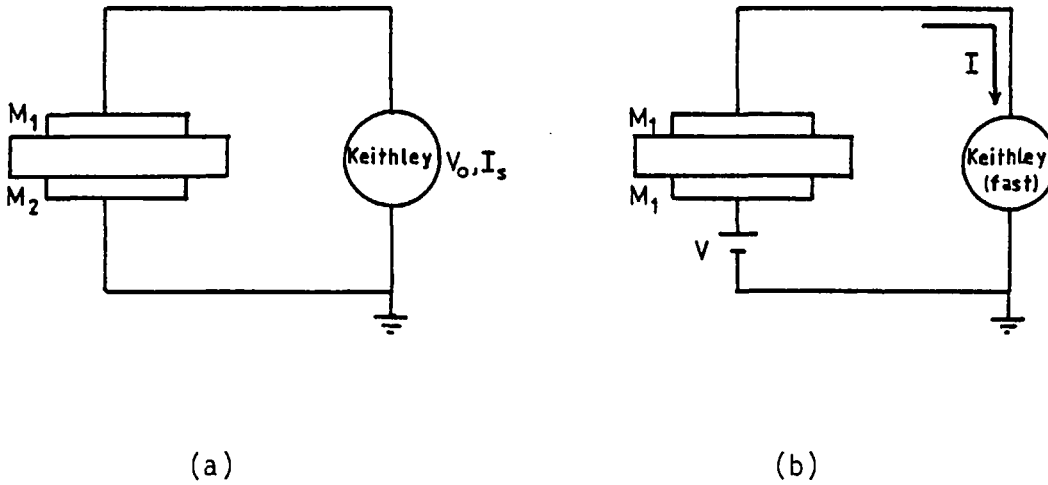


Fig. 4.8: Schematic diagrams of the measuring circuit (a) for the short-circuit current,  $I_s$  and open-circuit voltage,  $V_o$  and (b) for conduction current.

The open-circuit voltage,  $V_o$  is given by

$$V_o = \frac{R_e}{R_i + R_e} E \quad (4.1)$$

Assuming negligible the input impedance of the electrometer in the feedback mode, the short-circuit current,  $I_s$  is given by

$$I_s = \frac{E}{R_i} = \frac{R_i + R_e}{R_i R_e} V_o \quad (4.2)$$

On the other hand, when an external voltage,  $V$  is applied to the M<sub>1</sub>-Polymer-M<sub>1</sub> system, where the polymer is sandwiched between two identical metals M<sub>1</sub>, the conduction current  $I$  is given as (see Fig. 4.8b)

$$I = \frac{R_i + R_e}{R_i R_e} V \quad (4.3)$$

Two extreme cases can occur depending upon whether  $R_i$  is greater or smaller than  $R_e$ . By using eqns. (1) - (3), the following relations shown in Table VII can be obtained.

$R_i \gg R_e$ (Electronic)	$R_e \gg R_i$ (Ionic)
$V_o \approx \frac{R_e}{R_i} E$	$V_o \approx E$
$I_s \approx \frac{E}{R_i}$	$I_s \approx \frac{E}{R_i}$
$I \approx \frac{V}{R_e}$	$I \approx \frac{V}{R_i}$

Table VII: Schematic diagram for determining the predominant carrier species using the galvanic cell.

For a general cell reaction



the electromotive force is given by (Ruoff 1973)

$$E = E^\circ - \frac{RT}{nF} \ln \frac{A_M^m A_N^n \dots}{A_A^a A_B^b \dots} \quad (4.5)$$



where  $A$  is the activity coefficient,  $R$  the gas constant,  $F$  the Faraday constant,  $n$  the number of electric charges taking part in the cell reaction and  $E^0$  is the standard emf of the cell. The change in  $E$  with temperature variation is usually very small as compared with the resistance  $R_i$  due to the ionic carriers. For the sake of simplicity, it is assumed that  $E$  is constant for temperature and  $R_i$  is expressed as

$$R_i = R_{i0} \exp(A/kT) \quad (4.6)$$

where  $A$  is the activation energy and the other symbols have their usual meaning.

It can be concluded from Table VII that, if the ionic conduction is predominant ( $R_i \ll R_e$ ),  $V_0$  is almost independent of temperature and the temperature characteristics of  $I_s$  and  $I$  are identical, since the change in  $E$  with temperature is small. In the case of predominance of electronic conduction,  $V_0$  depends upon temperature and varies according to the temperature dependence of  $R_e/R_i$ . Also,  $I_s$  and  $I$  are different in activation energy.

Electrochemical effects as a source of emf in  $M_1$ -PET- $M_2$  have been studied by Vijn (1979). He proposes that the negative electrode of this battery reacts with water to form a metal oxide and protons. The protons thus released would be injected into PET as conducting species.

In another paper on the battery effect in PET, Crine et al (1979a) have expressed dissatisfaction with the previous model and propose that protons in PET are rather liberated by residual acid groups ( $\text{RCOOH} \rightarrow \text{RCOO}^- + \text{H}^+$ ) at about 80°C. The activation energy measured in their study was 1.38 eV.

#### 4.3.2 Experimental Results and Discussion

The purpose of this section is to present some experimental data concerned with the generation of spontaneous currents and open-circuit voltages in virgin polyamide films. The term 'virgin' film means in this context a sample which has never been electrically treated. Some models will be given to explain the observed behaviour. Once again, as done before, two systems will be discussed separately, i.e. symmetrical and asymmetrical electrodes.

##### 4.3.2.1 Symmetrical Electrodes

The polymer films used in the present experiment were prepared as described in Chapter III and the measurements were carried out in the vacuum cryostat. A great number of nylon films (about 120) were prepared in the course of the experiments. They were provided with similar metal electrodes (aluminium or gold) as explained in Chapter III. Only virgin devices were investigated in the present study. That means that the devices were not checked for continuity using an AVOM for example, so as not to introduce any electrical perturbation to the film. Numerous devices were faulty (short-circuited) when they were first placed in the cryostat. Pin-holes probably existed in the nylon film before evaporating the top electrode. These faulty devices were not used in the measurements. All the "good" devices investigated in this work revealed spontaneous currents when they were first heated in short-circuit conditions. It is worth mentioning that many devices failed during the heating process. The maximum value of the short-circuit current obtained at high temperature varied from sample to sample, but it sometimes reached the value of about  $1 \times 10^{-6}$  A.

Solvent-cast nylon films showed very complex initial internal fields. Figs. 4.9, 4.10 and 4.11 show some typical examples of the types

of spontaneous currents found when the nylon was sandwiched between similar electrodes. The peak found in Fig. 4.9 at about 60°C will be shown to correspond to the  $\alpha$  relaxation of the nylon, i.e. the glass transition  $T_g$  (section 4.5.3). The dipole alignment possibly stems from the way in which the sample is prepared. It is thought that the polymeric chains are preferentially oriented in the plane of the film by the solvent cast process, as proposed by Prest and Luca (1980). According to them the alignment of molecular segments occurs as the result of the competing effects of the rapidly increasing relaxation times of the concentrating solution (i.e. drying solution) and the time scales of the contracting process. It can also be seen in Fig. 4.9 that the short-circuit <sup>current</sup> during the second run was rather small.

Hot-pressed nylon films were also investigated. Figs. 4.12 and 4.13 show two typical examples of the spontaneous current generated when the device was first heated at a constant rate. The peak in Fig. 4.12, occurring in the region of 50°C, has a magnitude smaller than that of Fig. 4.9. The reason for that is probably due to the fact that dipole orientation occurs to a larger extent in solvent cast films.

The other high temperature peaks occurring above 60°C in Figs. 4.9, 4.10, 4.11 and 4.12 resemble the peaks found during the depolarisation process of the nylon electrets, as will be explained later on (sections 4.5.4 and 4.5.5). It is believed that those peaks have their origin in initial space charges embedded in the film. One manner in which a distribution of space charges inside a film could produce an external current is as follows. Let us consider a charge carrier  $q$  at  $x = x_0$  in a film of thickness  $d$ , as shown in Fig. 4.14.

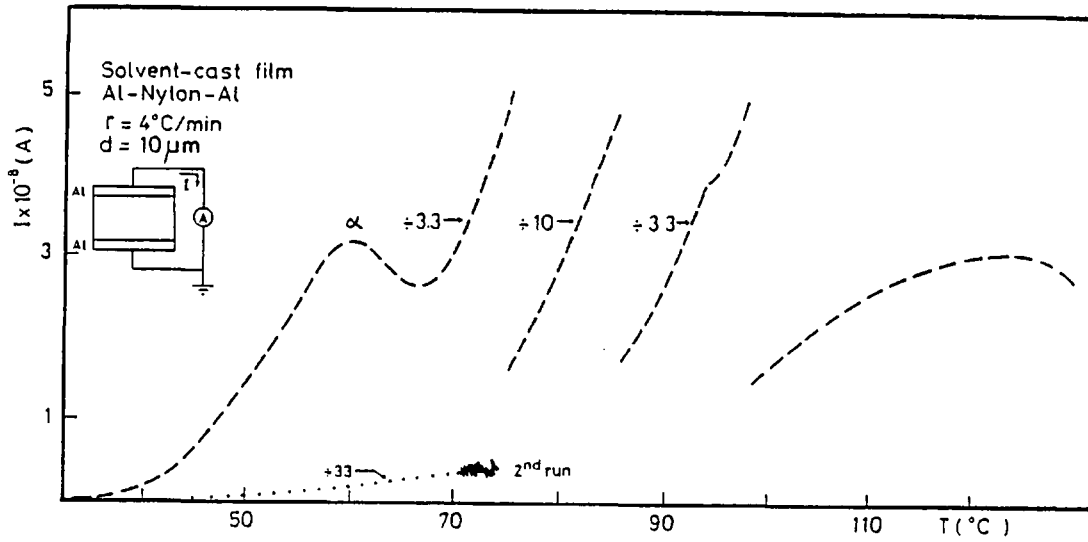


Fig. 4.9: Spontaneous current emission in solvent cast nylon film sandwiched between similar electrodes during the first and second heating.

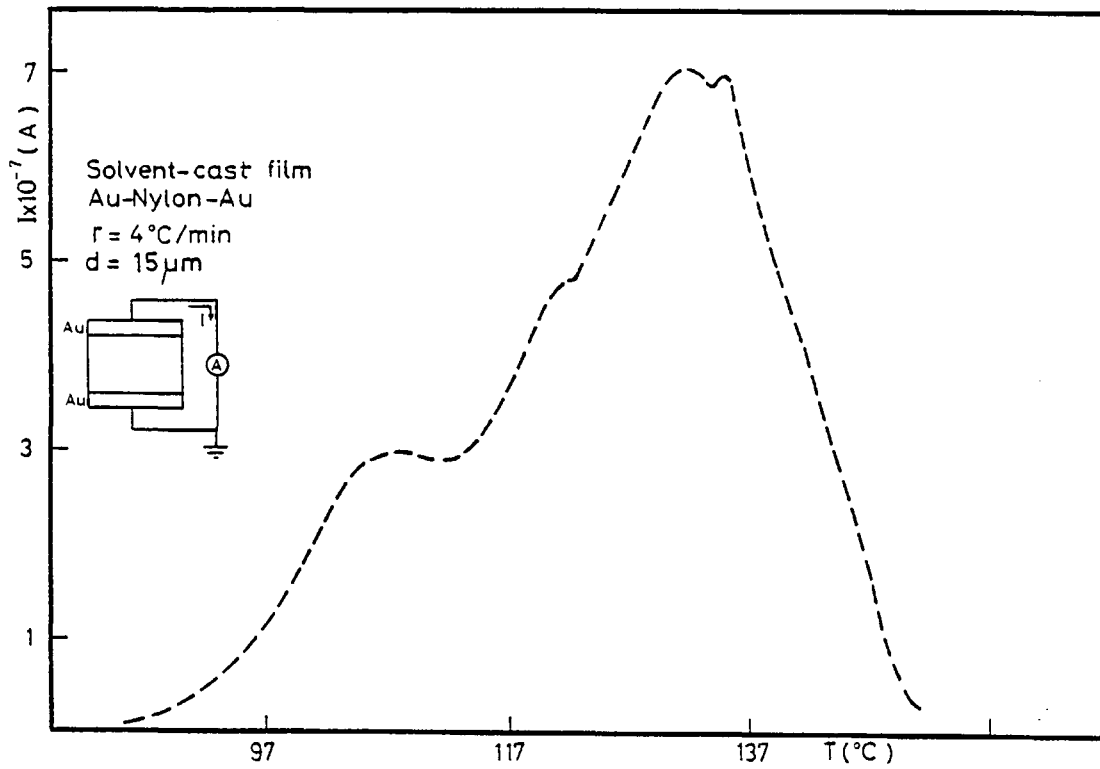


Fig.4.10: The short-circuit current from Au-nylon-Au system

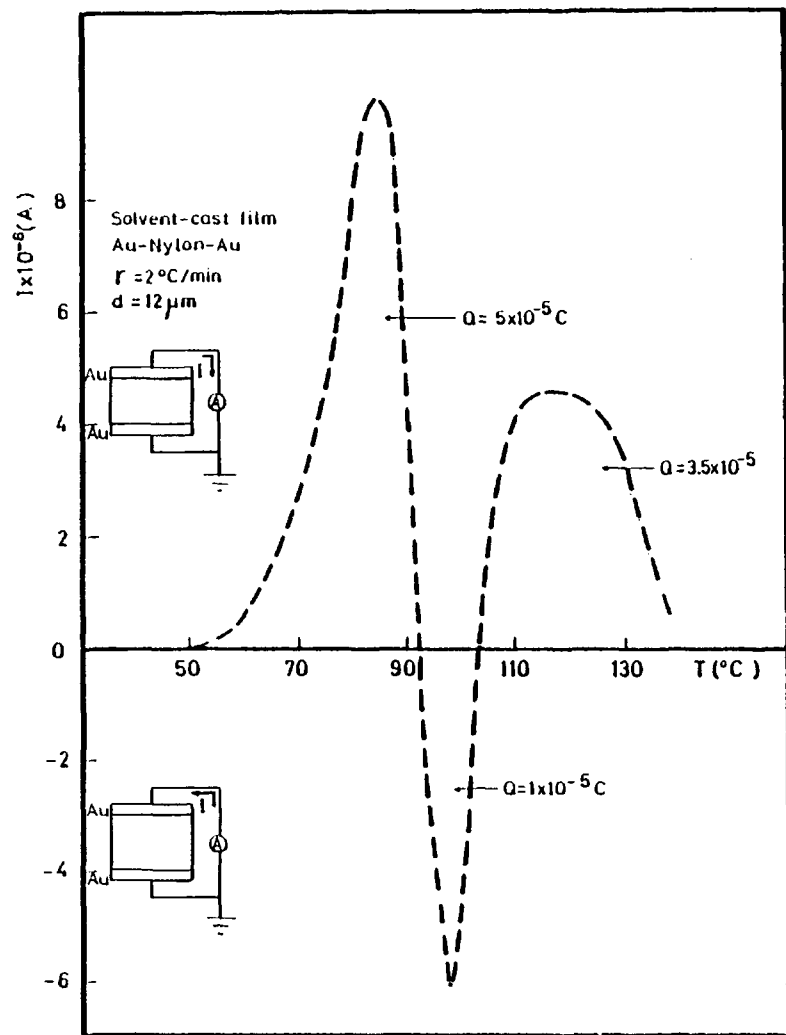


Fig. 4.11: The short-circuit current of unpolarised nylon film. The presence of peaks indicates that the polymer is initially not electrically isotropic.

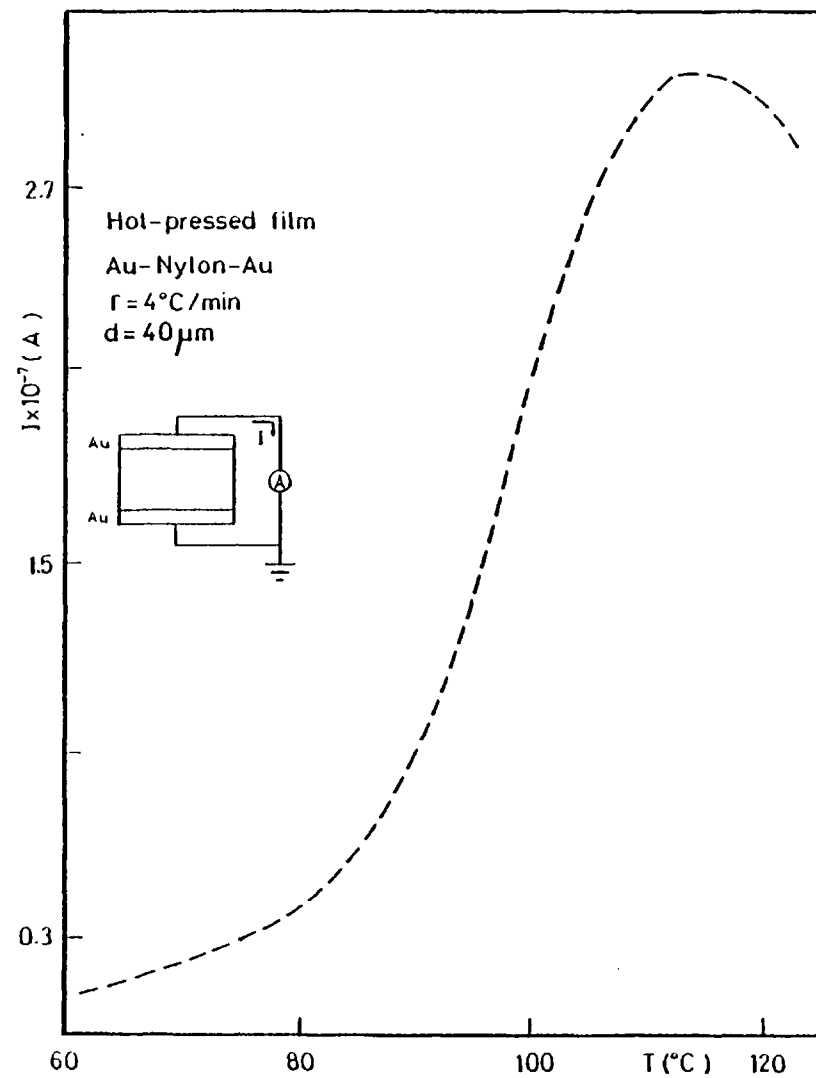


Fig. 4.12: Spontaneous current generation from a hot-pressed nylon film using Au electrodes.

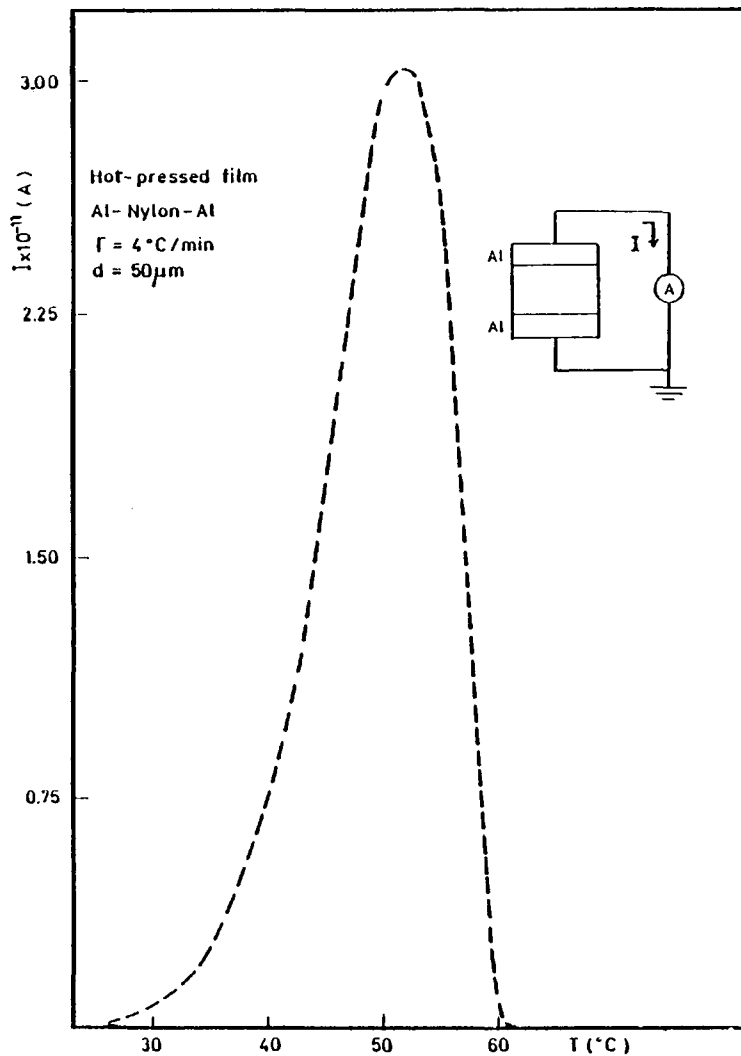


Fig. 4.13: Short-circuit current for a virgin sample of hot-pressed polyamide. Al electrodes.

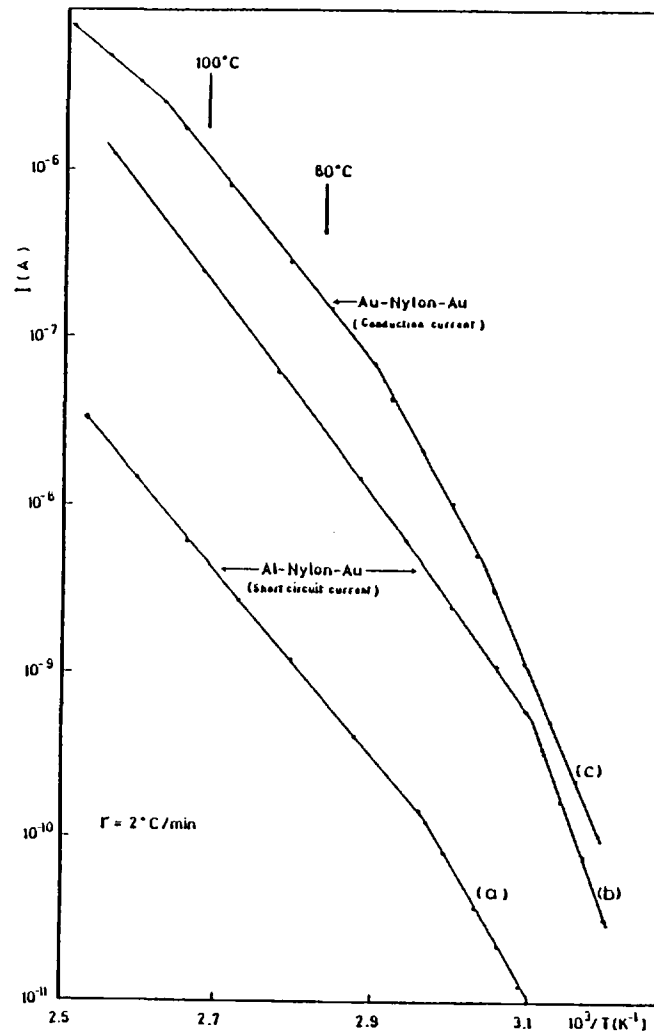


Fig. 4.16: Temperature dependence of the short-circuit current and the conduction current. Curves a and b correspond to hot-pressed and solvent cast nylon films respectively.

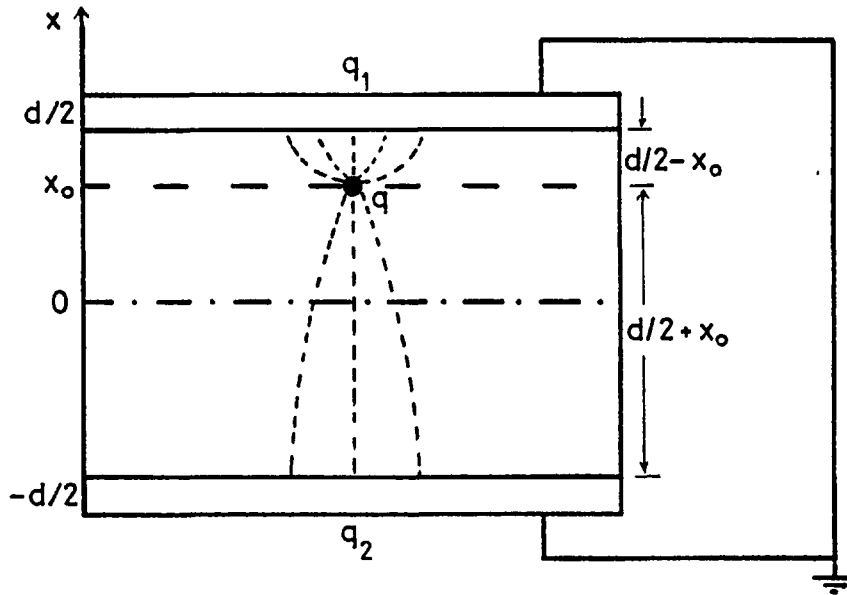


Fig. 4.14: Charge carrier  $q$  embedded in a polymer film

When the electrodes on the film are short-circuited, induced charges on electrodes,  $q_1$  and  $q_2$ , are given by

$$q_1 = -q \frac{C}{C_2} \quad q_2 = q \frac{C}{C_1} \quad , \quad q = -(q_1 + q_2)$$

where  $C$  is the capacitance between the electrodes,  $C_1$  is the capacitance between the upper electrode and the plane  $x = x_0$ , and  $C_2$  is the capacitance between the lower electrode and the plane  $x = x_0$ . When the polymer film is heated to high temperatures the charge  $q$  attains a sufficiently higher mobility, and moves towards the nearest electrode by the Coulomb attraction force of the induced charge. This motion changes  $x_0$  and hence  $q_1$ , producing an external current. A complicated initial space charge distribution in the film could make the short-circuit current first positive and then negative or vice versa.

A possible source of initial charges might be from impurities such as fragments of a polymerisation catalyst, absorbed water, and

degradation or dissociation products of the polymer itself. Protons are likely to participate in that charge distribution. There are two potential sources of protons: traces of water and self-ionisation of amide groups (Eley 1968).

It might be relevant to note here that charge separation occurs in dielectrics during changes of phases by the Costa Ribeiro effect (Costa Ribeiro 1943). So it is plausible that during the process of solidification from solution, charges are separated and the polyamide film ends up as an electret.

In summary, it can be stated, according to the experimental results obtained, that the polyamide films form a mechanoelectret in the process of preparation of the films.

#### 4.3.2.2 Asymmetrical Electrodes

When different kinds of electrodes are used on each side of the nylon film, the device behaves completely differently. The magnitude of the spontaneous current was rather large and it became reproducible in successive heating runs. Again, virgin samples were investigated and the way the devices were prepared was the same as the one explained in Chapter III. Aluminium and gold were used as metal electrodes (Silver dag and Aquadag were also tried to a lesser extent). It was found that the direction of the current was only determined by the combination of the metal electrodes. Fig. 4.15 illustrates the direction of the short-circuit current  $I_s$  obtained for the devices Au-nylon-Al and Al-nylon-Au. It can be seen that the short-circuit current flows in opposite directions when the electrodes are interchanged.



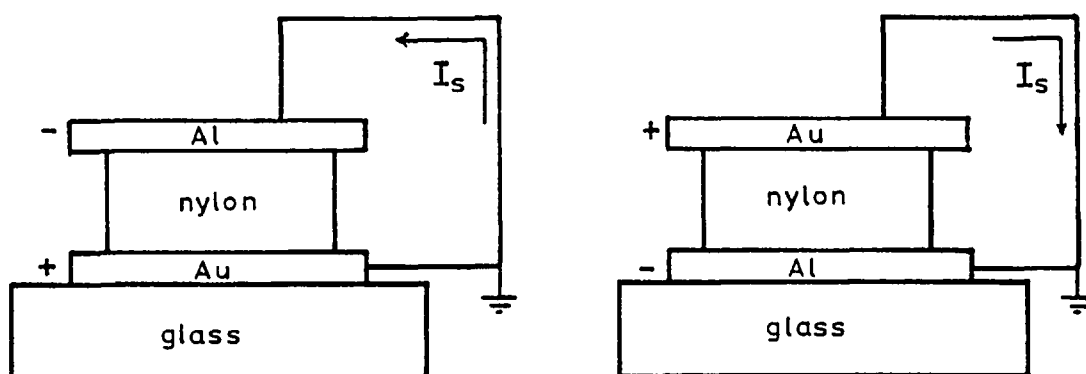


Fig. 4.15: Schematic diagram showing the direction of the short-circuit current,  $I_s$  for Al-nylon-Au and Au-nylon-Al structures.

This experiment indicates that the current is not due to the anisotropic properties of the nylon film or to a temperature gradient across the sample.

Typical log currents under short-circuit conditions as a function of  $1/T$  from the asymmetrical devices are shown in Fig. 4.16, (p.110). Curves (a) and (b) correspond to hot-pressed and solvent-cast nylon films respectively. It was also found that the direction of the current remains the same for heating as well as cooling. To obtain an indication of the amount of charge released from an Al-nylon-Au device, it was placed in an air oven at a temperature of  $70^\circ\text{C}$  and short-circuited. The short-circuit current,  $I_s$  was measured at regular intervals for one month. Fig. 4.17 gives the results obtained for two devices. The total charge released during that time was about 5 mC.

Another similar experiment was performed in vacuum. The device (Al-nylon-Au) was heated in short-circuit condition at  $4^\circ\text{C}/\text{min}$  and when the temperature was about  $85^\circ\text{C}$ , the heating was stopped and the temperature

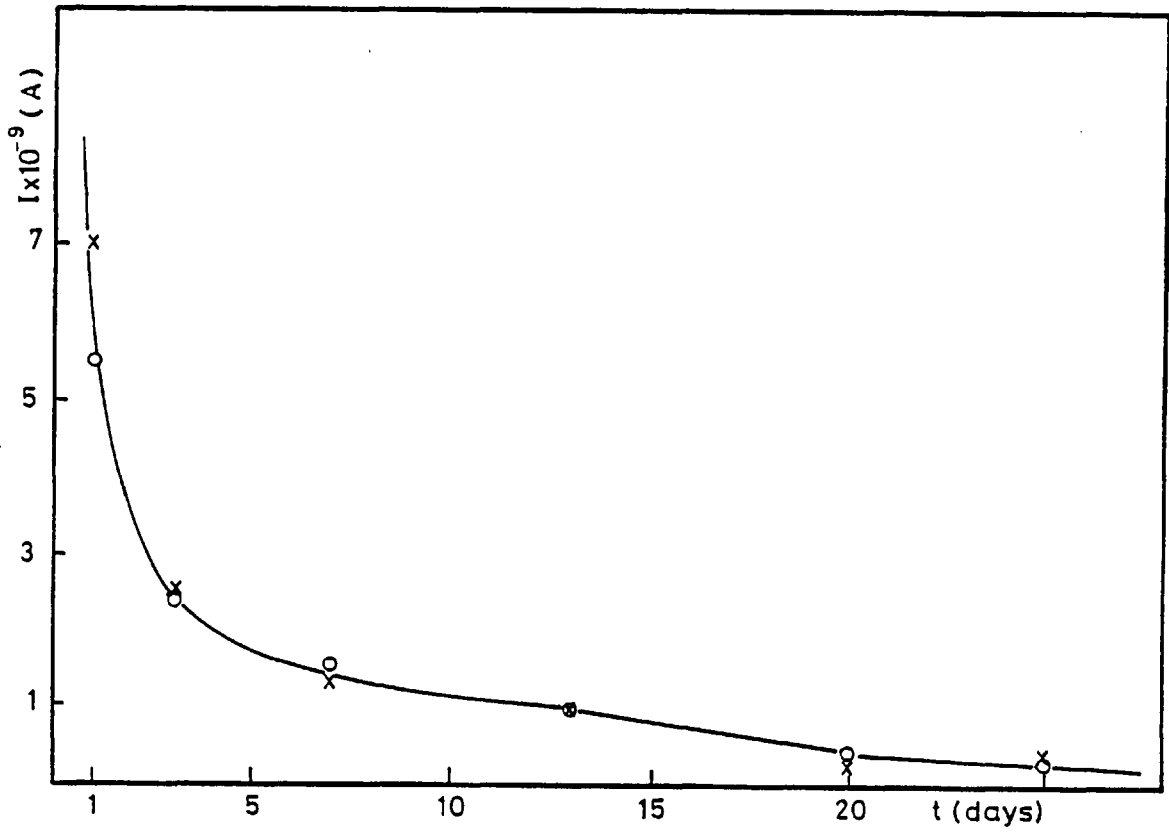


Fig. 4.17: Short-circuit current of two Al-nylon-Au devices at 70°C as a function of time. Thickness 12  $\mu\text{m}$

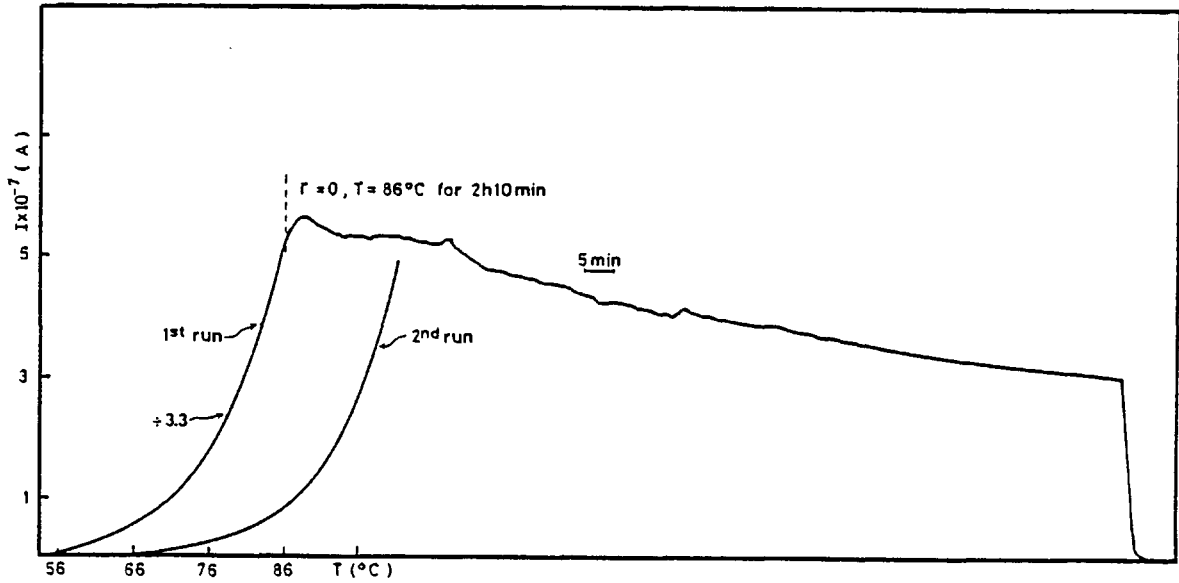


Fig. 4.18: Reversibility of the short-circuit current in an Au-nylon-Au device. Thickness 10  $\mu\text{m}$

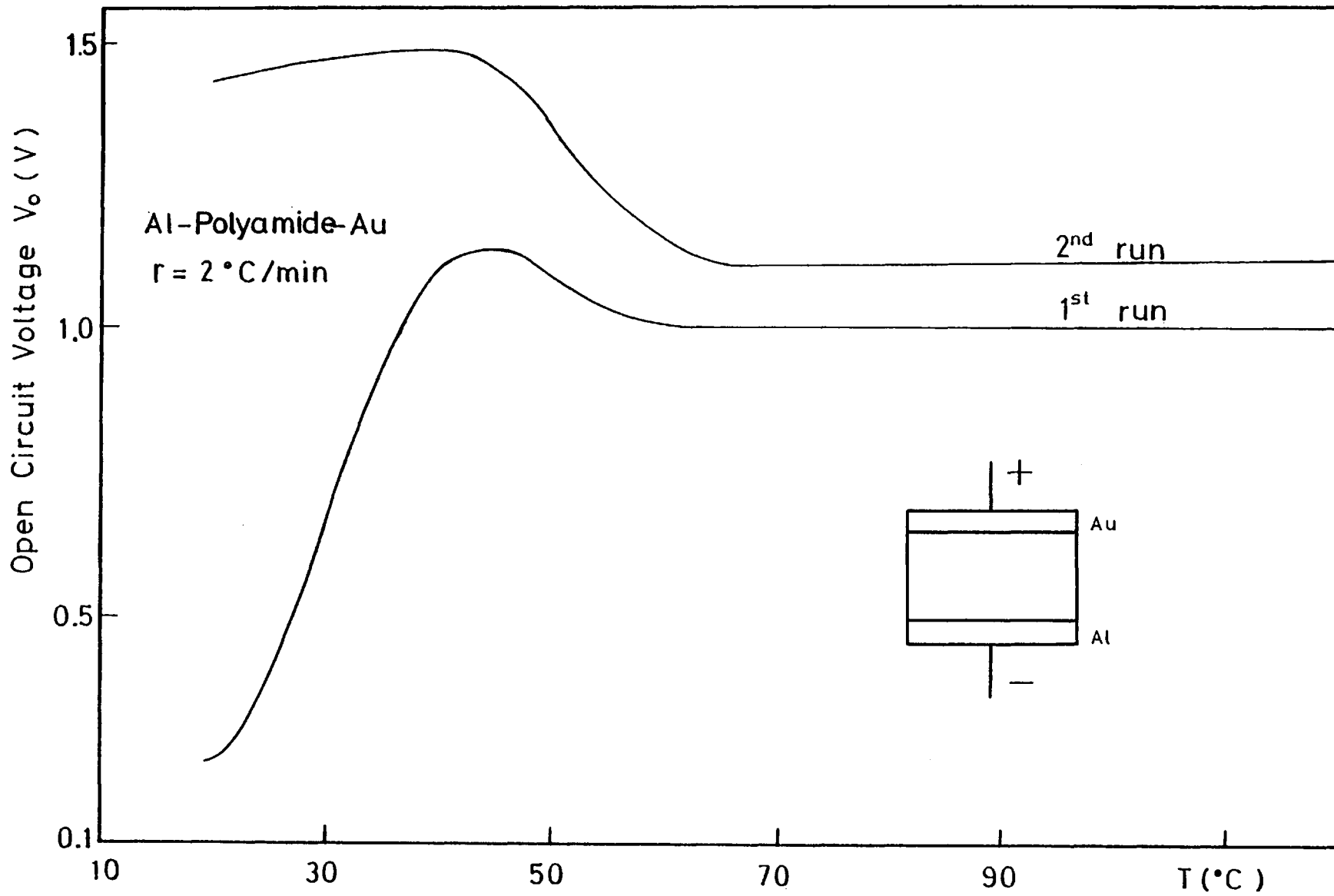


Fig. 4.19: The open-circuit voltage  $V_o$  as a function of temperature. Thickness  $10\ \mu\text{m}$ .

was maintained constant for 2 h 10 min. During that time the current was recorded as a function of time. The charge released during this time was about 3 mC. After that period of time the sample was cooled down and another run was done. The experimental results are shown in Fig. 4.18. As can be seen the device still gives a large current during the next run.

The variation of the open-circuit voltage  $V_0$  as a function of temperature was also investigated. A typical result is shown in Fig. 4.19. During the first heating run the value of  $V_0$  rose with ascending temperature from room temperature to about 45°C. From 45 to 70°C  $V_0$  dropped slowly and was constant after 70°C. In the next heating run  $V_0$  was almost constant from room temperature up to about 45°C. From 45 to about 60°C  $V_0$  dropped to about 1.1V and remained constant after that as the temperature increased.

Silver dag and Aquadag electrodes were also used in combination with aluminium. The following structure was prepared: an ultrasonically cleaned microscope slide was provided with an aluminium electrode and the nylon film was prepared by casting the polymer solution using the wire-wound bar as explained in Chapter III. Four silver dag electrode strips of dimensions  $20 \times 50 \text{ mm}^2$  were painted on the polymer surface. Three of these structures were connected as shown in Fig. 4.20.

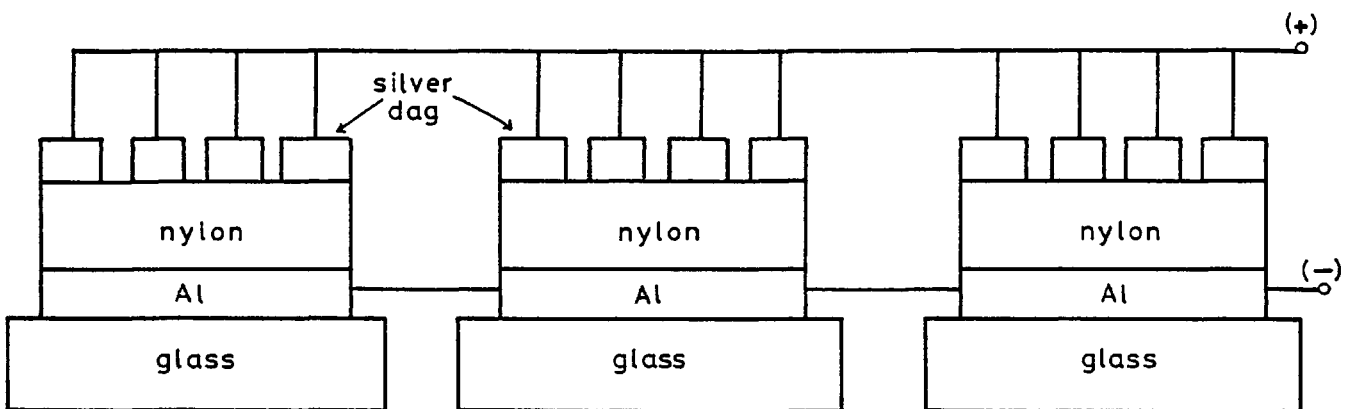


Fig. 4.20: Twelve parallel arrangements of silver dag-nylon-Al devices

The open-circuit voltage  $V_o$  measured at room temperature was 1.3V. The parallel arrangement was placed inside an air oven and heated in short-circuit conditions to about 120°C. After that, the devices were cooled to about 80°C. The open-circuit voltage, the initial short-circuit current, and the 3 and 10 minutes short-circuit currents were measured at that temperature. The results obtained are shown in Table VIII.

t(min)	$V_o$ (V)	$I_s$ ( $\times 10^{-5}$ A)
0	1.3	3.00
3	1.3	2.50
10	1.3	2.35

Table VIII:

It can be seen in Table VIII that the short-circuit current was rather large and that it decayed very slowly. The amount of charge released after 10 minutes was about 10 mC. Aquadag electrodes gave a lower performance when compared with silver dag. The external current released by the device Aquadag-nylon-Al was about 200 times lower than the silver dag-nylon-Al device.

Various kinds of origins of short-circuit currents in polymers have been reported in the past (Sawa et al 1977b). Table IX summarises these. A brief discussion will be given of each of these mechanisms. If a thermal gradient exists across the polymer film, charge carriers are expected to move (thermoelectricity). Because the short-circuit current measured changed direction when the Al and Au electrodes were interchanged (see Fig. 4.15), it seems that the current has no relation with the thermoelectric effect.

Nature	Condition required for generating the current	Origin
Thermoelectric	Temperature gradient	Thermo e.m.f.
Pyroelectric	Time variation of temperature	Temperature dependence of spontaneous polarisation (reversible)
Piezoelectric	Time variation of mechanical stress	Piezoelectric effect
Electrochemical	Film sandwiched between dissimilar metal electrodes	E.m.f. of cell

Table IX: Origin of short-circuit current in polymer films during heating

Pyroelectricity is the name given to the effect that is observed in certain materials which exhibit a change in polarisation when the temperature is raised. This effect is reversible and the direction of the current during heating is opposite to that of cooling. The present experimental results do not satisfy the second requirement because the short-circuit current does not change direction when the sample is cooled. Also, pyroelectric polymers are always previously polarised so that the effect is observed (poling process). The nylon films studied here have never been treated electrically.

Piezoelectricity has been reported to occur in polymers, either in bending, in elongational or in compressional conditions (Fukada and Furukawa 1981). Since none of these conditions occurred to the film, this mechanism can also be excluded.

As has been found experimentally, the short-circuit current observed in the devices has the following characteristics: (i) the current

flows from gold to aluminium through the external circuit and (ii) the direction of the current is always the same irrespective of whether the film is heated or cooled. These features agree well with the electrochemical mechanism as suggested by Ieda et al (1975). The present experimental results are interpreted as being due to the e.m.f. of the cell.

The model proposed by Sawa et al (1977a), which was discussed in section 4.3.1.2, to determine the carrier species in the galvanic cell was applied to the nylon studied in the present research. A symmetrical device (Au-nylon-Au) was prepared and the conduction current under an externally applied voltage of 2V was measured as the temperature was raised at 2°C/min. Curve (c) in Fig. 4.16 shows the temperature dependence of the conduction current  $I$ . Comparing curves (a), (b) and (c) in Fig. 4.16, it can be seen that between 80 and 100°C approximately the activation energy of the conduction current  $I$  shows good correlation with that of the short-circuit current  $I_s$ . The values of the activation energies measured for  $I$  and  $I_s$  were 1.15 and 1.20 eV respectively. The temperature dependence of the open-circuit voltage  $V_0$  given in Fig. 4.19, shows that  $V_0$  is constant above 70°C. Therefore it can be said, according to Table VII, that in the temperature region of 80-100°C the carrier species are ionic.

#### 4.3.3 Conclusions

It has been experimentally deduced that nylon films sandwiched in between dissimilar metal electrodes form a galvanic cell. In the temperature region of 80-100°C the predominant carrier species are ions because: (i)  $V_0$  is independent of temperature and (ii) the activation energies of the conduction current  $I$  and the short-circuit current are almost the same.

#### 4.4 D.C. CONDUCTION

This section deals with the conductivity measurements which were carried out at the very beginning of this research. Because transient electric currents flow from polymers under application or removal of an electric field, a brief discussion of these transients will be presented first. Experimental results will be given and compared with previous results on the nature of the d.c. conductivity in polyamides.

##### 4.4.1 Introduction

As was mentioned in Chapter I, transient charging and discharging currents occur in polymers after the application or removal of a step voltage. Fig.4.21a shows a schematic behaviour of these transient currents. According to the superposition principle, the discharge current is given by

$$I_d(t) = I_c(t) - I_c(t - t_c) \quad (4.7)$$

where  $t_c$ , the charging time, is an important factor for the correct determination of the discharging current. Assuming the Curie-von Schweidler law for the charging current, i.e.  $I_c \propto t^{-n}$ , it can be shown that the ratio of the error introduced into the measured discharge current to the true discharging current is given by

$$\frac{I_c(t)}{I_c(t+t_c)} = (1 + t_c/t)^{-n} \quad (4.8)$$

where  $t$  is now measured from the moment the sample is discharged. If  $t$  is one-tenth of the charging and  $n = 0.6$ , the percentage of error introduced in the measured discharge current is as high as 24%. It is important therefore to choose adequate charging time so as to keep the error low when making discharge currents.



#### 4.4.2 Hamon Approximation

Hamon (1952) has given an approximate method for deducing dielectric loss factor of a solid dielectric from the charging current that flows after the sudden application of a direct voltage,  $V$ . The theoretical equations for the permittivity  $\epsilon'(w)$  and dielectric loss factor  $\epsilon''(w)$  in terms of the transient current  $I(t)$  are

$$\epsilon'(w) - \epsilon_{\infty} = \int_0^{\infty} \phi(t) \cos wt \, dt \quad (4.9)$$

$$\epsilon''(w) = \int_0^{\infty} \phi(t) \sin wt \, dt \quad (4.10)$$

where  $\phi(t) = I(t)/C_G V$ ,  $C_G$  is the geometrical capacitance,  $t$  time and  $w$  the angular frequency ( $2\pi f$ ).

Many workers have found that  $\phi(t)$  can be approximated over a wide range of values by the empirical equation  $\phi(t) = At^{-n}$ , where  $A$  and  $n$  are constants for a given material. Placing  $\phi(t) = At^{-n}$  in eqn. (4.10) gives

$$\epsilon''(w) = Aw^{n-1} \Gamma(1-n) \cos n\pi/2, \quad 0 < n < 2 \quad (4.11)$$

where  $\Gamma(1-n)$  is the gamma function. Hamon expressed eqn. (4.11) in terms of  $\phi(t_1)$  at a particular time  $t_1$  as

$$\epsilon''(w) = \phi(t_1)/w \quad (4.12)$$

provided that  $w$  and  $t_1$  are related thus

$$wt_1 = [\Gamma(1-n) \cos n\pi/2]^{-1/n} \quad (4.13)$$

The expression on the right-hand side of eqn. (4.13) is almost independent of  $n$  in the range  $0.3 < n < 1.2$ , and, to an accuracy within  $\pm 3\%$ , can be taken as having the mean value 0.63. Then eqn. (4.12) takes the simple form

$$\epsilon''(\omega) = \phi(0.63/\omega)/\omega \quad (4.14)$$

or, alternatively

$$\epsilon''(\omega) = \phi(0.1/f)/2\pi f \quad (4.15)$$

Eqn. (4.15) can be expressed in terms of the transient charging current  $I(t)$  as a function of time after the application of a step voltage,  $V$

$$\epsilon''(f) = I(t = 0.1 f)/2\pi CgVf \quad (4.16)$$

#### 4.4.3 Measurements

Nylon films sandwiched between aluminium or gold electrodes were investigated. The samples were prepared as described in Chapter III. Before the experiments were carried out, the samples were short-circuited for one day at 90°C in vacuum. A typical discharge response after a charging time of 2000s is shown in Fig.4.21b for aluminium and gold metal electrodes. The exponent  $n$  measured from the slope of the graph was about 0.8. Therefore, the discharging currents were measured up to  $(t_c/d)$  only, so that the error remains within 19%.

A family of charging and discharging currents obtained at room temperature as a function of applied voltage is shown as  $\log I$  vs  $\log t$  plots in Figs. 4.22 and 4.23. It can be seen that the exponent  $n$  shows field independent behaviour, or a very weak field dependence. The charging currents become non-linear at long times, while at short times the linearity is almost complete. It was found that the difference  $I_c(t) - I_d(t)$  was not constant through the time range covered in the measurements, but above 50s it decreased slowly. The charging currents observed in nylon at different temperatures are represented in Fig. 4.24. Above 60°C, the

$t^{-n}$  dependence is no longer obtained except in more and more limited periods of time, probably due to the combined effects of a rapid decrease in relaxation times characteristic of a transient phenomenon and the progressive superposition of a steady-state conduction current growing exponentially with increasing temperature. Therefore it can be said that two regions of time-dependence can be observed: (i) below 60°C where the current falls continuously with time never reaching a limiting value, and (ii) above 60°C where there is very little change in current with time.

Fig. 4.25 shows a typical curve of the conductivity on a log scale plotted against the reciprocal of absolute temperature. Here the conduction current was obtained as the differences between the charging and discharging currents at corresponding times (300s). It can be seen that the current did not obey the equation  $\log I \propto A_c/2.3 kT$ , where  $A_c$  is the activation energy for conduction. However, the shape of the curve suggests two kinds of conduction mechanisms at least, one at low temperature and the other at high temperature. The activation energies measured at high and low temperatures were  $(1.21 \pm 0.10)$  and  $(3.00 \pm 0.24)$  eV respectively. The temperature range at which there is a change in the current, accompanied by a change in activation energy, suggests a close connection between the conductivity and the morphology of the polymer. In fact, this temperature range corresponds approximately to the glass transition temperature of the nylon as determined by differential thermal analysis (see Fig. 4.6).

At temperatures above 100°C the charging current transients were observed to rise to a maximum value before decaying again in the usual manner. A typical behaviour of the observed phenomenon is shown in Figs. 4.26 and 4.27. It can be seen that the current maxima were reached at shorter times as the temperature and polarising field were increased.

The field dependence of isochromel current transients observed at room temperature and 50°C are shown in Figs. 4.28(a) and (b). At room temperature no deviations from linearity were observed on increasing the applied field. As the temperature was increased, deviations from linearity became more apparent. Schottky plots were obtained above the glass transition temperature  $T_g$ . Fig. 4.29 shows a plot of  $\log I$  against  $E_p^{\frac{1}{2}}$  at 80 and 90°C. It can be seen that the curves are not linear in the range of applied fields. However, slopes of the curves were measured at high fields. The observed deviations from the linear Schottky plots at low fields are, sometimes, attributed to space charges and surface inhomogeneity. The values  $\epsilon_r$  calculated from the slopes ( $\beta_s/kT$ ), of these Schottky plots are 7.2 and 2.6 at 80 and 90°C. The value of the dielectric constant  $\epsilon_r$  is seen to decrease as the temperature increases, which is contrary to what one would expect.

Another dependence of  $I$  upon  $E$  such as  $\log I$  against  $E$  was examined. Such plot should yield a straight line with slope  $ea/2kT$  (see eqn. (1.13) if an ionic conduction mechanism is present in the sample. Fig. 4.30 shows this plot. From the gradient of the curves at high fields the average ionic jump distance measured was  $(39 \pm 4)$  and  $(56 \pm 6)$  Å at 80 and 90°C respectively. Different electrode materials did not affect markedly those currents.

The loss factor  $\epsilon''(f)$  was measured using the Hamon approximation (eqn. (4.16)) at temperatures above and in the region of  $T_g$ . A large relaxation, which will be called  $\rho$ , was found at frequencies between  $10^{-3}$  -  $10^{-4}$  Hz above  $T_g$ . Fig. 4.31 shows a plot of  $\log \epsilon''$  against  $\log f$  at temperatures of 80, 90 and 100°C. It can be seen that the relaxation shifts to lower frequencies as the temperature increases. For temperatures in the region of  $T_g$ , the plot of  $\epsilon''$  against  $\log f$  showed a loss peak which is characteristic of the  $\alpha$  process in polyamides (McCrum et al 1967).

Fig. 4.32(a) shows the plot of  $\log f_{\max}$  against  $1/T$  for the relaxation. The apparent activation energy of the process has been estimated to be about 1.1 eV. A plot of the relationship between the relaxation frequency and the d.c. conductivity is given in Fig. 4.33. It can be seen that it is approximately linear, indicating that the relaxation is due to bulk charge transport. The mechanism could involve localised carrier hopping between adjacent trapping sites in the amorphous regions (ionic relaxation loss mechanism) or an interfacial polarisation involving bulk morphology, as has been suggested by North et al (1978) for copolymers of butanedial terephthalate with poly(tetramethylene oxide terephthalate).

#### 4.4.4 Previous Studies

Before discussing the results of the present study, a summary of previous studies on the d.c. conductivity in polyamides will be made.

Baker and Yager (1942) first studied the dielectric loss and d.c. conductivity of nylon 66 and 610. They found two loss maxima, one at low frequency associated with a proton transfer mechanism, and one at higher frequencies associated with conventional dipole orientation losses. They also found a marked d.c. conductivity, for which they found an activation energy of 1.29 eV. Since the activation energy for the low frequency loss was 1.01 eV, similar to that found for conductivity, the latter process was also associated with proton transfer between amide groups. McCall and Anderson (1960) have extended these studies, and found that N-methylated polyamide 1010 gave a ten-fold lower conductivity than the corresponding simple polyamide, which gives support to the view that the current carriers are amide protons.

Eley and Spivey (1961) have investigated the d.c. conductivity in a series of polyamides. They suggest two processes determining the d.c. conductivity, according to the temperature range. For  $T < T_t$  (where  $T_t$  is

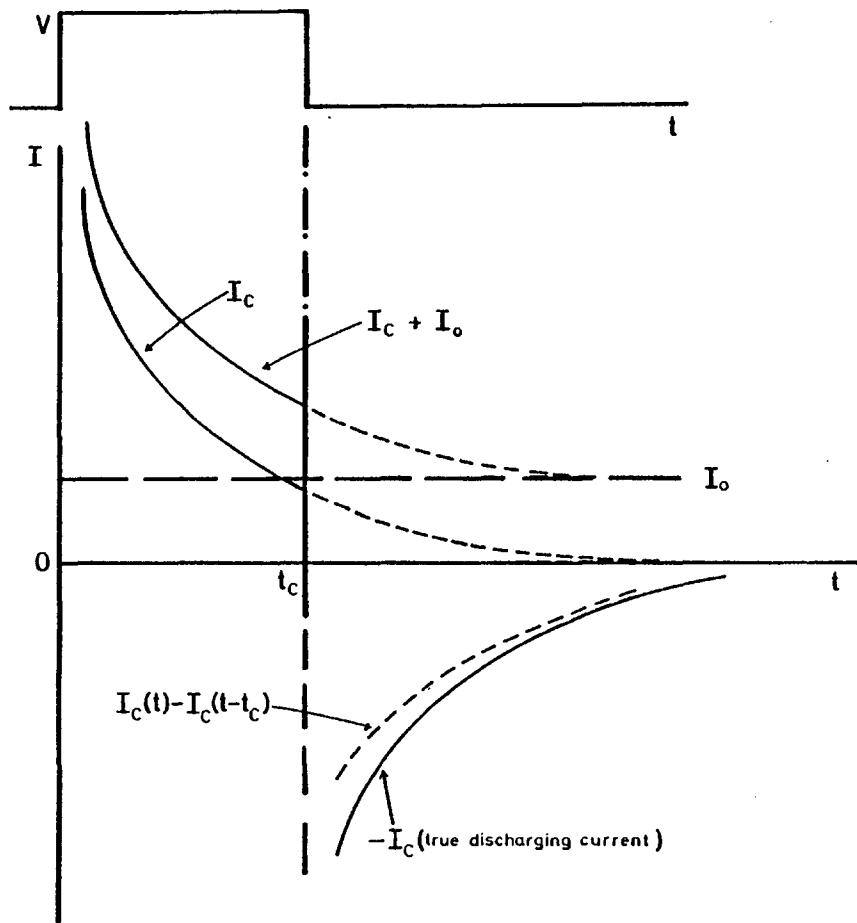


Fig. 4.21a: Schematic behaviour of charging and discharging currents in a solid dielectric.  $I_c$  = charging current;  $I_0$  = steady-state current.

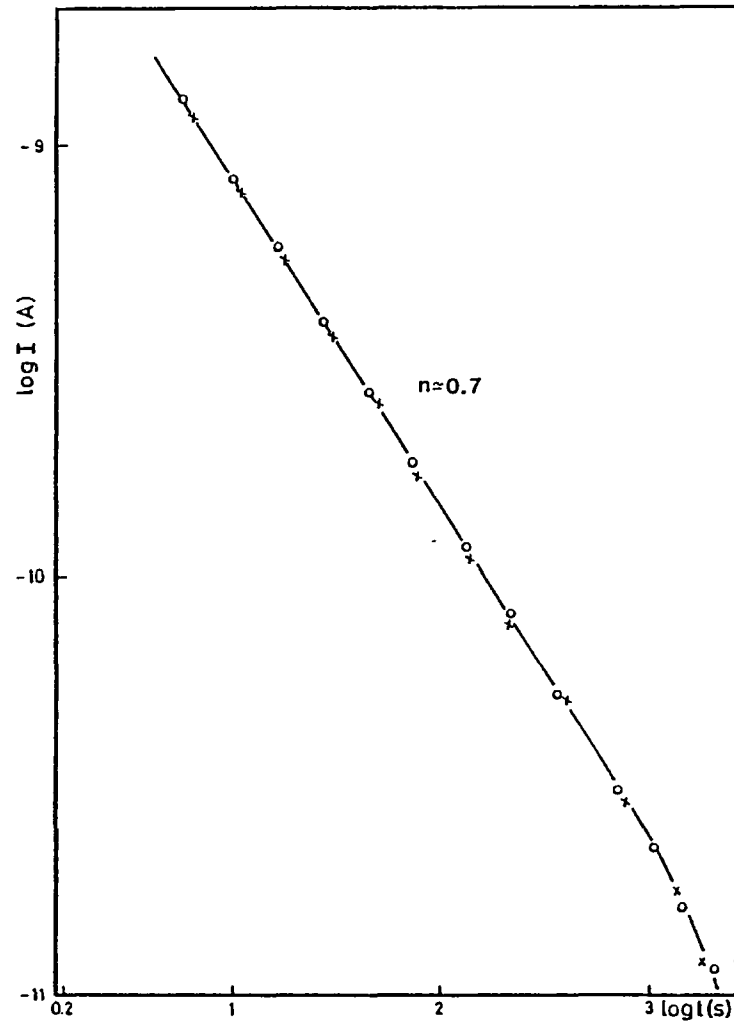


Fig. 4.21b: Discharge current for a charging time of 2000s. Aluminium (O), gold (X) electrodes.  $E_p = 10 \text{ kV/cm}$ ,  $T_p = 25^\circ\text{C}$ ,  $d = 6 \mu\text{m}$ .

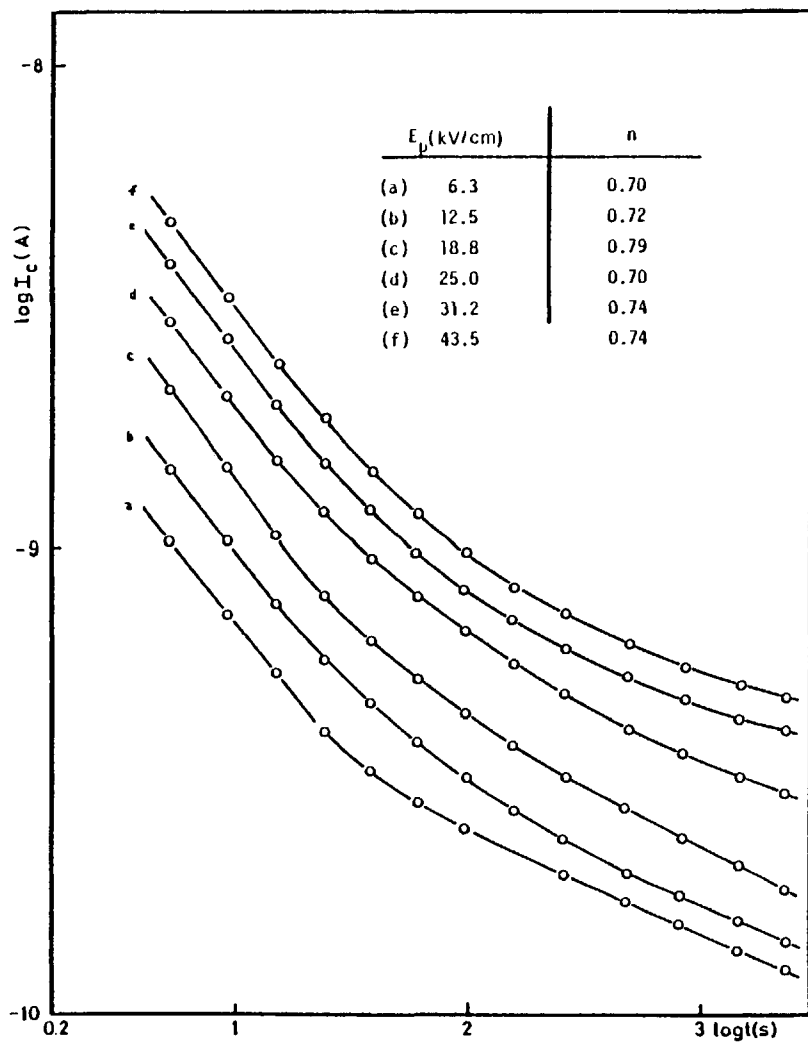


Fig. 4.22: Charging currents for several applied biases. Aluminium electrode.  $T_p = 25^\circ\text{C}$ ,  $d = 6 \mu\text{m}$ .

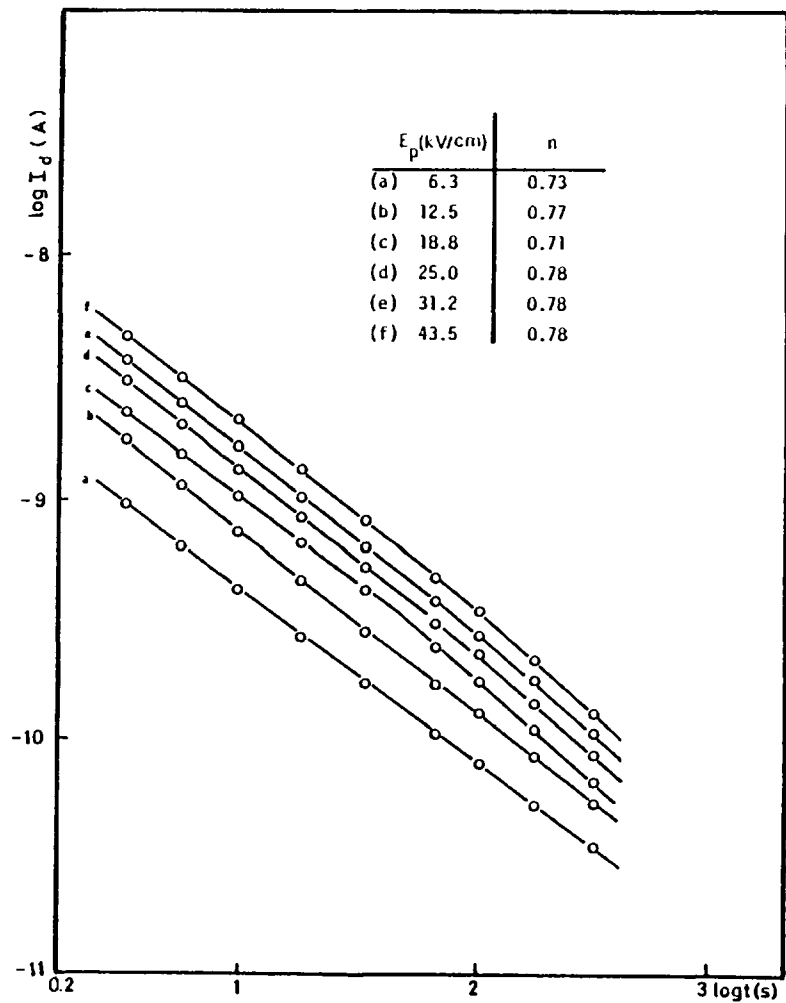


Fig. 4.23: Discharging currents for several applied biases. Aluminium electrode.  $T_p = 25^\circ\text{C}$ ,  $d = 6 \mu\text{m}$ .

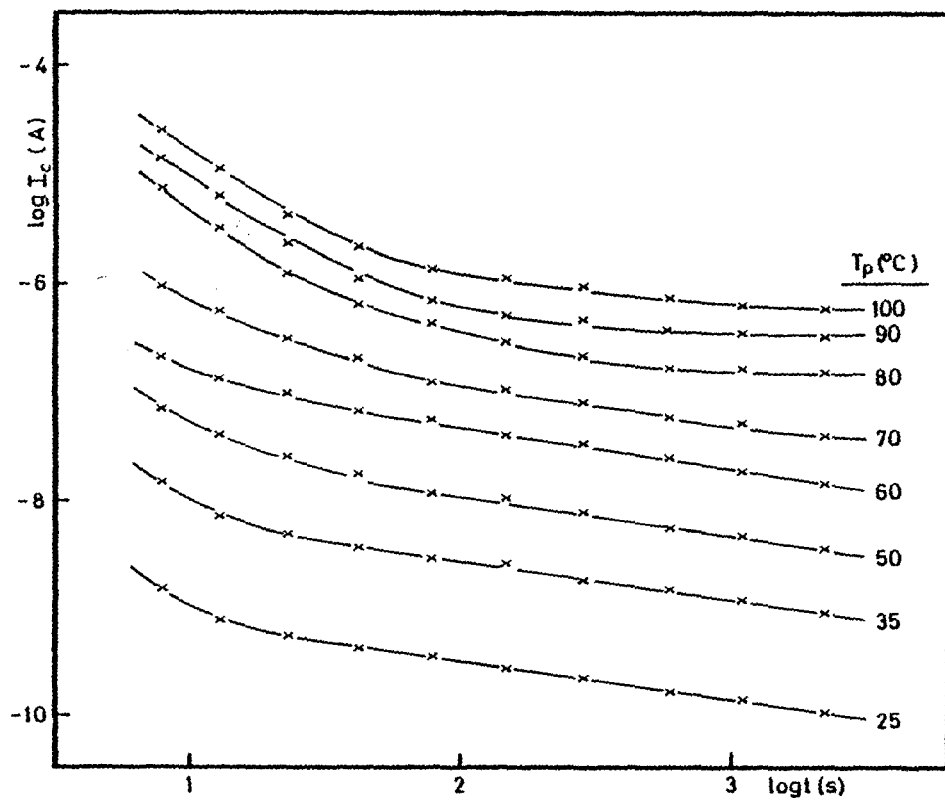


Fig. 4.24: Time dependence of charging currents in nylon above room temperature. Aluminium electrodes.  $V = 7V$ ,  $d = 10 \mu m$ .

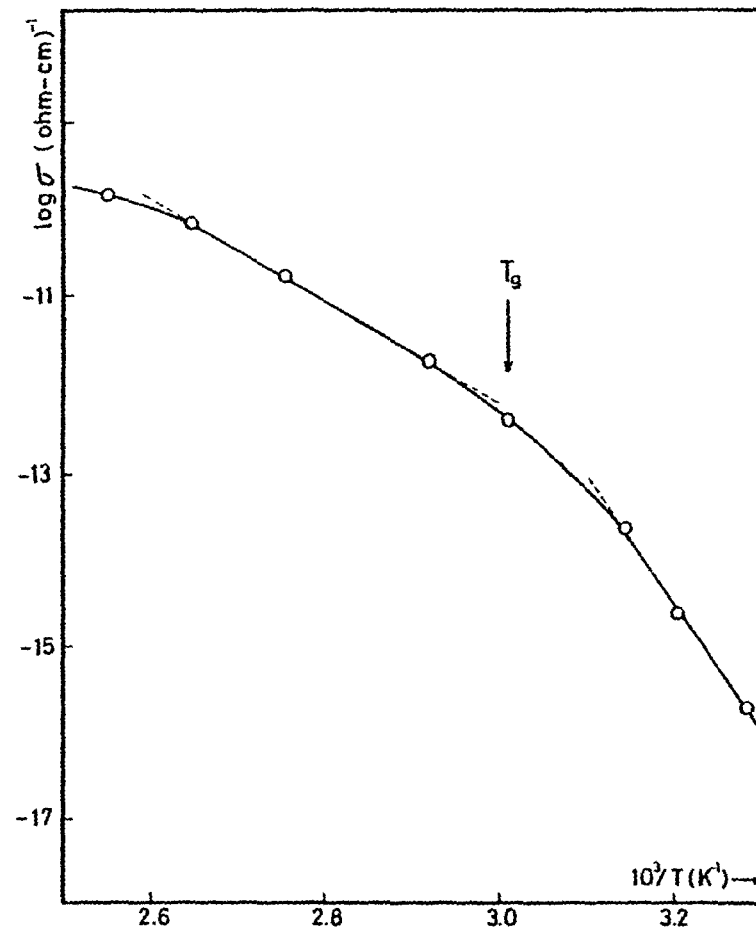


Fig. 4.25: Arrhenius plot for d.c. conduction. Aluminium electrodes.  $V = 20V$ ,  $d = 10 \mu m$ .



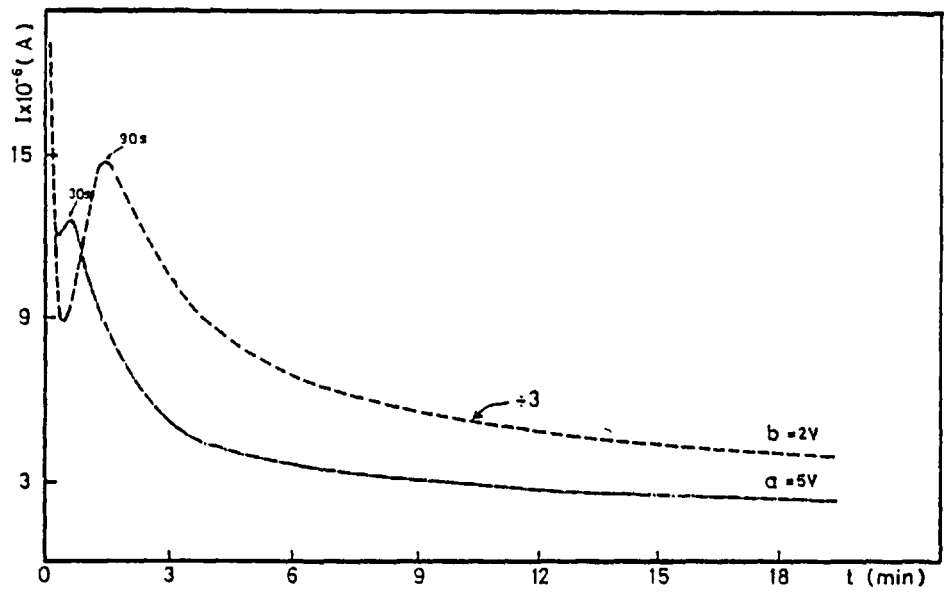


Fig. 4.26: Anomalous absorption currents in  $10 \mu\text{m}$  thick nylon samples with gold electrodes at  $140^\circ\text{C}$ .

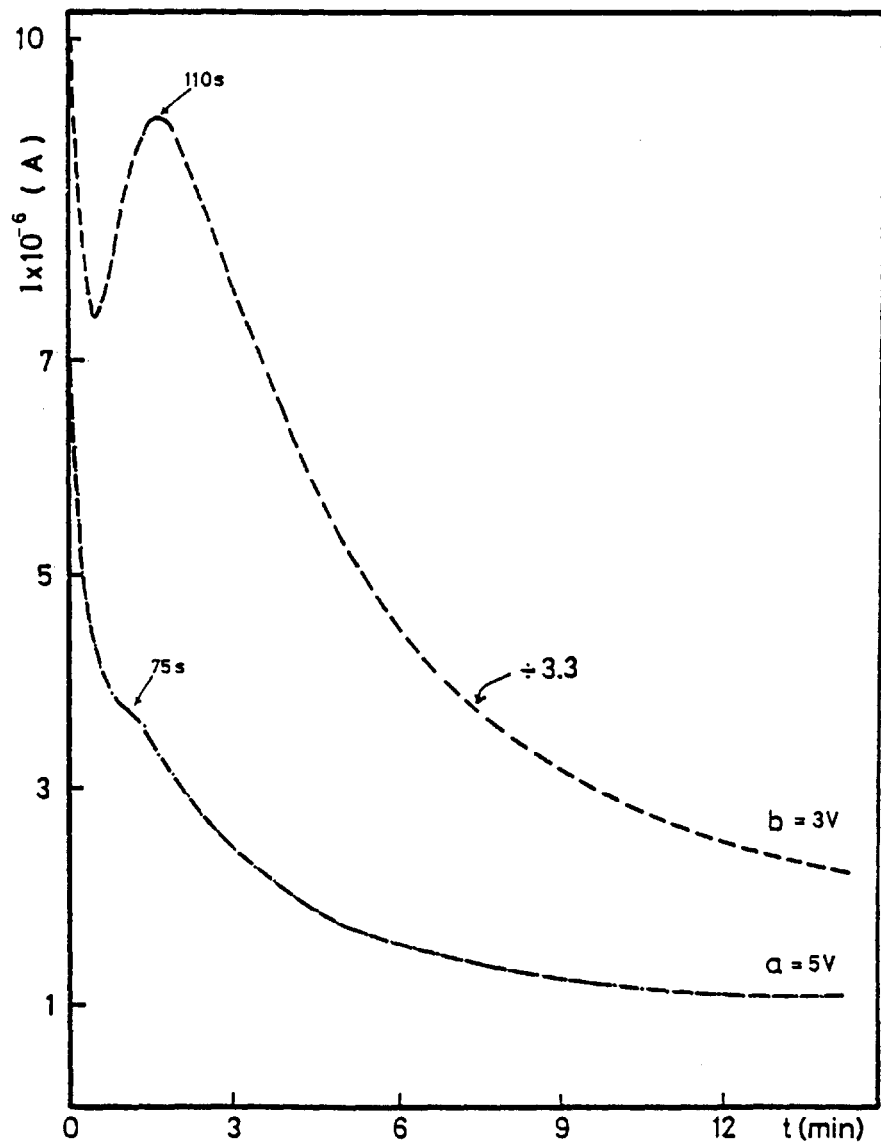


Fig. 4.27: Anomalous absorption currents in  $10 \mu\text{m}$  nylon sample with gold electrodes at  $125^\circ\text{C}$ .

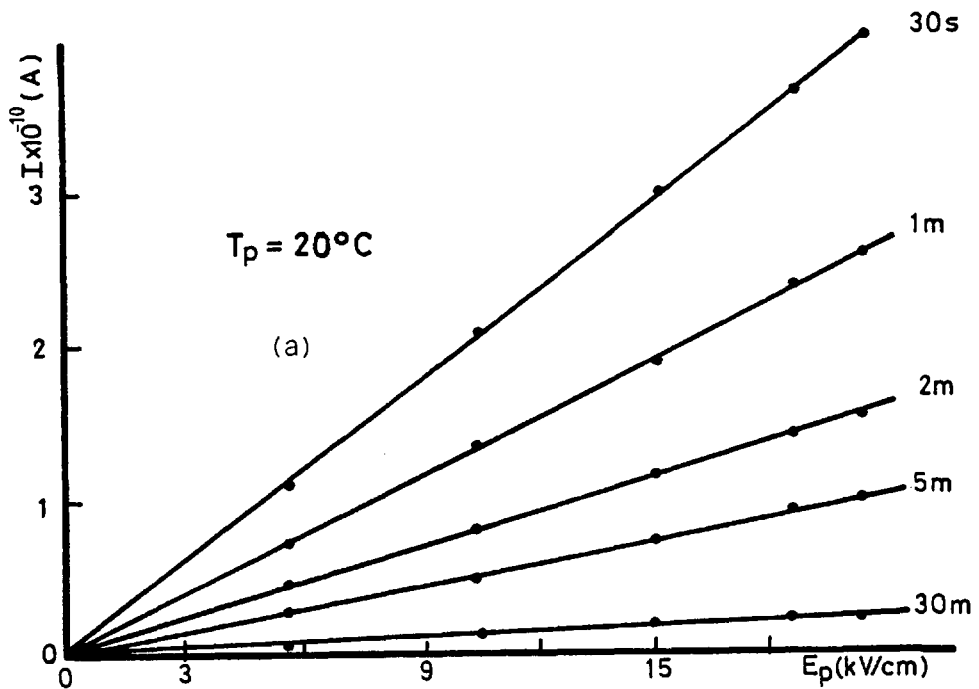
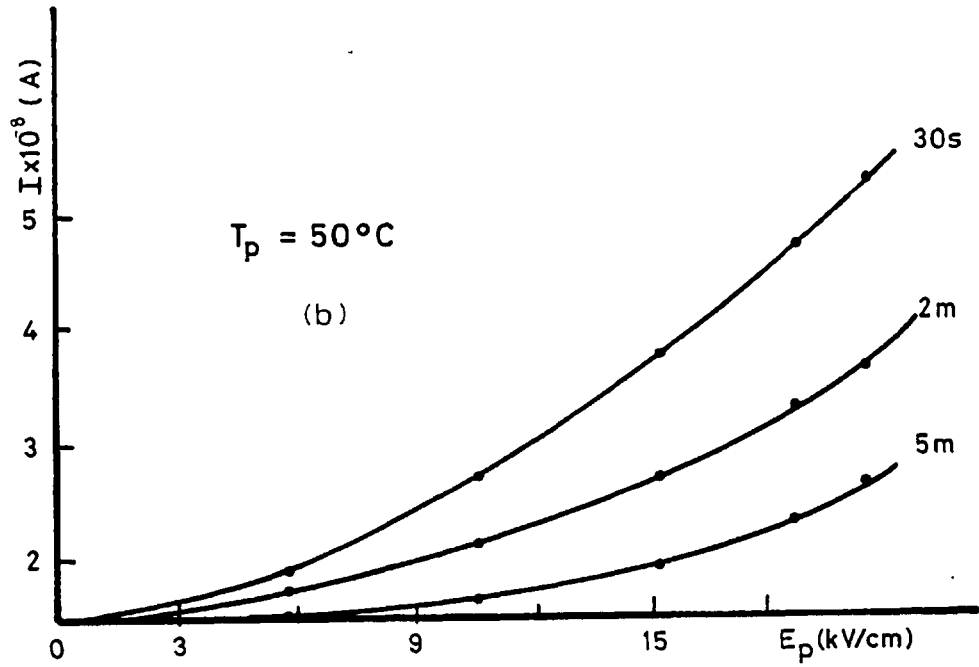


Fig. 4.28: Dependence of current on applied polarising field. Aluminium electrodes. Thickness  $10 \mu\text{m}$ .

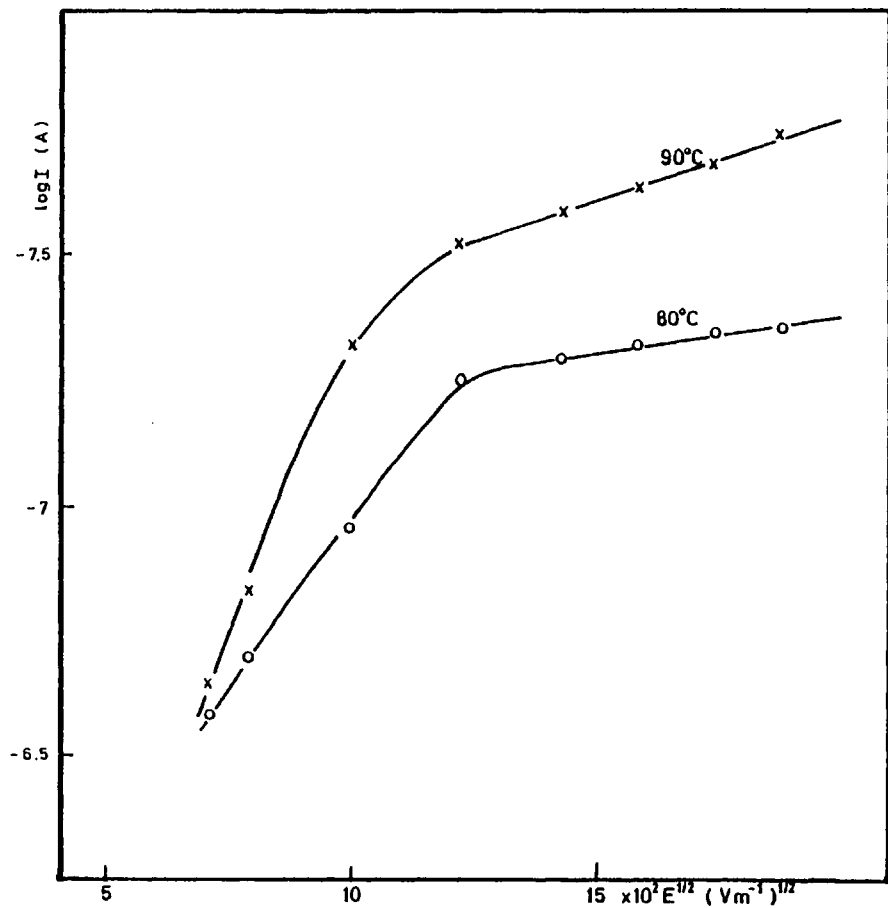


Fig. 4.29: Schottky plots for 10  $\mu\text{m}$  thick sample with aluminium electrodes.

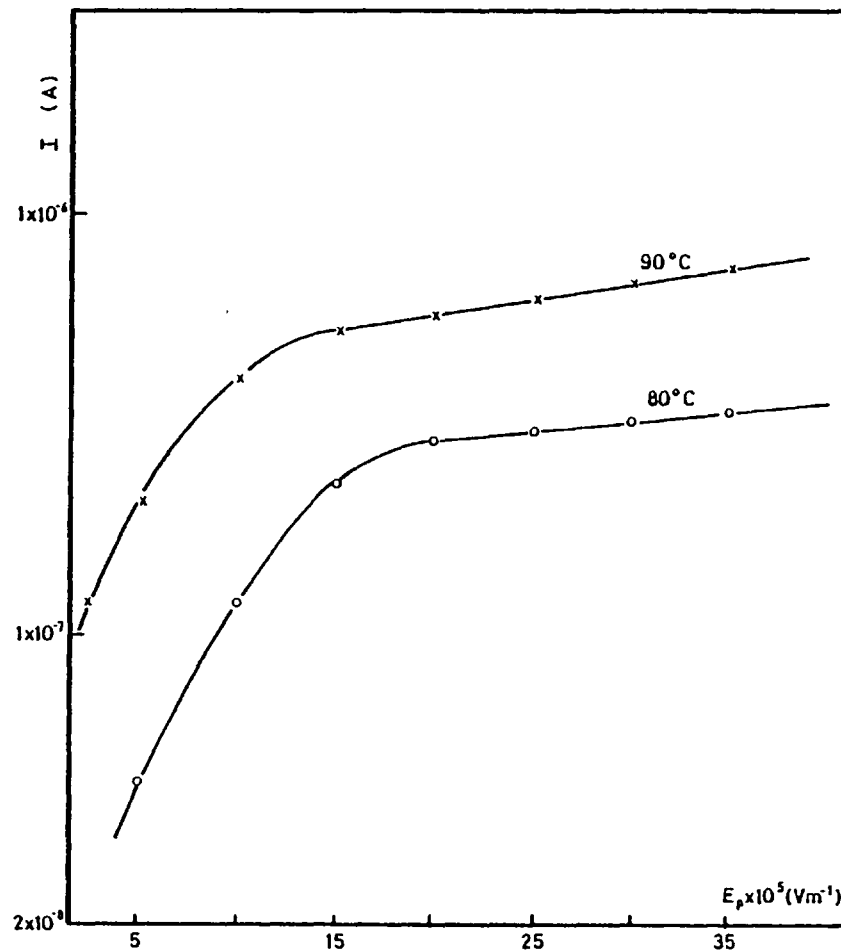


Fig. 4.30: Ionic conduction plot for nylon films with Al electrodes. Thickness 10  $\mu\text{m}$ .

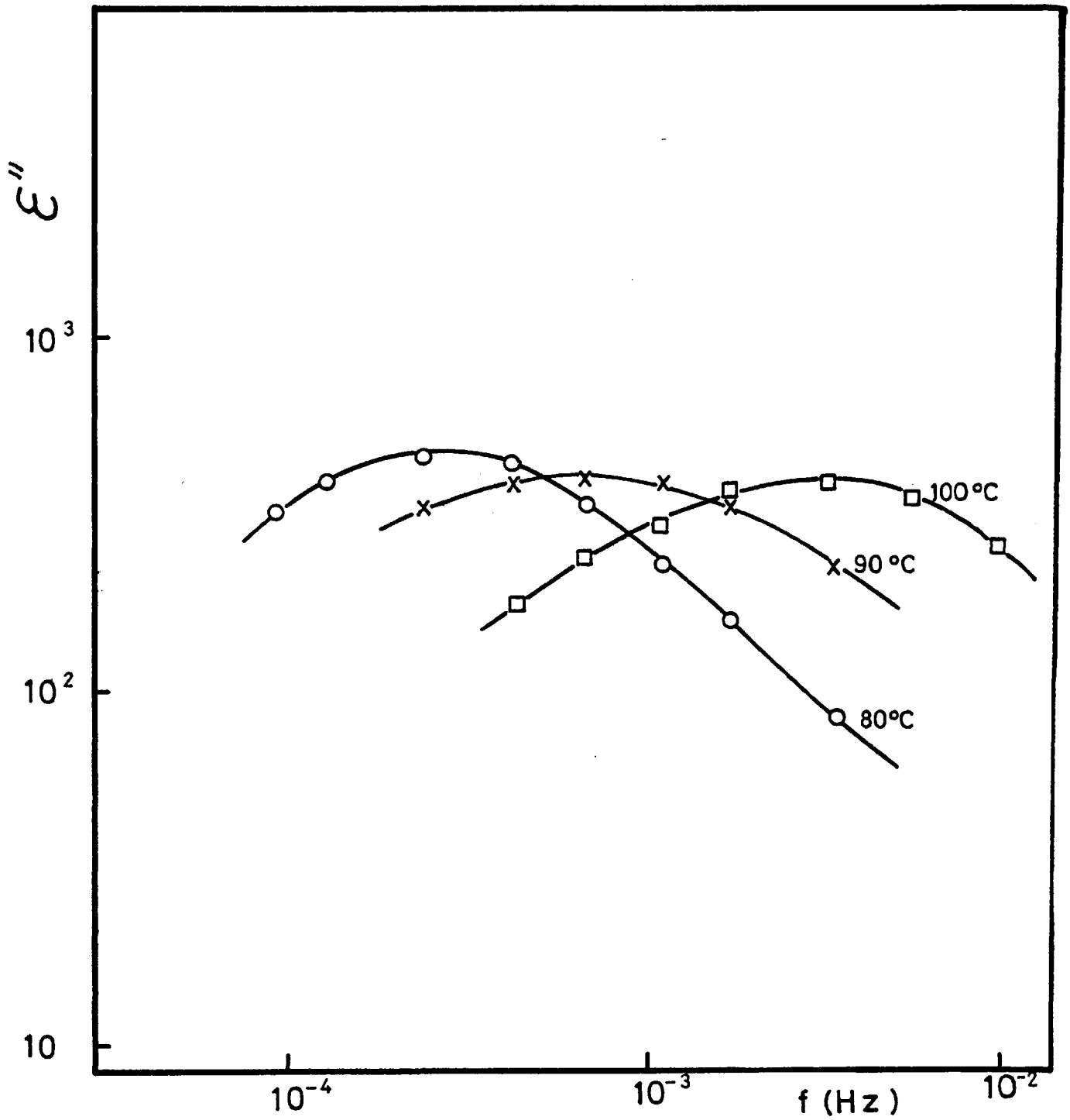


Fig. 4.31: Low-frequency dielectric behaviour of 10  $\mu$ m thick nylon at high temperatures. Gold electrodes and pre-applied field of 10 KV/cm.

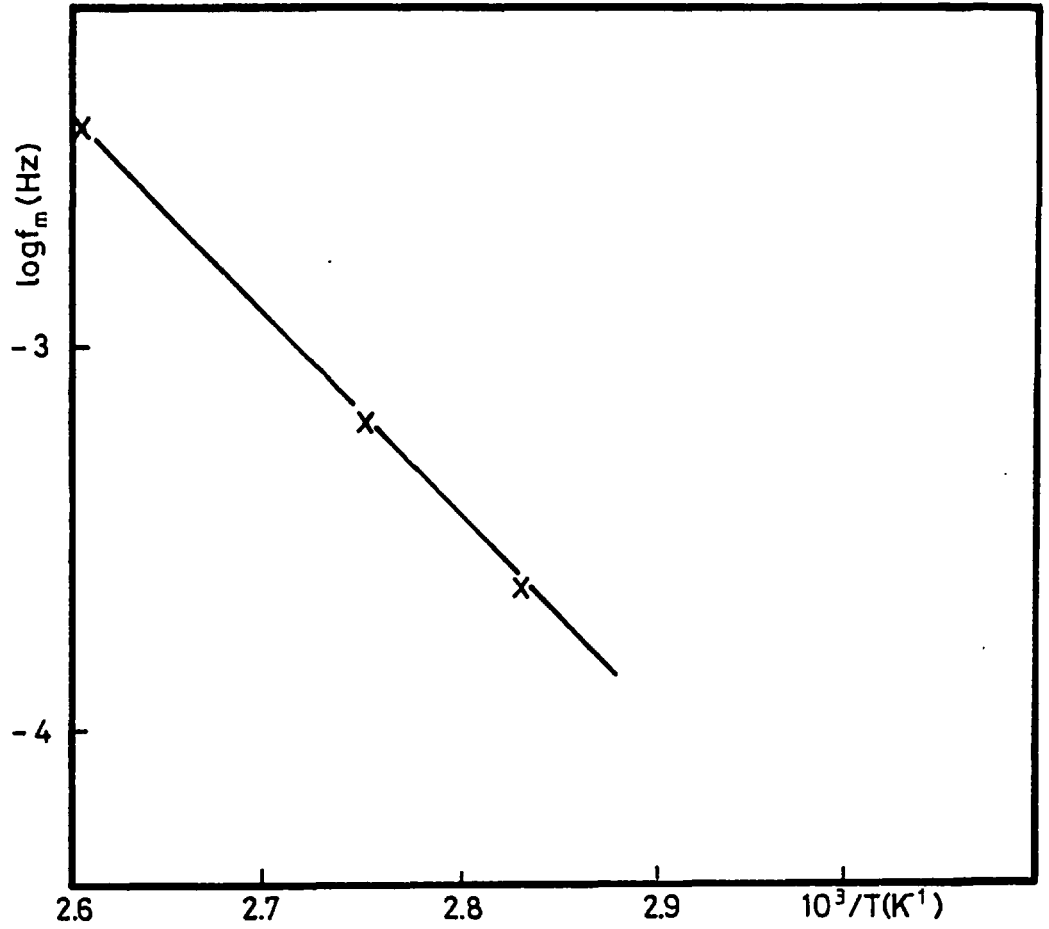


Fig. 4.32 :  $\log f_m$  against  $1/T$  for the dielectric  $\rho$  process in nylon.

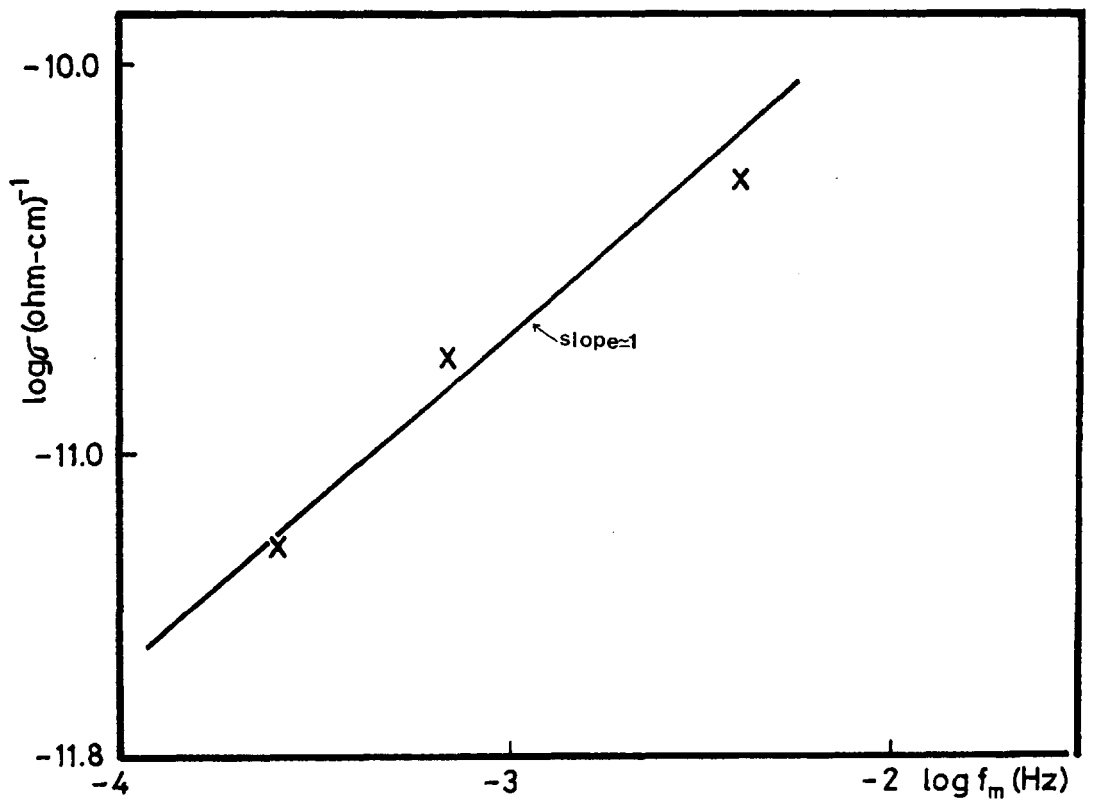
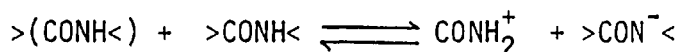


Fig. 4.33 : The relationship between d.c. conductivity and relaxation frequency for the low frequency process.

a transition temperature) the rate-determining step is the rotation of amide groups, and the activation energy will be the energy required to break the necessary number of hydrogen bonds required to free the segments. For  $T > T_t$  the rate-determining step is the self-dissociation of amide groups:



They concluded that the conductivity was ionic under all conditions.

Nakajima and Matsumoto (1963) have investigated the electric conduction in nylon 6. An electronic conduction mechanism was suggested to be operating at high temperatures. Hirota et al (1966) have measured the d.c. conduction in nylon 6 and 12. Activation energies measured were 2.52 and 1.87 eV respectively.

Seanor (1968) in his studies of the electrical conductivity in nylon 66 has concluded that at temperatures above 120°C the conduction involves the transport of both protons and electrons, while below this temperature to 80°C it is electronic. At still lower temperatures the nature of the conduction mechanism is still in doubt. These studies included the measurements of the volume of gas evolved from nylon. Above 120°C the gas evolved corresponded to about one-half of the volume calculated if the conduction process involved only protons. Below 120°C the gas evolved corresponded to a diminishing fraction of the total current until below 90°C no evolution of gas was observed.

Baird (1970) carried out d.c. conductivity measurements on nylon 610 and pip-10 polyamide (a polyamide with no hydrogen bonds) over the range of temperatures 35-150°C. He concluded that the electrical conduction in nylon 610 was electronic below about 100°C, with no significant contribution from protons, but above this temperature probably both electrons and amide protons contributed to its conductivity.

Isoda et al (1973) in their study of the electrical conductivity of nylon 66 observed three ranges of temperatures in the Arrhenius plot of conductivity: (i) below 97°C ( $A \approx 2$  eV), (ii) 97-250°C ( $A \approx 0.9$  eV), (iii) above 250°C ( $A \approx 0.8$  eV). For temperatures below 97°C the conductivity followed the WLF equation, indicating that chain rotation was the main molecular motion. Above 97°C the conductivity was ionic, impurity ions being the charge carriers and not the amide protons. Table X summarises the different values of the activation energies obtained for the most common nylons. As can be seen from the previous literature survey of the electrical conductivity of polyamides, the d.c. conductivity of nylons is really a matter of great complexity. Presumably these differences are due to the fact that the electrical conductivity in polyamides is influenced by the temperature, thermal history, physical structure of the sample, the amide concentration, chemical purity and state of polymerisation. In addition to these, moisture, adsorbed oxygen, residual solvent and impurities all play a role in determining the electrical conductivity. Unless these factors are recognised, it is not possible to make valid comparisons between the data of different workers.

#### 4.4.5 Discussion

As was observed in Fig. 4.24, two regions of current time dependence were observed above and below the glass transition respectively. This behaviour seems to be typical of polymers in general (Vanderschueren 1978) and thus appears that the time dependence of the transient currents is predominantly determined by the position of the measuring temperature with respect to the glass transition temperature. These temperature regions also correspond to the temperature at which a break in the  $\log \sigma$  vs.  $1/T$  curve was found. The value of  $T_g$  determined from DTA also corresponds to this change in the slope of the  $\log \sigma$  vs.  $1/T$  curve.

POLYAMIDE		COMMENTS	A(eV)
66 ) 610 )	(Baker and Yager 1942)	Activation energy for the low frequency loss = 1.01 eV	1.29
66 ) 610 ) 6 ) 6/66/610 )	(McCall and Anderson 1960)	Average value " " " " " "	1.73 1.52 1.30 1.43
66	(Eley and Spivey 1961)	Above 115°C Below 115°C	1.12 1.95 - 2.94
610	(Eley and Spivey 1961)	Above 82°C Below 82°C	1.27 2.20 - 2.96
6	(Nakajima and Matsumoto 1963)	60°C < T 100°C	1.8
6	(Hirota et al 1966)	Reference Temp. 65°C	2.52
66	(Seanor 1968)	Between 70-120°C > 125°C	2.18 1.30
66 ) 610 )	(Baird 1970)	Estimate - above T <sub>g</sub> Estimate - Above T <sub>g</sub>	1.86 1.86 1.55
66	(Isoda et al 1973)	Above about 90°C	0.9

TABLE X:



The loss peak found in the nylon at about  $T_g$  is characteristic of the  $\alpha$ -relaxation in polyamides (Hedvig 1977), and therefore is attributed to large scale Brownian motions of the dipoles. The dipoles responsible for this relaxation are probably the amide groups (section 4.1). This relaxation will be examined in more detail in section 4.5.3 using the electret effect.

It is believed that the steady-state current was positively found only at temperatures above  $T_g$ . The low temperature slope in Fig. 4.25 is therefore an arbitrary one and is not characteristic of a true conduction mechanism. It simply depicts the complex temperature dependence of distributed relaxation processes. The experiments presented here neither prove or disprove the point whether there exists another type of steady-state conductivity below  $T_g$ . However, in section 4.5.3 it will be seen that nylon electrets, polarised in the region of  $T_g$ , release a charge during constant heating, which is equal to the total charge measured from the charging current. This experimental result agrees with the fact discussed above about the non-existence of a true conduction current below  $T_g$ .

For temperatures above  $T_g$ , the Schottky-type field-assisted thermionic emission does not seem to operate in the sample because of the unrealistic values of the dielectric constant measured. The accepted value of the high frequency dielectric constant for polyamides is about 3.4 (Curtis 1961, Weast 1977). If one considers that electron liberation from sites in the bulk of the polyamide occurs (Poole-Frenkel effect, section 1.5.4.3(c)), the dielectric constant measured is about 20, which is considerably greater than the accepted ones. It should be mentioned that the problem of distinguishing experimentally between Poole-Frenkel and Schottky processes is not simple (Jonscher and Hill 1975). It should also be stated that the current was observed to be independent of the

electrode materials.

The present experimental data between 80-100°C seems to be in agreement with an ionic transport mechanism. Amborski (1962) has estimated the ionic jump distance in PET. It varies between 69-80Å in the temperature region 130-190°C. Another polymer which shows ionic conduction is PVC (Kosaki et al 1971). Above the glass transition, i.e.  $T > 90^\circ\text{C}$ , the jump distance varied between 35 and 55Å. The values of the jump distances measured in the present study are not too high when compared with other polymers. Assuming that the monomer unit of nylon is about 20Å (Kohan 1973) along the C axis, this would imply a hopping distance of about 2 monomer units. The glass transition temperature  $T_g$  can usually be identified by the onset of diffusional motion of large chain segments. At temperatures below  $T_g$  this motion is hindered by potential energy barriers. With increasing temperature the energy of the segments becomes large enough to overcome these barriers, and segmental motion occurs which results in an increase of the free volume of the system. The increase in free volume would also facilitate the motion of an ionic charge carrier at temperatures above  $T_g$  (see Fig. 1.7).

It is thought that closely associated with this ionic conduction mechanism is the low-frequency region of dielectric loss found in the polyamide above  $T_g$  (see Fig. 4.31). This low-frequency high temperature relaxation has been found in the past in polyamides. McCall and Anderson (1960) have attributed this loss to proton conduction through the amorphous regions of the nylon. The polymer consists of amorphous and crystalline regions, and ions are able to migrate through the amorphous regions. Ions which can move unobstructed to the electrodes are discharged and cause the direct current conductivity. Other ions are free to move over distances which are large in molecular terms but cannot reach the electrodes. For

example, these ions may be trapped at crystalline-amorphous phase boundaries. This creates a space charge and consequent polarisation. Owing to the relatively long distances the ions move, the polarisation is built up slowly, and thus corresponds to a low-frequency loss mechanism.

Hirota et al (1966) and Baird (1970) have also found this type of relaxation in polyamides. They agree that the relaxation mechanism involves the accumulation of space charges at the crystalline-amorphous interfaces. However, Isoda et al (1973) disagree with the Maxwell-Wagner type of relaxation and suggest that the mechanism responsible for this loss is the migration of ions with subsequent accumulation at the electrodes.

Relaxations at low frequencies and high temperatures have also been observed in other polymers, e.g. polyethylene-terephthalate (Das-Gupta and Joyner 1976), styrene-butadiene-styrene copolymers (North et al 1978) and polyvinylidene fluoride (Das-Gupta et al 1980). Almost all systems exhibiting interfacial polarisation have the following characteristics: (i) the loss is often of high magnitude ( $\epsilon'' > 100$ ) and (ii) the activation energy of the process mirrors that for d.c. conduction. This seems to indicate that the interfacial polarisation mechanism involves the same charge carriers as does d.c. conduction.

The activation energy of the  $\rho$  loss measured from Fig. 4.32 was estimated to be about 1.1 eV. This value agrees well with the activation energy for conductivity measured above  $T_g$ , i.e.  $(1.21 \pm 0.10)$  eV. Recalling the value of the activation measured in the galvanic cell experiment (see section 4.3.2.2) above 70°C, which was 1.2 eV, it appears then that the ionic conduction dominates the conduction process in the nylon films. However, according to the result of Fig. 4.33, the relationship between the relaxation frequency and d.c. conductivity is linear. This means that either an ionic relaxation loss mechanism and/or an interfacial polarisation involving bulk morphology could be involved.

Differential thermal analysis has shown that an exotherm transition exists in the nylon studied here above  $T_g$  (see Fig. 4.6). As was mentioned before, this transition has been called cold crystallisation and involves the nearest neighbours chain units in the amorphous regions. Such crystallisation occurs without molecular rearrangements and leads to the production of small crystallites. It is therefore not unreasonable to suggest that due to the creation of small crystallites in the bulk of the polyamide above  $T_g$ , charge carriers will accumulate at the interfacial boundaries. If this is so, the thermally stimulated discharge technique provides an excellent opportunity to verify that accumulation of charges does really occur in the bulk of the nylon. The experimental results of this technique will be presented in section 4.5.

It is worth mentioning that the  $\alpha$  loss has been observed with mechanical loss data (McCrum et al 1967), which is evidently related to the segmental motion in amorphous regions. The  $\rho$  loss has not been observed in mechanical loss data but in the dielectric loss data only.

The value of the activation energy measured above  $T_g$  appears close to the accepted one for protonic conduction, i.e. approximately 1.3 - 1.4 eV (Vijh 1978). However, it is not possible at the present stage to say whether the polarising species involved are protons and/or other ions. Usually it is hypothesised that the ionic species arise from some kind of self-ionisation process such as the ionisation of absorbed water  $H_2O \rightleftharpoons OH^+ + H^-$ . Eley and Spivey (1961) have suggested that self-ionisation of two adjacent amide groups could occur with an activation energy of about 0.7 eV. Seanor (1972) has given a possible process of generation and transfer of protons in polyamides as shown in Fig. 4.34.

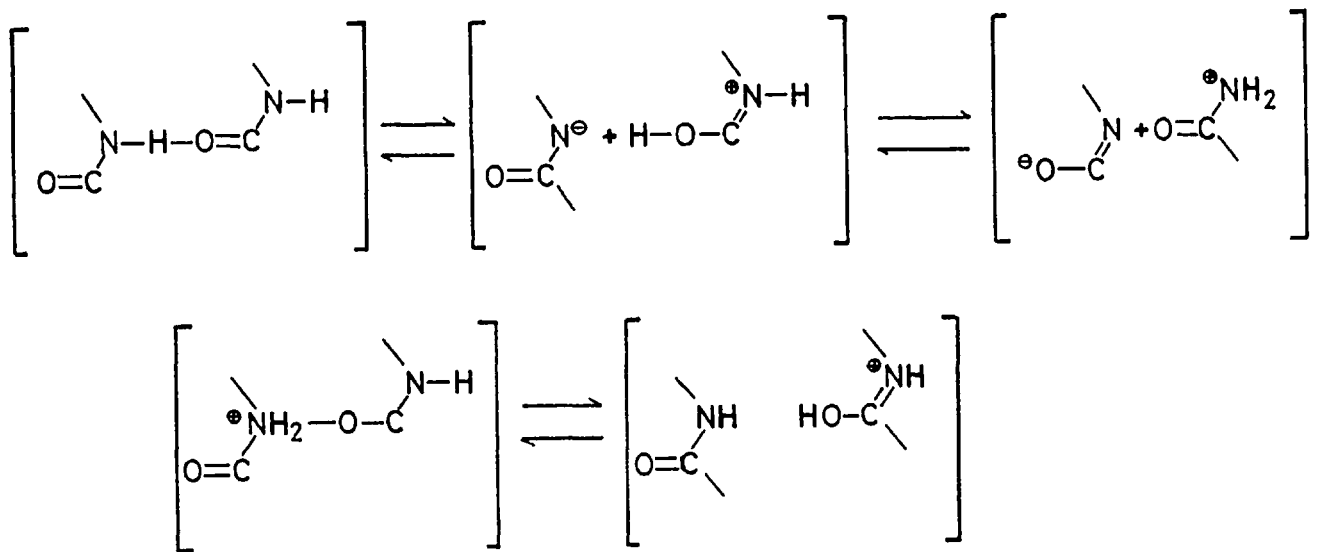


Fig. 4.34: Generation and transport of protons in nylon  
(Seanor 1972)

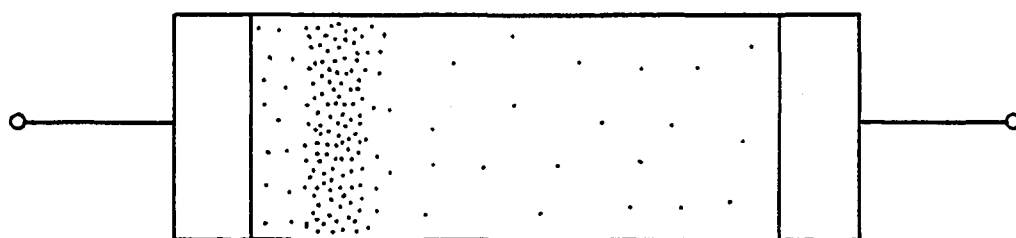
As was explained before, at temperatures above 100°C the charging current transients showed the presence of a peak. The current maxima occurred in the range of 20-100s and shifted to shorter times when the applied field increased. Similar current peaks have been observed in other polymers upon step voltage excitation by Fischer and Röhl (1977), Mizutani et al (1979, 1980) and Das-Gupta et al (1980). Because of the similarities to the current transients first observed by Many and Rakavi (1962), the current peaks observed were explained by the space charge build up of injected carriers. According to the transient SCLC theory, the current peak occurs at a time  $t_m$  given by (Mizutani et al 1980)

$$t_m = 0.786 \frac{d^2}{\mu V} \quad (4.17)$$

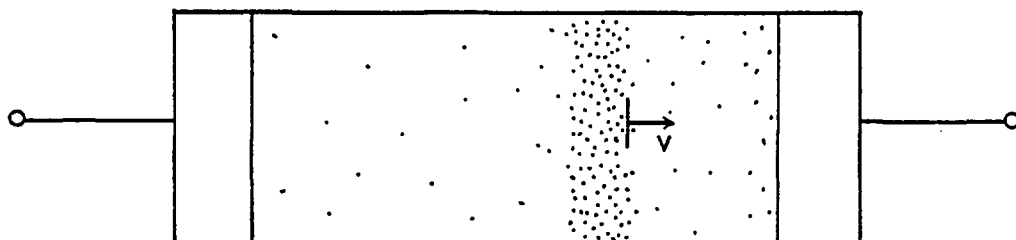
where  $V$  is the applied voltage,  $d$  the thickness of the sample and the mobility. The values of the mobility obtained by the previous authors ranged from  $10^{-8} - 10^{-11} \text{ cm}^2 \text{ V}^{-1} \text{ s}^{-1}$ . If one assumes that the current

peak observed in nylon has the same origin, the mobility obtained from the above equation is of the order of  $10^{-6} \text{ cm V}^{-1} \text{ s}^{-1}$ .

It is believed that the origin of these current peaks in nylon is still not clear, mainly because of the relatively low applied fields ( $\sim 3 \text{ kV/cm}$ ) and the fact that the peaks are observed with aluminium and gold electrodes. One could suggest the following simple model to explain the current peaks. At high temperatures there is a spontaneous formation of charge carriers which are situated asymmetrically in the polymer film. Upon application of the polarising field those charges drift towards the respective electrode, where eventually they might accumulate or discharge. Fig. 4.35 illustrates such a model.



(a) Before application of the field



(b) After application of the field

Fig. 4.35: Model to explain the anomalous current in nylon

#### 4.4.6 Conclusions

The present experimental evidence suggests that the transient currents observed at temperatures lower than the glass transition temperature, as a result of the application of low to moderate voltage steps may be essentially explained in terms of a dipolar relaxation mechanism or a number of such overlapping processes.

At temperatures above  $T_g$  a low frequency loss mechanism has been observed and has been attributed to a space charge relaxation. This process probably involves a combination of an ionic relaxation loss and interfacial polarisation mechanism. The interfacial polarisation mechanism is believed to be associated with the exothermic transition found in the DTA of the nylon.

#### 4.5 THERMALLY STIMULATED DEPOLARISATION CURRENT AT HIGH TEMPERATURE IN NYLON

##### 4.5.1 Introduction

This section deals with the electret effect in nylon films. The thermally stimulated discharge technique was used to study this effect between 0°C and temperatures close to the melting point, showing three prominent parts. An overall TSD spectrum of a solvent-cast nylon film is shown in Fig. 4.36. The electret was formed at 140°C with a polarising field strength of 20 kV/cm for a period of 30 minutes. The heating rate used was 6°C/min.

Three prominent peaks are observed to exist near 65, 110 and 138°C, and will be designated as  $\alpha$ ,  $\rho$  and  $\rho'$  respectively. The  $\alpha$  peak appears well separated from the other peaks. It can be seen that the amplitude of the  $\rho$  peak is high and that the  $\rho'$  peak is a broad one. Some overlapping exists between  $\rho$  and  $\rho'$ .

The properties and characteristics of the  $\alpha$  peak will be studied first with the aim of gaining some understanding of the molecular motions associated with this peak. Secondly, the  $\rho$  and  $\rho'$  peaks will be analysed and conclusions drawn according to their behaviour in different experimental conditions. Wherever possible conventional dielectric and mechanical measurements are compared with the TSD results.

##### 4.5.2 Experimental

The nylon films used in these experiments were prepared as described in Chapter III. Gold or aluminium was used for the metal electrodes. The apparatus used includes a Keithley 610 electrometer, a d.c. power supply, a temperature programme controller (Stanton Redcroft) and a Brians chart recorder. The samples were first heated at a constant rate (4°C/min) to high temperatures ( $\sim 130^\circ\text{C}$ ) before forming the electrets. This conditioning



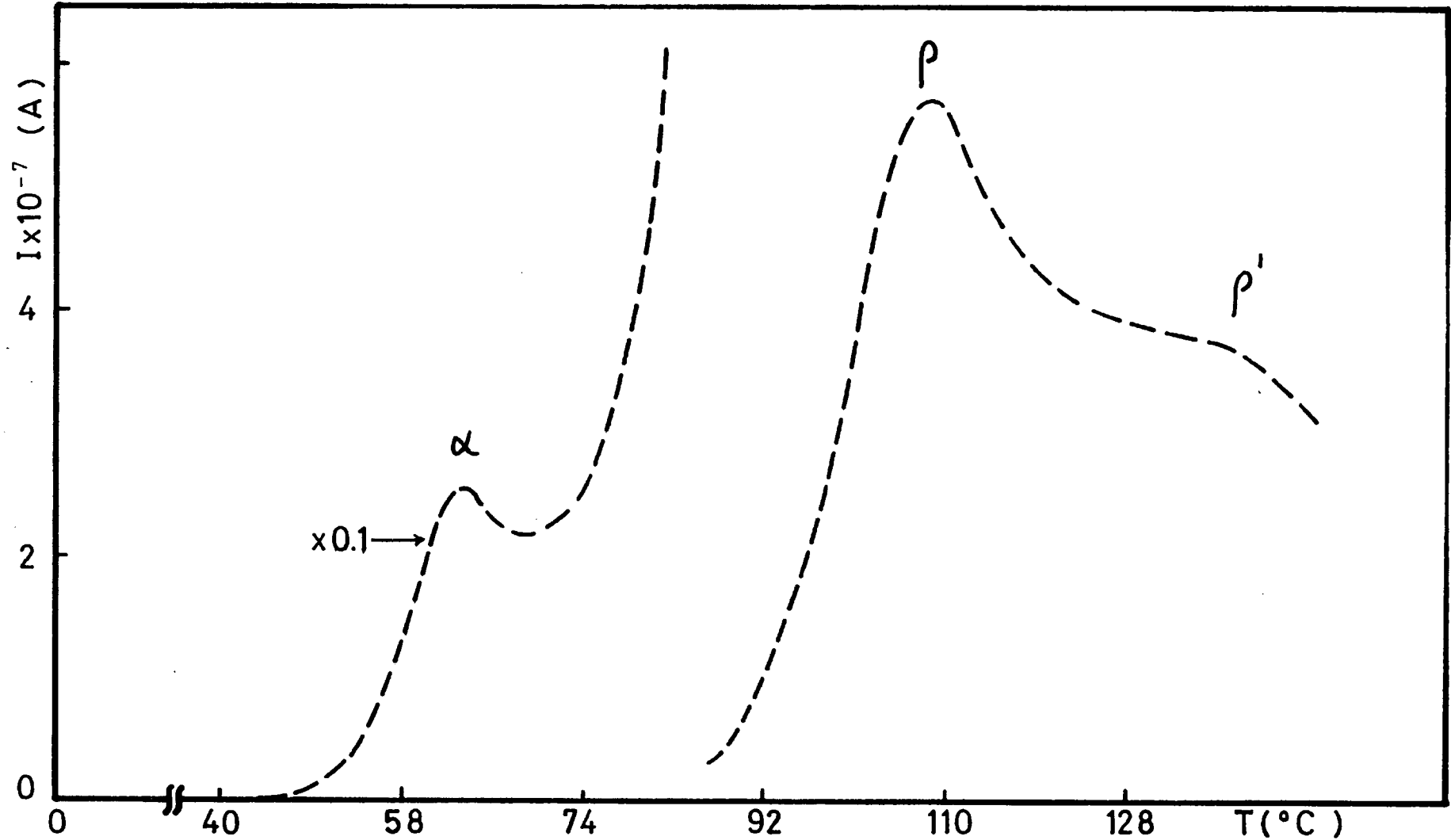


Fig. 4.36: Overall TSD current spectra obtained from 10  $\mu\text{m}$  solvent cast polyamide film. Au electrodes.  
 $T_p = 140^\circ\text{C}$ ,  $E_p = 18 \text{ kV/cm}$ ,  $r = 6^\circ\text{C/min}$ ,  $t_p = 30 \text{ min}$ ,  $T_o = 0^\circ\text{C}$ .

procedure was done in order to "wash" the sample. The polarising field  $E_p$  was applied at the polarising temperature  $T_p$  for a period of time  $t_p$ . Samples were subsequently cooled under the applied field to  $0^\circ\text{C}$ . Depolarisation currents were recorded while scanning the temperature in the range from  $0^\circ\text{C}$  to  $130^\circ\text{C}$  at a heating rate  $r$ . Thermally stimulated polarisation experiments (see section 2.4) as well as a.c. dielectric measurements were carried out on the films. All the experiments were performed in an evacuated cryostat.

### 4.5.3 The $\alpha$ -relaxation

#### 4.5.3.1 Results

The  $\alpha$  relaxation in nylon was studied as a function of polarising field, heating rate and polarising temperatures. The TSD spectra obtained from nylon formed at  $60^\circ\text{C}$  for periods of 2 minutes for different polarising fields and a heating rate of  $4^\circ\text{C}/\text{min}$  are shown in Fig. 4.37. All curves show a prominent peak centred at about  $60^\circ\text{C}$ . It can be seen that the maximum temperatures of those peaks are independent of the polarising field. The relationship between the maximum current of the TSD peak and the polarising field is shown in Fig. 4.38. The relationship is seen to be linear. By extrapolating the straight line it can be seen that it passes through the origin. Fig. 4.39 shows the dependence of the total charge released to the external circuit, which was obtained by integrating the TSD spectrum in terms of time from  $t = 0$  to  $t = \infty$ , on the polarising field was also found. Fig. 4.40 shows the TSD spectra for constant polarising field ( $5 \text{ kV}/\text{cm}$ ), polarising time (10 min) and heating rate ( $4^\circ\text{C}/\text{min}$ ), but varying polarising temperature. The peaks are seen to be increased in strength and to be shifted slightly to higher temperatures on increasing polarising temperature.

The method of varying the heating rate (see section 2.10.1.3) was utilised to estimate the activation energy of the process. Fig. 4.41 presents the plot of  $\log (T_m^2/r)$  against  $1/T_m$ , where  $T_m$  is the temperature at which the TSD shows a maximum and  $r$  is the heating rate. The slope of Fig. 4.41 gives an apparent activation energy for the  $\alpha$  peak of  $(2.1 \pm 0.1)$  eV.

To find out the effect of storage conditions, the polyamide electret was left in a short circuited condition for several periods of time under vacuum and at room temperature. Fig. 4.42 shows how the  $\alpha$  peak is affected by prolonged storage. It can be seen that even after 20 days of storage the amplitude of the peak had decayed very little.

The initial rise method was also used to estimate the activation energy of the  $\alpha$ -relaxation. Fig. 4.43(a) gives the results for different polarising fields of 0.8, 2 and 8 kV/cm, and polarising temperature and time of 60°C and 2 minutes respectively. Fig. 4.43(b) also shows results obtained under different forming conditions, i.e. polarising fields of 1.4 and 3 kV/cm, polarising temperature and time of 90°C and 10 minutes respectively. The apparent activation energy determined from the slope of the lines in Figs. 4.43(a) and 4.43(b) was independent of the forming conditions and the value obtained was about  $(1.9 \pm 0.1)$  eV in all cases.

Relaxation frequencies at different temperatures  $w(T)$  have been calculated by the total curve method, i.e. the BFG method (section 2.10.1.2). Fig. 4.44 is a plot of  $\log w(T)$  vs.  $1/T$  (a typical BFG plot). It can be seen that the plot is not a straight line. The apparent activation energy calculated from the linear part of the plot gave the value of 1.9 eV.

Thermally stimulated polarisation (TSP) runs were also investigated. A fresh sample was cooled with shorted electrodes to -20°C. At that temperature, the polarising field of 3 kV/cm was applied and the sample

heated at 4°C/min. The current which flowed in the external circuit was measured as a function of temperature. The result obtained is shown in Fig. 4.45. The same graph also shows the TSD on the same specimen, formed at 70°C for 5 min. The field applied and the heating rate used were the same as in the TSP run. The (+) sign indicates that positive charge was flowing to the electrode which had positive polarity.

The following experiment was performed to verify whether or not the released charge during TSD was equal to the frozen-in or stored charge. The polymer was polarised at 60°C for 2 minutes and subsequently cooled and shorted. At this moment the polymer contains a frozen-in or stored charge,  $Q_s$ , defined as the time-integral over the transient component of the charging current. The system is then discharged by reheating in a short-circuit condition. The released charge is defined as the time integral over the discharge transient, i.e. as  $Q_{TSD} = \int_0^{\infty} Idt$ . Fig. 4.46 shows the result obtained. It can be seen that the values of the stored and released charge obtained are the same within the experimental error.

In view of the fact that the relaxation obtained is not due to a single relaxation process, as evidenced from its dependence on the forming conditions, attempts were made to obtain the components by using special techniques. The thermal sampling technique (discussed in section 2.9.3) was used to investigate the  $\alpha$ -relaxation. The polarising field used was 11.4 kV/cm. The heating and cooling rates were 4 and 20°C/min respectively. The polarising windows were used  $\Delta T = 2, 3$  and 5K. The polarising temperature was scanned every 2, 3 and 5K. Various attempts to decompose the  $\alpha$  peak, by changing the thermal sampling parameters, were unsuccessful. The fractional polarisation technique which consists of applying the polarising field in limited temperature ranges during a slow cooling (typically 1°C/min) was also applied to the  $\alpha$ -relaxation. Again, no decomposition of

the peak was obtained.

Multistage TSD experiments (see section 2.9.2), which consist of interrupting the heating of increasingly higher temperatures, revealed that the dipole distribution did not arise from a distribution in activation energies. It is a common procedure in evaluating dielectric and mechanical relaxation data to introduce a distribution function to interpret the results. The distribution function of relaxation times for the  $\alpha$  dispersion has been calculated from measurements of TSD currents. The first order approximation of Schwarzl and Staverman (1952) (see section 2.7) was used to calculate the distribution function in characteristic relaxation times, i.e. in pre-exponential factors. The result obtained is shown in Fig. 4.47. The distribution is quite symmetrical which means that it can be represented by a Fuoss-Kirwood or Cole-Cole distribution (see Table V). The Fuoss-Kirwood distribution has been compared in Fig. 4.47 with the experimental distribution  $F(\tau_0/\tau_{om})$ . The agreement between the two curves is excellent. The distribution parameter used in the calculations was 0.77.

The symmetry properties of the  $\alpha$  peak were used to calculate the activation energy. The symmetry factor calculated had the average value of 0.5. Using the results given by Chen (1969b) the kinetic order found was about 1.7. By using eqns. (2.48), (2.49) and (2.50), the activation energy calculated was about 2.2 eV.

Despite the fact that this section is dealing with TSD measurements, it is interesting to mention that dielectric constants and losses were measured over the range of temperature -10 to 100°C at different frequencies. A single absorption and dispersion was obtained in this measuring temperature and frequency range. Figs.4.48 and 4.49 give a typical result obtained of the temperature dependence of dielectric constant  $\epsilon'$  and  $\tan \delta$ . In

general the absorption becomes more prominent as the frequency increases. The result obtained is typical of a polar polymer. The dependence of  $\tan \delta$  on temperature can be decomposed into two processes: one produced by purely dipole losses and the other caused by losses due to electrical conduction. It can also be seen that a sharp change in  $\epsilon'$  corresponds to the maximum of  $\delta$ . The temperature at which the absorption occurs is again in the region in which the TSD  $\alpha$  peak occurs.

#### 4.5.3.2 Discussion

Thermally stimulated discharge analysis of electrically polarised nylon films indicates persistent internal polarisation in all the specimens studied here. The occurrence of a maximum at about 60°C in the TSD spectrum suggests the onset of low frequency molecular motions in the polymer.

From Figs. 4.38 and 4.39 it is noted that the value of the current maximum and the charge released are proportional to the polarising field. This experimental result indicates that the induced polarisation is uniform due to dipole alignment rather than space charge. For the latter case one expects the induced polarisation to increase superlinearly with the polarising field.

Another strong evidence that a dipolar process is operating in the polymer is given in Fig. 4.45. The TSP experiment gives a peak characterised by the same position and approximate height as the TSD peak. The observation of a TSP peak cannot be understood by trapped space charge release since the nylon film was cooled under zero bias. In the TSP experiment, the orientation of the dipoles in the polymer is initially random. On heating the sample with the field applied, dipoles respond to the field as they become unfrozen near 60°C. This dipole alignment is observed by a corresponding peak at about 60°C in the current flowing in the external circuit.

It was noted in Chapter II that a dipolar TSD peak may arise from a single dipole relaxation or from a distribution relaxation, i.e. one with many relaxation times. The observed shift of the peak to higher temperatures as the polarising field and temperature increase is in favour of there being a distribution of relaxation times. Also, the shift of the peak with heating rate is in agreement with this fact as shown in Fig. 4.41.

The Staverman-Schwarzl transform (section 2.7), although it is only an approximation seems to be accurate enough for calculating the distribution function of relaxation times as shown in Fig. 4.47. It might be relevant to note here that the symmetrical Cole-Cole and Fuoss-Kirwood distribution functions do not differ much from the Gaussian distribution first advocated by Wagner, the only difference being that they fall off more slowly towards extreme values of  $U$  (Vanderschueren 1980). The occurrence of different relaxation frequencies is closely related to the complex structure of polymers which indicates the different configurations of the dipoles. For the  $\alpha$ -relaxations, which involve configurations rearrangements of the main chains, a distribution in  $\tau_0$  is more likely because the partaking molecular groups of various sizes and shapes will move at very different speeds when the polymer becomes rubbery.

In their study on nylon-66 Chattain et al (1973) used the TSD technique to investigate the  $\alpha$ -relaxation. The  $\alpha$  peak occurred at a temperature of about 66°C. Using the thermal sampling technique they claimed they were able to resolve the peak into four different processes, each having a relaxation time whose temperature variation followed an Arrhenius law. Table XI gives the peak temperatures and the corresponding activation energies of the isolated peaks found by them.

Peak	$\alpha_1$	$\alpha_2$	$\alpha_3$	$\alpha_4$
$T_m$ (°C)	23	45	58	67
A (eV)	0.55	0.85	1.31	2.09

Table XI:

Weber (1978) used the electret effect to study molecular motions in nylon 6. The  $\alpha$ -relaxation occurred at 70°C. No activation energy was calculated for that process. The relaxation was associated with large scale segmented motions at the glass transition temperature. The chain mobility increased by adding water and gave rise to the  $\alpha$  peak near 50°C.

Hino (1980) has used the thermal sampling technique to study molecular motions in several polymers. In particular, he has investigated nylon 6. He applies a bias  $V_p$  at the temperature  $T_p$  for a time  $t_p$ . The bias voltage is then removed at  $T_p$  and the sample cooled down in a short circuited condition very rapidly. He therefore isolates the TSD peaks due to dipoles with a single relaxation time involved in the distributed process. He found that the  $\alpha$ -relaxation, which occurred at 67°C, was distributed both in activation energy and in frequency factors. His results are presented in Fig. 4.51. If the length of the segments is distributed, the number of configurations of the chain will vary; hence an increase in the activation energy will increase the frequency factor.



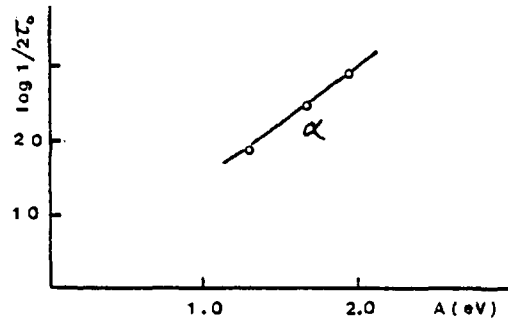
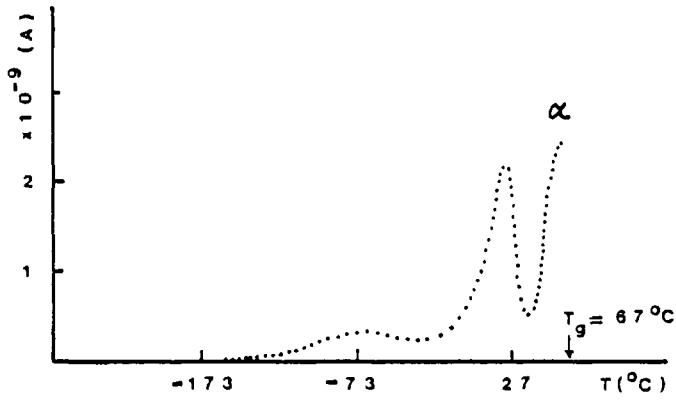


Fig.4.51: TSD and activation energy dependence of the frequency factor for nylon 6 (after Hino, 1980)

The  $\alpha$ -relaxation in polyamides has been investigated using dynamical mechanical and conventional dielectric measurements (McCrum et al 1967, Prevorsek 1971). The relaxation is believed to involve the motion of longer chain segments in the amorphous portions of the polymer. On the basis of cross-linked samples, Boyd (1959) concluded that these segments contain about 15 amide groups. Activation energies obtained for the  $\alpha$  peak varied between 1.52 and 2 eV. The temperature region in which the relaxation occurs agrees with the one found in the present study. It might be relevant to compare the amplitude of the TSD  $\alpha$  peak obtained here for the nylon terpolymer with that of the other monomers of nylon 6 and 66 found in the literature. The magnitude of the  $\alpha$ -relaxation found in this

investigation is larger than each of the more crystalline homopolymers. This is evidence which supports the amorphous assignment of the  $\alpha$ -relaxation.

Differential thermal analysis showed that the glass transition temperature of the nylon studied in this research lies in the region of 60°C. This value of  $T_g$  closely corresponds to the TSD  $\alpha$  peak obtained here.

It is known that the TSD method is characterised by a very low equivalent frequency ( $10^{-2}$  -  $10^{-4}$  Hz) as compared to the dielectric loss method ( $1$  -  $10^{12}$  Hz). The equivalent frequency (eqn. 2.18(a)) of TSD current measurements is estimated to occur at about  $2 \times 10^{-3}$  Hz. Fig.4.50 shows the relaxation maps of nylons 66, 6 and 610 (McCrum et al 1967, Hedvig 1977). It can be seen that the position of the TSD current peak is compatible with these maps, at least for nylon 66 and nylon 610. Also, the results of Fig. 4.48 agree well with the previous one, as far as the location of the TSD peak is concerned.

The upper value for polarisation arising from preferentially oriented amide groups, may be estimated by the following expression

$$P_{\max} = \mu N \quad (4.18)$$

where  $N$  is the number of amide dipoles per unit volume and  $\mu$  is the dipole moment of the amide group. The values of  $N$  and  $\mu$  are  $6 \times 10^{21}$  amide groups/cm<sup>3</sup> (McCall and Anderson 1960) and 3.7 Debye units (see section 4.1), respectively, yielding a value of  $P_{\max} = 7.4$  C/cm<sup>2</sup>. The largest value of the 60°C TSD peak is 4.5 C/cm<sup>2</sup>. This suggests that the amide groups have a large preferred orientation in the direction of the polarisation.

It is of interest at this point to consider briefly a theoretical predication for dipolar orientation in nylon films exposed to electric fields. For this purpose a calculation has been performed using the familiar Langeving equation for freely rotating dipoles  $P_L = N\mu^2 E_p / 3kT_p$  (see eqn. (2.1)). Calculation of  $P_L$  predicts values for the total

polarisation contributed by dipoles of the order of  $0.1 \mu\text{C}/\text{cm}^2$ , which is drastically lower than those obtained experimentally. The discrepancy between calculated and observed degrees of orientation suggest the presence of strong local fields in the condensed phase of the nylon. Local field effects would be important in nylon films due to the strong moment of the amide groups.

The activation energy obtained from the initial rise of the TSD curves (Figs. 4.43 and 4.44) is 1.9 eV. This is similar to the 2.1 eV obtained from Fig. 4.41. This has been discussed by van Turnhout (1975) who concludes that for a symmetrical distribution of relaxation times the plot  $\log I_{\text{rise}}(T) - \text{vs} - 1/T$  will have a slope  $mA/k$ , where  $m$  is the distribution parameter. Since  $m < 1$  it means that activation energies deduced from the initial rise current will be less than  $A$ , i.e.  $A_{\text{initial rise}} = mA$ . Thus one may estimate the value of  $m$  to be about 0.9. This value is close to the one used for the calculation of the distribution function (Fig. 4.47).

#### 4.5.3.3 Conclusions

The TSD technique has been found to be a powerful tool for investigating the molecular motions in nylon. The TSD  $\alpha$  peak obtained is well isolated and cannot be resolved in discrete components by application of the functional polarisation and thermal sampling techniques. It was found that the peak could be characterised by a continuous distribution of relaxation times resulting from a distribution in pre-exponential factors, as is often the case for  $\alpha$ -relaxations in polymers. It was found that differential thermal analysis and dielectric measurements had a good correlation with the TSD technique. Therefore, it might be concluded that the  $\alpha$ -relaxation is associated with large-scale segmental motions at the glass transition. The rigid glass becomes rubbery and the main chain motion becomes more and more active as the temperature is raised.

The apparent activation energy of the  $\alpha$  peak has been estimated by several experimental methods. Its value was about 2.0 eV and the equivalent frequency of the TSD peaks found was of the order of  $2 \times 10^{-3}$  Hz. Comparison

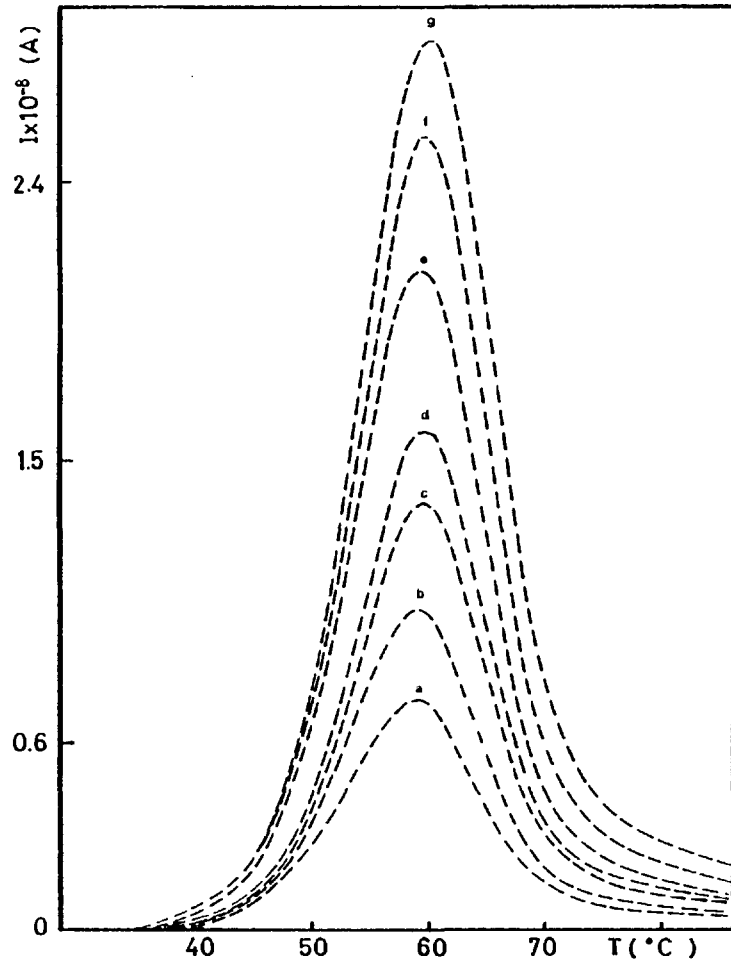


Fig. 4.37: Depolarisation current of nylon for various polarising fields,  $E_p$ . a,b,c,d,e,f and g correspond to 2.1, 2.9, 3.6, 4.3, 5.7, 7.1 and 7.9 kV/cm respectively.  $T_p = 60^\circ\text{C}$ ,  $t_p = 2$  min,  $r = 4^\circ\text{C}/\text{min}$ ,  $T_0 = 0^\circ\text{C}$ ,  $d = 7 \mu\text{m}$ .

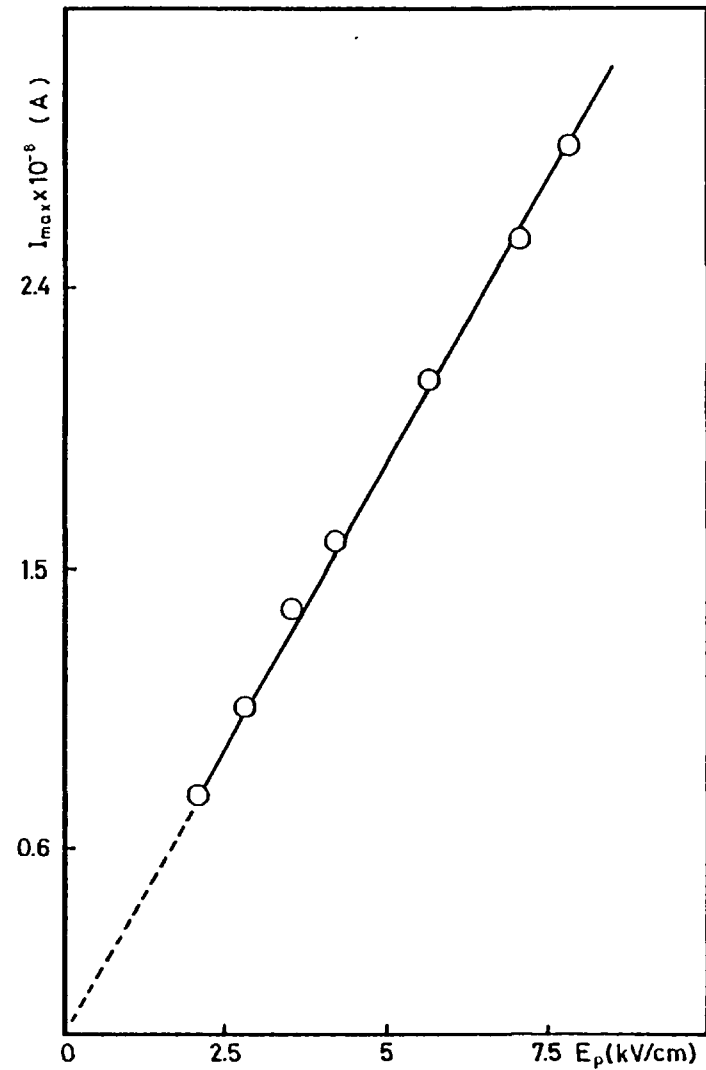


Fig. 4.38: Variation of the peak current with polarising field.

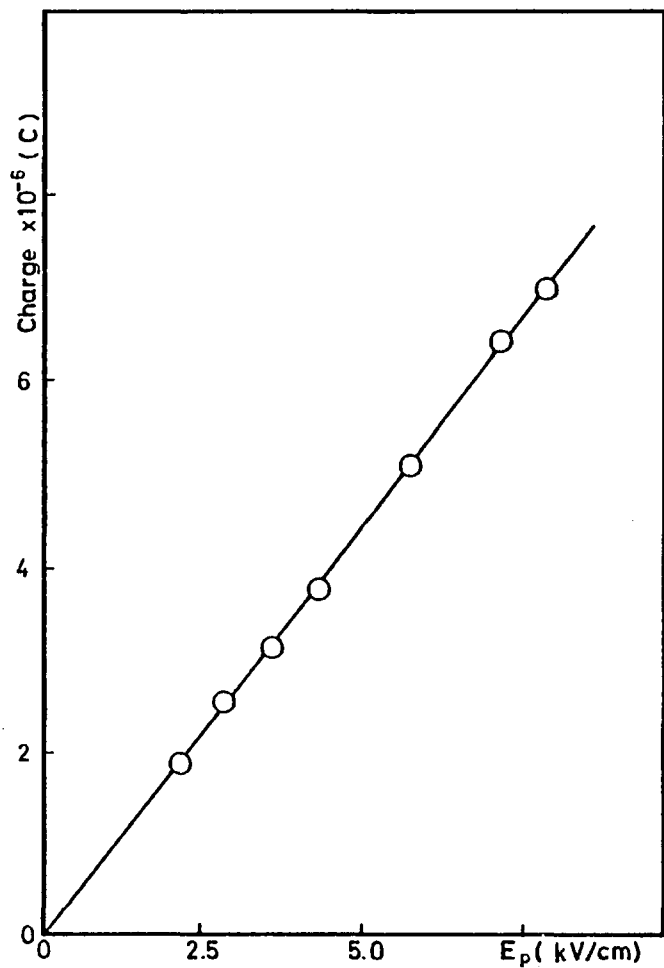


Fig. 4.39: Charge released to external circuit against polarising field.

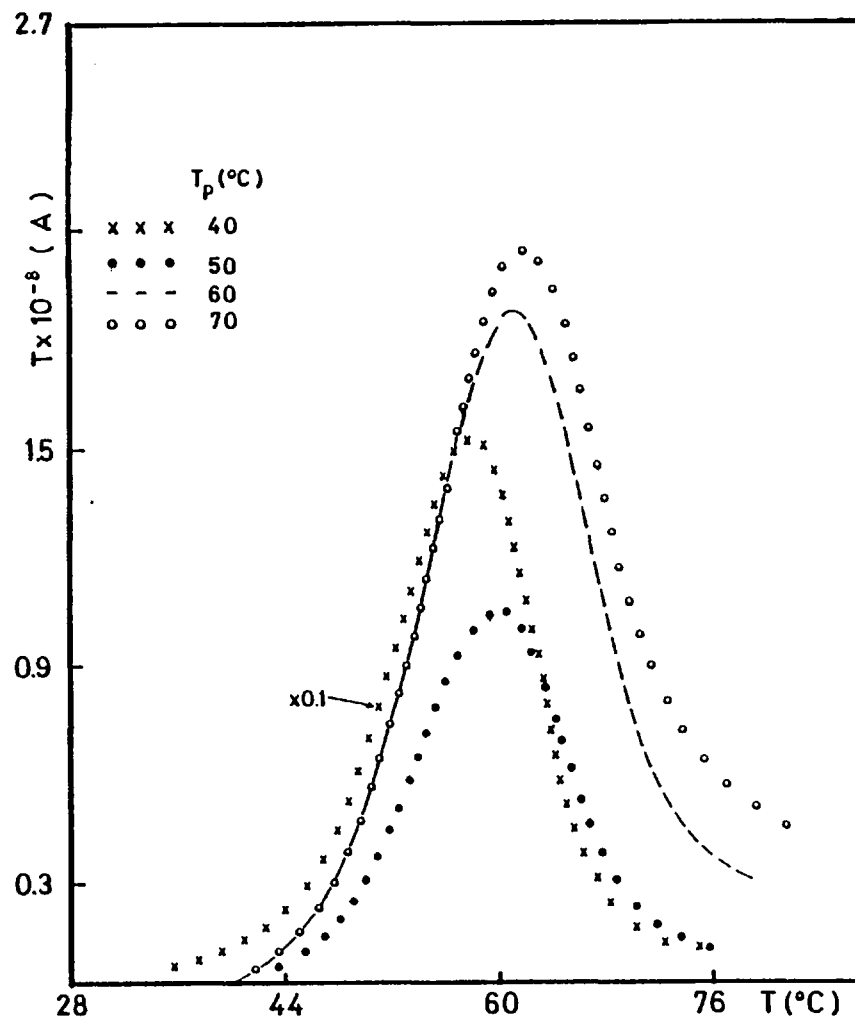


Fig. 4.40: TSD spectra as a function of polarising temperature.  
 $E_p = 5$  kV/cm,  $t_p = 10$  min,  $r = 4^\circ\text{C}/\text{min}$ ,  $d = 10$   $\mu\text{m}$ .

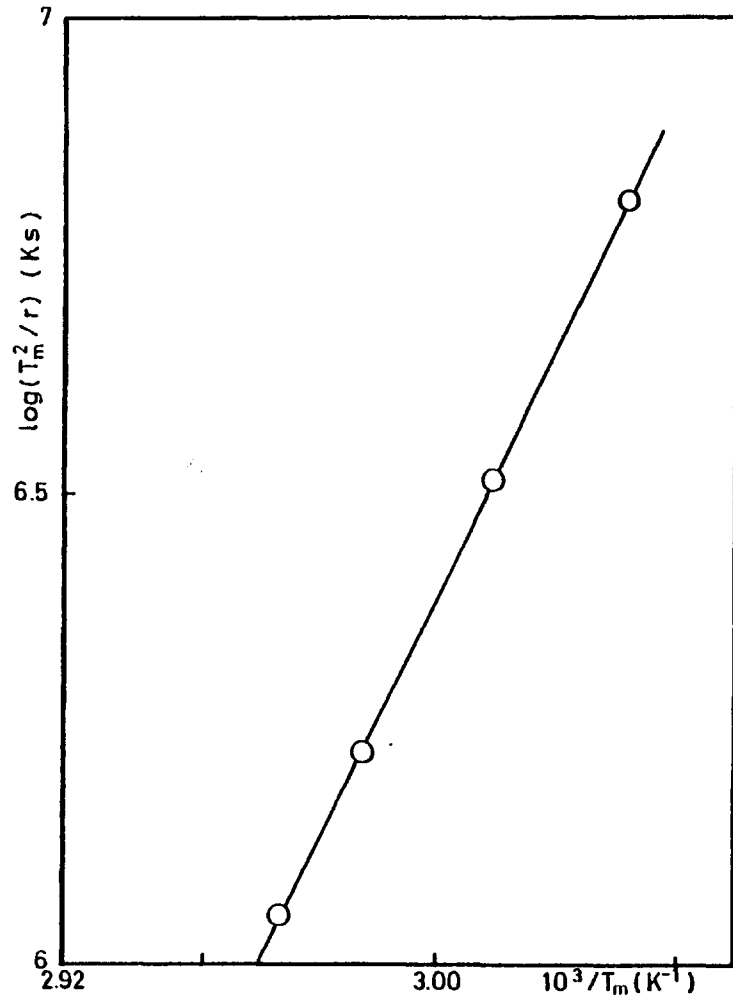


Fig. 4.41: Plot for calculating the activation energy of the  $\alpha$  peak from the temperature shift with heating rate of its TSD current maximum.

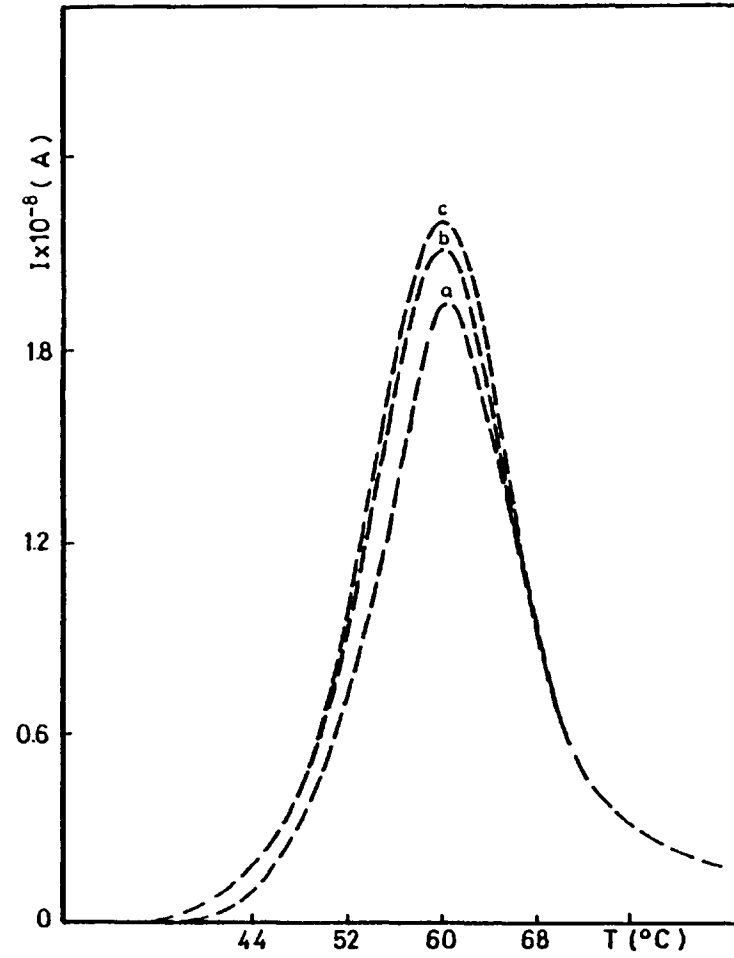


Fig. 4.42: Influence of prolonged storage on the  $\alpha$  relaxation. a, b and c correspond to 20 days, 20 hours and 5 min. respectively. Gold electrodes.  $E_p = 6$  kV/cm,  $T_p = 65^\circ\text{C}$ ,  $r = 4^\circ\text{C}/\text{min}$ ,  $d = 15$   $\mu\text{m}$ .

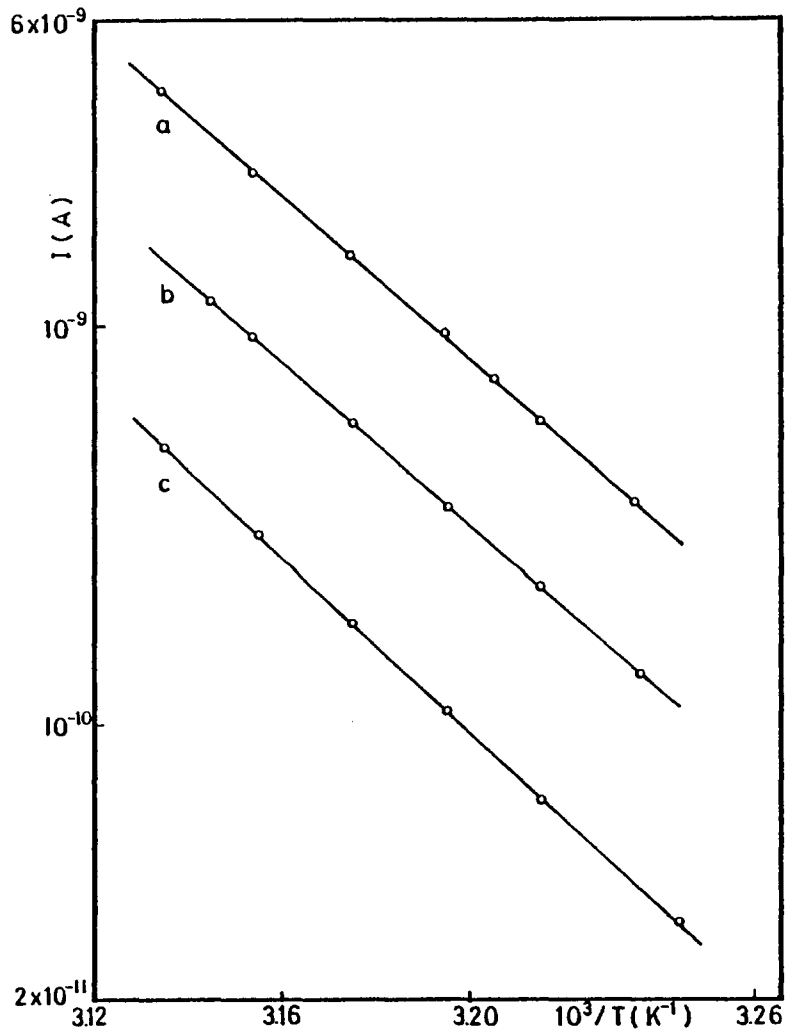


Fig. 4.43(a): Initial rise of the  $\alpha$  peak of a nylon electret. a, b correspond to 8.2 and 0.8 kV/cm respectively.  $T_p = 60^\circ\text{C}$ ,  $t_p = 2$  min,  $r = 4^\circ\text{C}/\text{min}$ .

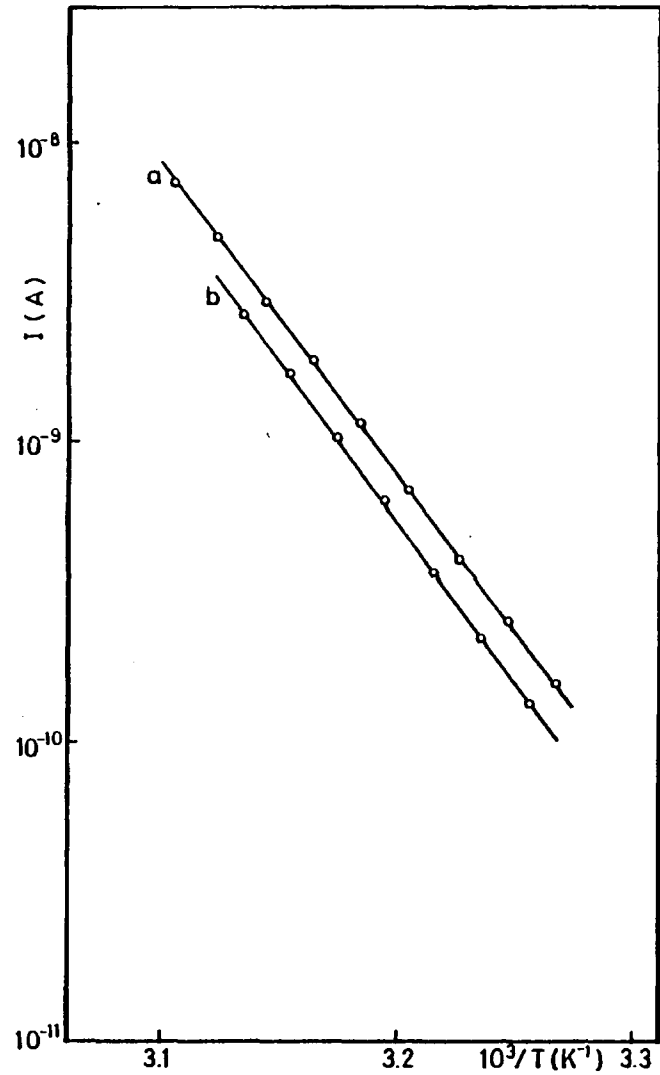


Fig. 4.43(b): The initial rise of the TSD  $\alpha$  relaxation of nylon. a and b correspond to 3 and 1.4 kV/cm,  $T_p = 90^\circ\text{C}$ ,  $t_p = 10$  min,  $r = 4^\circ\text{C}/\text{min}$ .

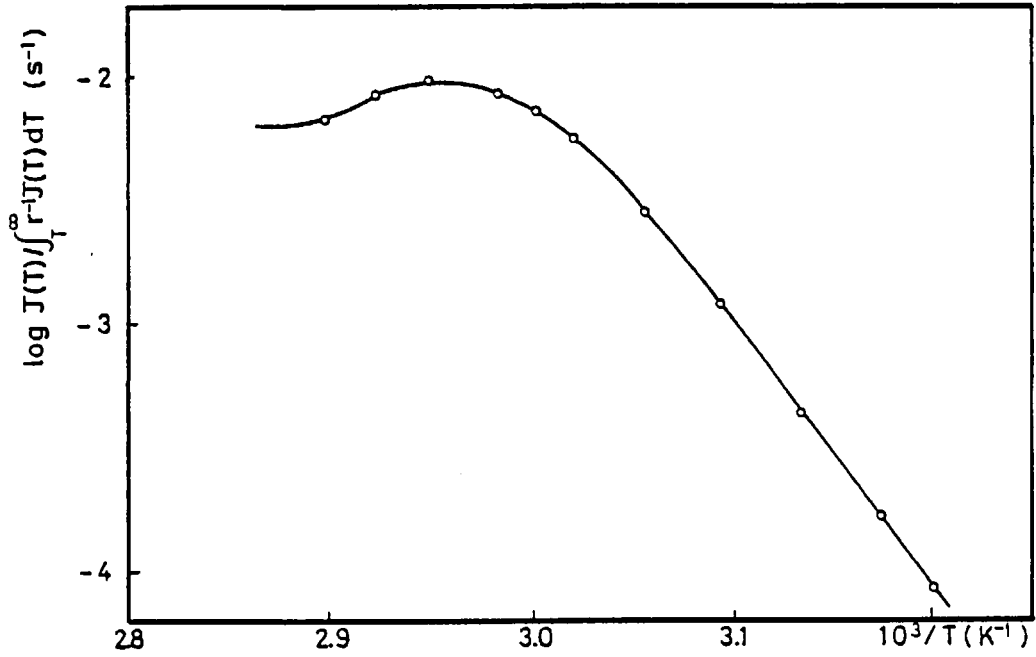


Fig. 4.44: BFG plot of the  $\alpha$  relaxation.  $T_p = 60^\circ\text{C}$ ,  $t_p = 2$  min,  $E_p = 7.8$  kV/cm,  $d = 7$   $\mu\text{m}$ .

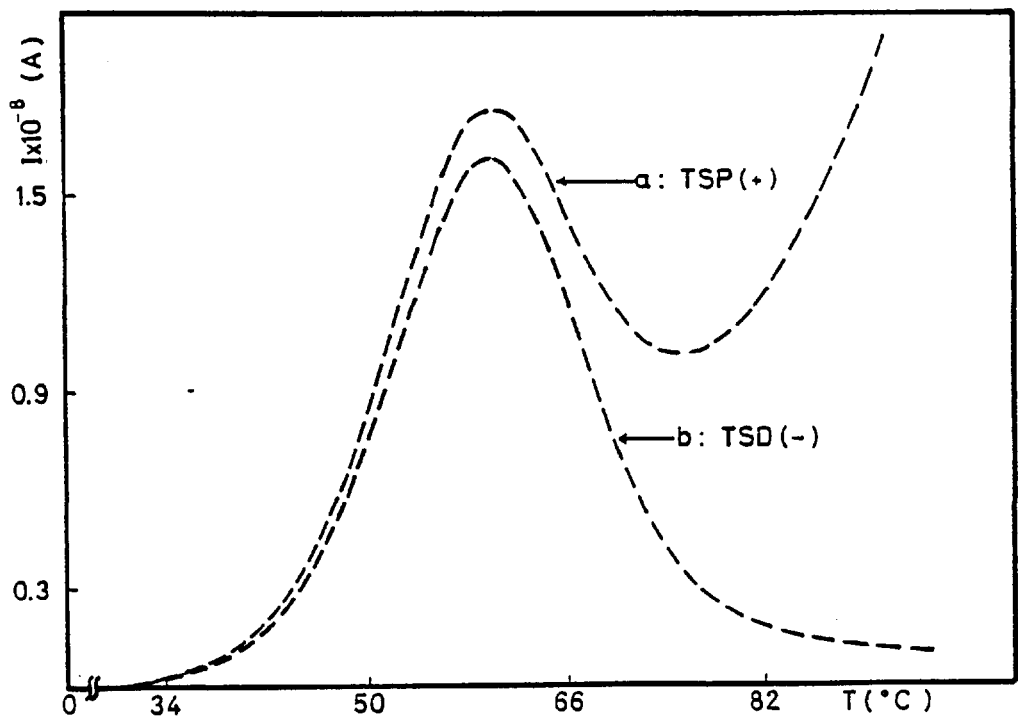


Fig. 4.45: Thermally stimulated polarisation and depolarisation current of the  $\alpha$  peak  $E_p = 3$  kV/cm. Poling conditions for TSD:  $T_p = 70^\circ\text{C}$ ,  $t_p = 5$  min,  $r = 4^\circ\text{C}/\text{min}$ .



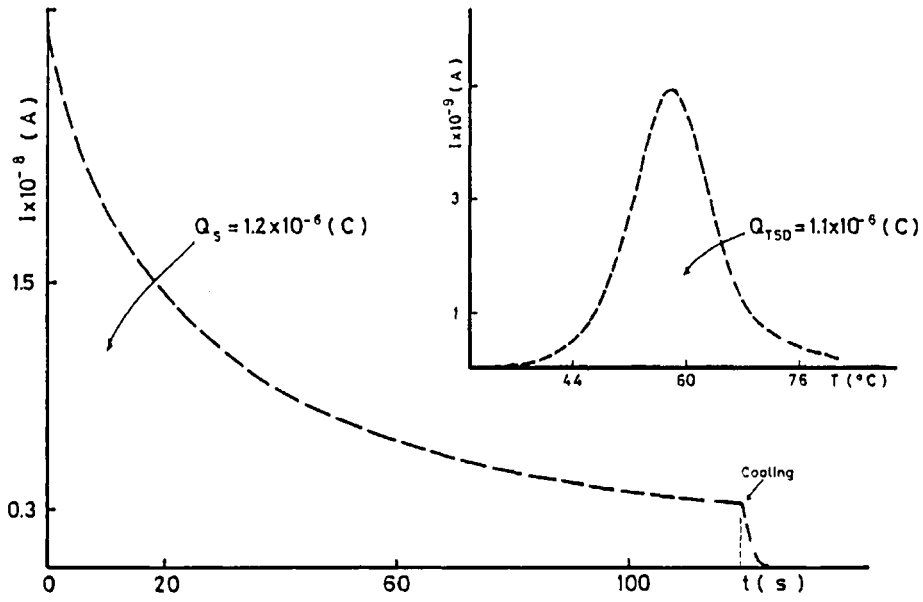


Fig. 4.46: Comparison between the charge adsorbed during formation of a nylon electret ( $Q_s$ ) and the charge released upon subsequent reheating ( $Q_{TSD}$ ).  $T_p = 60^\circ\text{C}$ ,  $t_p = 2$  min,  $r = 4^\circ\text{C}/\text{min}$ ,  $E_p = 5$  kV/cm.

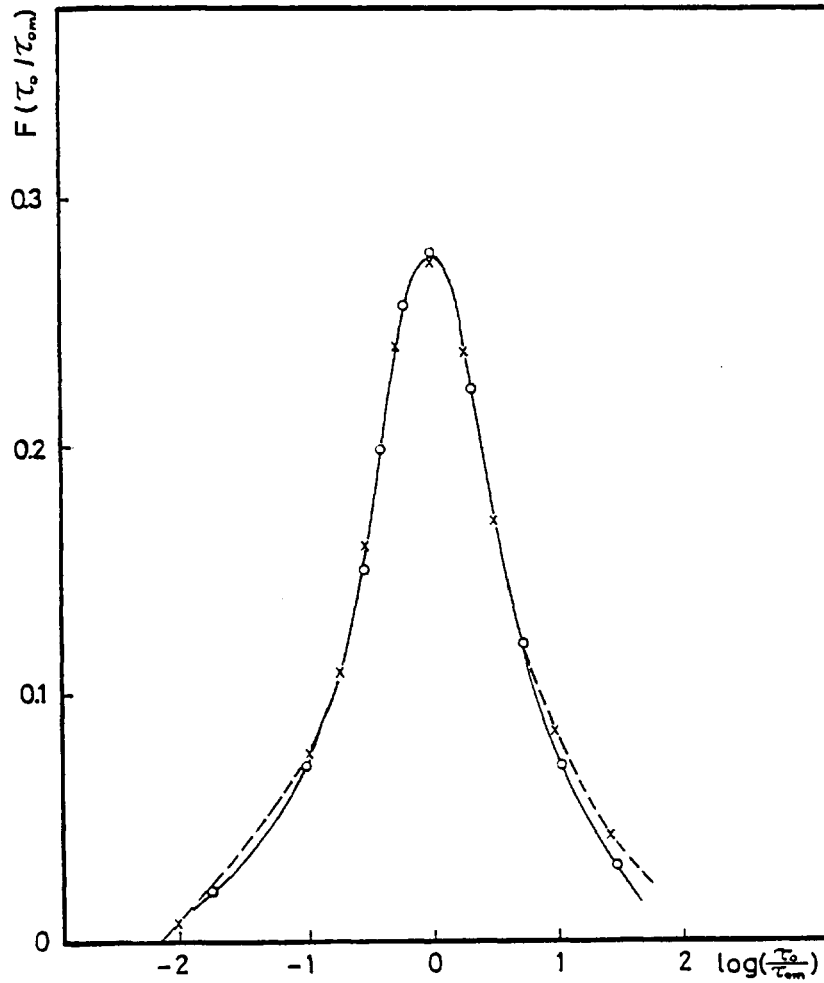


Fig. 4.47: Distribution of relaxation times in nylon, calculated from thermal depolarisation data (solid line) and from Fuoss-Kirkwood distribution with  $\bar{\gamma} \sim 0.3$  (dashed line).

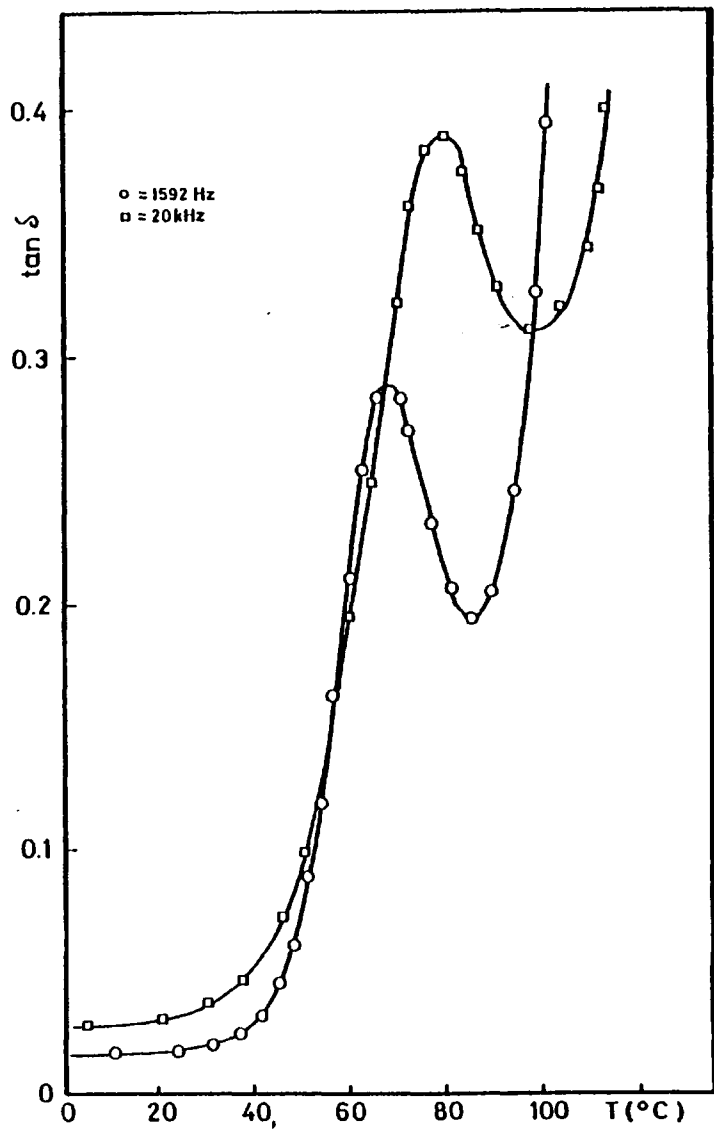


Fig. 4.48: Variation of  $\tan \delta$  against temperature.

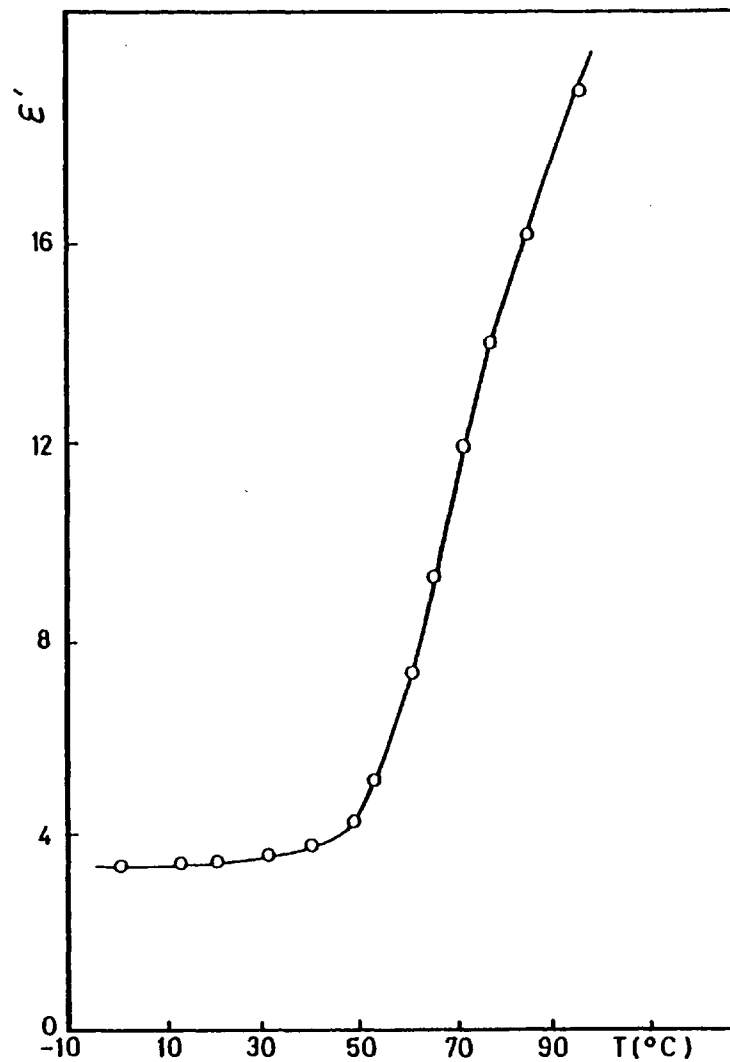
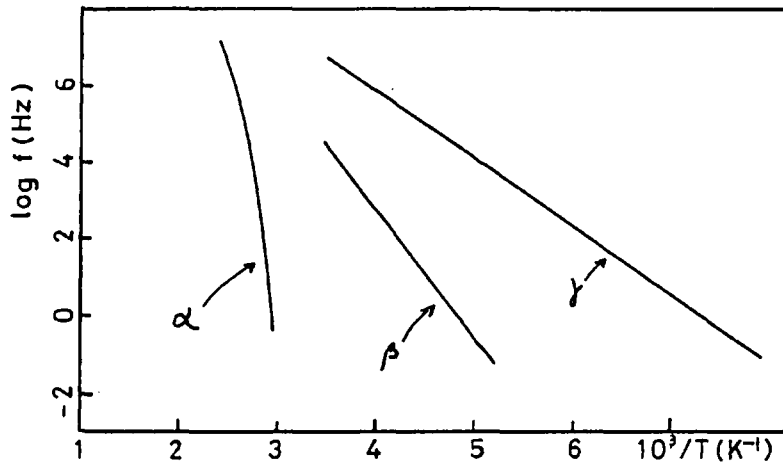
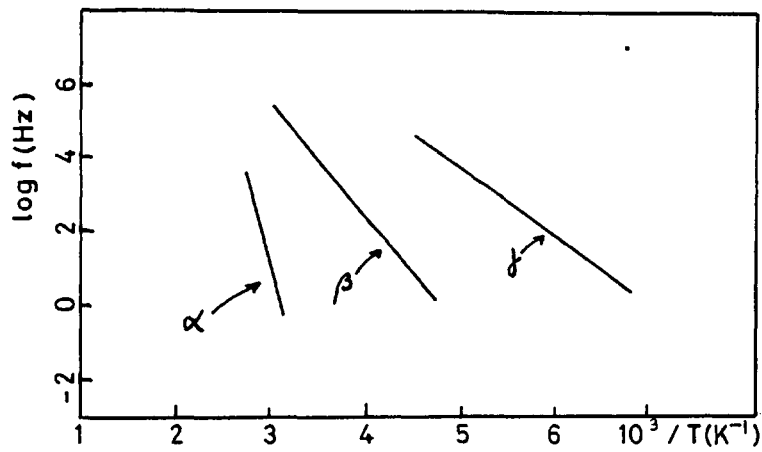


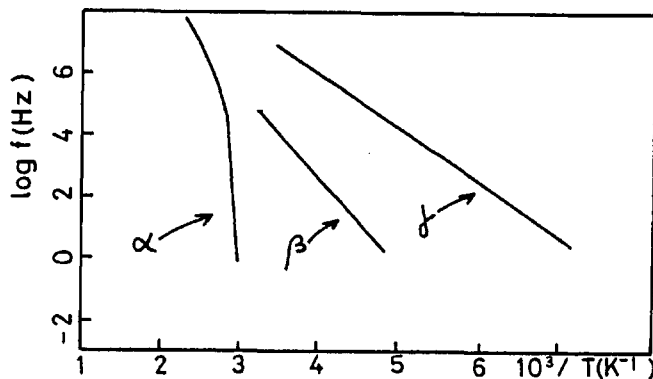
Fig. 4.49: Variation of permittivity with temperature.



Nylon-66



Nylon-6



Nylon-610

Fig. 4.50: Relaxation maps of nylon 6, 66 and 610 (McCrum et al 1967).

with previous workers (McCrum et al 1967) showed that this value is compatible with the  $\alpha$ -relaxations of nylon 66 and 610 determined by conventional dielectric measurements.

#### 4.5.4 The $\rho$ Peak

##### 4.5.4.1 Results

The  $\rho$  peak, observable at temperatures higher than that of the  $\alpha$ -relaxation process appeared in all the samples investigated. The current released had the opposite direction to that of the charging current.

The TSD spectra obtained from solvent cast polyamide films, charged at 80°C for periods of 30 min, for different polarising fields and heating rate of 6°/min are shown in Fig. 4.52 (gold electrodes). The small peak which appears at about 60°C corresponds to the  $\alpha$ -relaxation, which was discussed in the previous section. As can be seen the amplitude of the  $\rho$  peak is very large, which means that very high levels of persistent internal polarisation exist in the electret. The maximum temperature of these peaks is almost independent of the polarising field. A slight shift of the peak to higher temperatures occurs as  $E_p$  increases. However, the shift of the peak with  $E_p$  became more prominent when the polarising temperature was 90°C or higher, as shown in Fig. 4.53. The relationship between the maximum current of the TSD  $\rho$  peak and the polarising field is shown in the inset of Fig. 4.52 and is seen to be non-linear.

The total charge released to the external circuit during discharge, for several polarising temperatures, is shown in Fig. 4.54 as a function of the polarising field. The total charge was obtained by integrating the TSD spectrum with respect to time. The small contribution of the dipolar charge due to the  $\alpha$  peak was isolated by the peak cleaning method (Perlman and Unger 1974) and therefore will not be counted. As can be seen, the total charge,  $Q_p$ , released during the discharge process is not a linear function of  $E_p$ . It is worth noting also that the charge released becomes constant at higher polarising temperatures and fields. As one gradually

increases the polarising temperature, a regular increase in the amplitude of the  $\rho$  peak is first observed and this is followed by a saturation phenomenon. The reproducibility of the  $\rho$  peaks were good as shown in Fig. 4.55.

The influence of prolonged storage on the  $\rho$  peak was also investigated. The results are shown in Fig.4.56. In (a) the electret was depolarised immediately after being formed, while in (b) the electret was discharged after being kept in short-circuit condition at room temperature and in vacuum for one week. As can be seen very little charge was lost during storage.

To calculate the activation energy of the process, the method of varying heating rate was used. The position of the  $\rho$  peak for seven heating rates is listed in Table XII.

$r$ ( $^{\circ}\text{C}/\text{min}$ )	$T_m$ ( $^{\circ}\text{C}$ )
2	79
3	81
4	83.5
5	85
6	87.5
8	88
10	90

Table XII:

The temperature shift is small, but the results can be fitted to a straight line in a  $\log T_m^2/r$  vs  $1/T_m$  plot as shown in Fig. 4.57. From the slope of this line the apparent activation energy is 1.4 eV.

The dependence of the  $\rho$  peak on the material of the electrodes used was also studied. Fig. 4.58 presents the TSD peak obtained using  $\text{Al}$  evaporated electrodes. The  $\rho$  peak is still present and its amplitude is large. The charge released to the external circuit was about  $2 \times 10^{-4} \text{C}$ .

Hot pressed polyamide films, prepared by the method outlined in Chapter III, were also investigated. A typical TSD spectrum is shown in Fig. 4.59 for a 50  $\mu\text{m}$  film. It can be seen that the  $\alpha$ ,  $\rho$  and  $\rho'$  peaks are still present.

Another experiment done to investigate the  $\rho$  peak was to apply a collecting voltage  $V_c$ , much smaller than the polarising voltage  $V_p$ , during the TSD measurement. The Au-Polyamide-Au structure was polarised with  $V_p = 10\text{V}$  at  $90^\circ\text{C}$  for 30 min. After cooling down to  $0^\circ\text{C}$  the polarising voltage  $V_p$  was switched off, the structure short-circuited, and then the collecting voltage  $V_c$  ( $\approx 0.1 V_p$ ) was applied. The sample was then heated at a constant rate of  $4^\circ\text{C}/\text{min}$  and the current measured as a function of temperature. Fig. 4.60 shows the results obtained for two collecting fields of opposite polarity. In both cases (see (a) and (b) in Fig. 4.60) the TSD current flowed in the opposite direction that that of the formation current of the electret. It can be seen that the  $\rho$  peak occurs in the region of  $100^\circ\text{C}$  and is present in both cases.

Since the TSD  $\rho$  peaks are not broad and the amount of overlapping with the  $\alpha$  and  $\rho'$  peaks is small in the range of temperature  $80\text{-}100^\circ\text{C}$ , the graphical integration method was applied to these. Fig. 4.61 gives two typical curves of the quantity  $J(T)/\int_T^\infty r^{-1}J(T)dT$  plotted against  $10^3/T$ . It can be seen that only a partial linearisation at low temperatures can be achieved. When the temperature approaches the current maximum, the curves bend downwards. This gives an indication that one is not dealing with a single relaxation process. The temperature at which the peak occurred is also indicated on the graph. The values of the relaxation parameters calculated by the BFG method are listed in Table XIII.

$T_p$ (°C)	$T_m$ (°C)	$J_m \times 10^{-7}$ (A/cm <sup>2</sup> )	A (eV)	$\tau(T_m)$ (sec)	$\tau(300K) \times 10^7$ (sec)
80	91	4	1.70	140	1
90	101	7	1.70	83	3

Table XIII: Parameters of the  $\rho$  peak evaluated by BFG's method

The initial rise method was also utilised to calculate the activation energy of the peak. Table XIV presents the values obtained for different applied fields. The polarising temperature and time were 80°C and 30 min respectively. The heating rate was 4°C/min.

$E_p$ (kV/cm)	A (eV)
3	1.64
7	1.72
11	1.65
19	1.71
23	1.70
27	1.65
<hr/> $A = (1.68 \pm 0.10) \text{ eV}$	

Table XIV:

As can be seen the activation energy did not vary too much with  $E_p$ . An average value of 1.68 eV can be calculated for the activation energy.

The dependence of the charge released on heating rate was also investigated for the  $\rho$  peak. It was found that the amount of charge released decreased as the heating rate increased. A typical result found is presented in Fig. 4.62.

#### 4.5.4.2 Discussion

The TSD  $\rho$  peak in the polyamide investigated here occurs above the glass transition temperature. The fact that the charge released as a function of the polarising field is non-linear seems to be in agreement with a space charge polarisation mechanism. It is known that TSD arising from space charge polarisation due to electrons injected from the electrodes strongly depends on the collecting voltage  $V_c$  which is applied during TSD measurements, and that the sign of the current changes with  $V_c$  when it is smaller than  $V_p$  (Sawa et al 1974, Tanaka et al 1978 a, b). The results obtained in Fig. 4.60 provide experimental evidence in opposition to the injection mechanism. In general space charges tend to accumulate near the boundary of different materials. In homogeneous polymers they are expected to accumulate near the electrodes and in heterogeneous polymers on the interfaces within the material such as boundaries between crystalline and amorphous regions. The absence of any electrode dependence in the films investigated suggests that the electrode polarisation mechanism may not have been responsible for the TSD  $\rho$  peak and therefore the polarisation is mainly a bulk phenomenon.

Differential thermal analysis of the polyamide studied has shown that a crystallisation exotherm exists in the region of 80°C. This phenomenon has been called Cold Crystallisation and is assumed to involve the nearest neighbouring chain units in the amorphous regions. Such crystallisation occurs without molecular arrangements and leads to the production of small crystallites. Therefore it is believed that the  $\rho$  peak is associated with space charges trapped at the crystalline-amorphous interfaces. Similar TSD  $\rho$  peaks have been observed in polycarbonate, polyimide, polymethyl methacrylate and other copolymers (Vanderschueren and Gasiot 1979, van Turnhout 1980).



It might be relevant at this stage to correlate the thermally stimulated discharge technique with the conventional dielectric measurements. It is known, as was explained in section 4.4.1, that when a d.c. field is applied to a finite thickness of a non-ideal dielectric sandwiched between two plane parallel electrodes, there is, besides the rapidly changing current and the steady-state conduction current, a long-term slowly decaying current ( $\propto t^{-n}$  where  $n$  is  $\approx 1$ ). Similarly, on removal of the voltage and with the electrodes short-circuited, the fast component of the current is followed by a long-term slowly decaying current. The time dependence of the transient current may be used to calculate the dielectric loss factor  $\epsilon''$  at low frequencies (where the conventional bridge technique is not available), using the Hamon (1952) approximation (see eqn. (4.16)).

The variation of loss factor with frequency at temperature above  $T_g$  was measured in section 4.4.3 (see Fig. 4.30). A clear peak was observed in the high temperature low frequency range. It seems, therefore, that the thermally stimulated depolarisation technique, which commonly works in ranges of equivalent frequencies of  $10^{-2}$  -  $10^{-4}$  Hz, has revealed the  $\rho$ -relaxation found in section 4.4.3. Furthermore, the results of the d.c. transient technique closely correspond to the results of this section. Using eqn. (2.18a) one can estimate the equivalent frequency of the TSD  $\rho$  peak to be of the order of  $10^{-3}$  Hz.

Recalling the values of the activation energies found in the galvanic cell experiment (section 4.3.2.2) and d.c. conduction experiments (section 4.4.3), the following table can be formed.

Experiment	A(eV)
Galvanic cell	1.20
d.c. conduction	1.21
d.c. transient technique	~ 1.10
electret effect	1.4 - 1.7

Table XV:

It can be seen from Table XV that the activation energy determined from the electret resulted in a value larger than the others. Nevertheless those values agree well with the activation energy found by McCall and Anderson (1960).

According to Jonscher (1967) the activation energy associated with migration of ionic species over microscopic distances in amorphous solids is 0.6 - 0.8 eV or higher. Since the activation energies found in the present work are greater than 0.8 eV, the polarisation might possibly be produced by ionic species. This explanation is supported by the fact that an ionic conduction mechanism was found in the polyamide investigated here above 70°C using a galvanic cell consisting of Au-Polyamide-Al at low field. Also, the large amount of charge stored in the virgin films could be associated with ionic carriers. The type and source of ionic species is unknown, though contribution from protons cannot be ruled out. Activation energy for proton conduction in polymers seems to be in the region of 1.3 - 1.4 eV (Sacher 1970, Vijn 1978, Crine et al. 1979b).

The space charge TSD peak observed shows the characteristic of a distributed process, i.e. extension over a wide range of temperature and large increasing shifts of the maximum temperature with increasing polarising fields. However, attempts to interpret these observations, even qualitatively, in terms of a distribution of conductivity parameters have been surprisingly rare and, up to now, no theoretical effort has been

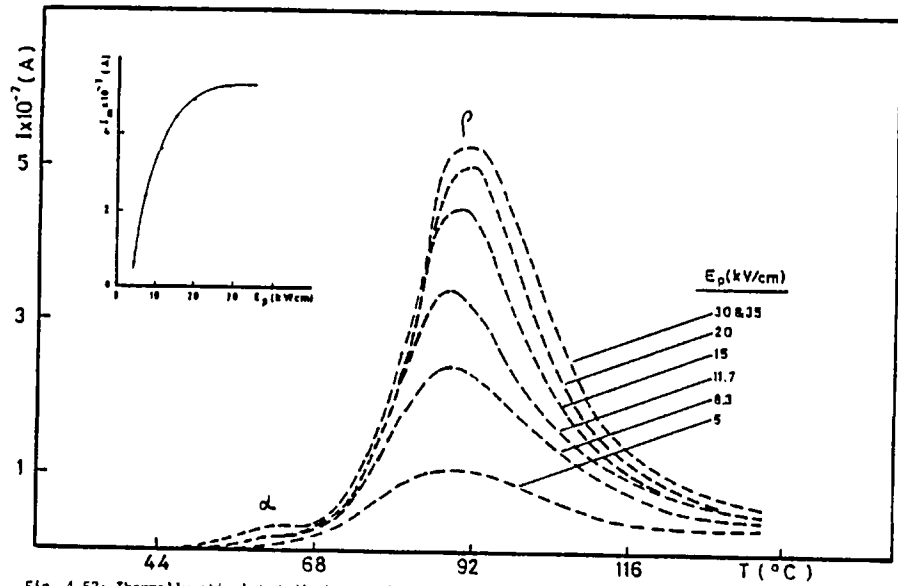


Fig. 4.52: Thermally stimulated discharge of nylon film 10  $\mu\text{m}$  thick polarised for 30 min. at 80°C with different polarising fields.  $r = 6^\circ\text{C}/\text{min}$ .  $T_0 = 0^\circ\text{C}$ . Au electrodes. Inset shows dependence of  $I_m$  against  $E_p$ .

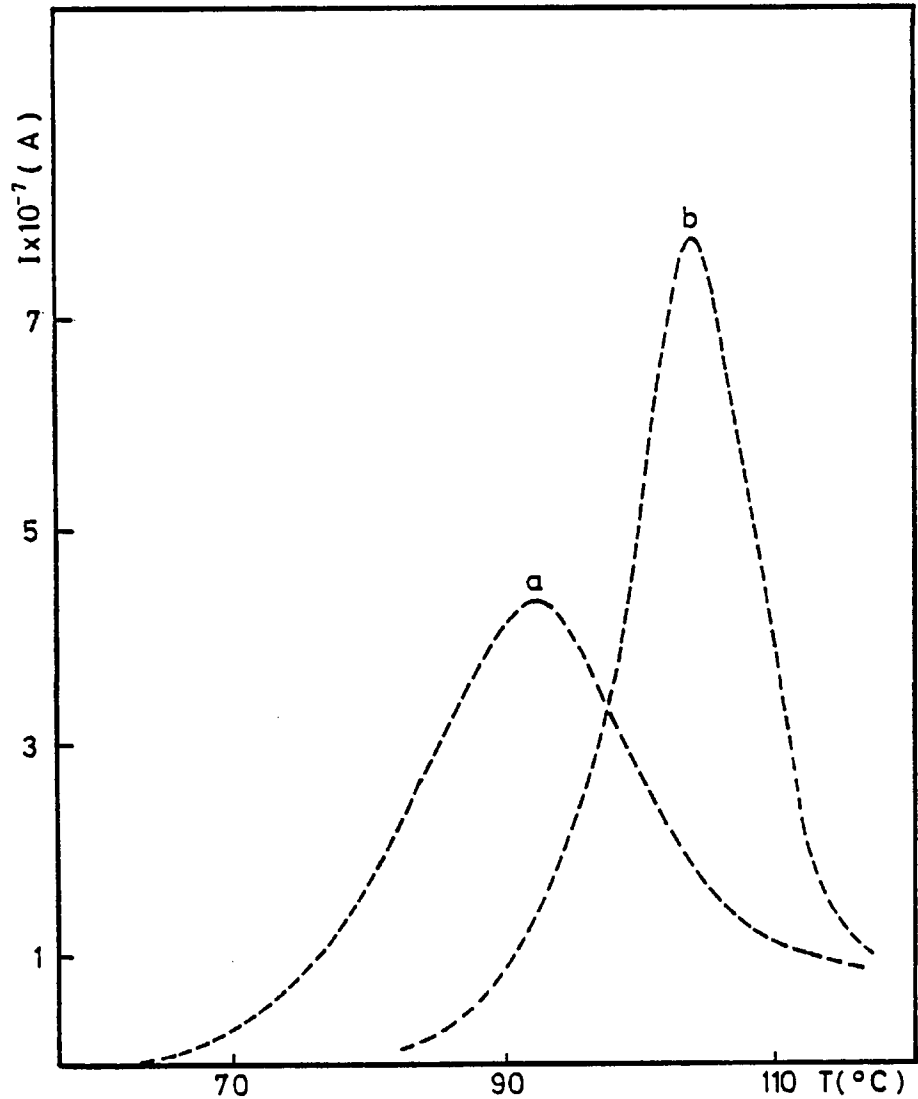


Fig. 4.53: Effect of the polarising field on the TSD  $\rho$  peak. a and b correspond to 1.67 and 18.3 kV/cm respectively.  $T_p = 90^\circ\text{C}$ .  $t_p = 30$  min.  $d = 10 \mu\text{m}$ .

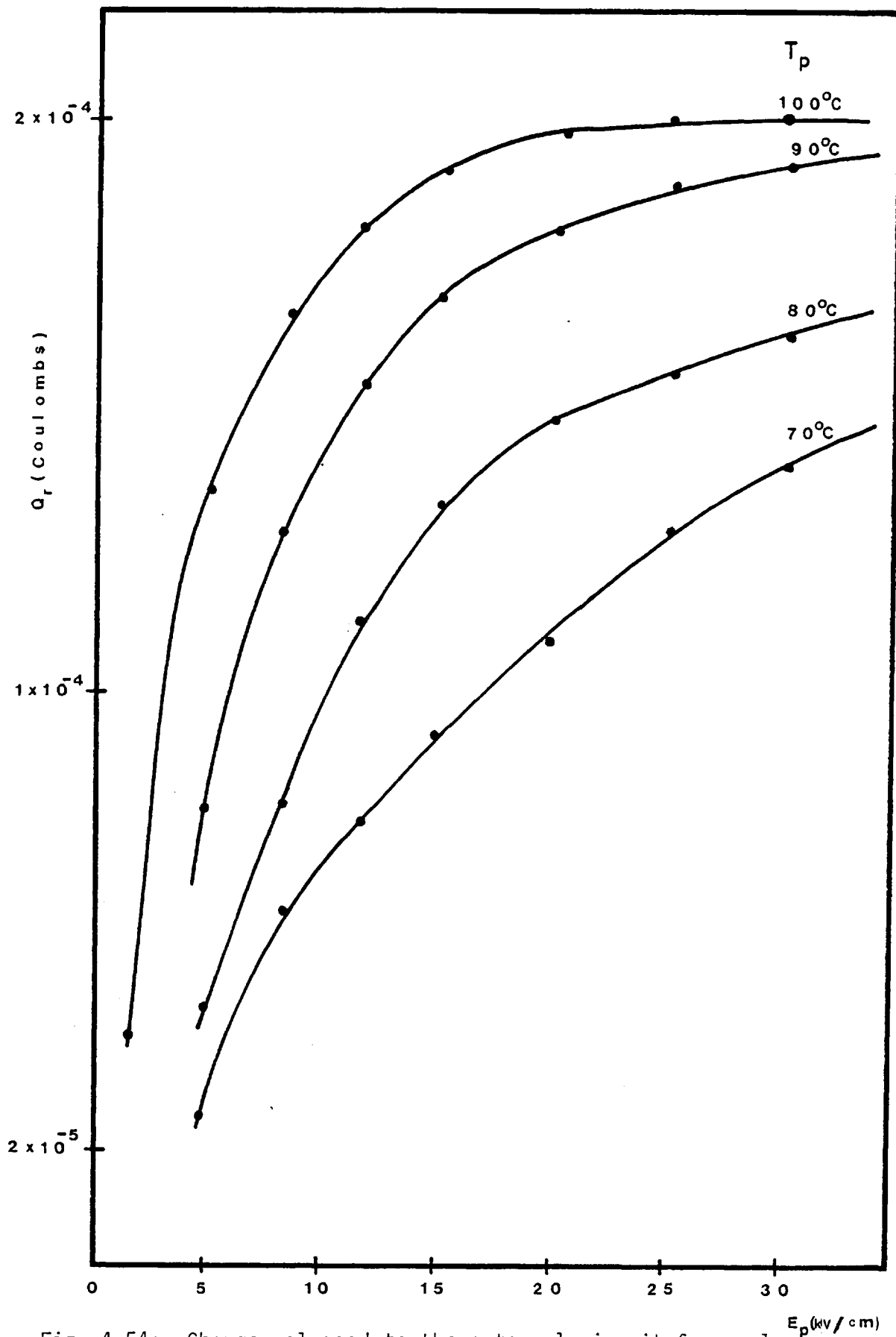


Fig. 4.54: Charge released to the external circuit from nylon electrets as a function of polarising field and temperature.  $r = 4^\circ\text{C}/\text{min}$ ,  $T_0 = 0^\circ\text{C}$ ,  $d = 10 \mu\text{m}$ . Au electrodes.

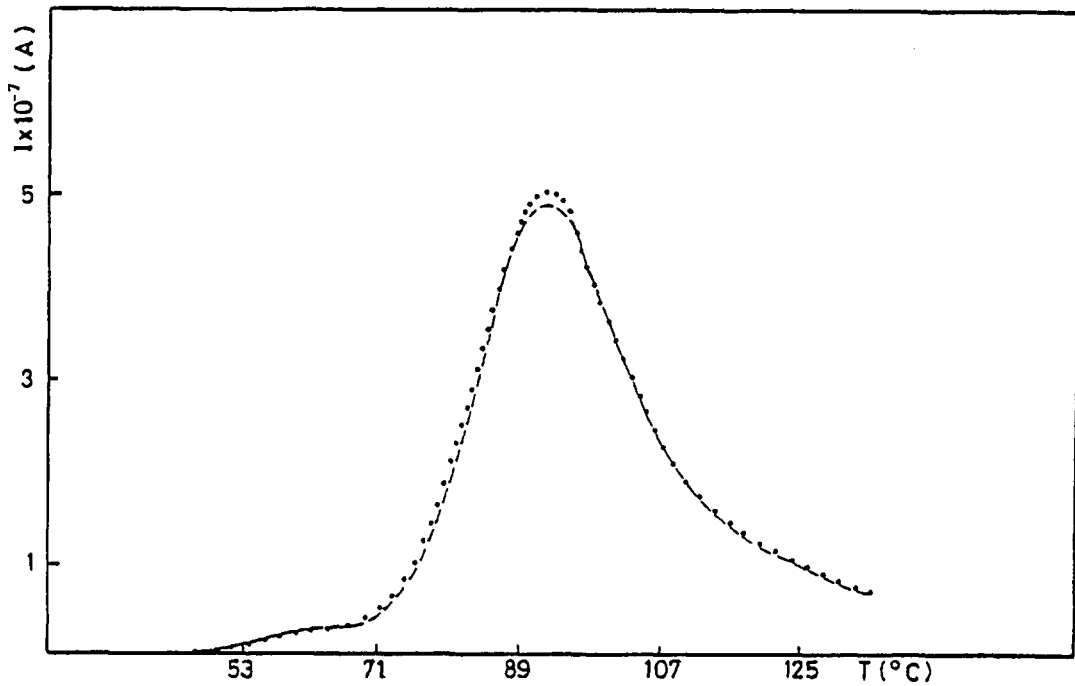


Fig. 4.55: Reproducibility of the TSD  $\rho$  peak  $E_p = 20$  kV/cm,  $T_p = 80^\circ\text{C}$ ,  $r = 6^\circ\text{C}/\text{min}$ ,  $T_0 = 0^\circ\text{C}$ , Au electrodes. The dashed curve corresponds to a discharge done 2 days after the first discharge (dotted curve)  $Q$  (dashed curve) =  $(1.50 \pm 0.10) \times 10^{-4}\text{C}$ ,  $Q$  (dotted line) =  $(1.52 \pm 0.10) \times 10^{-4}\text{C}$ .

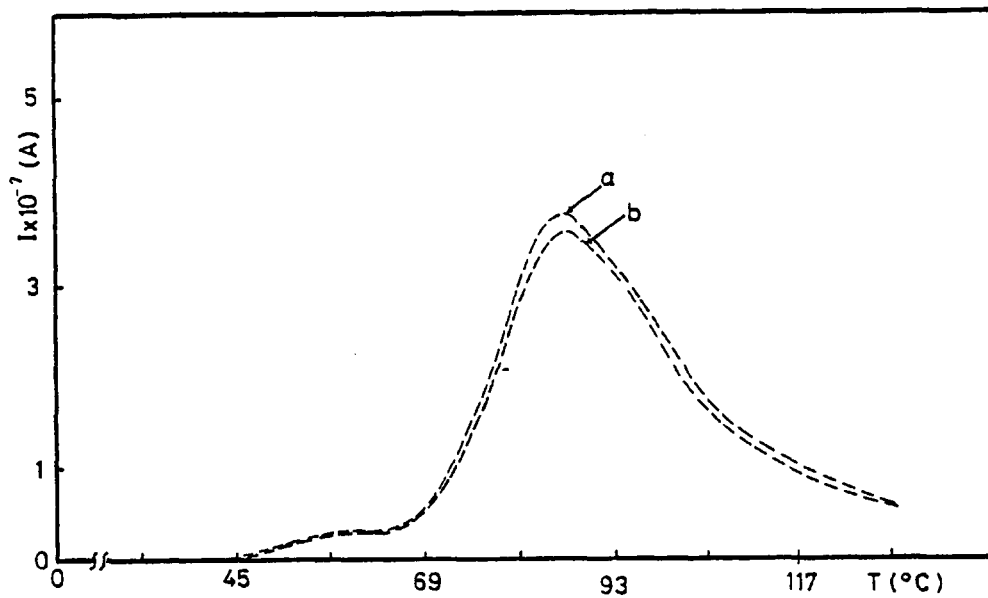


Fig. 4.56: Influence of prolonged storage at room temperature on the  $\rho$  peak. In a the nylon electret was depolarised immediately after being formed, while in b the electret was depolarised after 1 week.  $T_p = 70^\circ\text{C}$ ,  $t_p = 30$  min,  $E_p = 35$  kV/cm,  $r = 6^\circ\text{C}/\text{min}$ .

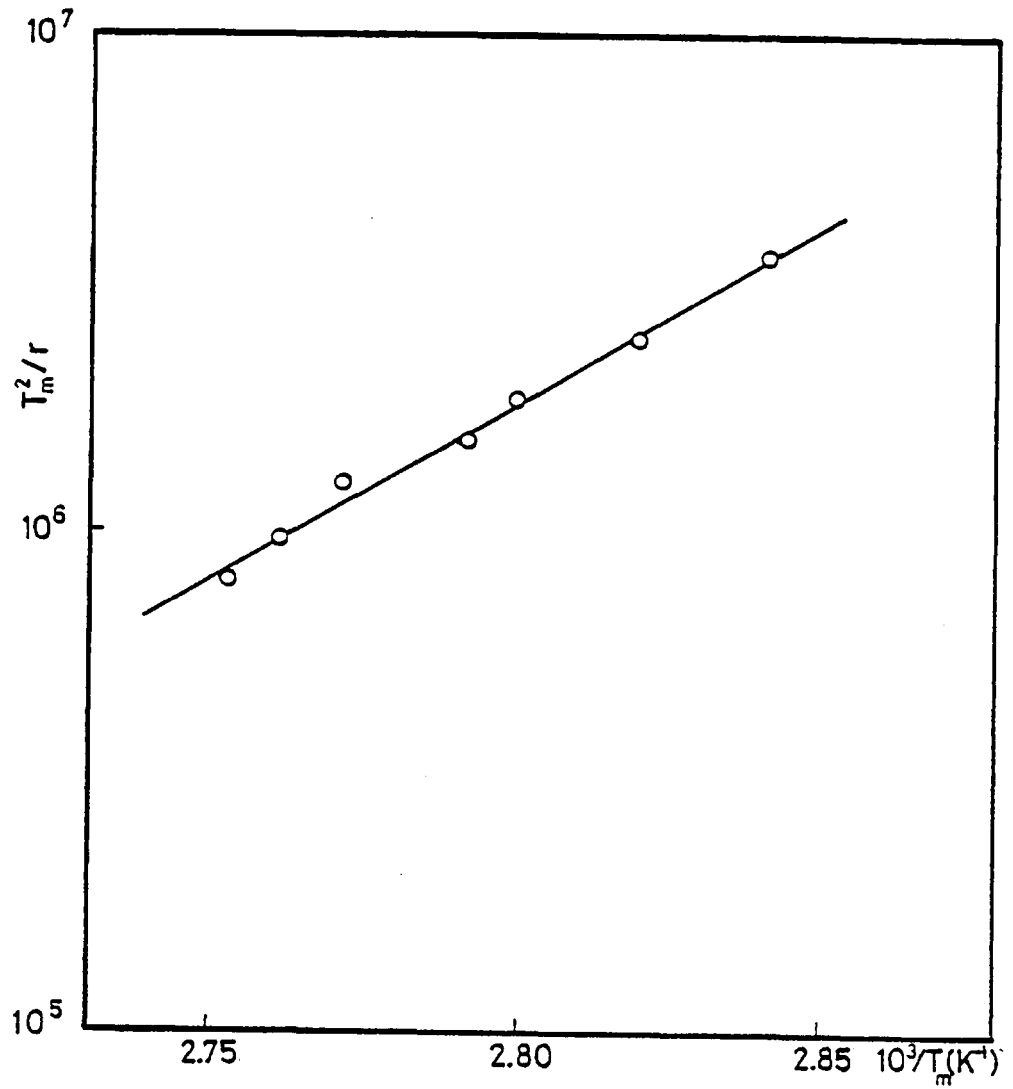


Fig. 4.57: Plot of  $\log (T_m^2/r)$  vs.  $1/T_m$  obtained from the TSD curves of polarised nylon films  $10 \mu\text{m}$  thick with  $E_p = 12 \text{ kV/cm}$ ,  $T_p = 90^\circ\text{C}$ ,  $t_p = 30 \text{ min}$ ,  $T_0 = 0^\circ\text{C}$ ,  $d = 10 \mu\text{m}$ .

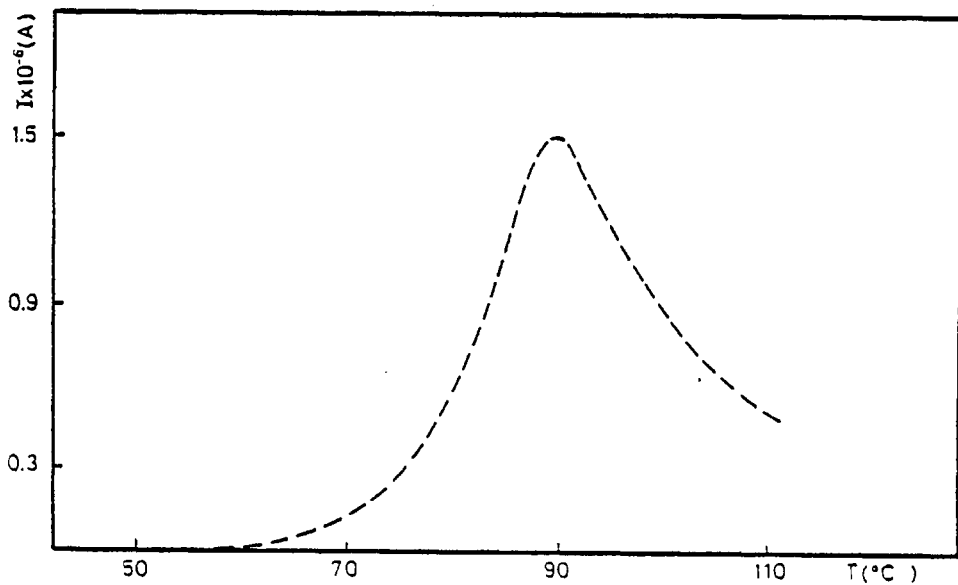


Fig. 4.58: TSD  $p$  peak obtained using aluminium electrodes.  $E_p = 3.6 \text{ kV/cm}$ ,  $T_p = 85^\circ\text{C}$ ,  $t_p = 40 \text{ min}$ ,  $d = 14 \mu\text{m}$ ,  $r = 4^\circ\text{C/min}$ ,  $T_0 = 0^\circ\text{C}$ .

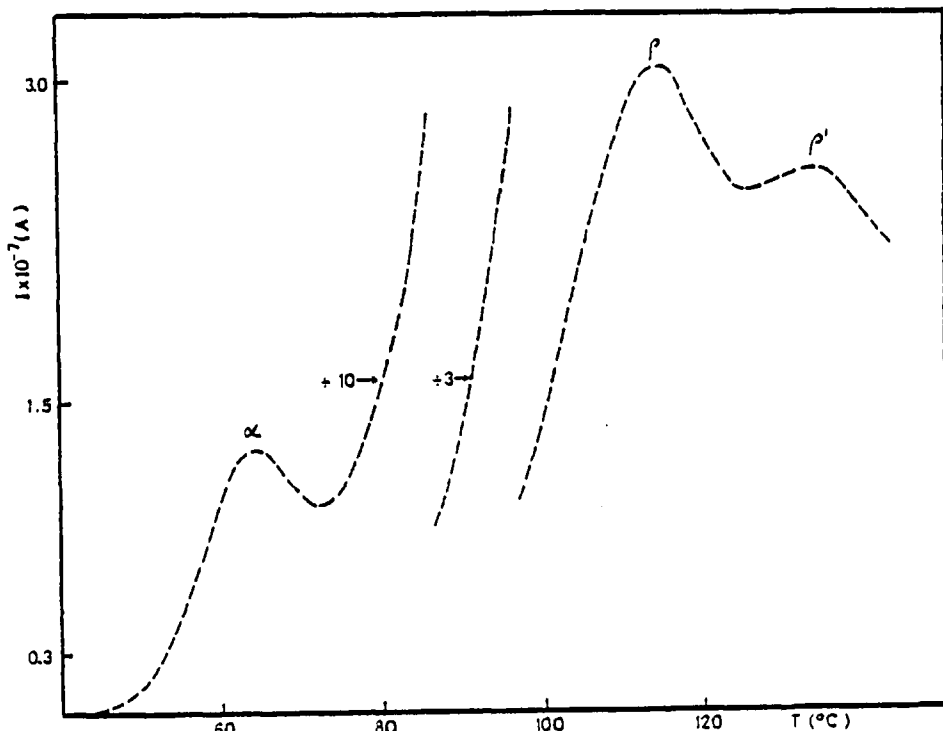


Fig. 4.59: TSD spectrum of not pressed nylon films. Au electrodes,  $T_p = 130^\circ\text{C}$ ,  $E_p = 2\text{ kV/cm}$ ,  $t_p = 19 \text{ min}$ ,  $T_0 = 0^\circ\text{C}$ ,  $d \approx 50 \mu\text{m}$ ,  $r = 4^\circ\text{C/min}$ .

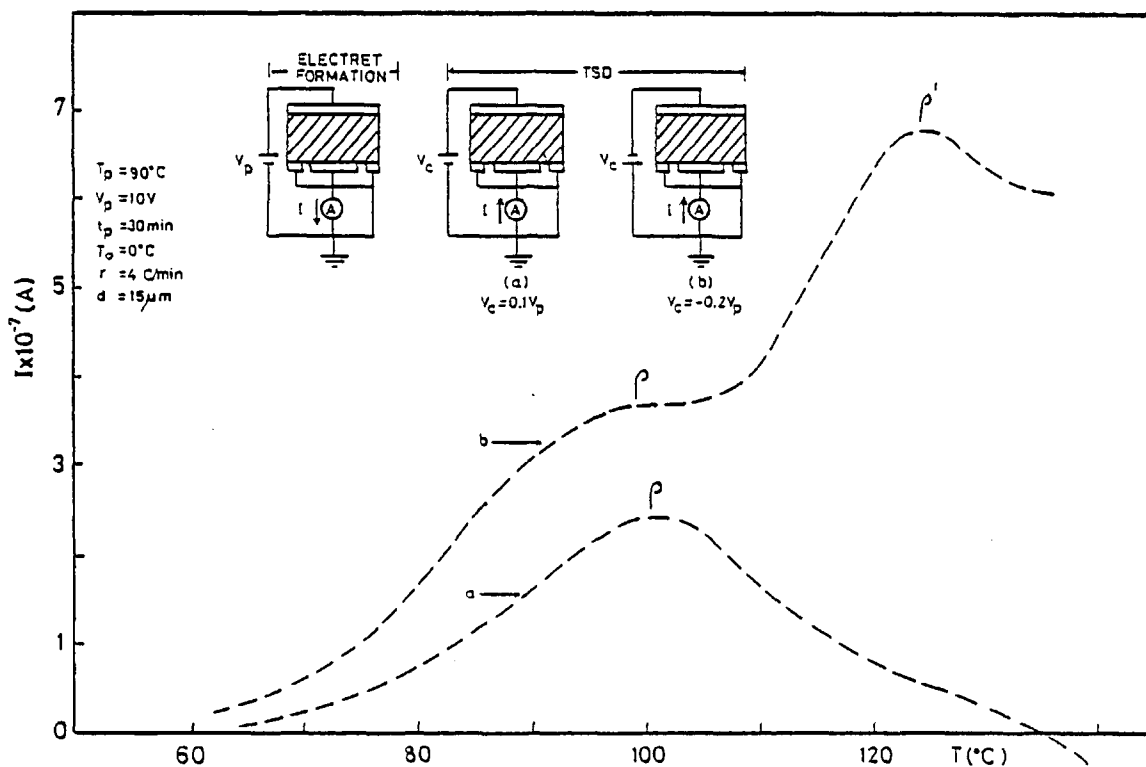


Fig. 4.60: TSD spectra of nylon film using the collecting voltage  $V_c$ .

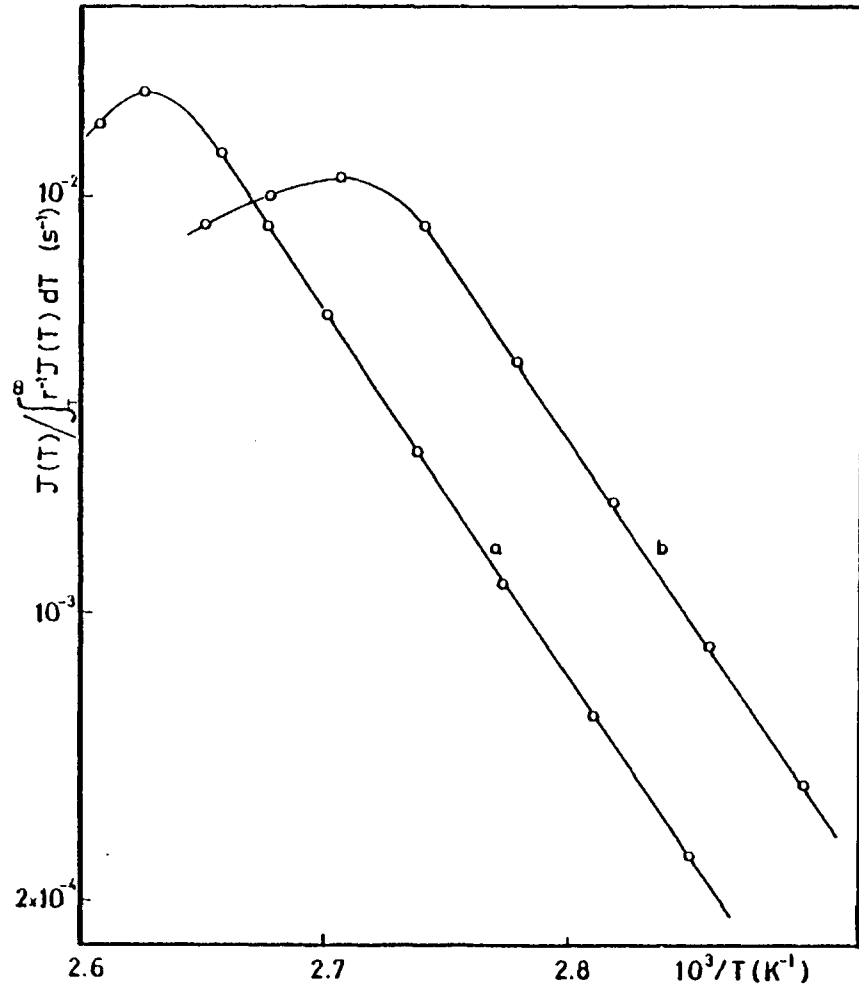


Fig. 4.61: BFG plot of the space charge peak in nylon. Curves a and b correspond to  $T_p = 80$  and  $90^\circ\text{C}$  respectively.  $r = 4^\circ\text{C}/\text{min}$ ,  $E_p = 11.5 \text{ kV}/\text{cm}$ ,  $T_0 = 0^\circ\text{C}$ ,  $t_p = 0^\circ\text{C}$ ,  $d = 12 \mu\text{m}$ .

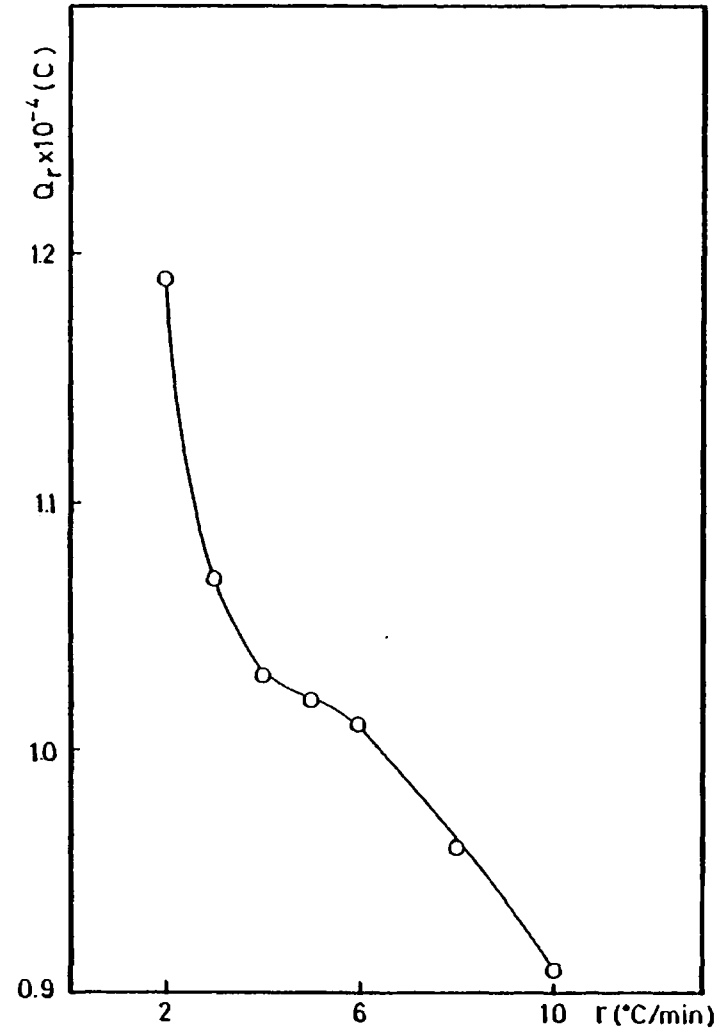


Fig. 4.62: Charge released to the external circuit as a function of heating rate.  $E_p = 12 \text{ kV}/\text{cm}$ ,  $T_p = 90^\circ\text{C}$ ,  $r = 4^\circ\text{C}/\text{min}$ ,  $t_p = 20 \text{ min}$ . Au electrodes,  $d = 10 \mu\text{m}$ .



devoted to derive suitable expressions for the current density or to calculate the involved distribution function. This is probably due to the fact that such a behaviour is a complex one. However, the author is well aware of the difficulties of the distribution of relaxation times approach.

It is believed that the polarisation is produced by the trapping or localisation of mobile charge carriers, migrating under the influence of the applied field, at the crystalline-amorphous interfaces. The accumulated charge is supplied by the unequal ohmic conduction currents arriving at the interfaces. The importance of this process in a variety of polymer systems has been emphasised recently (Baird et al 1971, Jux et al 1974, Das-Gupta et al 1980).

The results of Fig. 4.62 show that less charge is released to the external circuit as the heating rate is increased. This is in agreement with heterogeneous systems which do not obey Gross's invariance principle (see section 2.2).

#### 4.5.4.3 Conclusions

The thermally stimulated discharge technique has revealed the existence of a large persistent internal polarisation in the polyamide films investigated. The TSD  $\rho$  peak is found to occur above the glass transition temperature. The polarisation is believed to be associated with the accumulation of space charges at the crystalline-amorphous interfaces inside the polymer. During formation of the electret charges accumulate near the interfaces. These charges are frozen-in during the cooling down with the field maintained. During TSD the interfacial charges are neutralised because the local fields in the dissimilar parts of the polymer are reversed so that neutralising charges of opposite sign are conveyed to the interfaces by ohmic conduction. This neutralisation process

clearly is a transient one, giving rise to a  $\rho$  peak.

It has been found that the thermally stimulated discharge technique, which commonly works in ranges of equivalent frequencies of  $10^{-2}$  -  $10^{-4}$  Hz, could be revealed as a useful complementary tool for the dielectric study of polymer systems. In particular space charge peaks which can easily be obtained with TSD are also found in isothermal step-response measurements.

The activation energy for ohmic conduction approximately matches the activation energy obtained for the TSD  $\rho$  peak. This is understandable because the excess charges accumulated at the phase-boundaries originate from carriers that previously took part in the conduction process, and therefore have the same activation energy. The polarising species responsible for the interfacial polarisation are believed <sup>to be</sup> ionic carriers. *There was no much difference between the properties of solvent cast and hot pressed films.*

#### 4.5.5 The $\rho'$ Peak

##### 4.5.5.1 Results

At temperatures above 110°C, another prominent peak appears in the TSD spectrum of nylon. This peak has been called  $\rho'$  and overlaps with the  $\rho$  peak found at lower temperatures. It was intended to investigate this peak in detail, but due to its proximity to the crystalline melting point of the nylon, it presented many experimental difficulties. For example, the top electrode deteriorated after the heating and cooling procedures involved in a TSD experiment. Some discolouration of the film was also observed, probably due to degradation of the polymer. The peak cleaning technique of Perlman and Unger (1974) was used in an attempt to isolate the peak, but it proved unsuccessful. Therefore, few experimental results were obtained for this peak. Table XVI presents the experimental values obtained of the current maximum as a function of polarising field and temperatures. The heating rate was 6°C/min and gold electrodes were

Table XVI:

$$T_p = 110^\circ\text{C}$$

$E_p$ (kV/cm)	$I_{\text{max}} \times 10^{-7}$ (A)
5	2.3
8.3	4
11.6	3.8
15	3.4
20	4.4

$$T_p = 125^\circ\text{C}$$

$E_p$ (kV/cm)	$I_{\text{max}} \times 10^{-7}$ (A)
5	5.1
8.3	5.0
11.7	4.6
15	4.3
20	4.2

$$T_p = 140^\circ\text{C}$$

$E_p$ (kV/cm)	$I_{\text{max}} \times 10^{-7}$ (A)
3.3	5.6
8.3	6.1
11.7	5.5
20	5.8
25	5.0
	5.0

used. As can be seen the current maximum is almost independent of the polarising field.

The field dependence of the peak temperature  $T_m$  is shown in Fig. 4.63. It can be seen that the peak temperature is almost independent of the polarising field. Also, the peak temperature occurs in the region of 120-125°C. Aluminium electrodes gave a current maximum which was approximately three times lower than those of gold electrodes. For example,  $I_{\max}$  was  $1.7 \times 10^{-7} A$  when the nylon was depolarised at 6°C/min ( $E_p = 5 \text{ kV/cm}$  and  $T_p = 125^\circ\text{C}$ ).

#### 4.5.5.2 Discussion and Conclusions

As can be seen from the experimental results shown in Table XVI, there is a saturation of polarisation with low fields. This suggests that the polarisation is not due to dipole orientation but probably to a fixed number of charge carriers that exists in the nylon. It is thought that the polarising species responsible for the polarisation are ions which are deeply trapped near the electrodes, or neutralised at the electrode, where high temperature is required for reionisation. It is not known whether the carrier species are residual impurities or self-ionisation of the polymer. However, if one accepts that the number of carriers is fixed, the polarisation might be due to residual impurities.

At this point it might be relevant to recall that at high temperatures the charging current transients showed the presence of a peak (see section 4.4). Thus it is possible that the observed TSD  $\rho'$  peak be related to those transient current peaks (see Figs. 4.25 and 4.26). However, the final confirmation will require still more experimental work.

The  $\rho'$  relaxation might also have its origin in the so-called liquid-liquid relaxations. It is known that non-crystalline polymers

exhibit liquid-liquid transitions (see Chapter I). Lacabane et al (1980) have observed a liquid-liquid relaxation in polystyrene at temperatures above  $T_g$  using the TSD technique, which was attributed to molecular origin. On the other hand, Newman and McKnight (1981) have expressed dissatisfaction with the molecular origin of this type of relaxation and claimed that it is caused solely by the temperature dependence of the Newtonian viscosity of the material being studied above  $T_g$ .

#### 4.6 PYROELECTRIC EFFECT IN NYLON FILMS

The objective of this section is to present experimental evidence concerned with the finding that the nylon films studied in this work showed pyroelectricity. It is not claimed that this section represents a full study on that effect. Pyroelectricity in polyvinylidene fluoride will be discussed to get an insight of the observed effect, because it is the only polymer from which a suitable model has emerged to explain pyroelectric behaviour.

Nylon films sandwiched between metal electrodes were prepared as described in Chapter II. They were placed in the cryostat described as well in that chapter. The structure was heated or cooled at a constant rate and the pyroelectric current was recorded continuously using a Keithley electrometer model 602. Fig. 4.64 shows a typical temperature dependence of the pyroelectric coefficient, defined as  $dP/dT = J/r$ , which was calculated from heating/cooling currents  $J$ . The heating rate used was  $3^\circ\text{C}/\text{min}$ . It can be seen that the pyroeffect changes sign during cooling, and that some asymmetry exists. Nevertheless the effect is clearly visible. It is worth mentioning that the film became pyroelectric after the poling procedures to form the thermoelectrets. It is well known that the measured value of the pyroelectric effect depends on whether or not the sample is free to change its shape (Nye 1957). The "primary" pyroelectric

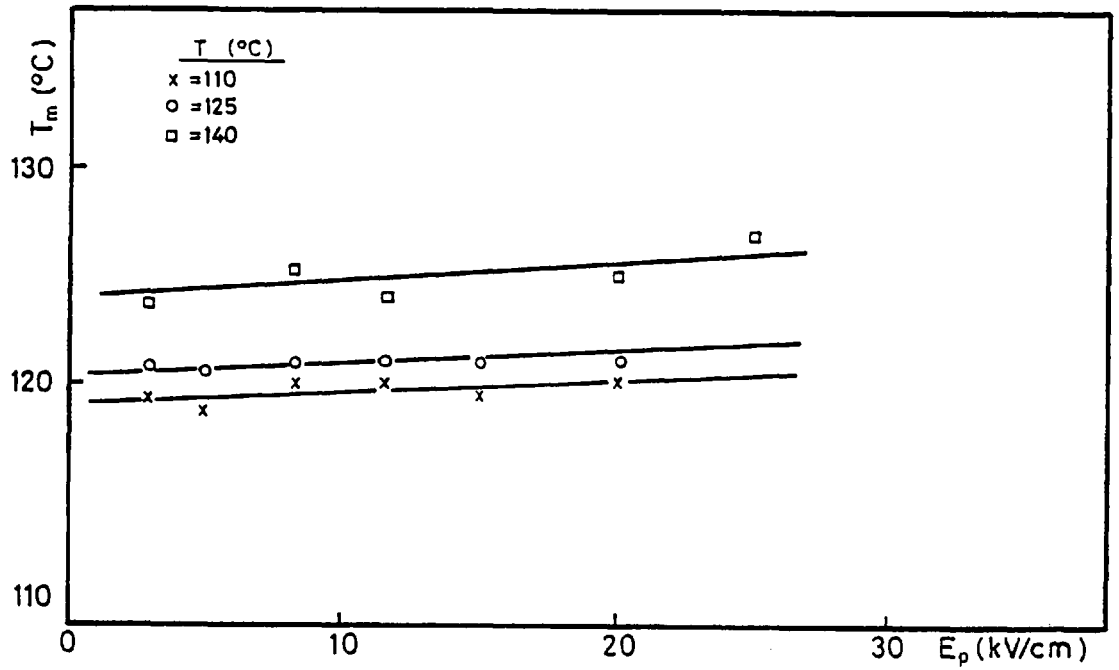


Fig. 4.63: Field dependence on  $T_m$

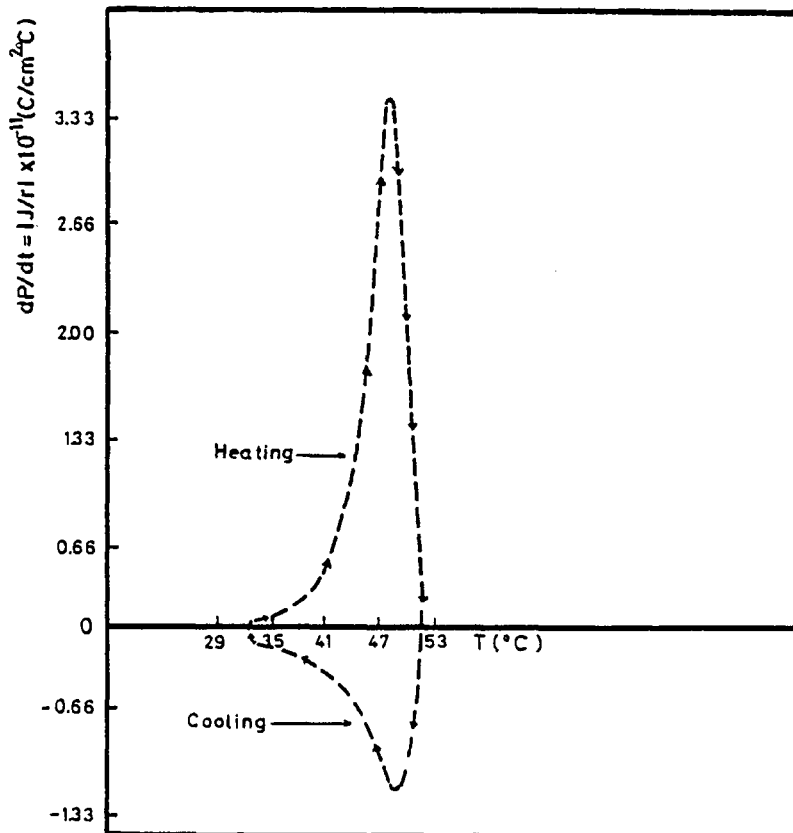


Fig. 4.64: Pyroelectric response observed in nylon films.

effect is defined as the effect measured when the shape and volume of the polymer film is held fixed as the temperature changes ("clamped" boundary conditions or constant strain). Usually, in a measurement on a bulk sample, the sample is free to expand or contract and the resultant strain causes a piezoelectrically induced polarisation ("secondary" effect) which adds to the strain-free case. A thin pyroelectric film rigidly attached to a substrate is free to expand along its thickness dimension only, but in the plane of the film it must expand or contract as determined by the substrate. By assumption, the film is sufficiently thin to cause negligible strains in the substrate. Thus, the film is in a state which is partially free and partially clamped.

Litt et al (1977) have observed reversible pyroelectricity in nylon 11. The effect is probably due to dipole orientation in the crystalline regions since this was not affected by the decay of the spontaneous current or by the glass transition temperature. Lee et al (1979) have shown that trapped charge in a polymer film coupled with the non-linear thermal expansion of the film can lead to a reversible pyroelectric current.

Polyvinylidene fluoride (PVDF) and other semicrystalline polymers are being used increasingly in transducer applications. Their advantages over ceramic materials include light weight, flexibility, toughness, ease of fabrication and low permittivity. The most frequently invoked mechanism for piezo- and pyroelectricity in PVDF is as follows. A large electric field causes crystallised segments of the polymer to rotate individually about their molecular axes and repack in polar crystal lamellar with preferential alignment in the direction of the applied field. These stable aligned crystals change their net polarisation when temperature or stress change largely because of dimensional changes.

Semicrystalline polymers consist of lamellar crystals mixed with amorphous regions. A schematic diagram of a spherulite within an unoriented semicrystalline polymer is shown in Fig. 4.65 (Broadhurst et al 1978). In the crystals the molecular segments are linear and roughly normal to the large crystal surfaces. It is believed that the piezo- and pyroelectric activity in PVDF and other semicrystalline polymers is due to the presence of oriented dipolar crystals. A schematic diagram showing dipole alignment and countercharge on a lamellar section of polar crystal is presented in Fig. 4.66.

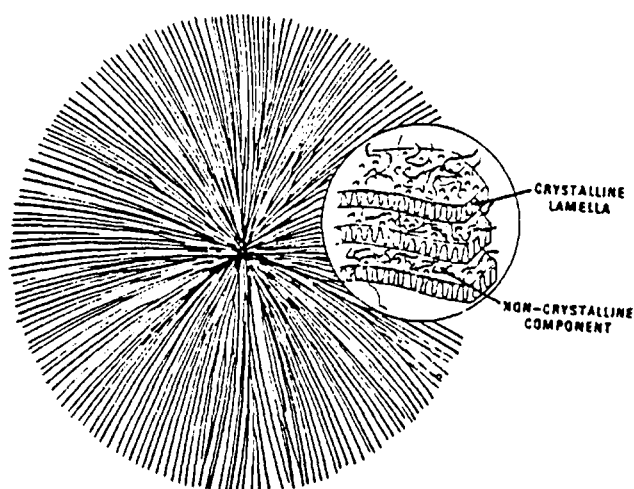


Fig. 4.65 Schematic diagram of a spherulite

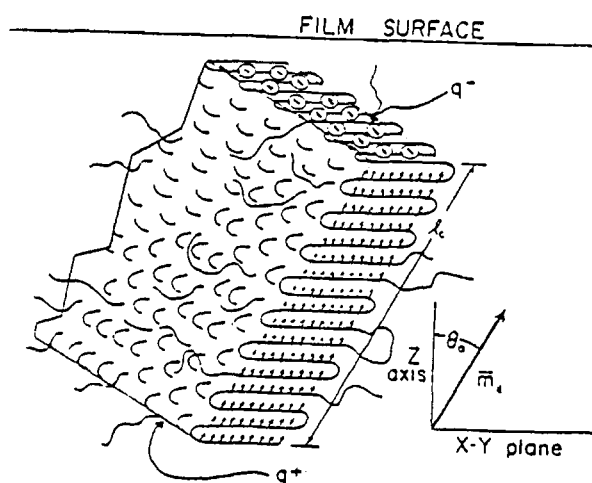


Fig.4.66 A schematic diagram showing dipole alignment of a polar crystal

Probably related to the pyroelectric effect in nylon is the fact that the films showed a current response under light illumination. Nylon films ( $\sim 10 \mu\text{m}$ ) with evaporated gold electrodes were short-circuited through the electrometer in vacuum. The samples were illuminated through the cryostat window from a 250W quartz halogen lamp. A manual chopper was utilised to interrupt the passage of light. The results obtained are shown in Fig. 4.67. As can be seen a square-wave response was obtained, probably because of the long response time of the film with the result that the



heating and cooling rates were constant during the on and off periods.

In conclusion it may be said that nylon appears to be an interesting material, which shows some pyroelectricity. It is believed that the poling process induces the thermally reversible electric polarisation in addition to the electrical polarisations  $\alpha$ ,  $\rho$  and  $\rho'$  which vanish upon the first heating of the sample.

#### 4.7 EFFECT OF BREATHING ON NYLON FILMS

The only purpose of this section is to present an experimental observation about the effect of breathing on the metallised surface of a metal-nylon-metal structure. This effect was not investigated in detail, and therefore it is not proposed to give a full account of it.

A metal-nylon-metal structure was short-circuited through a Keithley 602 electrometer at room temperature and atmospheric pressure. A large current was observed when the structure was breathed on one of its surfaces. The response of the device upon a short breath is illustrated in Fig. 4.68. It is not clear at the present what causes the generation of such a current, which sometimes reached the value of  $1 \mu\text{A}$ . However, moisture is believed to play an important role in such a behaviour.

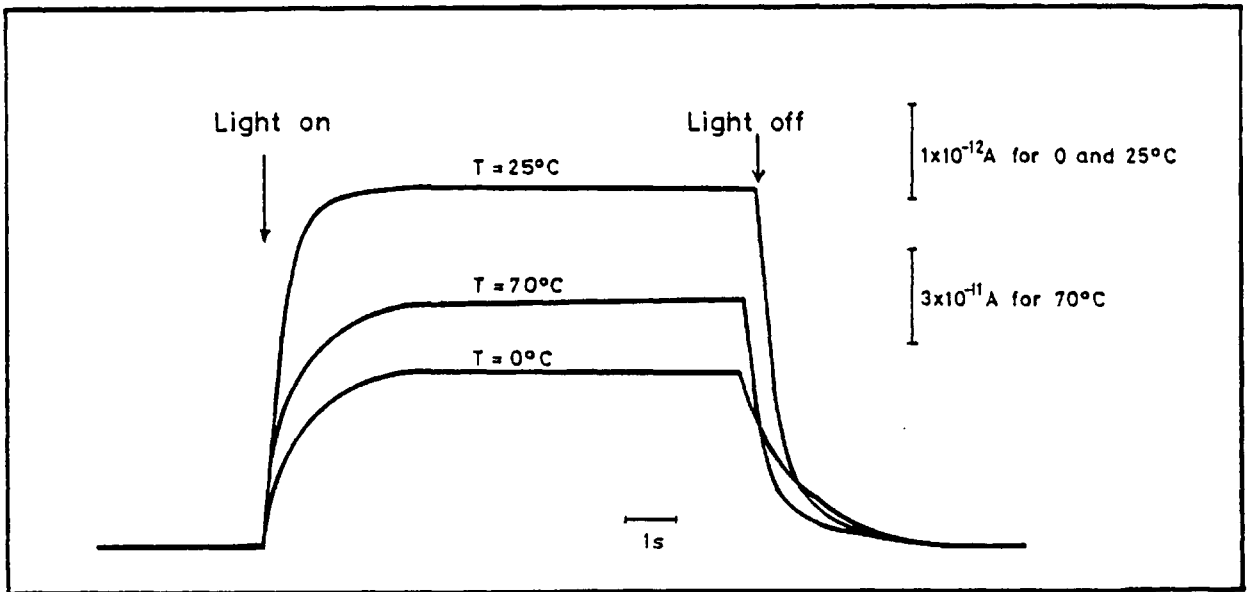


Fig. 4.67: Effect of light on nylon.

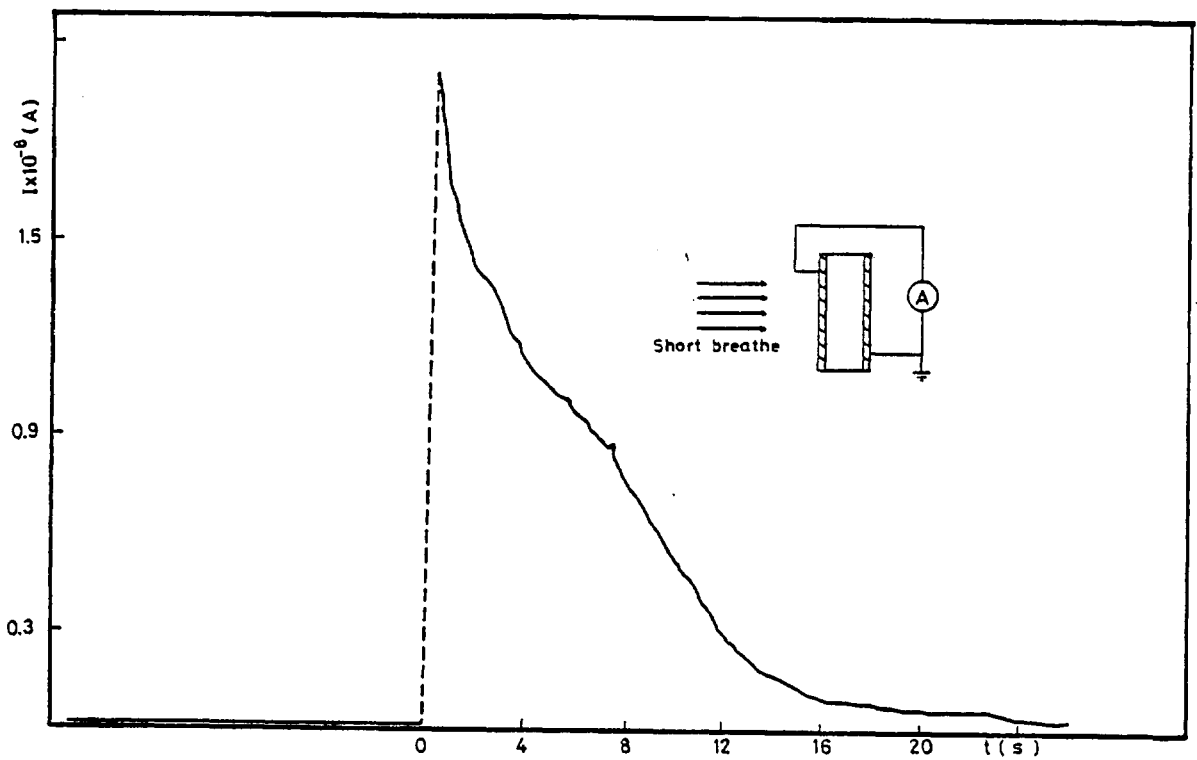


Fig. 4.68: Effect of breathing on nylon films

CHAPTER V

THERMALLY STIMULATED DISCHARGE CURRENTS IN POLYVINYL BUTYRAL FILMS

5.0 INTRODUCTION

Another polymer investigated in this work was polyvinyl butyral (PVB) (Butvar, Monsanto). PVB is a binder polymer resin with the structure shown in Fig. 5.1.

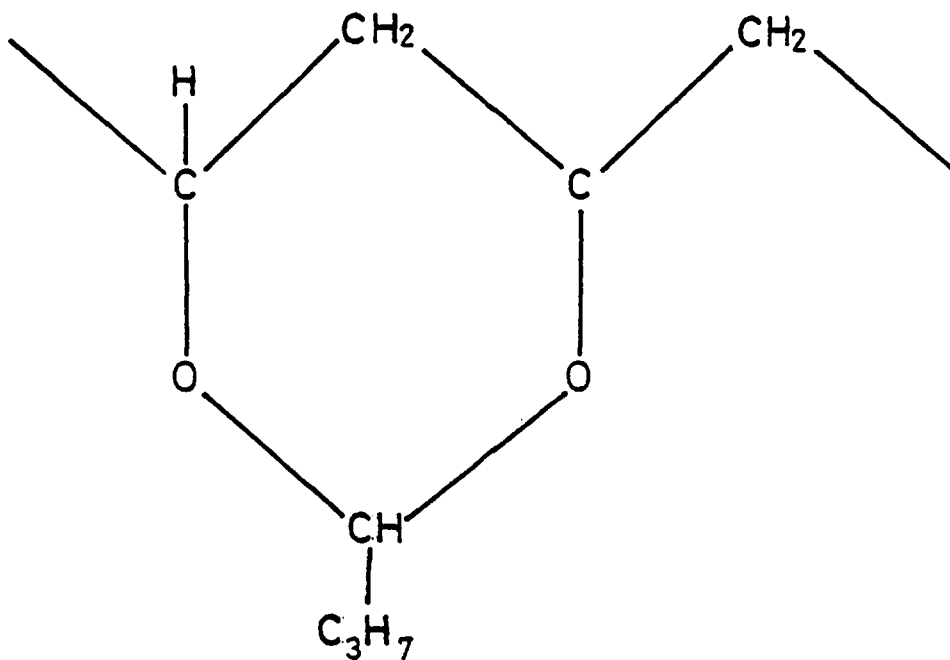


Fig. 5.1: PVB Structure

Under normal storage conditions the resin is unusually stable, therefore does not require any special handling. The resin is supplied in white, free-flowing powder. As can be seen in Fig. 5.1 the repeat units contain dipolar side groups which bridge across alternate carbon atoms. The permanent dipole moments are thus unable to reorient independently of the main chain.

The  $\alpha$ -relaxation in PVB was investigated using the TSD technique. The results obtained in the present study are compared with the only two

investigations found in the literature (Jain et al, 1974 and 1979) and conclusions drawn. Differential thermal analysis was also carried out on the samples. Transient charging and discharging currents and a.c. measurements were also performed.

## 5.1 EXPERIMENTAL

PVB was dissolved in mixtures of toluene and MEK by continuous stirring and gentle heating as described in section 3.1. Films were prepared by spreading the solution uniformly on an aluminium glass structure using the rod coater described in section 3.1, followed by drying in an air oven at 50°C for 30 mins. The films thus prepared were placed in vacuum for a day for further drying before they were overcoated with the top electrode using the guard ring configuration shown in Fig. 3.2. The thickness of the films was approximately 20  $\mu\text{m}$ .

## 5.2 RESULTS

The TSD spectra obtained from polyvinyl butyral formed at 80°C for periods of 240s for different polarising fields and a heating rate of 4°C/min are shown in Fig. 5.2. A well isolated peak is seen to exist. It can also be seen that the peak temperatures are independent of the polarising fields. The current maximum vs. polarising field is plotted in Fig. 5.3. The magnitude of  $I_m$  increases linearly with applied field  $E_p$ . By extrapolating the straight line position of the graph it can be seen that this passes through the origin. The effect of the polarising temperature on the TSD spectrum is shown in Fig. 5.4. It is found that the temperature maximum of the peak is a function  $T_p$ . The dependence of the peak temperature and current maximum on the heating rate is illustrated in Fig. 5.5. The apparent activation energy of the TSD peak was estimated using the method of varying heating rate. Fig. 5.6 shows the plot

$\log T_m^2/r$  vs.  $10^3/T_m$ . The activation energy calculated from the slope gives a value of about 2 eV. If one uses the initial rise method to calculate the activation energy from the peaks in Fig. 5.2 the value of 0.5 eV is obtained.

The TSD spectra was analysed using the BFG plot. It was found that the plot of  $\log \tau(s)$  vs.  $1/T$  was not a straight line. This means that the relaxation could be due to either a discrete or continuous spectrum of relaxation times. Further evidence for this distributed process was obtained by the dependence of the electret effect on the forming conditions. In order to investigate this complex relaxation, the thermal sampling(TS) technique was used. The heating rate used was 4°C/min. The polarising field was 5.5 kV/cm, the polarising and depolarising times were 4 minutes and the temperature window  $\Delta T = 5K$ . The polarising temperature was scanned every 5K. The cooling rate after polarisation was 20°C/min. Fig. 5.7 gives a set of current maxima obtained in a series of TS experiments. The envelope of the curves exhibits the typical TSD spectrum of PVB. The temperatures of the TS maxima,  $T_m$ , increased linearly with increasing polarising temperatures,  $T_p$ , as shown in Fig. 5.8. The variation of the activation energy with the polarising temperatures for the set of TS maxima is given in Fig.5.9. The quantity  $\Delta\epsilon = \epsilon_s - \epsilon_\infty$  was calculated from the total charges released in a TS experiment using the equation

$$\Delta\epsilon = \frac{1}{\epsilon_0 E_p} \int_{t_0}^{\infty} J(t) dt$$

The dependence of  $\Delta\epsilon$  on polarising temperature is presented in Fig. 5.10. Thermally stimulated polarisation experiments were also performed. The sample was cooled to -20°C in short circuit condition. At that temperature a polarising field  $E_p$  was applied. The sample was then heated at a constant

rate of 4°C/min. Fig. 5.11 shows the peak observed during TSP as well as the TSD peak.

The charging and discharging currents were also recorded as a function of polarising temperatures. Fig. 5.12 shows a typical example of these currents. It can be seen that the time dependence of the transient currents agree fairly well with the Curie-von Schneider law (section 4.4.1) and that the two types of currents are mirror images of one another. The exponent  $n$  measured from the slopes of the curves varied from 0.8 at 35°C to 1.2 at 60°C. The field dependence of the isochronal current transients observed at 45°C is shown in Fig. 5.13. As can be seen a linear (ohmic) dependence was obtained. Different electrode materials (aluminium, silver and graphite) did not affect markedly the transient currents. The dielectric loss factor was evaluated using the Hamon method (eqn. (4.16)) and Fig. 5.14 shows a typical plot of  $\epsilon''$  against temperature for two frequencies. A prominent peak is observed at about 60°C. Also, the peak is shifted slightly to lower temperatures by decreasing the frequency.

Dielectric measurements were carried out using the equipment described in section 3.6. Fig. 5.15 shows the plot of  $\tan \delta$  against temperature for frequencies of 2 and 15 kHz. As can be observed a single relaxation exists in the range of temperature covered. Also, it can be seen that as the frequency is increased, the peak shifts to higher temperatures. The temperature of the maximum of  $\tan \delta$  for given constant frequencies were plotted against frequency. The experimental points obtained were in close agreement with that of Fig. 5.18.

Differential thermal analysis was also carried out on PVB. Fig. 5.16 shows the DTA thermogram of PVB. As can be seen a sharp change occurs in the position of the base line, which is normally associated with the glass transition. The glass transition measured was 61°C.

Spontaneous currents in virgin PVB films, flowing under short-circuit conditions during a linear heating rate were also investigated. Fig. 5.17 shows a typical result obtained from the films. A rather small peak is seen to occur in the region of 60°C, as well as an increasing current for temperatures greater than 70°C.

### 5.3 DISCUSSION

The thermally stimulated depolarisation peak is seen to occur in the region of 58°C. The fact that the maximum of the current peak is proportional to the polarising field is a good indication that the induced polarisation is due to dipole alignment. Experimental evidence in favour of the dipole mechanism is given as well by the thermally stimulated polarisation experiments. As shown in Fig. 5.11 the TSP experiment gives a peak located in the region where the TSD peak occurs. From Fig. 5.4 it can be seen that the relaxation process is distributed because of the electret dependence on the forming conditions. This fact is also corroborated by the BFG plot which was found to be not linear and also by the shift of the peak with heating rate. The apparent activation energy of the process, calculated from the initial rise method was 2 eV. By means of the thermal sampling techniques it was possible to resolve the TSD peak into several components as shown in Fig. 5.7. The activation energies of the TS maxima are an increasing function of the polarising temperatures. It was also found that the pre-exponential factor was not constant in the same range of polarising temperatures. It may be said therefore that the relaxation obtained in PVB at 58°C is due to a continuous distribution of relaxation times, in which both the activation energy and the pre-exponential factor are distributed. The  $\alpha$ -relaxation in PVB has been obtained previously by Takahashi (1961 a , b) from dielectric and mechanical measurements. An apparent activation energy of 4 eV was calculated at 80°C. The

relaxation was associated with the segmental movements of the main chain and to the second-order transition of the polyvinyl butyral. The plot of logarithmic dispersion frequency against reciprocal of absolute temperature found by him is given in Fig. 5.18

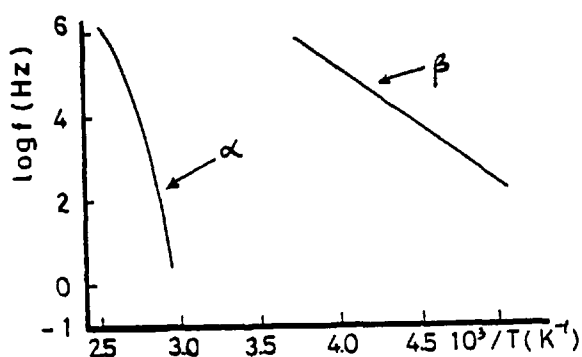


Fig. 5.18: Plot of logarithmic dispersion frequency against reciprocal of absolute temperature

The equivalent frequency of the TSD peaks found in the present study has been estimated to be of the order of  $2 \times 10^{-3}$  Hz. Comparing this value with the relaxation map given above it can be seen that the position of the TSD peak is compatible with the given dielectric relaxation.

Jain et al (1974) have investigated the TSD currents in PVB films. They observed two peaks in the TSD spectrum, namely a  $\beta$  peak at 77°C and an  $\alpha$  peak at 157°C. The  $\alpha$  peak, according to these authors, was due to the molecular motion involving the depolarisation of aligned dipoles connected to the main chain polymer chain, whereas the  $\beta$  peak resulted either from the local twisting of the main chain or from the motion of the side groups in the polymer chain. The activation energies, calculated from the initial rise method of the  $\beta$  and  $\alpha$  peaks, were 0.19 and 0.53 eV respectively.



In another paper Jain et al (1979) have also observed two relaxation processes at 74°C and 150°C using the TSD technique. Their activation energies, obtained from the initial rise method, were 0.36 and 0.66 eV. The relaxation at 74°C was assigned to the disorientation of aligned dipoles involving the acetate/hydroxyl side groups. The possibility that the charge associated with this peak was trapped and released at the glass transition was ruled out. In addition they indicated that this peak was due to a single relaxation process. The other peak, at 150°C, was associated with the release of trapped electrons/holes.

From the TSD study of both papers on PVB, it can be concluded that the relaxation observed in the region of 75°C was due to the motion of the polar-side groups acetate/hydroxyl.

It is well established (McCrum et al 1967) that most polymers and copolymers show a  $\alpha$ -relaxation. In PVC, for instance, this is a motion still within the polymer chain but locally more restricted than the motion corresponding to the glass transition. It involves 2-4 main chain atoms. In polymethyl methacrylate this motion is due to rotation of the ester side-group about the C-C bond which links it to the main chain. Another relaxation which is found in amorphous and semicrystalline polymers is the  $\alpha$ -relaxation which is always associated with the glass transition of the polymer (Meier 1978). Amorphous and semicrystalline polymers show a marked change in their physical properties at the glass transition. The glass transition process occurring at temperature  $T_g$  marks the freezing in (upon cooling) or the unfreezing (upon heating) of micro-Brownian motion of chain segments of 20-50 carbon atoms in length. This micro-Brownian motion is a semicooperative action involving torsional oscillation and/or rotations about the backbone bonds in a given chain as well as in neighbouring chains (see Chapter I).

The PVB films investigated show a transition at about 61°C as determined by differential thermal analysis. It is believed that this is the glass transition of the PVB studied here. The peak found in the TSD method occurs at about 60°C when using the heating rate of 8°C/min. In view of the good correlation obtained in  $T_g$  with both methods of thermal analysis, it is concluded that the TSD peak at about 60°C is associated with the glass transition of PVB and therefore due to the motions of large parts of the polymer chain.

The activation energy obtained from the initial rise of the TSD curves (Fig. 5.2) was 0.5 eV. This is in contrast to the 2 eV obtained from Fig. 5.6. This has been discussed by van Turnhout (1975) who concludes that for a symmetrical distribution of relaxation times the plot of  $\log I_{\text{rise}}(T)$  - vs -  $1/T$  will have a slope  $mA/k$  where  $m$  is the distribution parameter. Since  $m < 1$  it means that activation energies deduced from the initial rise current will be less than  $A$ , i.e.  $A_{\text{initial rise}} = mA$ . Thus in this case the value of  $m$  may be estimated to be about 0.25. This is in general agreement with values of  $m$  which may be obtained by examination of published a.c. loss-data (McCrum et al 1967) extrapolated to the frequency-temperature range of the TSD rise currents.

The charging and discharging currents observed in PVB show the expected behaviour of a dipolar relaxation mechanism, i.e. reversibility of the transient phenomenon, linear dependence on field strength and independence of electrode materials. The results of Fig. 5.14 show good correlation with the location of the TSD peak. The dielectric dispersion obtained from a.c. measurements (Fig. 5.15) agrees well with the results of Takahashi (1961). This dispersion is related to the segmental movements of the main chain.

The presence of a peak around 60°C in never polarised PVB (see Fig. 5.17) films, undoubtedly corresponds to the  $\alpha$ -relaxation in PVB, i.e. the glass transition. Thus, it can be said that during the method of preparation of the films some orientation of dipoles occurs in the bulk of the polymers.

#### 5.4 CONCLUSIONS

Two thermal techniques, namely TSD and DTA, have been used to investigate the  $\alpha$ -relaxation in PVB films. The TSD technique gives a peak at temperatures corresponding to that of the second-order transition determined by DTA. It follows therefore that the TSD peak is associated with the motion of large segments of the main polymer chain. It was also shown, by using the thermal sampling technique, that the  $\alpha$ -relaxation is due to a distributed process involving a distribution in activation energies and in natural frequencies. TSD and the better-established techniques of d.c. step-response and a.c. response were found to be consistent with each other.

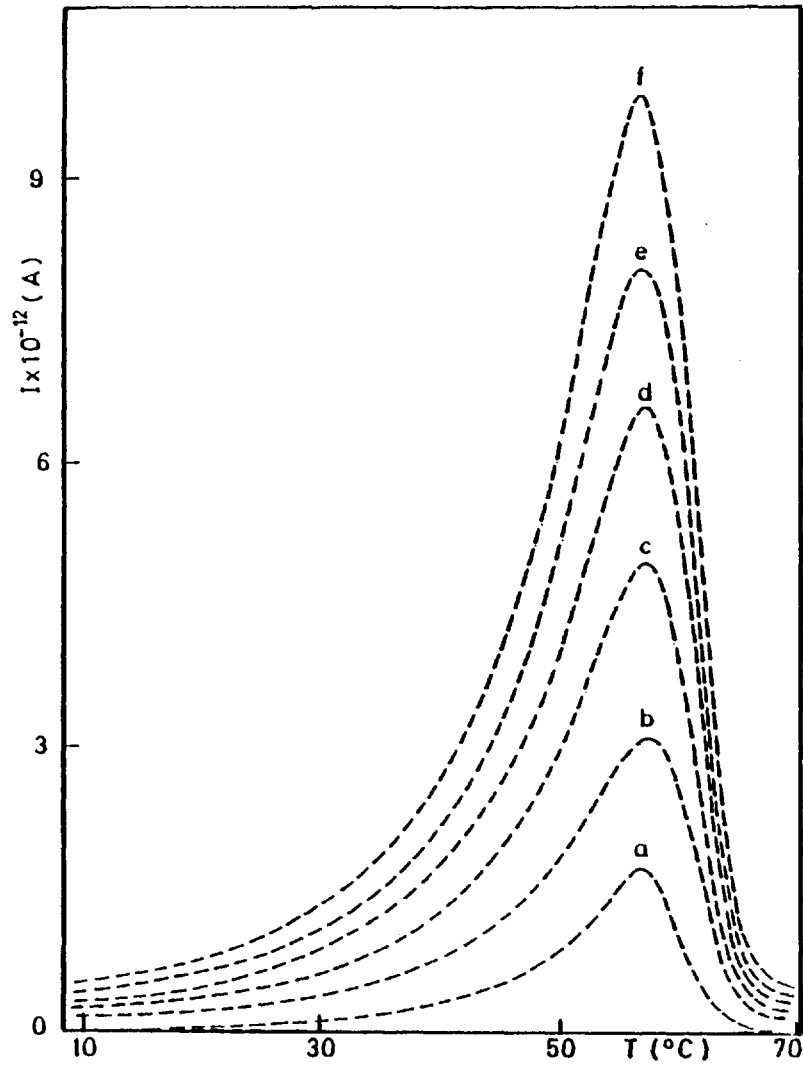


Fig. 5.2: TSD spectra of PVB poled at 80°C for 240s. Curves a,b,c,d,e and f correspond to  $E_p$  of 1,1.8,2.7,3.6,4.6 and 5.4 kV/cm respectively.  $\nu = 4^\circ\text{C}/\text{min}$ ,  $T_0 = 0^\circ\text{C}$ .

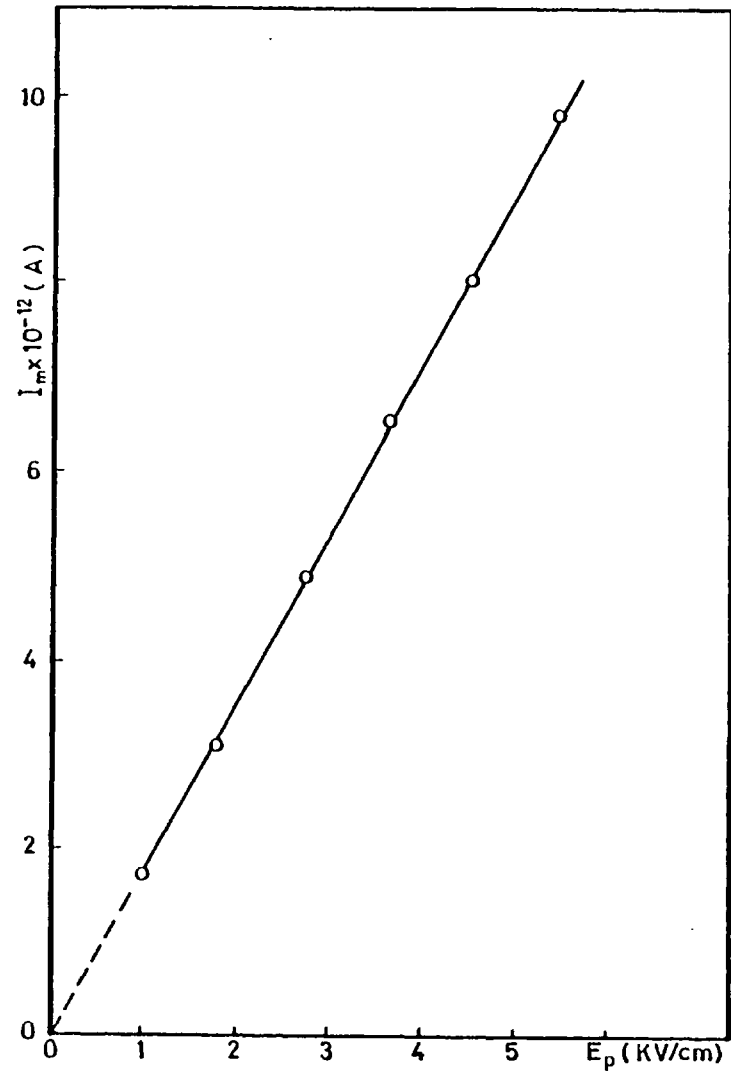


Fig. 5.3: Dependence of current maximum upon polarising field.

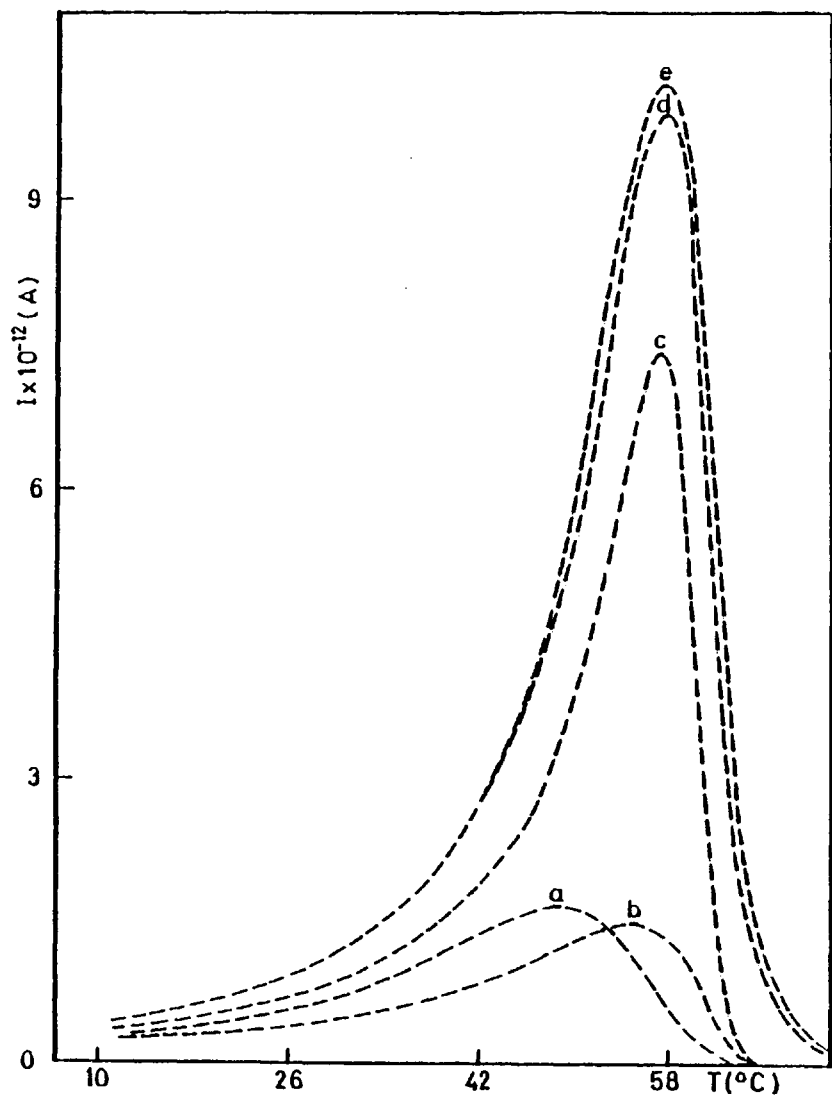


Fig. 5.4: Depolarisation currents of PVB films poled for 240s with  $E_p = 6$  kV/cm. Curves a,b,c,d and e correspond to 40,45,50, 60 and 70°C respectively.  $r = 4^\circ\text{C}/\text{min}$ ,  $T_0 = 0^\circ\text{C}$ .

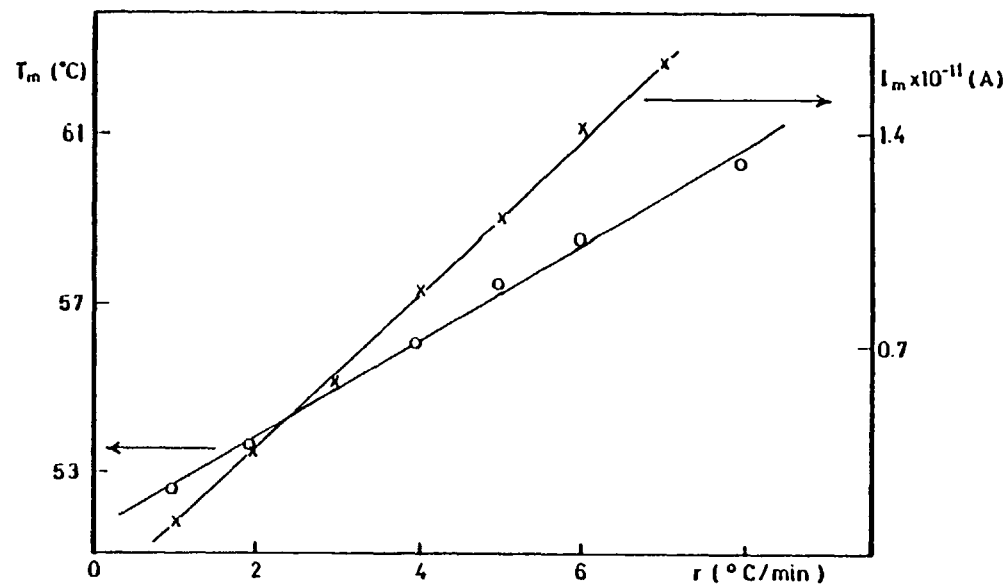


Fig. 5.5: Peak temperature and current maximum  $I_m$  as a function of heating rate.

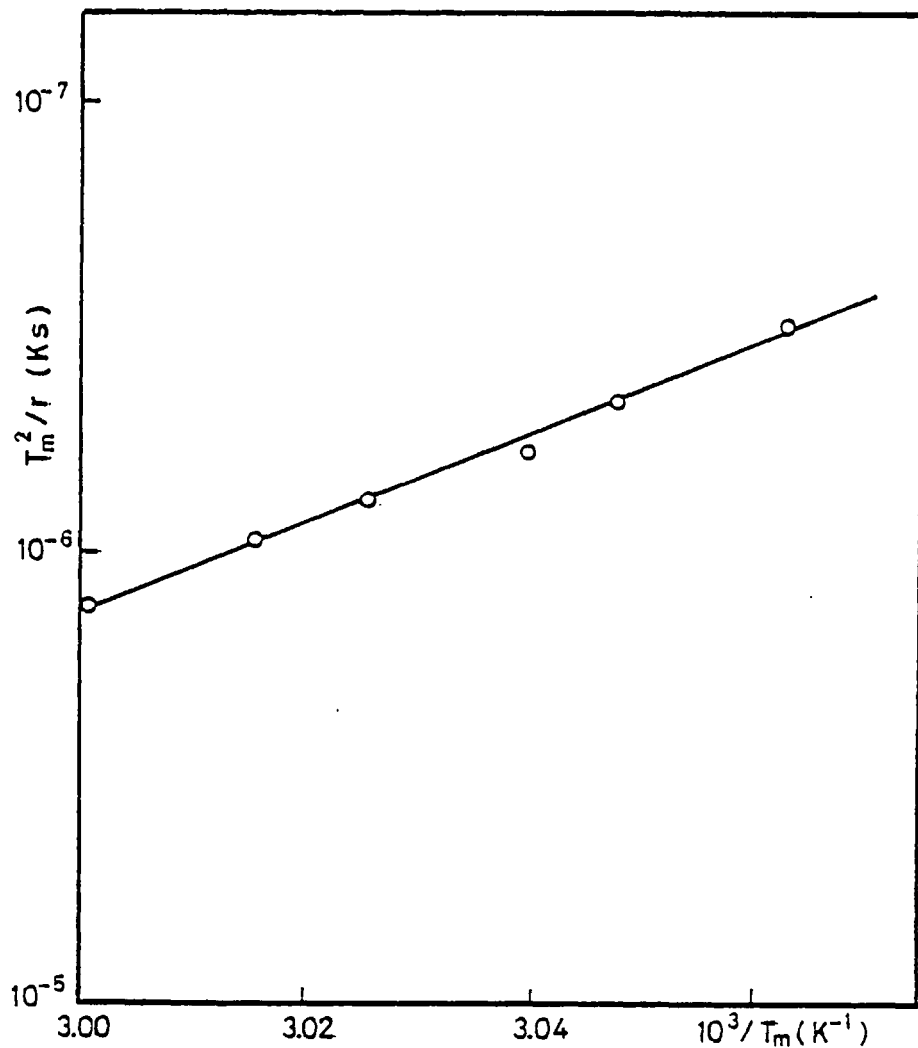


Fig. 5.6: Plot of  $\ln T_m^2/r$  against  $1/T_m$ .

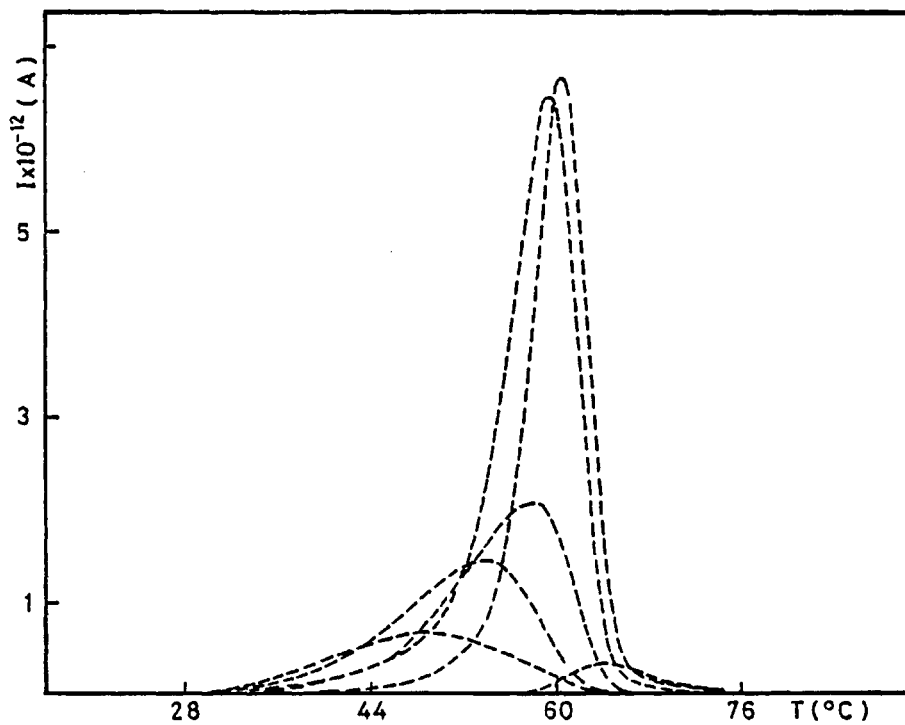


Fig. 5.7: Series of thermal sampling maxima in PVB films. The temperature window is 5°C.

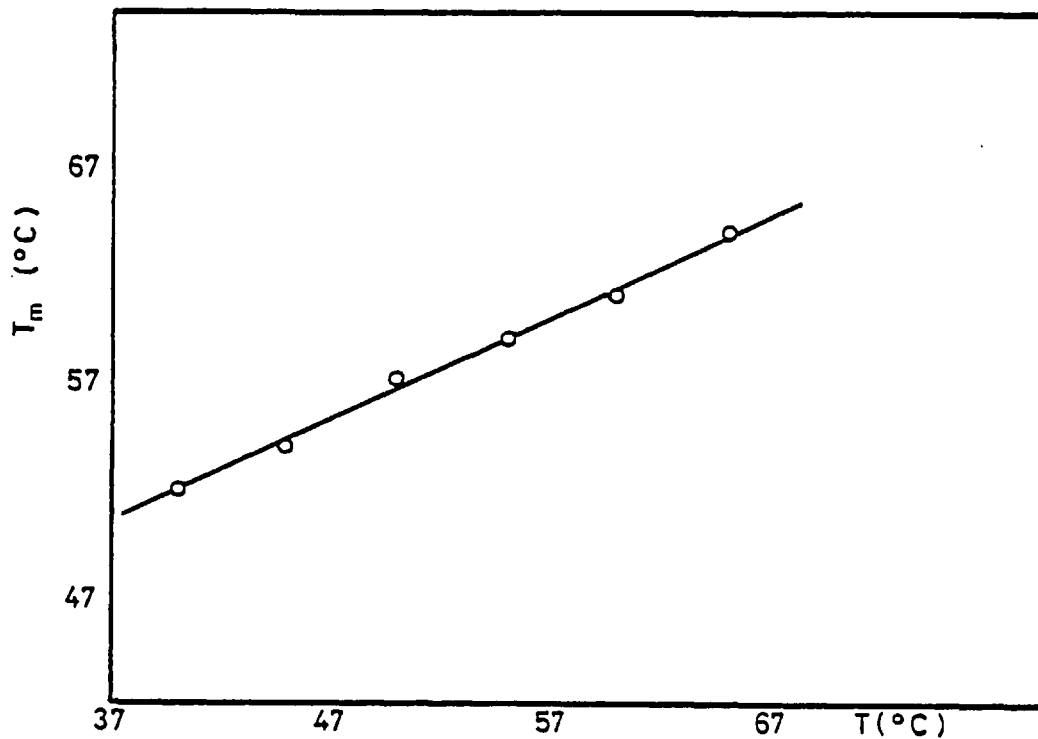


Fig. 5.8: Dependence of the temperatures of the TS maxima,  $T_m$ , as a function of polarising temperature.

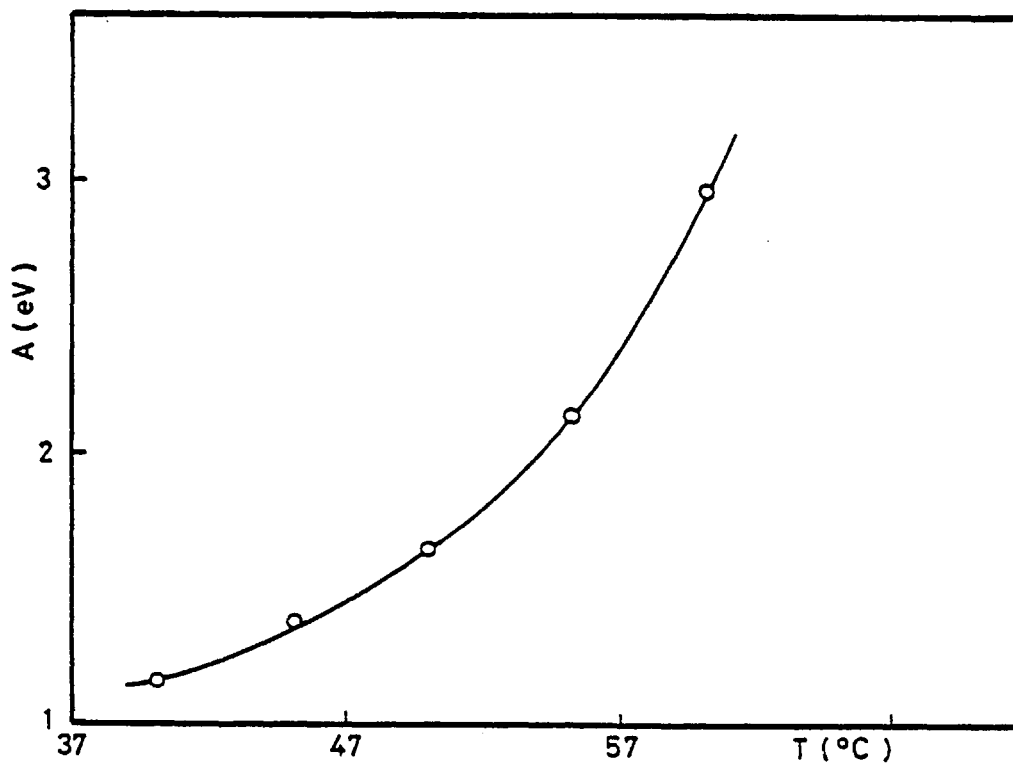


Fig. 5.9: Activation energy against temperature obtained from the TS experiment.

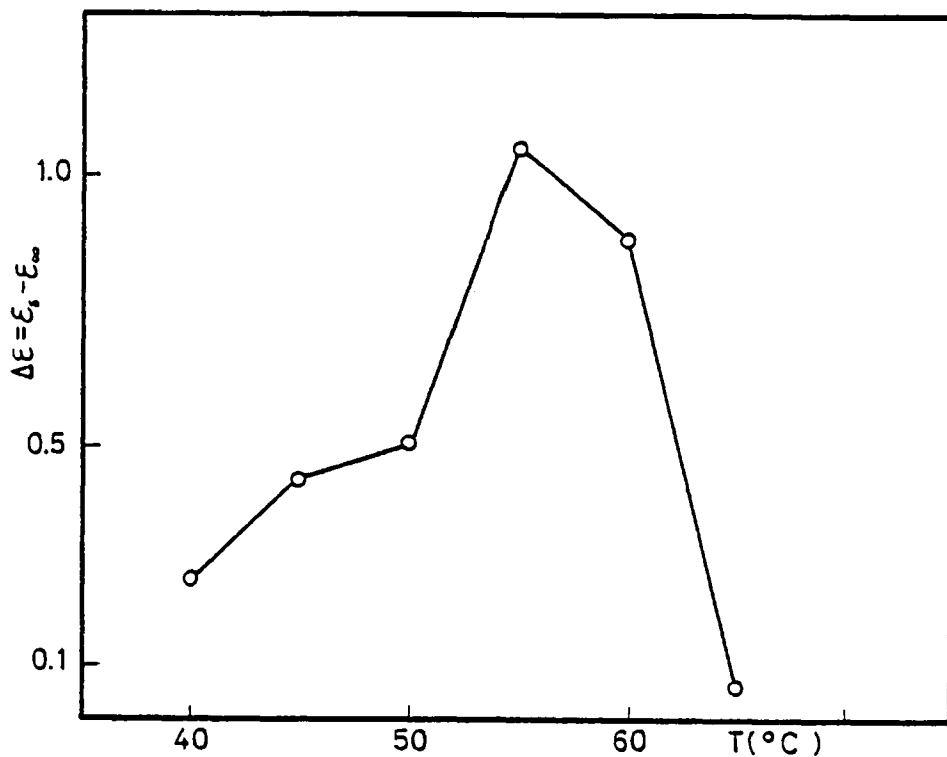


Fig. 5.10: Values of  $\Delta\epsilon$  plotted against polarising temperatures for the TS runs shown in Fig. 5.7.

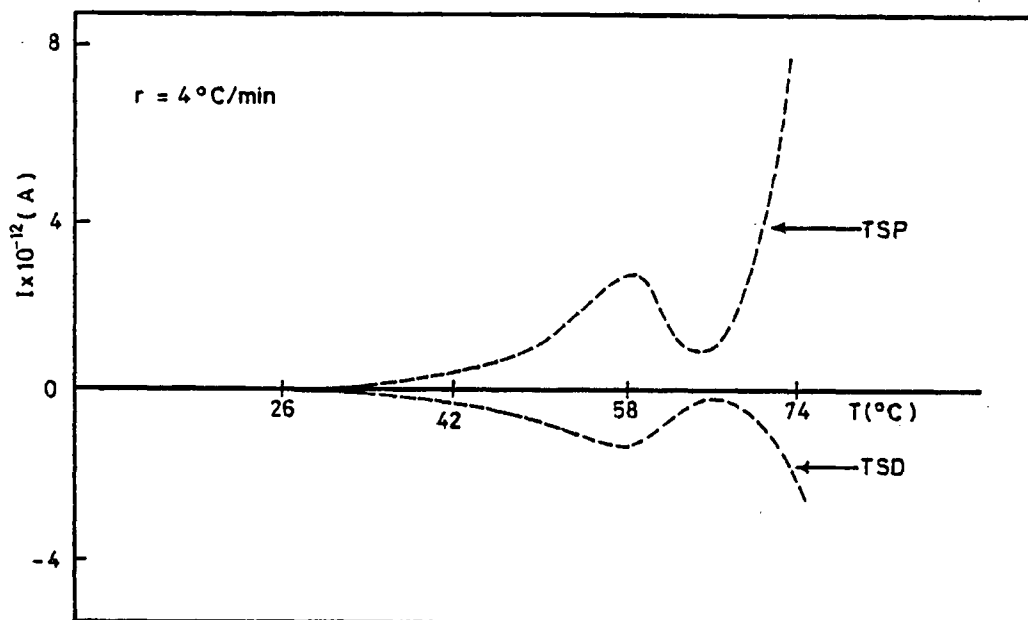


Fig. 5.11: TSP and TSD currents in PVB films.



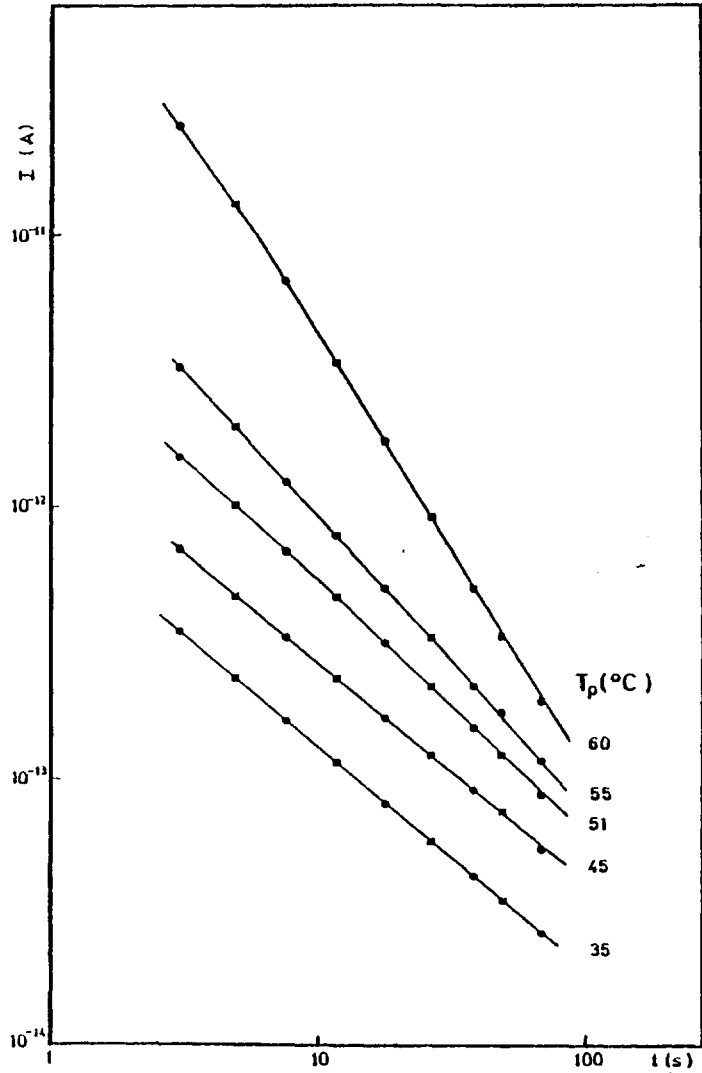


Fig. 5.12: Charging (●) and discharging (■) currents in PVB as a function of polarising temperature  $T_p$ . Aluminium electrodes,  $E_p = 10$  kV/cm,  $10 \mu\text{m}$  thickness.

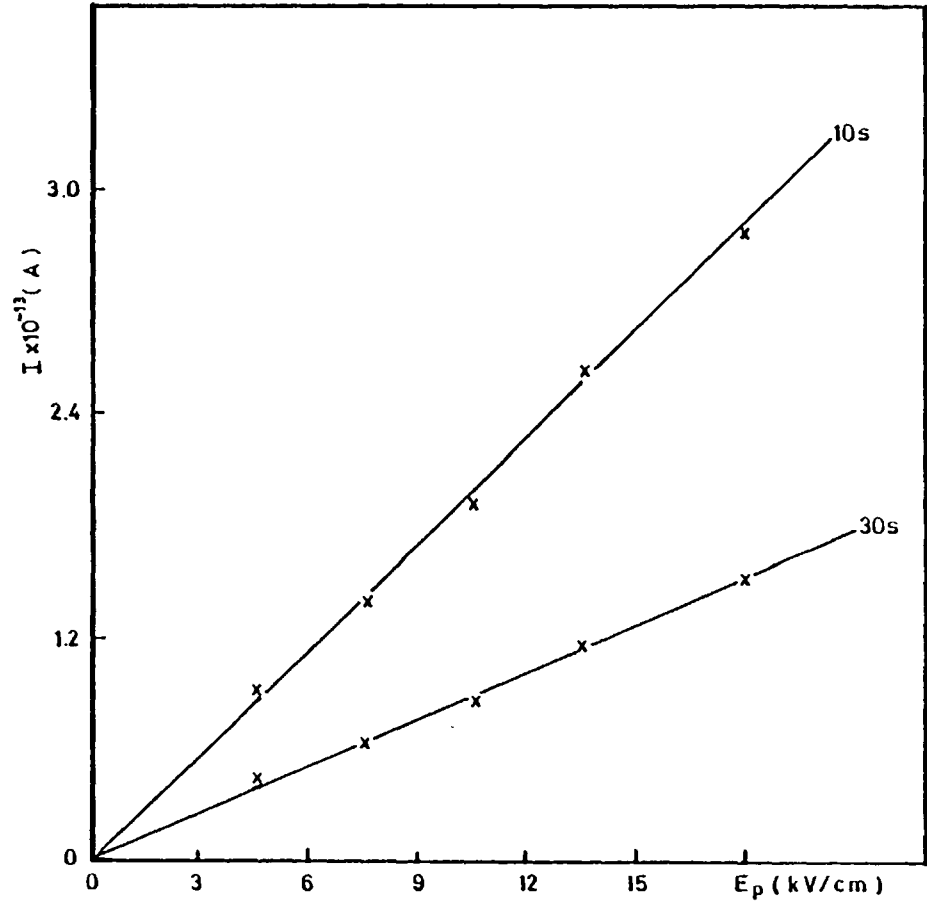


Fig. 5.13: Field dependence of ioschronal discharging currents in PVB at  $45^\circ\text{C}$ .

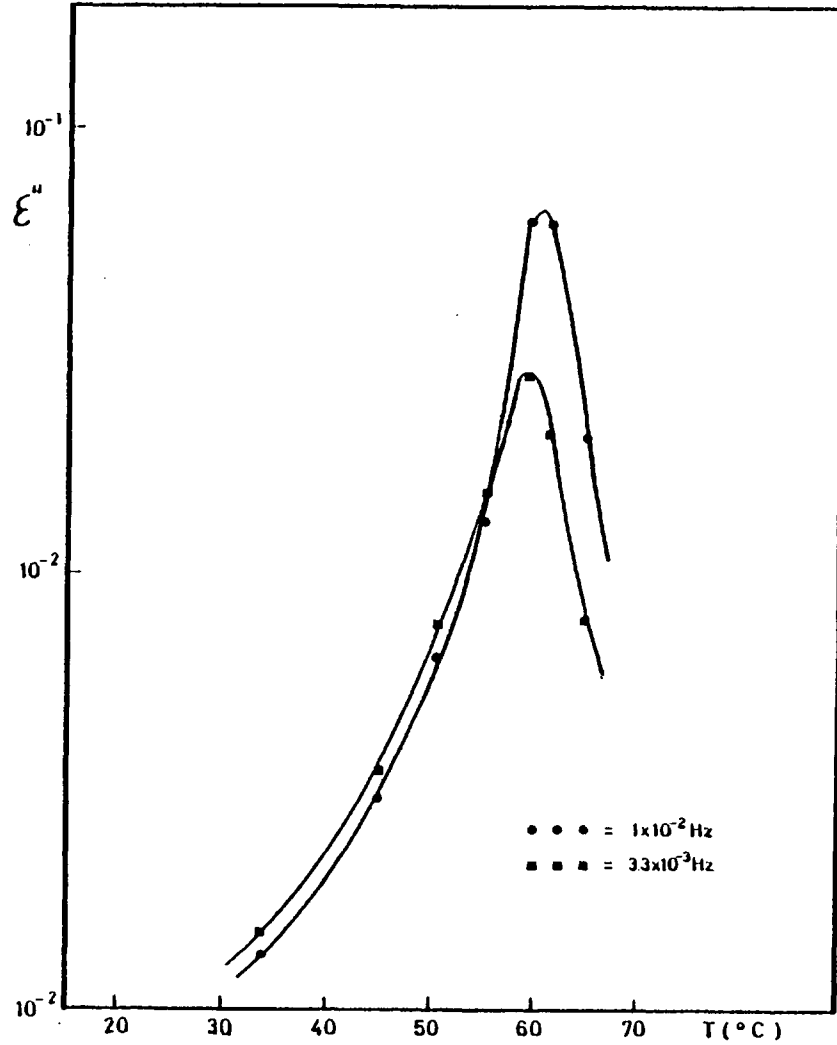


Fig. 5.14: Temperature dependence of dielectric loss  $\epsilon''$  calculated using Hamon method.

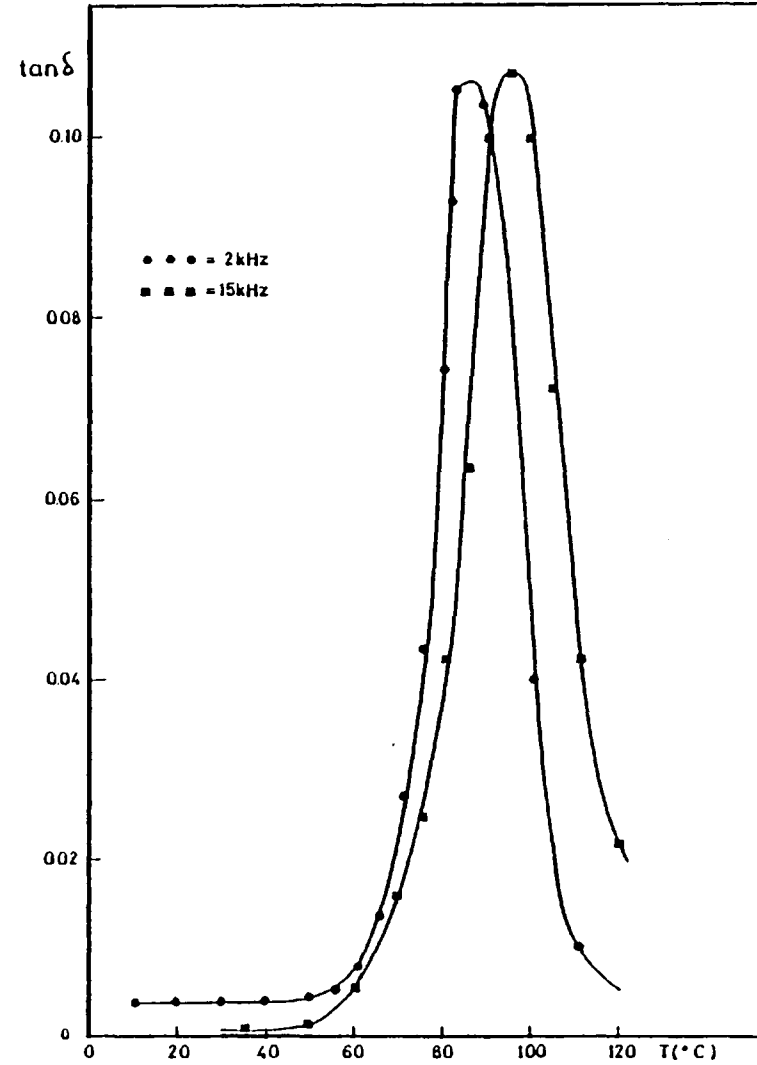


Fig. 5.15: Temperature dependence of  $\tan \delta$  for two frequencies.

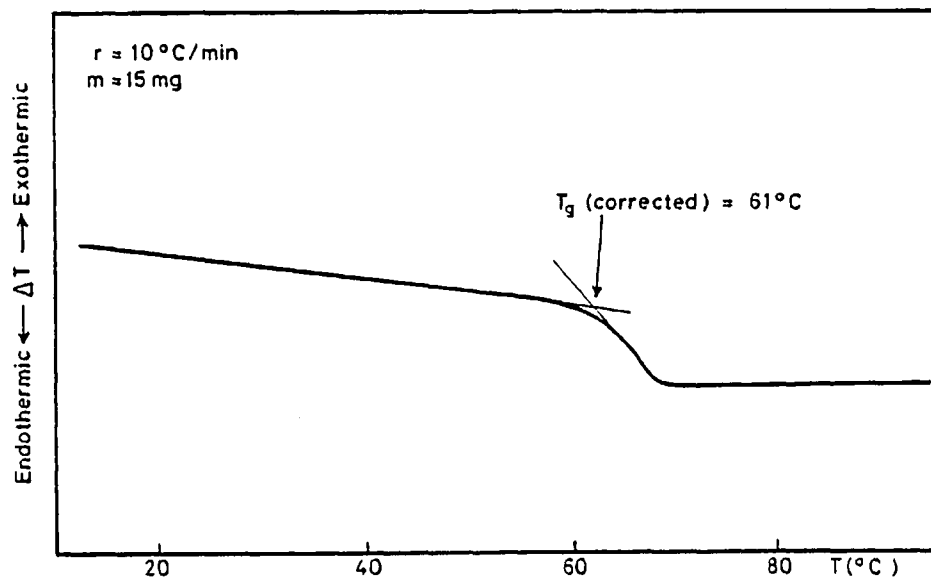


Fig. 5.16: The glass-transition curve for PVB films.

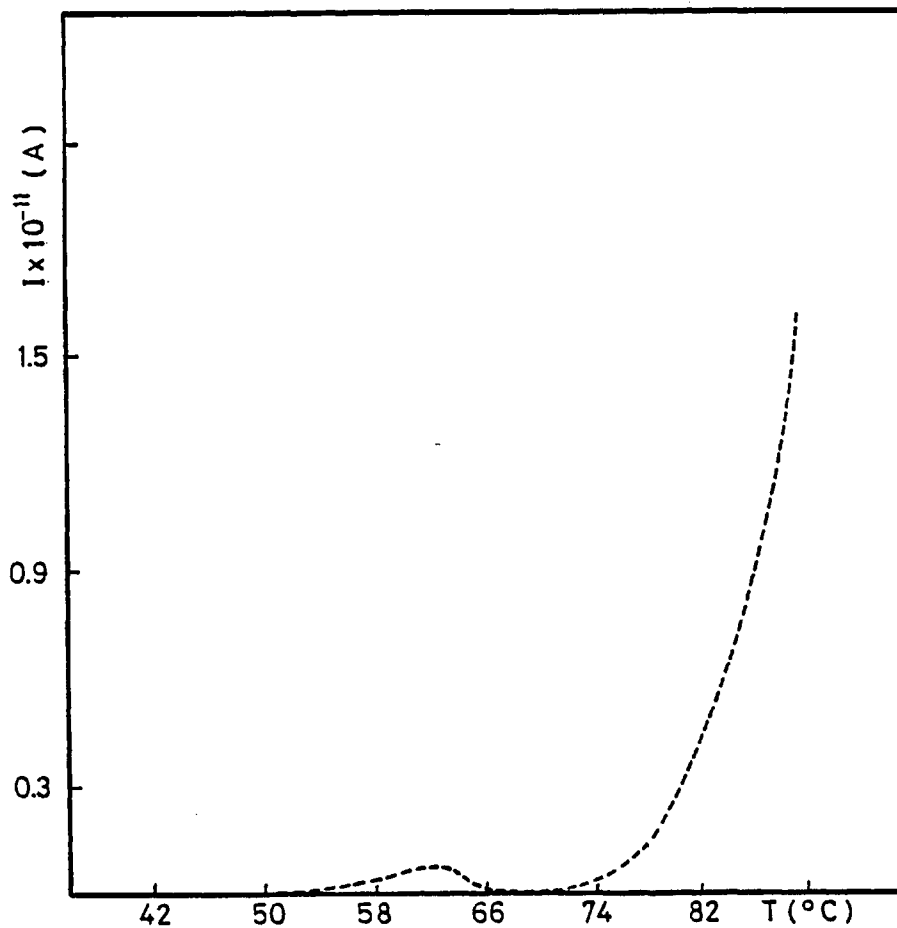


Fig. 5.17: Spontaneous current obtained from a virgin sample of PVB.  $r = 4^\circ\text{C}/\text{min}$ .

CHAPTER VI

6.1 FINAL CONCLUSIONS

A review on the electrical properties of polymers has been given together with some experimental techniques usually applied to study them. This is a subject which is inherently interdisciplinary in nature, being closely allied with the mechanical properties of polymers on the one hand, and with the semiconductive properties of inorganic substances on the other.

A versatile experimental system has been designed and constructed to investigate the electrical properties of polymers. The cryostat is suitable for investigating the electret effect as a function of polarising field and heating rate.

The results of this research have shown that the TSD technique is a powerful tool for investigating molecular motion in polymers. This is particularly the case for polar polymers, where the TSD current shows the increasing freedom of movement of the molecular dipoles through the glass transition. TSD research has not been confined to electrets, but has now become widely accepted as an important spectroscopic technique for investigating the dielectric and electrical behaviour of solids in general.

The objectives of TSD studies are to understand the molecular origins of the dielectric and space-charge relaxations observed, and to predict the impact of these relaxations on the electrical properties of a material in a satisfactory manner.

The most promising approach for improving the precise description of TSD peaks is to correlate them with results from complementary techniques, such as d.c. step response, a.c. response and DTA measurements.

The glass transition temperature determined by TSD in nylon and polyvinylbutyral films showed good correlation with those determined by DTA. This means that TSD offers an alternative approach for the determination of  $T_g$ 's in polymers, a fact that is being increasingly adopted in many laboratories.

An appreciable current was found under short-circuit conditions during the heating of virgin nylon films sandwiched between similar electrodes. Peaks were observed in the spectra, showing that the virgin polyamide films were not electrically isotropic. This is an important finding which should be carefully considered when investigating electrical properties of polymers, otherwise errors could arise due to the presence of such complex charge distributions. It can be said that a mechanoelectret is formed during the process of preparation of the nylon films.

When dissimilar metal electrodes are used on nylon films, a short-circuit current is observed which is reproducible in repeated heating cycles. It is believed that the observed current is of an electrochemical nature. The possibility of making use of this phenomenon for plastic dry cell batteries cannot be ruled out. This also needs further attention while studying TSD or the d.c. conductivity of polymers in addition to new technological applications.

A space charge relaxation ( $\rho$  peak) was observed in nylon films using TSD at about 90°C. It is believed that charges are trapped at the crystal boundaries during the poling process, because the amorphous phase is probably more conductive (Maxwell-Wagner effect). During discharge of the electret, the excess charges are considered to be neutralised by opposed carriers replenished at the phase boundaries by the unequal ohmic conduction currents. The polarising species responsible for this polarisation are probably ions. This gives TSD a special advantage over conventional measurements, for as it is always the case with  $\rho$  peaks, they are not

observed in dielectric or mechanical measurements, and therefore such crystallisation effects are not noticed. The activation energy measured for the  $\rho$  peak is close to that of proton conduction in polymers, i.e. 1.3-1.5 eV. However, it cannot be concluded that protons are the polarising species responsible for that relaxation, although their participation in it cannot be ruled out.

## 6.2 Future Work

It might be interesting to study in more detail the observed pyroelectricity in the nylon films, in order to see if the pyroelectric coefficient could be improved. Also, piezoelectric studies could be carried out in future investigations.

The gaseous effects on the nylon films is a phenomenon which deserves to be investigated further. For example, it might be interesting to see the feasibility of these devices as breath analysers.

The author has observed the existence of another peak in PVB at about 180°C. It might be relevant to study this relaxation to see whether or not it is of molecular origin.

Finally, the battery effect found in nylon films could be investigated using other kinds of metal electrodes, for instance Zn, Sn, Pb, Cu, etc. in order to optimise performance.

REFERENCES

- Adam G and Gibbs J H 1965 J. Chem. Phys. 43 139-46
- Adamec V and Calderwood J H 1975 J. Phys. D: Appl. Phys. 8 551-60
- Adamec V and Calderwood J H 1978 J. Phys. D: Appl. Phys. 11 781-800
- Amborski L E 1962 J. Polym. Sci 62 331-46
- Baird M E 1970 J. Polym. Sci 8 739-45
- Baird M E et al 1971 Polymer 12 159-75
- Baker W O and Yager W A 1942 J. Amer. Chem. Soc. 64 2171-77
- Billmeyer F W 1971 Textbook of Polymer Science (New York: Wiley)
- Blythe A R 1980 Electrical Properties of Polymers (London: Cambridge UP)
- Boyd R H 1959 J. Chem. Phys. 30 1276-83
- Boyer R F 1966 J. Polym. Sci. C14 261-81
- Boyer R F 1975 J. Polym. Sci. : Symp. No 50 189-242
- Boyer R F 1977 in Encyclopaedia of Polymer Science and Technology Ed. N. Bikales. Suppl. II (New York : Wiley) 745-839
- Booth G L 1968 in The Science and Technology of Polymer Films Ed. O J Sweeting Vol I (New York : Interscience) chap 11
- Broadhurst M G, Davies G T and McKinney J E 1978 J. Appl. Phys. 49 4992-97
- Bucci C and Fieschi R 1964 Phys. Rev. Lett. 12 16-19
- Bucci C A and Riva S C 1965 J. Phys. Chem. 26 363-74
- Bucci C and Fieschi R 1964 Phys. Rev. Lett. 12 16-19
- Bucci C, Fieschi R and Guidi G 1966 Phys. Rev. 148 816-23
- Bunn C W and Garner E V 1947 Proc. Roy. Soc. Lon. A189 39-70
- Chattain D et al 1973 J. Polym. Sci. Polym. Phys. Ed. 11 1631-40
- Chen R 1969a J. Appl. Phys. 40 570-85
- Chen R 1969b J. Electrochem. Soc. 116 1254-57
- Chybicki M 1977 Phys. Stat. Sol. 39 271-8
- Cohen M H and Turnbull D 1959 J. Chem. Phys. 31 1164-69
- Costa Ribeiro J (1943) An. Acad. Brasil. Cien. April p15
- Creswell R A and Perlman M M 1970 J. Appl. Phys. 41 2365-75

- Crine J P, Piron D L and Yelon A 1979a J. Appl. Phys. 50 3762-63
- Crine J P, Piron D L and Yelon A 1979b Ann. Rept. Conf. Elec. Ins. Dielect. Phenom. (NAS : Washington DC) 226-33
- Curtis A J 1961 J. Res. NBS 65A 185-96
- Daniel V V 1967 Dielectric Relaxation (New York : Academic Press)
- Das-Gupta D K and Joyner K 1976 J. Phys. D : Appl. Phys. 9 2041-48
- Das-Gupta D K, Doughty K and Brockley 1980 J. Phys. D : Appl. Phys. 13 2101-14
- Davies D K 1969 British J. Appl. Phys. 2 1533-37
- Doolittle A K 1951 J. Appl. Phys. 22 1471-75
- Duke C B and Schein L B 1980 Physics Today 42-48
- DuPont 1976 Technical Sheet on Elvamide
- Eguchi M 1925 Phil. Mag 49 179
- Eley D D and Spivey D I 1960 Trans. Farad. Soc. 56 1432-42
- Eley D D 1968 in Organic Semiconducting Polymers Ed J E Katon (London : Edward Arnold) Ch 5
- Fischer P and Röhl P 1976 J. Polym. Sci. Polym. Phys. 14 543-54
- Fischer P and Röhl P 1977 Prog. Colloid of Polym. Sci. 62 149-53
- Fukada E and Furukawa T 1981 Ultrasonics 31-39
- Garlick G F J and Gibson A F 1948 Proc. Phys. Soc. 60 574-90
- Gibbs J H and DiMarzio E A 1958 J. Chem. Phys. 28 807-13
- Gill W D 1972 J. Appl. Phys. 43 5033-40
- Gross B 1949 J. Chem. Phys. 17 866-72
- Gross B 1968 J. Electrochem. Soc. 115 376-381
- Gross B 1971 Endeavour XXX, 115-19
- Gross B 1972 J. Polym. Sci. : Polym. Phys. Ed 10 1941-47



- Hamon B V 1952 Proc. I E E (Lond) 99 151-5
- Hayashi S et al 1979 Charge Storage, Charge Transport and Electrostatics with their Applications Ed Y Wada (Tokyo : Kodansha) 277-81
- Haslam J et al 1972 Identification and Analysis of Plastics (London : Iliffe)
- Heaviside O 1892 Electrical Papers (London : McMillan) p488
- Hedvig P 1973 J. Polym. Sci. 42 1271-1274
- Hedvig P 1977 Dielectric Spectroscopy of Polymers (Bristol : Adam and Hilger Ltd.)
- Heijboer J 1978 Molecular Basis of Transitions and Relaxations Ed D J Meier (London : Gordon and Breach) 75-102
- Hill N E et al 1969 Dielectric Properties and Molecular Behaviour (London : van Nostrand) Ch I
- Hino T 1980 I E E E Elect. Insul. 15 301-11
- Hirota S et al 1966 Kolloid Z Z Polym. 213 109-15
- Hirsch J and Tahmasbi A R 1980 Sol. St. Comm. 34 79-81
- Hosemann R 1972 Crit. Rev. Macromol. Sci. 1 351-97
- Hummel D O and Scholl F 1972 Infrared Analysis of Polymers, Resins and Additives (New York : Wiley)
- Ieda et al 1975 J. Appl. Phys. 46 2796-98
- Isoda S et al 1973 Jpn. J. Appl. Phys. 12 1799-1805
- Ito D and Nakakita T 1980 J. Appl. Phys. 51 3273-77
- Jain K, Rastogi A C and Chopra K L 1974 Phys. Stat. Sol. 21 (85-92)
- Jain K, Kumar N and Mehendru P C 1979 J. Electrochem. Soc. 126 1958-63
- Jonscher A K 1967 Thin Solid Films 1 213-34
- Jonscher A K 1975 Nature 253 717-719
- Jonscher A K 1977a Phys. Stat. Sol. 84 159-166
- Jonscher A K 1977b J. Electrostat. 3 53-68
- Jonscher A K and Hill R M 1975 Physics of Thin Films V8 (New York : Academic Press)
- Jux J T, North A M and Kay R 1974 Polymer 15 799-804

- Kaufmann H S 1977 Introduction to Polymer Science and Technology (New York : Wiley)
- Ke B 1962 J. Appl. Polym. Sci. 6 624-28
- Keiss H and Rehwald W 1980 Colloid of Polym. Sci. 258 241-51
- Keithley 1972 Instruction Manual Model 610C p6
- Kohan M I 1973 Nylon Plastics (New York : Wiley)
- Kosaki M, Sugiyama K and Ieda M 1971 J. Appl. Phys. 42 3388-92
- Lacabane C, Goyaud P and Boyer R F 1980 J. Polym. Sci. Polym. Phys. Ed 18 277-84
- Lee H, Salomon R E and Labes M M 1979 J. Appl. Phys. 50 3773-74
- Lengyel G 1955 J. Appl. Phys. 37 807-10
- Lewis T J 1976 Annual Reports Conf. on Elect. Insul. and Dielect. Phenom. (NAS-NRC Washington DC) 533-61
- Lewis T J 1978 Polymer Surfaces Ed D T Clark and Feast W J (Chichester : Wiley) 65-89
- Lilly A C and McDowell J R (1968) J. Appl. Phys. 39 141-47
- Litt M H, Hsu C and Basu P 1977 J. Appl. Phys. 48 2208-12
- Lowell J 1977 J. Phys. D : Appl. Phys. 10 65-71
- Lowell J and Rose-Innes A C 1980 Adv. Phys. 29 947-1023
- Many A and Rakavi G 1962 Phys. Rev. 126 1980-88
- Martin E H and Hirsch J 1972 J. Appl. Phys. 43 1001-15
- McCall D W and Anderson E W 1960 J. Chem. Phys. 32 237-41
- McCrum N G, Read B E and Williams G 1967 Anelastic and Dielectric Effects in Polymeric Solids (London:Wiley)
- McKeever S W S and Hughes D M 1975 J. Phys. D : Appl. Phys. 8 1520-29
- Mehendru P C et al 1977 Phys. Stat. Sol. 42 403-7
- Mier D J 1978 Molecular Basis of Transitions and Relaxations (London : Gordon and Breach)

- Miyamoto T et al 1973 J. Appl. Phys. 12 5372-76
- Mizutani T, Ieda M and Jordan I B 1979 Jpn. J. Appl. Phys. 18 65-70
- Mizutani T, Tsukahara T and Ieda M 1980 J. Phys. D : Appl. Phys. 13 1673-9
- Mort J 1980 Advances in Physics 29 367-408
- Mott N F and Davies E A 1979 Electronic Processes in Noncrystalline Materials  
(Oxford : Clarendon Press)
- Murata Y 1979 Jpn. J. Appl. Phys. 18 1-8
- Nakajima T and Matsumoto Y 1963 Rep. Prop. Polym. Phys. Jap. 6 241-44
- Nakamura S, Sawa G and Ieda M 1979 Jpn. J. Appl. Phys. 18 995-6
- Neumann R M and Macknight W J 1981 J. Polym. Sci. Polym. Phys. Ed 19 369-70
- Norian K H 1977 PhD Thesis London University
- North A M et al 1978 Polymer 19 913-22
- Nye J F 1957 Physical Properties of Crystals (Oxford : Oxford U P) pp 78 and  
189
- O'Dwyer J J (1973) The Theory of Electrical Conduction and Breakdown  
in Solid Dielectrics (Oxford : Clarendon Press)
- Ong P H and van Turnhout J 1973 Electrets, Charge Storage and Transport  
in Dielectrics Ed M M Perlman (Princeton : The Electrochemical Society)  
213-29
- Perlman M M 1971 J. Appl. Phys. 42 2645-52
- Perlman M M and Unger S 1974 J. Appl. Phys. 45 2389-93
- Perlman M M, Sonnonstine T J and St. Pierre J A 1976 J. Appl. Phys. 47 5016-21
- Pethig R 1979 Dielectric and Electronic Properties of Biological Materials  
(New York : Wiley)
- Pfister G 1977 Phys. Rev. B 16 3676-87
- Pfister G and Abkowitz M A 1974 J. Appl. Phys. 45 1001-8
- Prest W M and Luca D J 1980 J. Appl. Phys. 51 5170-74
- Prevorsek D C 1971 J. Polym. Sci. 9 867-86

- Radhakrishna S and Haridoss S 1978 J. Appl. Phys. 49 301-3
- Reucroft P J and Ghosh S K 1973 Phys. Rev B 8 803-7
- Ruoff A L 1973 Materials Science (London : Prentice-Hall)
- Sacher E 1970 J. Macromol. Sci. Phys. B4 449-52
- Sacher E 1972 J. Macromol. Sci. Phys. B6 151-65
- Sacher E 1976 Ann. Rept. Conf. Elect. Ins. Dielect. Phenom. (Washington D C : NAS) 33-37
- Saito N et al 1963 Solid State Phys. 14 (New York : Academic Press) 344-502
- Sawa G et al 1974 Jap. J. Appl. Phys. 13 1547-53
- Sawa G et al 1977a J. Appl. Phys. 48 2414-18
- Sawa G, Lee D C and Ieda M 1977b Jap. J. Appl. Phys. 16 359-64
- Schaffert R M 1975 Electrophotography (New York : Wiley)
- Schwarzl F and Staverman J 1952 Physica 18 791-98
- Seanor D A 1968 J. Polym. Sci. 6 463-77
- Seanor D A 1972 Electrical Properties of Polymers in Polymer Science V2 Ed A D Jenkins (Amsterdam : North-Holland) 1187-1280
- Sessler G M 1977 International Symposium on Electrets and Dielectrics Ed Acad. Bras. Cien. (Rio de Janeiro) 321-35
- Sessler G M 1978 Annual Reports Conf. on Elect. Insul. and Dielect. Phenom. (NAS-NRC Washington D C) 3-10
- Sessler G M and West J E 1975 J. Electrostat. 1 111-118
- Sessler G M and West J E 1966 J. Acoust. Soc. Am. 40 1433-40
- Simmons J G 1971 Conduction in Thin Films (London : Mills and Boon Ltd)
- Street G B and Clarke T C 1981 IBM J. Res. Develop. 25 51-57
- Stupp S I and Carr S H 1975 J. Appl. Phys. 46 4120-23
- Stupp S I and Carr S H 1977 J. Polym. Sci. Polym. Phys. Ed. 15 485-95

- Takahashi Y 1961a J. Appl. Polym. Sci. V 468-77
- Takahashi Y 1961b J. Phys. Soc. Jap. 16 1024
- Takayanagi M et al 1963 Rept Prog. Polym. Phys. (Jap) 6 121-25
- Tanaka T et al 1978a J. Appl. Phys. 49 784-87
- Tanaka T et al 1978b J. Appl. Phys. 49 2490-93
- Vandershueren J 1977 J. Polym. Sci. Polym. Phys. Ed 15 873-80
- Vanderschueren J 1980 Macromolecules 13 973-77
- Vanderschueren J and Gasiot J 1979 Top. Appl. Phys. 37 135-223
- Vanderschueren J and Linkens A 1977 J. of Electrostat. 3 155-61
- Vanderschueren J and Linkens A 1978 J. Appl. Phys. 49 4195-4205
- Vanderschueren J. et al 1980 J. Appl. Phys. 51 4967-75
- van Turnhout J 1971 Advances in Static Electricity Ed. W.F. de Geest  
(Brussels : Auxilia) 164-94
- van Turnhout J 1975 Thermally Stimulated Discharge of Polymer Electrets  
(New York : Elsevier)
- van Turnhout J 1980 Top. Appl. Phys. 33 81-125
- Vijh A K 1978 J. Appl. Phys. 49 3621-24
- Vijh A K 1979 J. Appl. Phys. 50 3764-65
- Wada Y and Hayakawa R 1976 Jpn. J. Appl. Phys. 15 2041-57
- Ward I M 1979 Mechanical Properties of Polymers (Chichester : Wiley)
- Weast R C 1977 Handbook of Chemistry and Physics (Ohio : CRC Press) E-60
- Weber G 1978 Die Macromol. Chem. 74 187-202
- Williams M L, Landel R F and Ferry J D 1955 J. Amer. Chem. Soc. 77 3701-07
- Wintle H J 1972 The Radiation Chemistry of Macromolecules Ed. M Dole  
(New York : Academic Press) 109-125
- Wintle H J 1974 J. Noncryst. Sol. 15 471-86

Yamashita K et al 1979 Charge Storage, Charge Transport and Electrostatics  
with their Applications Ed. Wada Y (Tokyo : Kodansha) 427-31

Zielinski M and Kryszewski M 1977 Phys. Stat. Sol. (a) 42 305-14

Zielinski M, Jeszka J K and Kryszewski M 1980 Phys. Stat. Sol. (a) 58  
385-92